The physical processes that drive galaxy evolution - from massive galaxies to the dwarf regime

Author:

Ryan Jackson

Supervised by:

Prof. Sugata Kaviraj

Prof. James Geach

Centre for Astrophysics Research

School of Physics, Astronomy and Mathematics

University of Hertfordshire

Submitted to the University of Hertfordshire in partial fulfilment of the requirements of the degree of Doctor of Philosophy.

October 2021

Abstract

The study of galaxy formation and evolution is a cornerstone in astrophysics, as galaxies connect together all scales of the Universe. The physical processes that govern galaxies therefore needs to be fully understood if we are to understand how our Universe works. The various morphologies of galaxies we see today indicate that there are multiple processes at play, that act both on and within galaxies. In our currently accepted paradigm, galaxies are expected to assemble mass through merging and gas accretion, therefore these are critical processes that must be understood across the range of galaxy masses. We can now combine observational data from wide-are surveys with state of the art cosmological simulations to study how these processes drive galaxy evolution across cosmic time.

In this thesis we have used cosmological simulations (Horizon-AGN and `NewHorizon`) to study how physical processes shape galaxies. Firstly, we explore an unusual population of extremely massive ($M_* > 10^{11} M_\odot$) spheroids, in the Horizon-AGN simulation, which exhibit anomalously low ex-situ mass fractions. This indicates that they form without recourse to significant merging, contrary to the common belief. These systems form in a single minor-merger event (with typical merger mass ratios of 0.11 - 0.33), where the satellite orbit is virtually co-planar with the disc of the massive galaxy. The merger triggers a catastrophic change in morphology, over only a few hundred Myrs, coupled with strong in-situ star formation. While this channel produces a minority (~5 per cent) of such galaxies, our study demonstrates that the formation of at least some of the *most massive* spheroids need not involve major mergers - or any significant merging at all - contrary to what is classically believed.

We also look at how extremely massive disc galaxies form in both simulations and in the nearby Universe. We show that extremely massive ($M_* > 10^{11.4} M_\odot$) discs are created via two channels. In the primary channel (accounting for 70% of these systems and 8% of massive galaxies) the most recent, significant merger (mass ratio > 1:10) between a massive spheroid and a gas-rich satellite 'spins up' the spheroid by creating a new rotational stellar component, leaving a massive disc as the remnant. In the secondary channel (accounting for 30% of these systems and 3% of massive galaxies), a system maintains a disc throughout its lifetime, due to an anomalously quiet merger history. These massive discs have similar black-hole masses and accretion rates to massive spheroids, providing a natural explanation for why some powerful AGN are surprisingly found in disc galaxies.

In an observational follow-up we use UV-optical and HI data of massive galaxies, from the SDSS, GALEX, DECaLS and ALFALFA surveys to test the predictions from Horizon-AGN. Observed massive discs form ~13 per cent of the population, in good agreement with the simulation (~11 per cent). ~64 per cent of massive discs exhibit tidal features indicative of recent minor mergers in the deep DECaLS images. The incidence of these features is at least four times higher than

in low-mass discs, indicating that minor mergers play a significant role in the formation of these systems. The empirical star-formation rates agree well with Horizon-AGN's predictions and, for a small galaxy sample with HI detections, the HI masses/fractions are consistent with the range predicted. The good agreement between theory and observations indicates that extremely massive discs are indeed remnants of recent minor mergers between spheroids and gas-rich satellites.

We also look into the origins of dwarf low surface brightness galaxies (LSBGs), which are expected to dominate the galaxy number density. Using `NewHorizon`, a high-resolution cosmological simulation, we study the origin of LSBGs and explain why, at similar stellar mass, they exhibit a large observed spread in surface brightness. `NewHorizon` galaxies populate a well-defined locus in the surface brightness - stellar mass plane, with a spread of $\sim$3 mag arcsec^{-2}, in agreement with deep SDSS Stripe data. We find that galaxies with fainter surface brightnesses today are born in regions of higher dark-matter density. This results in faster gas accretion and more intense star formation at early epochs. The stronger resultant supernova feedback flattens gas profiles at a faster rate which, in turn, creates shallower stellar profiles (i.e. more diffuse systems) more rapidly. A small minority of dwarfs depart from the main locus towards high surface brightnesses, making them detectable in past wide surveys (e.g. standard-depth SDSS images). These systems have anomalously high star-formation rates, triggered by recent, fly-by or merger-driven starbursts. We note that objects considered extreme/anomalous at the depth of current datasets, e.g. 'ultra-diffuse galaxies', actually dominate the predicted dwarf population and will be routinely visible in future surveys like LSST.

Finally, we look at a population of galaxies that go against our current theoretical paradigm. Recent observations have found local dwarfs with extremely low dark matter content, potentially bringing the validity of the standard model into question. We use `NewHorizon` to demonstrate that sustained stripping of dark matter, in tidal interactions between a massive galaxy and a dwarf satellite, naturally produces dwarfs that are dark-matter-deficient. The degree of stripping is driven by the closeness of the orbit of the dwarf around its massive companion, and produces dwarfs with halo-to-stellar mass ratios consistent with the findings of recent observational studies. $\sim$30 per cent of dwarfs show some deviation from normal dark matter fractions due to dark matter stripping, with 10 per cent showing high levels of dark matter deficiency ($M_{halo}/M_{\star}<10$). The creation of these galaxies is, therefore, a natural by-product of galaxy evolution and their existence is not in tension with the standard paradigm.

This thesis examines galaxy populations that appear to go against the currently accepted paradigm, in both the massive and dwarf galaxy regime. We show that galaxy evolution is a very complicated problem and that it is possible to form different galaxy populations through many processes. By using a cosmological simulation based on ΛCDM we also show that the

existence of these populations do not pose a challenge to this model and are, in fact, readily explained by it.

Declaration

I declare that no part of this work is being submitted concurrently for another award of the University or any other awarding body or institution. This thesis contains a substantial body of work that has not previously been submitted successfully for an award of the University or any other awarding body or institution.

The following parts of this submission have been published previously and/or undertaken as part of a previous degree or research programme:

1. Chapter 2: this has been published as Jackson et al., 2019, *Monthly Notices of the Royal Astronomical Society*, **489**, 4679.

2. Chapter 3: this has been published as Jackson et al., 2020, *Monthly Notices of the Royal Astronomical Society*, **494**, 5568.

3. Chapter 4: this has been submitted as Jackson et al. to the *Monthly Notices of the Royal Astronomical Society*.

4. Chapter 5: this has been published as Jackson et al., 2021, *Monthly Notices of the Royal Astronomical Society*, **502**, 4262.

5. Chapter 6: this has been published as Jackson et al., 2021, *Monthly Notices of the Royal Astronomical Society*, **502**, 1785.

Except where indicated otherwise in the submission, the submission is my own work and has not previously been submitted successfully for any award.

Acknowledgements

I dedicate this work to my late grandparents Gwen and Ray Carr, whose enthusiasm for life and unconditional love helped make me the person I am today.

Contents

List of Figures

List of Tables

Chapter 1

Introduction

Galaxies are a fundamental component of our Universe, therefore understanding their formation and evolution is one of the key research areas in astronomy. The study of galaxies links together other research areas in astronomy, as they connect the large scale structure of the Universe to the gas, stars and planets that are contained within them. We therefore require a complete understanding of the processes that govern galaxies if we are to truly understand how our Universe works.

The existence of galaxies other than the Milky Way was first demonstrated by Hubble (1926), who created a classification scheme to identify galaxies by their shape (Figure 1.1). This classification scheme breaks galaxies down into four classes: spirals, lenticular, ellipticals and irregular. At the time the way these different morphologies related to one another, if at all, was not known. However, over time observational studies have shown that at high redshift galaxies tend to have more disc-like morphologies, with high rates of star formation and blue colours (Wuyts et al., 2011; Conselice et al., 2014; Buitrago et al., 2014; Shibuya et al., 2015). Whereas low redshift galaxies are dominated by massive quenched galaxies with elliptical morphologies and red colours (Bernardi et al., 2003; Buitrago et al., 2013; Madau and Dickinson, 2014; Kaviraj, 2014b). Given this, it is therefore plausible that these morphologies encode information about the history of each galaxy, and the processes that have formed it.

We are now in an age of large datasets, allowing us to study galaxies and processes that govern them in a statistical way. These recent wide-area surveys (such as SDSS (Abazajian et al., 2009)) have allowed for the study of millions of galaxies across a large part of cosmic time and, with modern computational methods, large-volume cosmological simulations can be performed to examine how physical processes shape galaxies (Dubois et al., 2014a; Vogelsberger et al., 2014b; Schaye et al., 2015). By combining these two datatsets it has become possible to study how galaxies we see in the local Universe have formed over time. We now believe that the
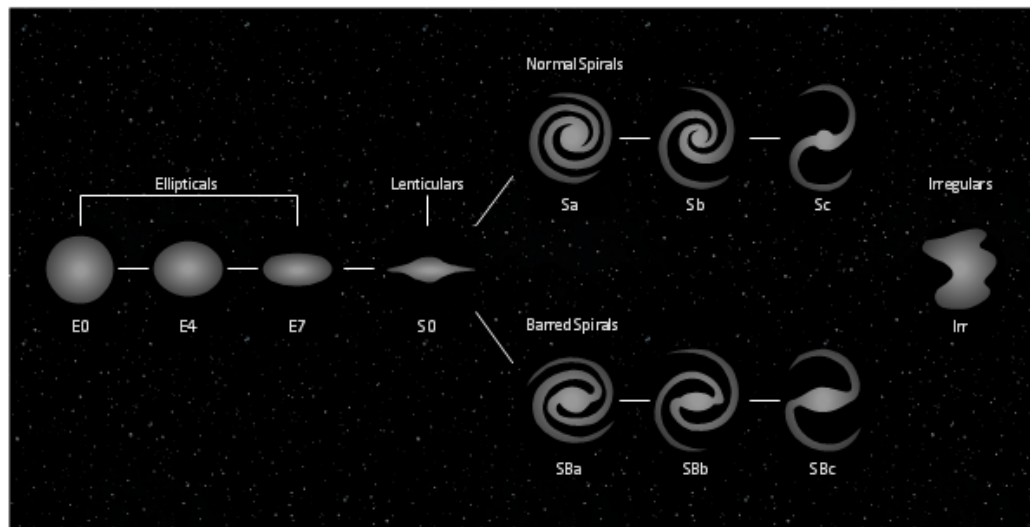
FIGURE 1.1: The Hubble sequence classification scheme, used to morphologically identify galaxies.

morphologies of galaxies form a sequence, with galaxies typically evolving from star-forming spirals to quenched ellipticals (e.g. Conselice, 2014).

Although the study of galaxies has come a long way since the days of Hubble, there are still many areas that are poorly understood. A particular area that has recently come to prominence is the study of dwarf galaxies. Recent theoretical work (e.g. Martin et al. (2019), Chapter 5) has shown that the these galaxies dominate the number density of galaxies but are almost entirely missed in current wide-area surveys, as they are below the surface brightness limits. As our models are statistically calibrated to the subset of bright galaxies, our understanding of the physics of galaxy evolution remains potentially highly incomplete. Therefore upcoming deep-wide survey instruments (e.g. HSC-SSP, LSST, JWST and EUCLID), which will allow us to study galaxies in the low surface brightness regime, have the capacity to alter our current understanding of galaxy evolution. These new observing tools are supplemented by the next generation of high-resolution simulations (`NewHorizon` (Dubois et al., 2020), Illustris-TNG (Nelson et al., 2019), allowing us to make predictions for these surveys and understand how processes operate over a large range of stellar masses and redshift.

1.1 The formation of galaxies

A detailed process of how galaxies form is still a major open question, the current theoretical model is known as the bottom-up model (White and Rees, 1978; Searle and Zinn, 1978). This theory states that small structures form first, with these smaller structures merging together over time to create ever larger structures resulting in hierarchical galaxy formation (White and Rees,

1978; Cole et al., 2000). In our current cosmological model (ΛCDM (Rees and Ostriker, 1977)), the Universe is constructed of four components: radiation, baryons, dark matter and dark energy.

Although on large scales the Universe appears to be homogeneous and isotropic, small scale inhomogeneities do exist. These manifest themselves as regions of the Universe that are slightly under and over dense compared to the average (discovered by analysis of the Cosmic Microwave Background (Komatsu et al., 2009; Dunkley et al., 2009)). These high-density regions contract due to gravity and eventually collapse, bringing in material from their surroundings. This in turn causes the under-dense regions to become ever sparser. Inside these over-dense regions, dark matter halos begin to form and acquire angular momentum, through halo mergers and/or tidal interactions. These dark matter halos will then begin to accrete more dark matter and merge together in order to increase in mass (Peebles, 1982; Blumenthal et al., 1984).

Following recombination, baryons (in the form of gas) fall into these over-dense regions as they are no longer coupled to photons in an ionised plasma. As the gas can cool radiatively, it is able to condense into cold gas, which eventually settles into rotationally supported discs at the centre of the dark matter halo (Fall and Efstathiou, 1980). Within these discs, clumps are formed which collapse to form stars, which constitute the beginnings of a galaxy (Conselice et al., 2014; Somerville and Davé, 2015). These proto-galaxies then begin to assemble more mass over cosmic time until they resemble the galaxies that we see in the local Universe.

1.1.1   Mass assembly in galaxies

One of the key predictions of the hierarchical formation model of galaxy evolution is that galaxies merge over cosmic time to create ever larger galaxies (see Figure 1.2). These mergers are split into two types: major mergers where galaxies have similar masses (mass ratios greater that 1:4) and minor mergers where one galaxy is significantly larger than the other (mass ratios less that 1:4 and greater that 1:10). The merging of galaxies (both major and minor) is believed to be an important driver of galaxy evolution (Steinmetz and Navarro, 2002) such as stellar mass assembly, triggering bursts of star formation and causing morphological transformations.

Merging is therefore an obvious candidate when considering which processes are capable of increasing the stellar mass of galaxies. Both major and minor mergers result in the stellar mass of the smaller galaxy being accreted by the larger companion, and therefore increasing its own mass. It is also possible for the merger to bring in gas via the smaller galaxy, increasing the gas reservoir available for star formation (e.g. Tonini et al., 2016). The merger process itself is capable of driving strong star formation episodes, such as in Figure 1.3, where gas is driven towards the central regions of the galaxy, which rapidly increases its gas density causing star formation (Mihos and Hernquist, 1996).
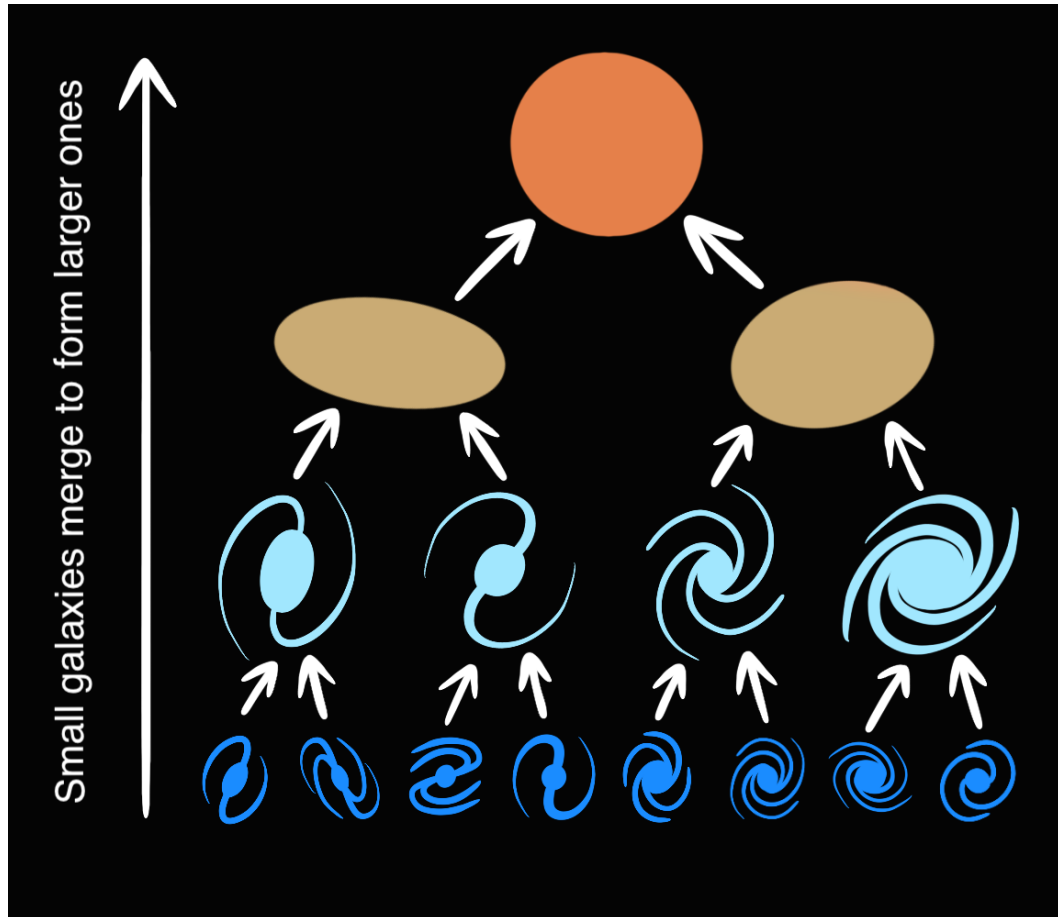
FIGURE 1.2: Hierarchical galaxy formation. Small galaxies merge together over cosmic time to form ever larger galaxies.

As star formation is reliant on gas, the occurrence of a merger by itself is not sufficient to result in an increase in star formation. In order for star formation to be triggered, the merger typically needs to be gas-rich, meaning one of the galaxies must have a large amount of cold gas which can fuel the star formation (Tonini et al., 2016). That being said, galaxies with the highest star formation rates, at a given redshift, typically show evidence of undergoing a merger (Sanders and Mirabel, 1996; Ellison et al., 2013). Therefore at high redshift, where mergers are more common and the Universe is generally more gas-rich, merging could be responsible for large amounts of the mass assembly of galaxies (Mihos, 2000; Conselice, 2007).

Although mergers contribute to both the stellar mass assembly and star formation budget of galaxies, in order to reach the observed rates of star formation an additional source of gas is required. At high redshift, galaxies with $M_\star > 10^{11} M_\odot$ must accrete gas at around $100 M_\odot \text{yr}^{-1}$, with this gas accretion responsible for $66 \pm 20\%$ of all new star formation between $1.5 < z < 3$ (Conselice et al., 2013). This process is therefore a major component of galaxy evolution and is potentially more important in forming new stars than merging (Martin et al., 2017).

There are multiple methods by which gas accretion onto galaxies could occur. The most

FIGURE 1.3: An image of a starburst galaxy (the Antennae Galaxies), which formed via the collisions of NGC 4038 and NGC 4039. Credit NASA/ESA.

prominent sources of this gas are believed to be the intergalactic medium (IGM), satellite galaxies and recycled feedback gas, see Figure 1.4 (Putman, 2017). Accretion from the IGM occurs along filaments connected to the galaxy's dark matter halo and is expected to be the dominant source of gas accretion for a galaxy (Joung et al., 2012). Satellite galaxies also have their gas reservoirs stripped by ram pressure from the circumgalactic medium of their host galaxies. Although most satellites do not provide much gas, larger ones such as the large Magellanic Clouds could provide fuel for extended star formation. Finally feedback methods (such as active galactic nuclei or supernovae) are capable of removing gas from a galaxy's disc into the halo, making it an abundant source of fuel for future star formation events as it cools.

Most of the gas inside the halo is hot, ionised gas that is gravitationally bound (Croton et al., 2016). Therefore, as gas is accreted, it is shock heated at the halo's virial radius to the virial temperature. As this heating occurs at the edges of the halo, rather than closer in to the galaxy, it requires a long time for the gas to cool and collapse onto the galaxy (Rees and Ostriker, 1977; White and Rees, 1978). This is what is termed 'hot mode' accretion and is believed to occur
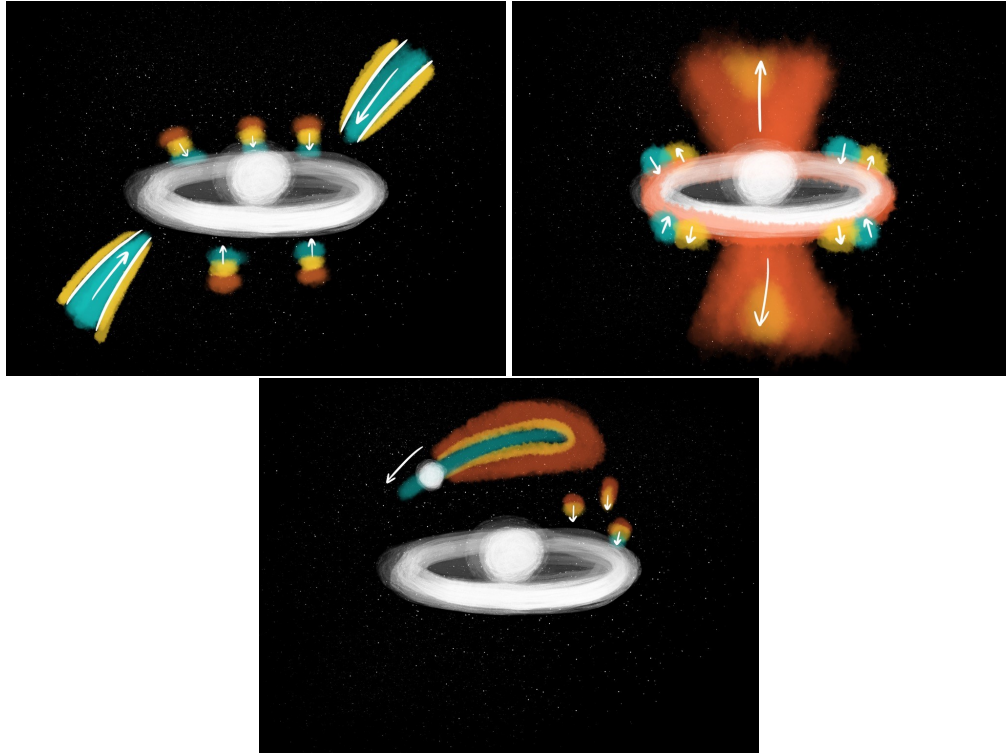
FIGURE 1.4: The three expected sources of gas accretion with gas temperature represented by colour (blue being cold gas to red being hot gas), modified from Putman (2017). Top-left: Accretion from the IGM along filaments onto the galaxy. Top-right: Feedback processes heat gas causing it to rise into the galaxy halo, the gas cools and falls back onto the galaxy. Bottom: Satellite galaxies are stripped of their gas as they pass through the circumgalactic medium of the larger galaxy.

predominantly in massive galaxies where these shocks can be stabilised (Birnboim and Dekel, 2003; Dekel and Birnboim, 2006).

In low mass halos, and at high redshift, 'cold' mode accretion is the dominant method of gas accretion, due to the relative high density of filamentary gas and the lack of a hot halo. This stops the formation of a stable shock, resulting in rapid cooling rates for gas (e.g. Kereš et al., 2005; Dekel et al., 2009; Benson and Bower, 2011). These cold accretion flows are, therefore, capable of bringing gas directly from the cosmic web and onto the central parts of galaxies, whilst also potentially providing angular momentum to the system (Kereš et al., 2005; Pichon et al., 2011). Cold flows are therefore believed to be a main driver of galaxy mass assembly, as most galaxies will experience this mode of accretion at some point.

Once gas is obtained by a galaxy, either via merging or gas accretion, it needs to be converted into stars in order for the galaxy to grow. The detailed process of star formation in galaxies is still a major research area in astronomy but some seemingly fundamental relations seem to exist. Most star forming galaxies seem to be converting gas to stars at a steady rate, this is shown when star formation rate is plotted against stellar mass. The 'main sequence' of galaxy formation is formed from these star forming galaxies that show the general trend of increasing star formation rate

with increasing stellar mass (Brinchmann et al., 2004; Elbaz et al., 2011; Speagle et al., 2014; Schreiber et al., 2015). This main sequence is a tight relationship, galaxies that fall off from this are either highly star forming (starbursts) or have been quenched. The reason that increasing stellar mass is correlated to increasing star formation rate is likely due to a larger amount of gas available in more massive galaxies. Indeed the Kennicutt-Schmidt law (Kennicutt, 1998) shows a relationship between the surface density of star formation and gas density of a galaxy. This suggests a larger relationship between the availability of gas in the Universe and the number of star forming galaxies found. Observations have shown that the cosmic star formation history, the evolution of SFR with redshift, increases from z=0 to a peak around z=2 before decreasing again (Madau and Dickinson, 2014). Many of these high redshift galaxies do not show signs of morphological disturbances and so are likely fueled by gas accretion (e.g Elbaz et al., 2007). The decline of star formation at low redshift is therefore likely due to the shutdown of gas supply to massive galaxies and the exhaustion of gas within galaxies (Hernquist and Springel, 2003; Schaye et al., 2010).

These relationships seem to govern the passive star formation in galaxies across cosmic time, however galaxies do not necessarily evolve in isolation and interactions with other galaxies can potentially disrupt this star formation, and even change the shape of a galaxy entirely.

1.1.2   Morphological transformations: the role of mergers

The evolution of the morphological mix of galaxies shows a gradual change from disc-dominated to elliptical-dominated, over cosmic time (e.g. Conselice et al., 2014). Morphological transformations, the conversion of spiral galaxies to ellipticals, is believed to be primarily triggered by galaxy mergers (Toomre, 1977; Barnes, 1992a; Di Matteo et al., 2007; Conselice et al., 2009a; Taranu et al., 2013; Negroponte and White, 1983; Naab et al., 2014a,b; Deeley et al., 2017; Martin et al., 2018). The strong gravitational torques generated by nearly equal mass-ratio mergers are capable of efficiently moving material from rotational orbits into the random, chaotic ones that make up elliptical systems. In addition, many ellipticals show signatures of rapid change in their stellar populations (e.g. Wild et al., 2016), and internal structure (e.g. Rodrigues et al., 2017), which would indicate a major merger in their recent history. Due to these findings the bulk of studies have highlighted the important role of major mergers, as the primary cause of morphological transformation (Toomre, 1977; Negroponte and White, 1983; Dubois et al., 2016).

However, more recent work (e.g. Welker et al., 2017; Martin et al., 2018) has highlighted the role that minor mergers may play in these morphological transformation (see Chapter 2). As low mass galaxies far outnumber their more massive counterparts, minor mergers are expected to occur at a much higher frequency than major mergers. Many massive spheroids that are in the

FIGURE 1.5: An image of Arp-Madore 2026-424, two equal mass galaxies merging. Credit NASA, ESA, J. Dalcanton, B.F. Williams, and M. Durbin (University of Washington).

process of forming at $z \sim 2$, the epoch at which the morphological mix of the Universe appears to change most rapidly (e.g. Conselice et al., 2014), do not show tidal features and extended halos that should be visible if they were forming via major mergers (at least at the depth of current data) (e.g. Kaviraj et al., 2013; Williams et al., 2014; Lofthouse et al., 2017). This suggests that there must be other channels (e.g. minor-merger-triggered disc instabilities, Zolotov et al. (2015)), not involving major mergers, that may give rise to a significant fraction of spheroidal systems at high redshift.

Given the lack of depth of current surveys, the effect of minor mergers on galaxy evolution remains relatively unexplored, although forthcoming instruments like LSST, EUCLID and JWST (e.g. Tyson, 2002; Robertson et al., 2017; Gardner et al., 2006; Laureijs et al., 2011) will enable the first statistical studies of minor-merger-driven galaxy evolution. Much of our current understanding of the role of this process therefore comes from theoretical work, in particular hydrodynamical simulations of cosmological volumes (e.g. Vogelsberger et al., 2014b; Schaye et al., 2015; Khandai et al., 2015; Kaviraj et al., 2017).
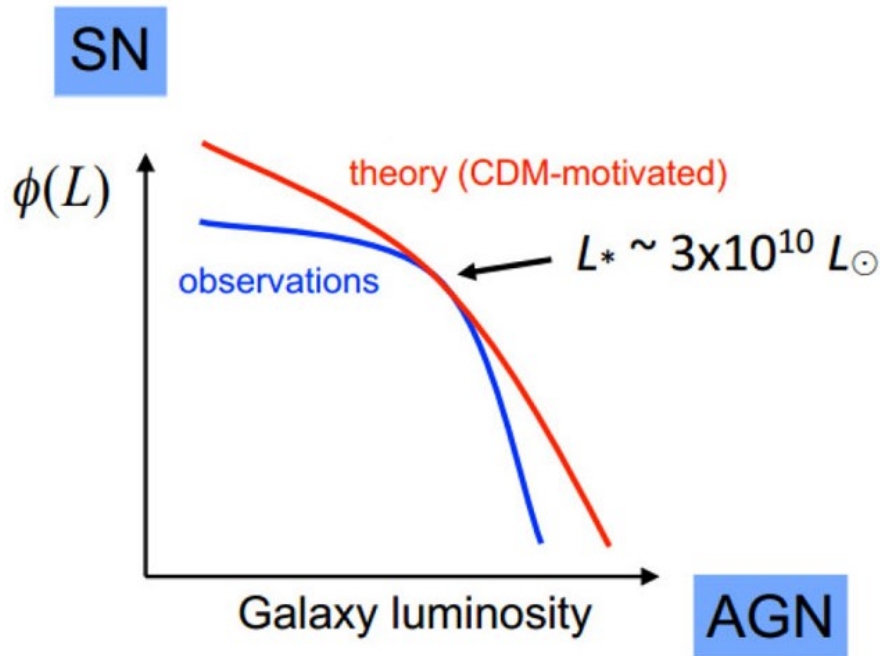
FIGURE 1.6: The galaxy luminosity function from both observations (blue) and theory (red), from Silk and Mamon (2012). The discrepancy between theory and observations in the low and high mass ends show the impact of feedback in regulating the number of galaxies in the Universe. At the low mass end supernovae feedback is able to disrupt the star formation of dwarf galaxies. Whereas at the high mass end AGN feedback is believed to be responsible for quenching galaxies.

1.1.3 Feedback processes and environment

In the standard ΛCDM model we expect that most baryonic material should cool and eventually form stars, if no other processes act upon it. However, observations of the galaxy luminosity function do not match these theoretical predictions (Figure 1.6). This means that there must be physical processes, that operate within galaxies, to prevent gas from cooling or reheat the gas that has cooled. These processes are therefore capable of suppressing star formation in galaxies at both the high and low mass end.

In low mass galaxies ($\sim M_\star < 10^{10} M_\odot$), where the gravitational potential wells are relatively weak, feedback from supernovae and stellar winds are efficient at removing baryons from galaxies (Silk, 2011). This feedback works by providing energy to the cold, star forming gas in galaxies, thereby removing the fuel needed for star formation. This heated gas outflows from the galaxy and into the halo where it can later cool and infall again (Dong et al., 2003). The star formation efficiency of these galaxies is reduced in a repeating cycle, as more stars are formed stellar feedback increases which re-quenches star formation (Hayward and Hopkins, 2017).

For galaxies that are more massive, the energy of stellar feedback is insufficient to quench galaxies, as the binding energy of the gas is too high. In this regime the dominant feedback process is believed to be energy released from an accreting supermassive black hole (SMBH) at

the galaxy's centre (e.g. Di Matteo et al., 2005; Cattaneo et al., 2009; Beckmann et al., 2017). When the SMBH is accreting matter, and emitting energy, they are referred to as active galactic nuclei (AGN). This AGN feedback is believed to occur in two modes, known as the jet and quasar modes, that operate via different mechanisms depending on the accretion onto the black hole (Fabian, 2012). The jet mode, which occurs at lower accretion rates and outputs lower energies, is believed to be important for keeping the medium around galaxies hot via kinetic energy from the jets (e.g. Antonuccio-Delogu and Silk, 2008; Wagner and Bicknell, 2011). This prevents the cooling of hot gas, contained within the halo, back onto the galaxy. In quasar mode, which occurs when there is rapid accretion onto the black hole (usually close to the Eddington rate), orbital energy from the matter accreting onto the SMBH is emitted as radiation which heats the surrounding medium. This radiation heats gas and quenches star formation on small scales within the galaxy (e.g. Veilleux et al., 2013).

A galaxy's environment is also known to have an effect on its morphology (Dressler, 1980; Dressler et al., 1997; Postman and Geller, 1984; Balogh et al., 1999). In the local Universe we find that denser environments (such as galaxy clusters) tend to have a higher fraction of elliptical galaxies, whereas comparatively sparse environments are prone to hosting more disc-like and star forming galaxies. This is likely due to the processes which operate in these dense environments, with tidal forces, ram-pressure and an increase in mergers all proposed as methods for quenching star formation and creating morphological transformations.

1.2 Cosmological simulations

Although current observational studies are able to answer many key questions on galaxy evolution, understanding how the physical properties and environments influence galaxies over cosmic time is difficult to answer with observations alone. We therefore require large volume simulations, that are consistent with observable properties, which can be used to study this evolution and make predictions that are testable. However, running such simulations is incredibly computationally demanding. In order to capture both large-scale structure and the internal evolution of galaxies these simulations need to simulate over a large dynamical range.

Simulations using semi-analytical models have been successful in reproducing many of the bulk properties of galaxies over a significant fraction of cosmic time (e.g. Somerville and Primack, 1999; Cole et al., 2000; Benson et al., 2003; Bower et al., 2006; Croton et al., 2006). This technique works by employing approximations derived from more detailed numerical simulations, and empirical calibrations from data, to probe galaxy formation. However, recent advances in computing power has given rise to full hyrdodynamical simulations which implement the evolution of dark matter and baryons self-consistently. These simulations still require recipes in order to model physical processes but these are applied at much smaller scales then in previous

simulation techniques. The combination of large volume, and high resolution, offered by these simulations has, for the first time, allowed for detailed predictions that can be compared to observations (e.g. Dubois et al., 2014a; Vogelsberger et al., 2014b; Schaye et al., 2015; Khandai et al., 2015; Taylor and Kobayashi, 2016; Kaviraj et al., 2017).

1.2.1   The Horizon simulations: Horizon-AGN and `NewHorizon`

Throughout the work in this thesis, we make use of the Horizon-AGN and `NewHorizon` simulations (Dubois et al., 2014a; Kaviraj et al., 2017; Dubois et al., 2020). In the following sections we will describe some of the key properties and recipes used in both simulations, as well as how they compare to observations.

Horizon-AGN is a cosmological hydrodynamical simulation (Dubois et al., 2014a), which employs RAMSES (Teyssier, 2002a), an adaptive mesh refinement (AMR) hydrodynamics code. The simulation is a cube with $L_{box} = 100\ h^{-1}$ comoving Mpc and uses WMAP7 ΛCDM initial conditions (Komatsu et al., 2011a). Horizon-AGN contains 1024^3 dark matter particles on an initial 1024^3 cell gas grid, which is refined using a quasi Lagrangian criterion, when 8 times the initial total matter resolution is reached in a cell. This refinement continues down to 1 kpc in proper units (which therefore sets the minimum cell size and the spatial resolution of the simulation). The simulation has a dark-matter (DM) mass resolution of 8×10^7 M$_\odot$, gas mass resolution of $\sim 10^7$M$_\odot$ and stellar mass resolution of 4×10^6 M$_\odot$. Unlike other simulations over similar volumes, such as EAGLE (Schaye et al., 2015), Horizon-AGN is only tuned to match the M$_{BM}$ - M$_*$ and M$_{BM}$ - σ_* relations at z=0. Therefore it is well suited to studying whether the assumed sub-grid physics is capable of producing the bulk properties of galaxies.

The `NewHorizon` cosmological, hydrodynamical simulation (Dubois et al., 2020), is a high-resolution simulation, produced using a zoom-in of a region of Horizon-AGN. For `NewHorizon`, the Horizon-AGN grid is resampled at higher resolution (using 4096^3 uniformly-distributed cubic cells), with the same cosmology as used in Horizon-AGN. The high-resolution volume occupied by `NewHorizon` is a sphere which has a radius of 10 comoving Mpc, centred on a region of average density within Horizon-AGN (see Figure 1.7 for the full dynamical range). `NewHorizon` has a DM mass resolution of 10^6 M$_\odot$, stellar mass resolution of 10^4 M$_\odot$ and a maximum spatial resolution of 34 pc [1]. The simulation has been performed down to $z = 0.25$.

Star particles in Horizon-AGN are formed using a standard 2% efficiency per free fall time (Kennicutt, 1998) in gas with density above the critical theshold of 0.1 H cm^{-3}. This star formation follows a Schmidt law and the assumed initial mass function (IMF) is Salpeter. Horizon-AGN includes prescriptions for both stellar and AGN feedback. Stellar feedback includes momentum, mechanical energy and metals from Type Ia/Type II supernovae (SNe), with the Type Ia SNe

---

[1]The gravitational force softening is equal to the local grid size.
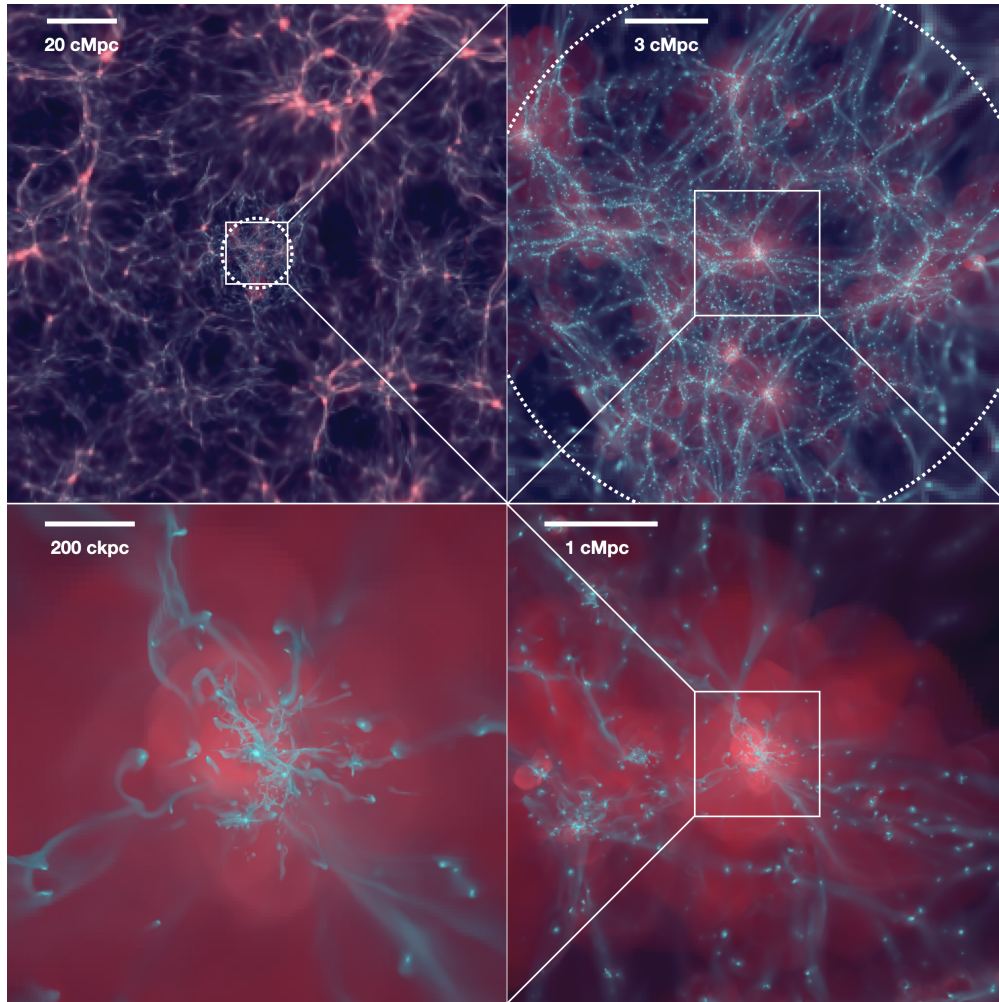
FIGURE 1.7: Sequential zoom (clockwise from top left) showing the dynamical range which is covered by `NewHorizon` (from Dubois et al. (2020)). The projected density (silver blue colors) and projected temperature (red) of the simulation are shown at redshift $z = 2$. The dashed white circles encompass the initial volume of `NewHorizon`, with the remainder being the volume of Horizon-AGN (and the low-resolution region in `NewHorizon`). Each panel is a zoomed-in version of the previous one (shown by the white square in the previous panel), the panel sizes are 142, 18, 4.4 and 1.1 comoving Mpc width respectively.

implemented following Matteucci and Greggio (1986), assuming a binary fraction of 5% (Matteucci and Recchi, 2001). Feedback from Type II SNe and stellar winds is implemented using STARBURST99 (Leitherer et al., 1999, 2010), via the Padova model (Girardi et al., 2000) with thermally pulsating asymptotic branch stars (Vassiliadis and Wood, 1993).

Compared to Horizon-AGN, star formation in `NewHorizon`, occurs at above a hundred times larger gas density, and a varying gravoturbulent-based star formation efficiency is used instead of assuming a constant 2% efficiency. Feedback from stars in `NewHorizon` only includes Type II SNe, and ignores stellar winds and Type Ia SNe. In addition, `NewHorizon` adopts a mechanical scheme for SNe instead of a kinetic solution (Dubois and Teyssier, 2008b). The assumed IMF is also changed to a Chabrier type, and thus the mass loss, energy, and yield are all increased.

Black holes (BHs) are implemented as 'sink' particles and form in dense star-forming regions, where the gas densities are above a critical threshold ρ_0, where $\rho_0 = 1.67 \times 10^{-25}$g cm^{-3} (equivalent to 0.1 H cm^{-3}), and the stellar velocity dispersion is larger than 100 kms^{-1}. Initial (seed) BH masses are 10^5M$_\odot$ and BH growth occurs either via gas accretion or via mergers with other BHs. This growth is tracked self-consistently, based on a modified Bondi accretion rate (Booth and Schaye, 2009), which is capped at Eddington. BHs impart feedback on ambient gas via two modes, depending on the accretion rate. For high Eddington ratios (> 0.01), 1.5 per cent of the energy is injected into the gas as thermal energy (a 'quasar' mode). For Eddington ratios that are less than 0.01, bipolar jets are used with velocities of 10^4 kms^{-1}, which constitutes a 'radio' mode with an efficiency of 10 per cent (Dubois et al., 2012, 2014a). These parameters are chosen to produce agreement with the local M$_{BH}$-M$_*$ and M$_{BH}$-σ_* relations (e.g. Häring and Rix, 2004), as well as the local cosmic BH mass density (Dubois et al., 2012; Volonteri et al., 2016).

Compared to Horizon-AGN, `NewHorizon`, now includes massive black hole (MBH) spin evolution, which affects several parts of MBH mass growth and feedback. The spins of these MBHs are evolved self-consistently through gas accretion in the quasar mode and coalescence of black hole binaries (Dubois et al., 2014b), which modifies the radiative efficiencies of the accretion flow (following the models of thin Shakura & Sunyaev accretion discs) and the corresponding Eddington accretion rate, mass-energy conversion, and bolometric luminosity of the quasar mode (Shakura and Sunyaev, 1973). The quasar mode imparts 15% of the bolometric luminosity as thermal energy into the surrounding gas. The radio mode employs a spin-dependent variable efficiency and spin up and spin down rates that follow the simulations of magnetically-choked accretion discs (see e.g. McKinney et al., 2012).

1.2.2   Comparison to observations

In order for these simulations to make predictions for observations, they need to be able to reproduce an array of observable quantities that trace the evolution of galaxies to ensure they are representative of real galaxy surveys (see Figure 1.8). For Horizon-AGN, Kaviraj et al. (2017) and Volonteri et al. (2016) found that the simulation successfully traced the evolution of stars and BHs in massive galaxies, e.g. the morphological mix of massive galaxies (M$_* > 10^{10.5}$ M$_\odot$) in the nearby Universe (Dubois et al., 2016), stellar mass/luminosity functions, rest-frame UV-to-near-infrared colours, the cosmic star formation history, the position of galaxies on the star formation main sequence (Kaviraj et al., 2017) and the demographics of BHs over cosmic time. However, a key tension exists at the low mass end of the mass function, where the simulation over-predicts the number of dwarf galaxies.
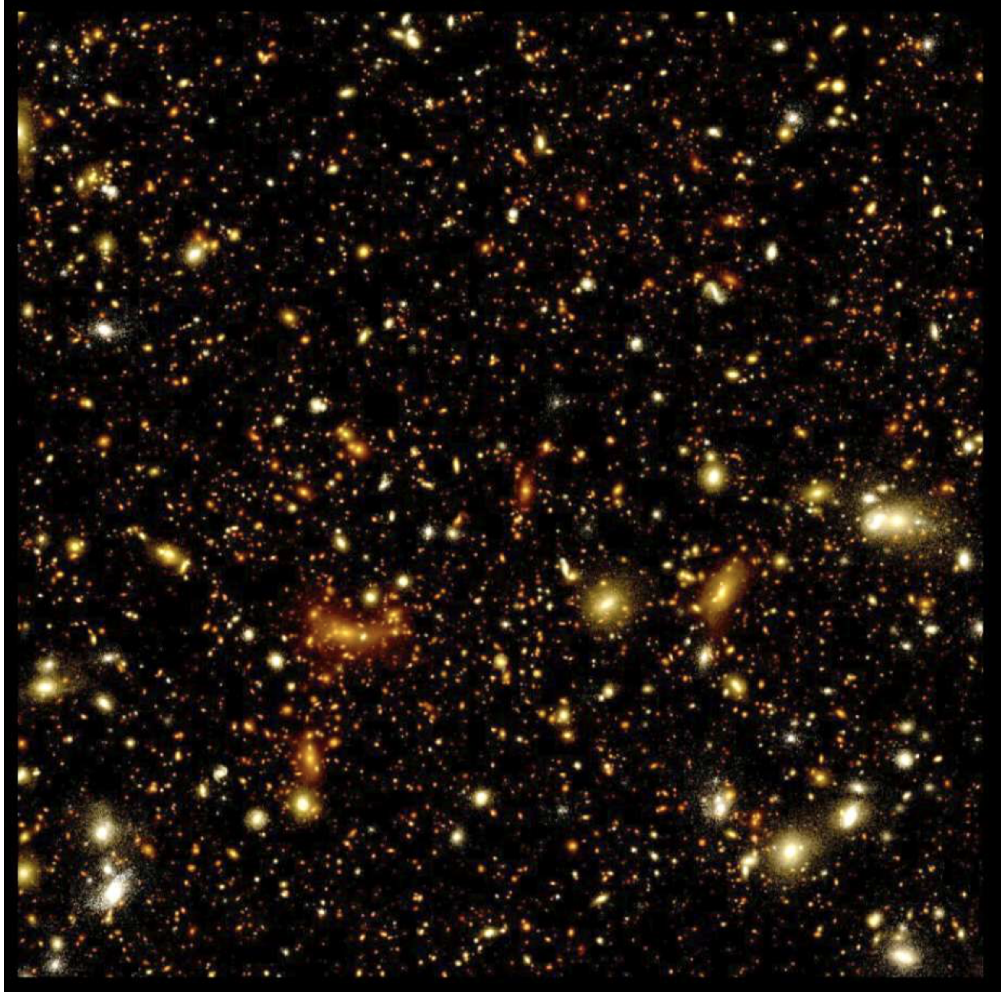
FIGURE 1.8: A 14 arcmin^2 composite image from the Horizon-AGN lightcone (Pichon et al., 2010), in the u, r and z filters (from Kaviraj et al. (2017)). The image is created using star particles between 0.1 < z < 5.8 and has a resolution of 0.15"/pixel.

Despite its smaller volume, `NewHorizon` is also successful at reproducing a broad number of galaxy properties (Dubois et al., 2020), as well as creating realistic looking galaxies on small scales, as shown in Figure 1.9. The cosmic SFR density, evolution of sSFR with stellar mass, Kennicutt-Schmidt relation, size-mass relation, Tully-Fisher relation and metallicities of stars and gas all agree reasonably well with observations. However, the same overproduction of dwarf galaxies is observed in the stellar mass function (see Figure 1.10). This is particularly noteworthy given the changes made to the implementation of SN feedback in `NewHorizon` from Horizon-AGN. This feature is something that will be examined in future work (see Chapter 8 for more details).
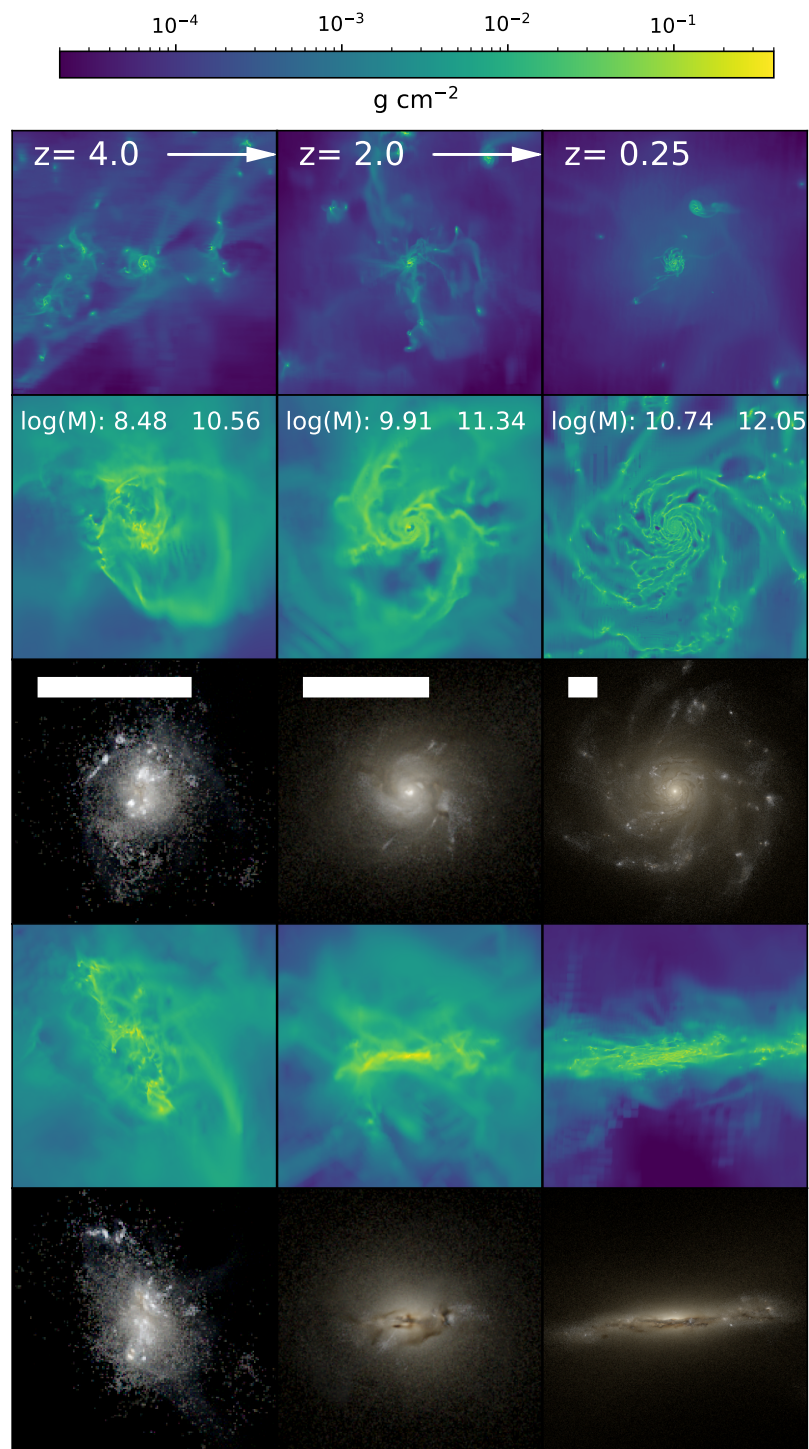
FIGURE 1.9: Projection of the gas density and mock observations of a massive galaxy in `NewHorizon` (from Dubois et al. (2020)). The first row shows gas density projections a of 1.4 Mpc at different epochs, the second and fourth rows are zoomed-in gas density projections with face-on and edge-on views of the galaxy, respectively. Third and fifth rows are mock images in face-on and edge-on direction, using the radiative transfer code SKIRT. The stellar mass and halo mass of the galaxy at each redshift is given in the second row. The white bar in third row indicates 5 kpc (comoving).
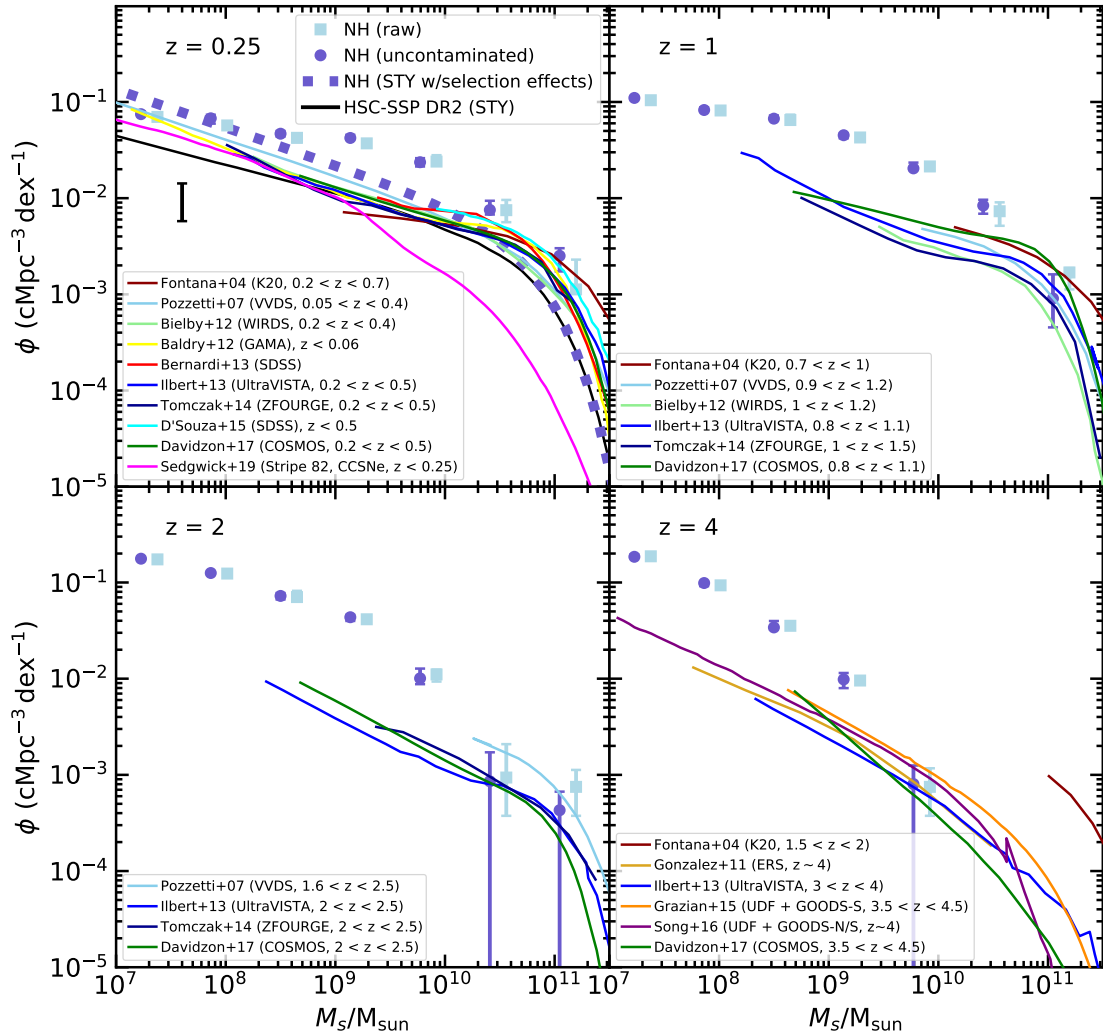
FIGURE 1.10: Galaxy stellar mass function at various redshifts in `NewHorizon` and the HSC-SSP survey (from Dubois et al. (2020)). Light blue squares indicate the mass function for all `NewHorizon` galaxies whereas purple circles indicate only uncontaminated galaxies. The HSC mass function (calculated from 100 random pointings from a volume of the HSC-SSP deep layer with the same volume as `NewHorizon`) is shown by the black line and the black error bar indicates the 90 percentile scatter in the mass function at the low-mass end. Additional mass functions from literature are also shown for comparison and are shown by the other coloured lines (Sedgwick et al., 2019b; Davidzon et al., 2017; Tomczak et al., 2016; Song et al., 2016; Grazian et al., 2015; D'Souza et al., 2015; Fontana et al., 2014; Bernardi et al., 2013; Ilbert et al., 2013; Baldry et al., 2012; Bielby et al., 2012; González et al., 2011; Pozzetti et al., 2007). Finally the thick purple dotted line indicates the `NewHorizon` mass function constructed using the Sandage et al. (1979) method ("STY"), this includes selection effects that would commonly affect the observed mass functions. The `NewHorizon` mass function lies in the upper range of the observational mass function at z=0.25, although it lies above at the low-mass end. At higher redshifts the discrepancy between the `NewHorizon` and observational mass functions become more apparent, especially at the low-mass end.

1.3   Overview

The aim of this thesis is to understand which processes drive galaxy evolution, across a range of stellar masses, to produce the diverse populations of galaxies that we see today. In order to do this the use of cosmological simulations, and comparisons to data, are invaluable as they allow us to trace the physical processes across cosmic time. This work focuses particularly on galaxy populations that appear to go against the generally accepted paradigm, and attempts to reconcile their existence with how we currently understand our Universe to work.

In Chapter 2 we examine a population of massive spheroid galaxies, with low ex-situ mass, in Horizon-AGN. Spheroids are believed to form primarily via major mergers, which would result in a significant ex-situ mass fraction, therefore a non-negligible population of spheroids with low ex-situ mass potentially challenges this paradigm. We use Horizon-AGN to track the formation of these galaxies, finding that their formation is the result of the orbital features of the minor merger that formed them.

In Chapter 3 we study the formation of extremely massive disc galaxies in Horizon-AGN. Beyond the knee of the mass function, galaxies are believed to primarily increase their stellar mass via mergers. As mergers generally destroy discs, the existence of galaxies with $M_\star > 10^{11.4} M_\odot$ that have a disc is not expected. We find that these galaxies constitute 11% of galaxies in this mass range and form via two distinct channels. We also provide some key observables so that these galaxies can be found in current and future observations.

Similarly in Chapter 4, we use data from SDSS, GALEX, DECaLS and ALFALFA to identify and compare extremely massive disc galaxies in observations to those in Horizon-AGN. We find that the observed properties of these observed massive discs, in terms of morphological fractions, SFRs and HI properties are in good agreement with the predictions from Horizon-AGN. This suggests that massive disc galaxies in the real Universe are likely to have been formed via the same mechanisms. Therefore, the existence of these galaxies, at least at the frequency found in this study, is not in conflict with the standard hierarchical paradigm and is expected in a ΛCDM Universe.

In Chapter 5 we look at the formation of low surface-brightness-galaxies in the dwarf regime using the `NewHorizon` simulation. These galaxies, which are defined as systems that are fainter than the surface-brightness limits of current wide area surveys, dominate the number density of galaxies at low mass ($M_\star < 10^9 M_\odot$). This has ramifications for galaxy evolution theories as it means that our understanding is predicated on a subset of bright galaxies that we can see with current instruments. In this study we examine how these galaxies form and evolve and the processes that dictate this evolution. As well as examining whether a galaxy's surface brightness at low redshift can be linked to its location in the cosmic web. Finally, we look at the

population of dwarf galaxies that are visible in today's wide-area surveys and show that they are not representative of the complete dwarf galaxy population.

In Chapter 6 we examine whether dark-matter-deficient galaxies, such as those found in van Dokkum et al. (2018a), can be formed in `NewHorizon`. These galaxies potentially challenge the ΛCDM paradigm, as dwarf galaxies are expected to be dark matter rich. These observed dwarf galaxies appear to have lower dark matter fractions than much more massive galaxies, with some being as low as unity. Such galaxies are wholly unexpected in the standard model of galaxy formation. We examine whether such galaxies exist in the `NewHorizon` simulation, which uses a ΛCDM cosmology. Where galaxies with anomalous dark matter fractions are formed, we examine whether the properties of such galaxies match with those predicted from observations, and examine the mechanisms for their formation.

In Chapter 7 we present a summary of the main conclusions to each of the studies in this thesis and attempt to set these conclusions in the wider field of astronomy. Finally in Chapter 8 we set out plans for future work.

Chapter 2

Massive spheroids can form in single minor mergers

2.1 Introduction

Understanding the processes that alter the morphological mix of the Universe and, in particular, drive the formation of spheroidal galaxies, is a key topic in galaxy evolution studies. Observations indicate that, while the massive galaxy population in the early Universe was dominated by objects with discy morphologies (Wuyts et al., 2011; Conselice et al., 2014; Buitrago et al., 2014; Shibuya et al., 2015), their counterparts in the local Universe are dominated by systems that are spheroidal in nature (Bernardi et al., 2003; Kaviraj, 2014b).

Morphological transformation, i.e. the conversion of rotationally-supported discs into slowly-rotating, dispersion-dominated spheroids, is believed to be triggered primarily by galaxy mergers (Toomre, 1977; Negroponte and White, 1983; Barnes, 1992b; Di Matteo et al., 2007; Conselice et al., 2009b; Oser et al., 2010; Dubois et al., 2016; Naab et al., 2014a; Rodriguez-Gomez et al., 2017; Welker et al., 2018; Martin et al., 2018). The past theoretical literature has often highlighted the important role of 'major' mergers (mass ratios greater than $\sim 1:3$), as potentially the primary driver of morphological transformation (Toomre, 1977; Negroponte and White, 1983; Solanes and Perea, 2015; Willett et al., 2015; Solanes et al., 2018). The strong gravitational torques generated by nearly equal mass-ratio mergers efficiently move material from rotational orbits into the random, chaotic ones that make up spheroidal systems. This appears to be generally true, except in cases where the progenitors are extremely gas-rich, in which case residual gas from the merger can rebuild a disc, resulting in a remnant that still shows significant rotation (e.g. Springel and Hernquist, 2005; Font et al., 2017; Martin et al., 2018a).

Observations lend general support to this picture. The evolution of the morphological mix of galaxies shows a gradual increase in the fraction of spheroids over cosmic time (e.g. Butcher and Oemler, 1984; Dressler et al., 1997; Conselice et al., 2014). Many spheroids show signatures of rapid change in their stellar populations (e.g. Blake et al., 2004; Bundy et al., 2005; Ferreras et al., 2009; Wong et al., 2012; Carpineti et al., 2012; Kaviraj, 2014b; Wild et al., 2016), and internal structure (e.g. Tacconi et al., 2008; McIntosh et al., 2008; Kaviraj et al., 2012a; Huertas-Company et al., 2015; Rodrigues et al., 2017), indicating a major merger in their recent history.

However, both theoretical and observational work in the recent literature (e.g. Zolotov et al., 2015; Fiacconi et al., 2015; Welker et al., 2017; Martin et al., 2017, 2018a) has highlighted the potentially important role of minor mergers (mass ratios less than $\sim 1 : 3$), which, by virtue of their higher frequency, may significantly influence the evolution of massive galaxies. For example, many massive spheroids that are in the process of forming at $z \sim 2$, the epoch at which the morphological mix of the Universe appears to change most rapidly (e.g. Conselice et al., 2014), do not show tidal features and extended halos that should be visible if they were forming via major mergers (e.g. Williams et al., 2014; Lofthouse et al., 2017). Indeed, recent studies have shown that (multiple) minor mergers are capable of re-distributing stellar orbits in galaxies and creating spheroidal, slowly rotating remnants (e.g. Bournaud et al., 2007; Qu et al., 2011; Taranu et al., 2013, 2015; Moody et al., 2014).

Minor mergers are capable of enhancing both star formation (e.g. Knapen et al., 2004; Ellison et al., 2008; Carpineti et al., 2012; Kaviraj, 2014b) and black-hole accretion rates (e.g. Kaviraj, 2014a; Pace and Salim, 2014) and, at low redshift, may account for more than half of the star formation budget in the Universe (Kaviraj, 2014a). Furthermore, the observed evolution in the sizes of massive (early-type) galaxies is also largely attributed to this process (e.g. Trujillo et al., 2006; Newman et al., 2012). A growing body of evidence therefore points towards minor merging being a significant driver of not only morphological transformation but also of the stellar mass buildup, black-hole growth and size evolution of massive galaxies.

Despite these examples, the impact of processes like minor mergers remains difficult to study observationally. This is because the surface-brightness of merger-driven tidal features scales with the mass ratio of the merger (e.g. Peirani et al., 2010; Kaviraj, 2010), and thus the efficient identification of minor mergers typically requires deeper imaging than that offered by current large-area surveys (e.g. van Dokkum, 2005; Duc et al., 2011; Kaviraj, 2014a; Kaviraj et al., 2019). Given this lack of survey depth, the effect of minor mergers on galaxy evolution remains relatively unexplored, although forthcoming instruments like LSST, EUCLID and JWST (e.g. Tyson, 2002; Robertson et al., 2017; Gardner et al., 2006; Laureijs et al., 2011) will enable the first truly statistical studies of minor-merger-driven galaxy evolution.

Much of our current understanding of the role of this process therefore continues to come from theoretical work e.g. from semi-analytical models (e.g. Somerville and Primack, 1999; Cole

et al., 2000; Benson et al., 2003; Bower et al., 2006; Croton et al., 2006) and, more recently, from cosmological hydro-dynamical simulations (e.g. Dubois et al., 2014a; Vogelsberger et al., 2014b; Schaye et al., 2015; Khandai et al., 2015; Taylor and Kobayashi, 2016; Kaviraj et al., 2017).

It is worth noting that exploring the role of various processes in driving morphological transformation ideally requires a simulation with a cosmological volume. While the past literature has often employed isolated and idealised simulations of galaxy mergers (e.g. Barnes, 1988; Hernquist and Spergel, 1992; Bois et al., 2011), such simulations exclude the broader effects of environment and gas accretion from the cosmic web. Furthermore, since the parameter space (e.g. orbital configurations, mass ratios etc.) explored by these studies is typically small, statistical conclusions about the importance of various processes that drive morphological change are difficult to draw. This can be particularly important for channels, like the one studied here, that are relatively rare.

The consensus view from simulations is that morphological transformation and the creation of spheroids can proceed via various channels and shows a complicated dependence on factors such as mass ratios, gas fractions, environments and orbital configurations (see the study by Martin et al. (2018) which quantifies these dependencies in detail). Here, we describe a channel for spheroid formation in which a *single* minor merger creates a massive ($M_* > 10^{11} \mathrm{M_\odot}$) spheroidal system. In this process, the satellites approach the more massive merging progenitor on a trajectory that is close to being co-planar to the plane of the massive disc. Notwithstanding the low mass ratios of many of these mergers, these events are able to trigger a catastrophic change in morphology over just a few hundred Myrs, coupled with an episode of strong in-situ star formation, that creates a slowly-rotating, massive spheroidal system from an otherwise typical disc galaxy.

This chapter is organised as follows. In Section 2.2, we briefly describe the Horizon-AGN simulation and how galaxies, mergers and morphologies are defined. In Section 2.3, we describe the properties of the spheroidal galaxies studied here and follow the evolution of their stellar and gas mass and morphology over cosmic time. In Section 2.4, we explore the properties of the progenitor systems (e.g. the gas fraction and clumpiness of the more massive galaxy and the orbital configuration of the merger) and investigate how such spheroids form via single minor-merger events. We summarise our findings in Section 2.5.

2.2 Horizon-AGN Simulation

In this study, we use the Horizon-AGN cosmological hydrodynamical simulation (Dubois et al., 2014a), which employs RAMSES (Teyssier, 2002a), an adaptive mesh refinement (AMR) hydrodynamics code. Horizon-AGN simulates a 100 h^{-1}coMpc^3 volume, with WMAP7 ΛCDM initial conditions (Komatsu et al., 2011a). The simulation contains 1024^3 dark matter particles on an initial 1024^3 cell gas grid. This is refined according to a quasi Lagrangian criterion, when 8 times the initial total matter resolution is reached in a cell. This refinement can continue until 1 kpc in proper units. Horizon-AGN has dark-matter and stellar-mass resolutions of 8×10^7 M$_\odot$ and 4×10^6 M$_\odot$ respectively.

The simulation includes prescriptions for feedback from both stars and AGN. Continuous stellar feedback is employed including momentum, mechanical energy and metals from stellar winds, Type Ia and Type II supernovae (SNe). Type Ia SNe are implemented following Matteucci and Greggio (1986), assuming a binary fraction of 5% (Matteucci and Recchi, 2001). Feedback from Type II SNe and stellar winds is implemented using STARBURST99 (Leitherer et al., 1999, 2010), which employs the Padova model (Girardi et al., 2000) with thermally pulsating asymptotic branch stars (Vassiliadis and Wood, 1993).

Black Holes (BHs) are implemented as 'sink' particles, with initial masses of 10^5M$_\odot$, and grow via gas accretion or coalescence with other BHs. When gas accretes onto a central BH it imparts feedback on ambient gas via two methods, depending on the accretion rate. When there is a high ratio of gas accretion to the Eddington rate (Eddington ratios of > 0.01), 1.5 per cent of the energy is injected into the gas as thermal energy (a 'quasar' mode). However, when Eddington ratios are less than 0.01, bipolar jets are employed with velocities of 10^4 km s^{-1}, which constitutes a 'radio' mode with an efficiency of 10 per cent. For more details of the baryonic recipes used in the simulation, we refer readers to Dubois et al. (2014a, 2016) and Kaviraj et al. (2017).

Horizon-AGN produces good agreement with an array of observational quantities that trace the aggregate growth of stars and BHs, particularly in massive galaxies. For example, in the stellar mass range $M_* > 10^{10.5}$M$_\odot$, it reproduces the morphological mix of the nearby Universe (Dubois et al., 2016; Martin et al., 2018a), the evolution of the stellar mass/luminosity functions, restframe UV-optical-near-infrared colours, the cosmic star formation history and the star formation main sequence (Kaviraj et al., 2017; Martin et al., 2017), galaxy merger rates at $z > 1$ (Kaviraj et al., 2015) and the evolving demographics of BHs over cosmic time (Volonteri et al., 2016). However, the simulation overproduces the number densities of very low-mass galaxies at low and intermediate redshift (which is typical of all simulations in this class of models). The rest-frame UV colours of galaxies in the red sequence are also typically too blue, indicating that feedback processes employed in the model do not suppress star formation completely in 'passive' galaxies. Note, however, that since the star formation rate density in the red sequence

is negligible compared to that in the blue cloud this does not affect the overall reproduction of galaxy properties.

2.2.1 Identifying galaxies and mergers

In each snapshot of the simulation galaxy catalogues are produced using the ADAPTAHOP structure finder (Aubert et al., 2004) applied to the star particles. Structures are selected when the local density, calculated for each particle using the nearest 20 neighbours, exceeds the average matter density by a factor of 178. A minimum of 50 particles is required for a structure to be identified, which imposes a minimum galaxy stellar mass of $\sim 2 \times 10^8 M_\odot$. Merger trees are produced for each galaxy from $z = 0.06$ to $z = 3$, with a typical spacing between time steps of ~ 130 Myr, using the method described in Tweed et al. (2009).

2.2.2 Morphologies

Following Martin et al. (2018), we define galaxy morphology using stellar kinematics, specifically V/σ, which is the ratio between the mean rotational velocity (V) and the mean velocity dispersion (σ). Galaxies with higher values of V/σ are rotationally-supported i.e. disc galaxies, while those with lower V/σ values are pressure-supported spheroidal systems.

In order to obtain V/σ, the coordinate system is rotated so that the z-axis is oriented along the stellar angular-momentum vector. V is then defined as V_θ, the mean tangential velocity component in cylindrical co-ordinates. The velocity dispersion (σ) is calculated by taking the standard deviations of the radial (σ_r), tangential (σ_θ) and vertical star particle velocities (σ_z) and summing them in quadrature. V/σ is then defined as:

$$\frac{V}{\sigma} = \frac{\sqrt{3}\bar{V}_\theta}{\sqrt{\sigma_r^2 + \sigma_z^2 + \sigma_\theta^2}} \tag{2.1}$$

As described in Martin et al. (2018), galaxies are separated morphologically by considering a range of values for V/σ and comparing how the corresponding predicted early-type fractions compare to local observations (Conselice, 2006). The value of V/σ which produces the best agreement with the observed morphological mix of the Universe is then used to separate early- and late-type galaxies. This V/σ threshold is 0.55 (see Figure 1 in Martin et al., 2018) i.e. galaxies with $V/\sigma > 0.55$ are considered to be discs, while those with $V/\sigma < 0.55$ are spheroids. Note that the systems we study in this chapter have V/σ values that are significantly lower than 0.55 i.e. these galaxies are firmly in the spheroid regime. We note that the highest V/σ in Horizon-AGN is 2.11, which is lower than observed values. This is because the spatial resolution results in the bulge components of discs being slightly too massive.
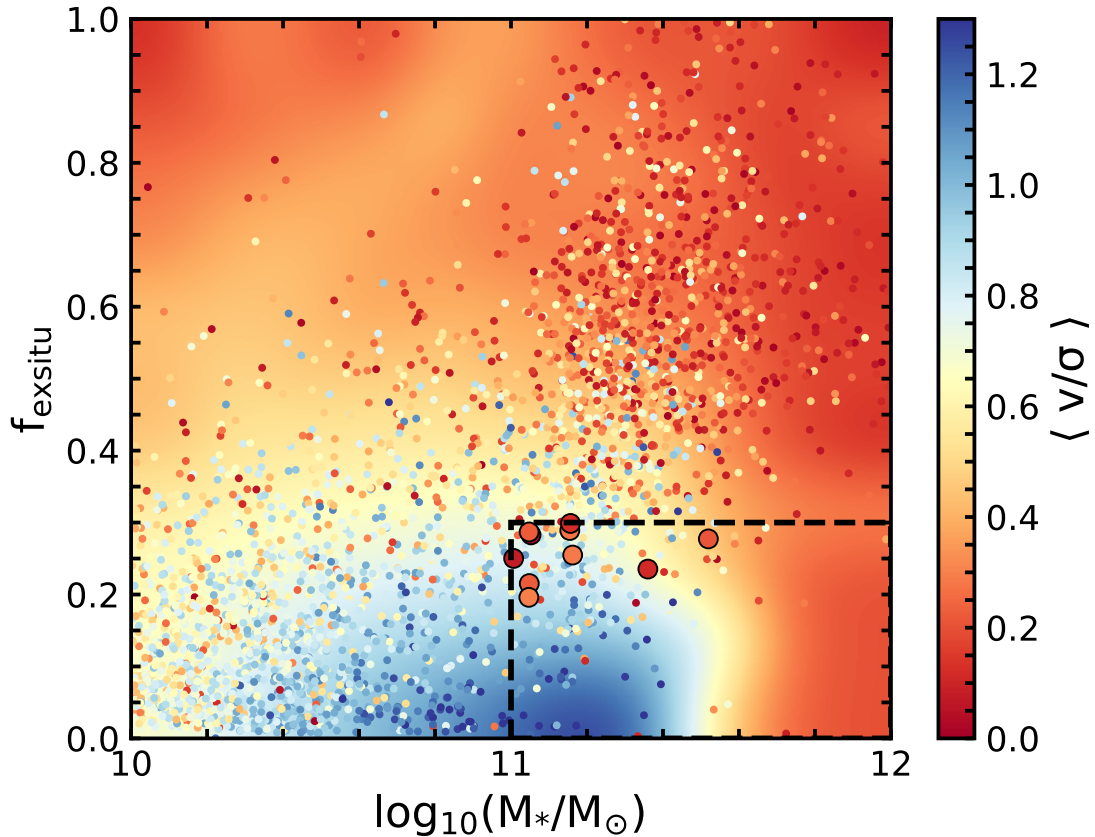
FIGURE 2.1: 2D histogram showing the fraction of ex-situ mass vs stellar mass of galaxies in the Horizon-AGN simulation at $z = 0.06$. The individual points show a random selection of galaxies and the background colour is derived using a cubic spline interpolation over all galaxies. The colour coding indicates the value of V/σ of both the background and the individual points. Massive spheroids typically exhibit large fractions of ex-situ stellar mass. The spheroids in this study have $V/\sigma < 0.3$, $f_{exsitu} < 0.3$ and stellar mass $> 10^{11} M_\odot$, and are shown using the large outlined points in the bottom right-hand corner of the plot. Note that we do not consider objects that may have $V/\sigma < 0.3$ but are in ongoing mergers, as the V/σ values of such objects are highly transient and the morphology of the remnant is uncertain.

2.3 Spheroidal galaxies with low ex-situ mass fractions

2.3.1 Sample selection and properties of the galaxies

In a recent study Martin et al. (2018a) have used Horizon-AGN to perform a detailed study of how mergers drive the change in the morphological mix of the Universe over cosmic time. Not unexpectedly, spheroidal galaxies, particularly those more massive than the knee of the galaxy mass function ($M_* > 10^{11} M_\odot$), typically have rich merger histories. As a result, they usually exhibit very high ex-situ mass fractions. Ex-situ mass is defined as stellar mass that is directly accreted from external objects, rather than having been formed in-situ in the main (i.e. most massive) branch of the merger tree of the galaxy in question (Martin et al., 2018a). Therefore, gas accreted from another galaxy, but converted into stars in the main galaxy, would not count as

1	2	3	4	5	6	7	8	9	10	11
ID	M_*	M_*/M_i	V/σ	R_e	μ_e^r	Density	f_{exsitu}	Merger z	Merger mass	Rel. ϕ_{max}
	$(10^{11}M_\odot)$			(kpc)	(mag arcsec^{-2})	perc.			ratio	
1841	2.28	1.97	0.12	10.39	21.08	0.30	0.24	0.4	0.15	63.7
5119	1.42	1.51	0.28	12.28	22.43	0.26	0.29	0.95	0.11	20.52
1078	1.33	6.33	0.10	10.87	21.55	0.82	0.29	2.45	0.33	27.22
1956	1.45	3.63	0.27	12.43	22.22	0.75	0.25	1.3	0.17	37.02
8233	1.11	1.54	0.24	7.66	21.57	0.53	0.21	0.3	0.24	18.51
9675	1.01	1.77	0.07	9.26	21.69	0.10	0.25	0.6	0.17	9.75
18163	1.11	1.71	0.30	7.34	20.60	0.17	0.20	0.25	0.20	8.16
3341	1.13	3.55	0.03	11.53	22.83	0.77	0.28	2.1	0.15	9.12
184	3.36	2.85	0.16	10.07	19.75	0.92	0.28	0.9	0.27	31.38
952	1.13	2.69	0.23	8.98	21.95	0.04	0.29	0.4	0.20	32.82

TABLE 2.1: Properties of the spheroids studied in this chapter (cols 1-8) and properties of the mergers that create them (cols 9-11). Columns are as follows: (1) Galaxy ID (2) Stellar mass in units of $10^{11}M_\odot$ (3) Ratio of stellar mass of the spheroid to the mass of the progenitors before the merger (4) V/σ (recall that the boundary between discs and spheroids is $V/\sigma \sim 0.55$) (5) Effective radius (R_e) in kpc (6) Effective surface brightness (i.e. the average r-band surface-brightness within R_e) (7) Local environment, expressed in terms of the percentile in local density (values greater than 0.9 indicate cluster environments, values in the range 0.4 - 0.9 indicate groups and values below 0.4 indicate the field) (8) The fraction of ex-situ stellar mass (9) Redshift of the merger (10) Stellar mass ratio of the merger and (11) Ratio of the maximum star-formation rate in the merger remnant during the phase where the morphological transformation is fastest (shown by the grey regions in Figure 2.3) and the average value of the observational star formation main sequence, for $M_* = 10^{11}M_\odot$, at the redshift of the merger that creates these spheroids.

ex-situ mass. Figure 2.1 shows a 2-D histogram of galaxies in Horizon-AGN at the last snapshot ($z = 0.06$), with the ex-situ stellar mass fraction plotted against stellar mass. Points indicate individual galaxies, while colours indicate their V/σ ratios.

While most massive spheroids show high ex-situ mass fractions, there exists a small, 'anomalous' population of spheroidal systems with unusually low ex-situ mass fractions (<0.3), that are more typical of discs. These objects are the focus of this study. We select galaxies that (1) have stellar masses greater than $10^{11}M_\odot$, which puts them beyond the knee of the galaxy mass function (see e.g. Kaviraj et al., 2017) where major mergers have classically been thought to be essential for building up galaxy mass (e.g. Bell et al., 2004; Bundy et al., 2006; Faber et al., 2007), (2) exhibit $V/\sigma < 0.3$ i.e. are firmly in the spheroid regime and (3) have very low ex-situ mass fractions ($f_{exsitu} < 0.3$) at the final timestep of the simulation. The f_{exsitu} threshold is not arbitrary but chosen at the approximate mass-ratio demarcation between major and minor mergers ($\sim 1:3$), making it unlikely that these galaxies have undergone major mergers. As we show below, while they have not undergone major interactions, these systems are the products of single minor mergers with a specific set of properties. Note that simulated galaxies in this mass regime have very complete merger histories. For example, the merger histories of galaxies with $M_* > 10^{11}M_\odot$ are close to 90 per cent complete for mass ratios greater than $\sim 1:10$ out to $z \sim 3$, and almost 100 per cent complete out to $z \sim 1$ (see Figure 1 in Martin et al., 2018a).
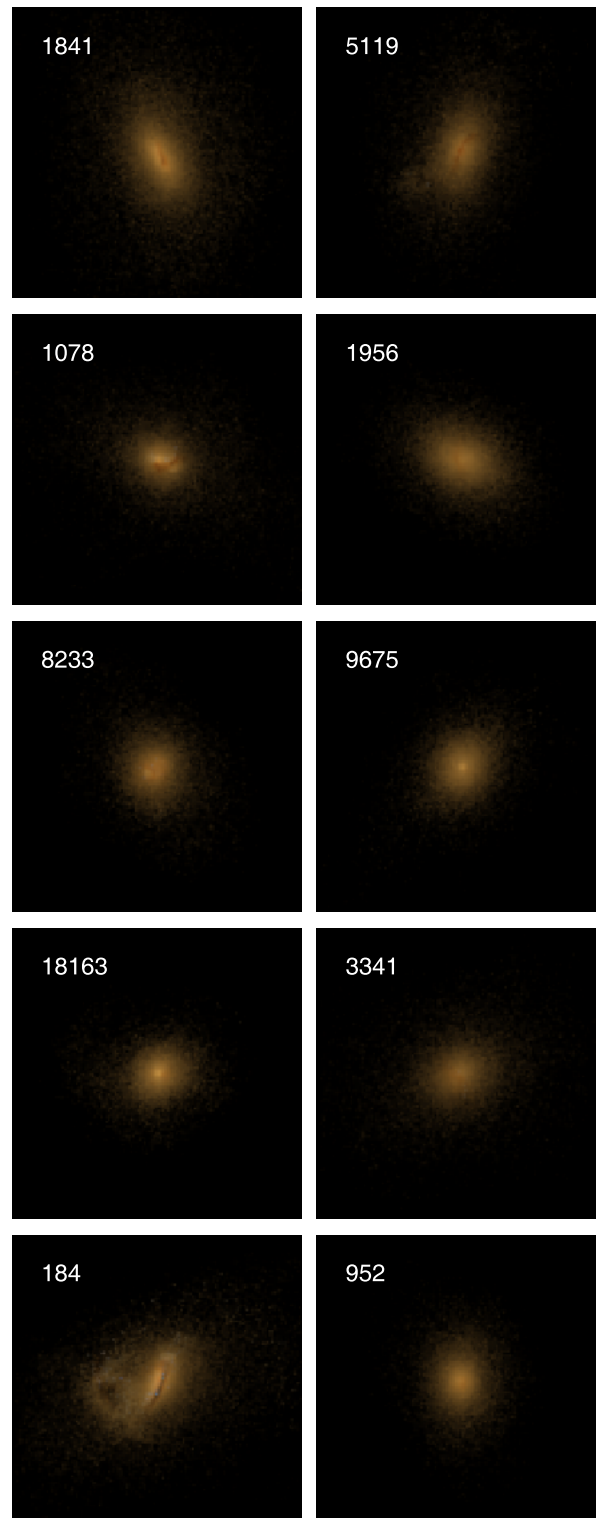
FIGURE 2.2: Mock *gri* images of the spheroids studied in this chapter. The ID of each galaxy (same as in the tables) is shown in the panels. The procedure for constructing the images is described in Section 3.1. The angular resolution of the images is 1.05 arcsec/pixel.

Our initial selection yields 20 galaxies, half of which exhibit, on visual inspection of their images, strong morphological disturbances (i.e. are in ongoing mergers). As the V/σ of merging objects can be extremely spurious (Martin et al., 2018a), the final values of V/σ for these systems are uncertain. We also examine visual morphology from these images to confirm that these galaxies are spheroids, therefore not relying on V/σ alone. Thus, we study only the 10 systems (indicated by the large points in Figure 2.1) that are morphologically settled spheroids. This represents ∼ 5 per cent of spheroids ($V/\sigma < 0.55$) that have $M_* > 10^{11} M_\odot$.

Figure 2.2 shows mock *gri* images of these galaxies (note the clearly spheroidal morphologies). To produce these images we use the Bruzual and Charlot (2003) stellar population synthesis models, with a Chabrier (2003) initial mass function, to calculate intrinsic spectral energy distributions (SEDs) of the constituent star particles within each galaxy. Dust-attenuated SEDs are then calculated using the SUNSET code, as described in Kaviraj et al. (2017), with line-of-sight optical depths calculated assuming a dust-to-metal ratio of 0.4 (e.g. Draine and Li, 2007). The attenuated SEDs of star particles are then convolved with the SDSS g, r and i band filter response curves to produce mock images of each galaxy. The images include a Gaussian point spread function with 1.2 arcsecond FWHM, but do not include a background or shot noise.

This population of galaxies consists of extremely massive, slowly-rotating spheroids in the local Universe that have formed without recourse to a significant amount of merging, since only a small fraction of their stellar mass has been directly accreted from external sources. It is worth noting that the cuts in V/σ and f_{exsitu} made here are conservative i.e. we intentionally select very low values of V/σ and f_{exsitu} in order to cleanly isolate systems that have virtually no mergers in their assembly histories, yet are both massive and spheroidal. It could be reasonably expected, however, that the processes that drive the formation of these spheroids may also play some role in the creation of spheroids which have higher (i.e. more typical) values of V/σ and f_{exsitu}.

In Table 2.1, we summarise key properties of these spheroids: the stellar mass today, the fractional increase in stellar mass after the merger that creates these systems, the V/σ, effective radius, effective surface-brightnesses in the r-band[1], the local environment at the present day and the peak star formation rate (SFR) as a fraction of the average SFR of an equal mass galaxy at the redshift of the merger ('Rel. ϕ_{max}').

Following Martin et al. (2018), we estimate local environment by ranking each galaxy by its local number density, which is calculated using an adaptive kernel density estimation method (Breiman et al., 1977). Galaxies are then sorted into percentiles of density, so that galaxies in the 0-40th percentile range inhabit environments that roughly correspond to the 'field', those in the 40-90th percentile range inhabit 'groups' and those in the 90-100th percentile range inhabit environments typical of 'clusters'. We refer readers to Martin et al. (2018) for more details of this procedure. Rel. ϕ_{max} is calculated by dividing the maximum spheroid SFR by the average

---

[1]The effective surface brightness is defined as the mean surface brightness within an effective radius.

value of the observational star-formation main sequence for $M_* = 10^{11} M_\odot$ at the redshift of the merger that creates these spheroids. The star-formation main sequences are taken from Lee et al. (2015) ($0.3 < z < 1.2$), Karim et al. (2011) ($0.3 < z < 2.5$), Whitaker et al. (2012) ($0.3 < z < 2.5$) and Tasca et al. (2015) ($2.5 < z < 5.0$).

Table 2.1 shows that the current mass of the spheroids is several factors ($\times 1.5$ - 6.3) larger than the mass of their progenitor systems. The effective radii (R_e) are typically larger than the typical value of R_e for spheroids of such masses in the present-day Universe (~4 kpc; Bernardi et al. (2010)) and the effective surface-brightnesses of these objects are somewhat fainter than that of typical massive spheroids (~18 mag arcsec^{-2}, e.g. Blanton et al., 2005; Driver et al., 2005). Indeed, the effective surface-brightness of some of these systems is close to the surface-brightness limit of current large surveys like the SDSS (~23 mag arcsec^{-2}, e.g. Kniazev et al. (2004)). The local environments of our spheroids span the full range of density percentiles, from systems that are in the field to one object which is in a cluster. These events are, therefore, not strongly correlated with a particular type of local environment. Finally, the SFRs of these spheroids show significant enhancements above the average SFR of similar-mass galaxies at the redshifts of their mergers.

2.3.2 Creation in single minor mergers

Table 2.1 also summarises the properties of the mergers that create the spheroids in this study. The redshifts of these events do not show a preference for a particular epoch. The mass ratios indicate that the events are minor mergers, albeit with a wide range of values, ranging from events that are close to being major mergers (mass ratios close to ~1:3) to those where the mass ratios are as low as ~1:10. It is worth noting that many of these spheroids exhibit prominent dust lanes (see Figure 2.2) which are considered to be signposts of recent minor mergers (see e.g. Kaviraj et al., 2012a).

We proceed by exploring the evolution of the properties of the more massive galaxy (stellar mass, ex-situ stellar mass, gas mass, effective radius and V/σ) in the minor mergers that create these spheroids. We follow these properties between $z = 0.06$ and $z = 3$ and focus on changes in these characteristics before and after the minor-merger event in question. Note that, in all cases, the massive galaxy in these mergers is firmly in the disc regime *before* the merger takes place.

In Figure 2.3 we show the evolution of these properties for two galaxies, in order to illustrate the process (the evolution is similar for other spheroids in our sample). In each panel, we highlight in grey the redshift at which the merger occurs. The left-hand panels show the evolution in V/σ. After the event the galaxies undergo a catastrophic decrease in V/σ which can drop from the disc regime $V/\sigma > 0.55$ well into the spheroid regime within only a few hundred Myrs (which represents only a few dynamical timescales). The V/σ ratio does not recover after the
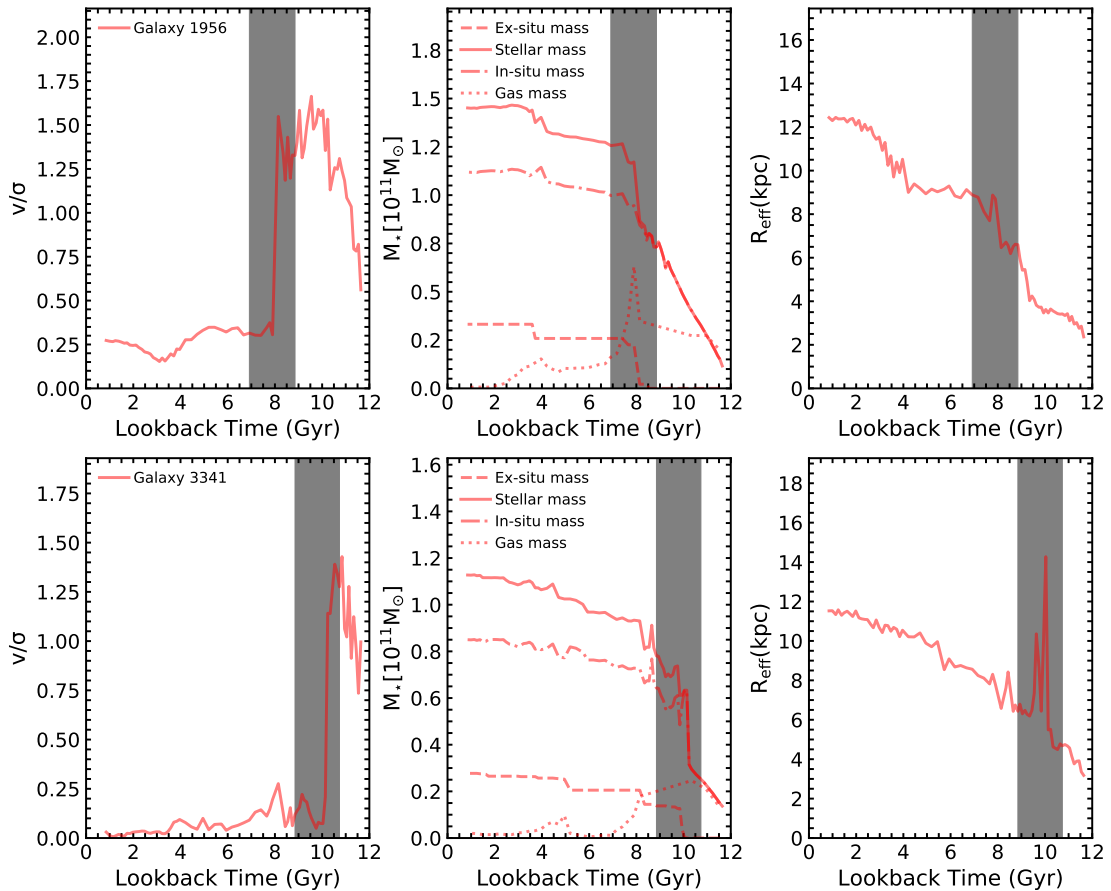
FIGURE 2.3: The evolution of the properties of the progenitor system of the spheroids in this study. The top and bottom rows show the evolution of two typical galaxies in our sample. The grey region indicates the epoch at which the merger event takes place. Left: Evolution in V/σ of the more massive galaxy. Middle: Change in the stellar mass (solid), ex-situ (i.e accreted) mass (dashed), in-situ mass (dashed-dotted) and gas mass (dotted) of the more massive galaxy. The near-step change in the ex-situ mass around the time of the merger indicates the stellar mass brought in by the accreted satellite. Right: Change in the effective radius of the more massive galaxy. In all cases, the merger results in a catastrophic (and permanent) decrease in V/σ, followed by a period of significant star formation and an increase in the effective radius of the galaxy.

merger, indicating that a disc does not reform after the event. We note that, while some of these spheroids do undergo further mergers (typically events with very low mass ratios), the creation of the dispersion-dominated system takes place in a *single* minor-merger event. An analysis of the angular momentum budget indicates that the angular momentum lost by the stars during these mergers is largely transferred to the dark matter halo.

The rapid formation of these spheroids is in contrast to the average morphological change of the general massive spheroid population (Figure 11 in Martin et al., 2018a), in which the mean V/σ changes from the disc regime to values close to 0.3 over Hubble time (note, however, that this is not the same as the average change in V/σ in individual typical spheroids where the morphological change can be bursty and changes fastest during merger events). For the spheroids in this study, a similar change in V/σ is achieved within only a few hundred Myrs.

1	2	3	4
ID	M$_*$ (10^{11}M$_\odot$)	Rel. f$_{gas}$	Rel. clumpiness
1841	1.16	1.15±0.13	0.79±0.05
5119	0.94	0.99±0.15	1.17±0.08
1078	0.21	0.89±0.36	0.84±0.06
1956	0.40	1.19±0.27	1.55±0.11
8233	0.72	1.23±0.17	1.61±0.11
9675	0.57	1.53±0.26	1.65±0.12
18163	0.63	1.20±0.16	2.06±0.15
3341	0.23	1.08±0.39	1.22±0.23
184	1.01	1.42±0.20	0.74±0.05
952	0.42	1.47±0.31	0.62±0.04

TABLE 2.2: Properties of the more massive progenitor of the spheroids studied in this chapter. Columns: (1) Galaxy ID, (2) Stellar mass in units of 10^{11}M$_\odot$, (3), (4) Gas fraction and stellar clumpiness respectively, relative to the mean of a control sample at the merger redshift.
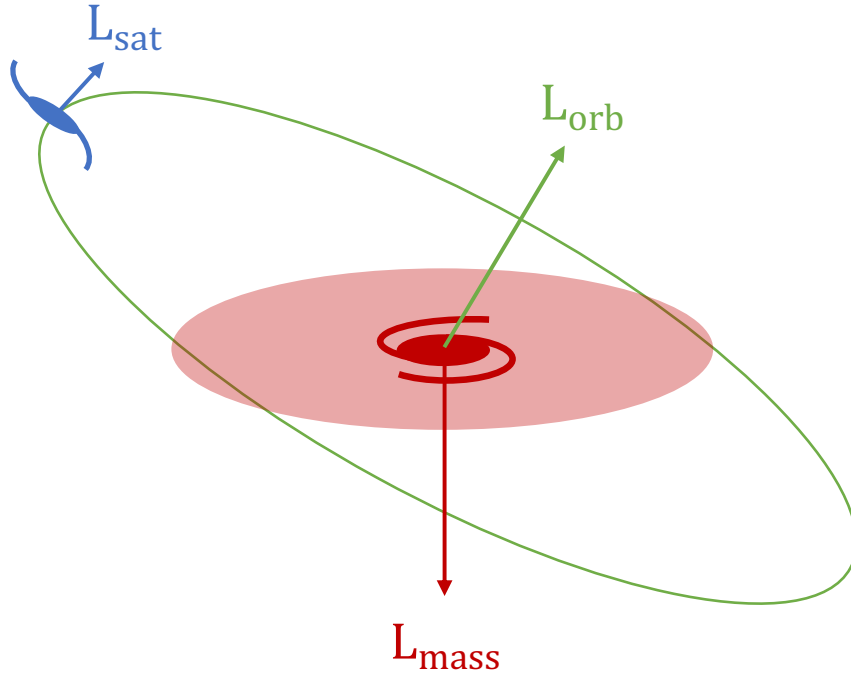
FIGURE 2.4: Diagram indicating the vectors used to describe the orbital configuration of the mergers. The angles between vectors are defined in the standard way, in the common plane containing both vectors.

The middle panels show the change in the stellar mass of the galaxy (solid line), the ex-situ i.e. accreted stellar mass (dashed line) and the gas mass of the system (dotted line). The step change in the ex-situ mass (dashed line) around the time of the merger indicates the stellar mass brought in by the accreted satellite. The galaxies undergo strong stellar mass growth during

the merger, with high star-formation rates (demonstrated by the steep gradient of the solid line), a corresponding decrease in the gas mass as it is consumed as the merger progresses, and an increase in the effective radius (right-hand panels). In many cases the gas mass increases prior to the star formation event, due to gas brought into the system by the satellite. It is worth noting that these merger remnants do not undergo compaction, akin to minor-merger-driven disc instabilities that are expected to take place in the gas-rich high redshift Universe (Dekel and Burkert, 2014; Zolotov et al., 2015; van Dokkum et al., 2015b) Instead, they continue to grow in stellar mass and size after the merger.

2.4   Properties of the progenitor system

We proceed by exploring why these minor mergers have such a profound and unusual impact on the morphology of the remnant, by studying properties of the progenitor system that are likely to contribute to the observed evolution of the morphology, stellar mass and effective radius of the remnant. It is important to study the progenitors of these systems to see if these galaxies are predisposed in some way to be disproportionately effected by minor mergers. We focus on three characteristics: the gas fraction and clumpiness of the more massive progenitor and the orbital configuration of the merging galaxies.

Disks in the early Universe ($z > 2$) can be gas-rich and clumpy and more susceptible to gravitational instabilities that can be triggered by events such as minor mergers (e.g. Swinbank et al., 2012; Zolotov et al., 2015; Saha and Cortesi, 2018). Even though the redshifts of the mergers that create our spheroids are typically much lower than the epoch of such gas-rich disks, it is worth considering whether the more massive progenitors may be anomalously gas-rich and/or clumpy, compared to control samples at similar redshifts. Note that we have also examined whether the merging satellites have properties that diverge from other galaxies of similar stellar masses at the merger redshifts in question, but find that they are not anomalous. In any case, given the typically low mass ratios of these events, the properties of the spheroidal remnants are driven more by those of the more massive progenitors, which are, therefore, more pertinent to our analysis.

In a similar vein, the outcome of a merger can be dependent on the orbital configuration of the progenitor system (e.g. Naab and Burkert, 2003; Chilingarian et al., 2010; Solanes and Perea, 2015; Martin et al., 2018a). It is, therefore, worth exploring whether the progenitors of these spheroids show a pattern in their relative trajectories that may explain the properties of their remnants.

2.4.1   Gas fraction and clumpiness of the more massive progenitor

We begin by comparing the gas fraction and clumpiness of the more massive progenitor, at the timestep before the merger, to a control sample of 200 randomly selected disc galaxies at the same redshift which have stellar masses within 10 per cent of the galaxy in question. The gas fraction is defined as:

$$f_{gas} = \frac{M_{gas}}{M_\star + M_{gas}}, \tag{2.2}$$

where M_{gas} and $M_\star$ are the total gas and stellar masses in the progenitor system respectively. Column 3 in Table 2.2 shows the ratio of the gas fractions in the more massive progenitors just before the merger to those in the control samples. For many systems these ratios are actually lower than the median values for similar disc galaxies at the same redshift, while for the others the ratios are less than ∼1.5. Compared to galaxies at intermediate redshift (where most of our spheroids form), gas fractions in the gas-rich early Universe are expected to be almost an order of magnitude larger (see Figure 4 in Martin et al., 2018a), indicating that, on the whole, the more massive progenitors in these mergers are not anomalously gas-rich.

We proceed by comparing the clumpiness of the more massive progenitor to the control samples[2]. Since we are interested in the *relative* clumpiness, compared to that of other galaxies at the same redshift, we simply use the star-particle distributions for this exercise. To measure the clumpiness in the stars we follow Conselice (2003) and Hambleton et al. (2011). We first apply a Gaussian filter with a standard deviation of $0.3 \times r_{20}$, where r_{20} is the radius that contains 20 per cent of the galaxy's stellar mass surface density (Conselice, 2003), and then subtract the original image from the smoothed one, which leaves the high-frequency structure as a residual. The absolute signal in this residual image is then summed and divided by the sum of that in the original image to yield a value for the clumpiness.

We study the ratio of the clumpiness of the more massive progenitors to control samples at the redshift of the merger. Column 4 in Table 2.2 shows that many of the progenitor systems are substantially *less* clumpy than their control samples and that the clumpiness of the more massive progenitors is within 46 per cent of the mean values of the control samples in all cases. On the whole, the ratios do not indicate that the more massive progenitors of our spheroids have anomalously high values of clumpiness.

Hence, the progenitor systems do not appear to be atypical, either in terms of their gas fractions or their clumpiness. These properties are, therefore, unlikely to be the key factors behind the rapid morphological transformation observed in these mergers. This is in contrast to the galaxies

---

[2]Note that, given the spatial resolution of the simulation, we are largely exploring kpc-scale clumps (Elmegreen et al., 2013; Cava et al., 2018) in this exercise.

studied in Chapter 3 which, despite having similarly low ex-situ mass fractions, have much higher gas fractions than spheroids of comparable mass. The evolution of the morphology of these galaxies is very different and is studied in detail.

2.4.2   Orbital configurations

We proceed by investigating whether the merger progenitors may have a specific orbital configuration which plays a role in the observed properties of the remnant. The orbital configurations are calculated at the closest timestep before coalescence. Figure 2.4 describes the vectors used to quantify the orbital configuration of the mergers. We study two key aspects of the orbital configuration: the angle between the spin (i.e. angular momentum) vectors of the two merging galaxies (i.e. whether the merger is prograde or retrograde) and the angle between the angular momentum vector of the satellite orbit and the spin of the more massive galaxy.

The top panel of Figure 2.5 shows the alignment of the spin vectors, defined using the star particles, of the two galaxies. Positive values of $\cos(\theta)$ indicate mergers where the spin vectors of the discs of the two galaxies point in the same direction. Negative values of $\cos(\theta)$ indicate mergers where the spin vectors of the discs of the two galaxies do not point in the same direction. The red dotted line indicates the distribution from a control sample (constructed as described in Section 2.4.1 above). As might be expected, neither the control sample nor the progenitors of our spheroids show any preference for aligned or misaligned spin mergers. The relative spins of the two merging galaxies are therefore not the principal cause of the properties of the remnant.

Finally, we study the orientation of the orbit of the satellite relative to the disc of the more massive galaxy. We first measure the angular momentum vector of the satellite orbit, defined as $L_{orbit} = M_{sat}.(r \times v)$, where v and r are the velocity and position vectors of the satellite with respect to the massive galaxy respectively, and then calculate the angle between L_{orbit} and the spin vector of the massive progenitor. Thus, a value of 0 for $\cos\theta$ represents a satellite whose orbit is exactly perpendicular to the disc of the more massive progenitor. A value of 1 indicates that the satellite orbit is exactly co-planar with the plane of the disc of the more massive progenitor and prograde with its spin, while a value of -1 indicates that the satellite orbit is co-planar with the plane of the disc of the more massive progenitor, but retrograde with its spin.

We find that, unlike the control sample which exhibits a flat distribution in orbital configurations (although it shows a slight, expected tendency towards prograde co-planar orbits, as satellites in the inner parts of halos tend to align with the central galactic plane, see Welker et al. (2018)), the progenitors of our spheroids strongly favour satellite trajectories that are close to co-planar with the disc of the more massive progenitor (regardless of whether the mergers are prograde or retrograde). Such trajectories are likely to be those that are able to deliver the orbital energy of the satellite into the disc of the more massive progenitor in the most efficient manner (e.g. Cox

et al., 2008), which likely enables even a small satellite (recall that the lowest mass ratio in the progenitors of our spheroids is 0.11) to quickly destroy the disc of the massive progenitor and create a dispersion-dominated system.

In Figure 2.6, we combine the information in the two histograms from Figure 2.5 by plotting the angles between the spin vectors of the two galaxies against the angle between the satellite orbit and the spin of the massive galaxy. Our systems show no preference for either the relative spins of the two galaxies to be aligned or the satellite orbit to be prograde or retrograde. In addition, there appears to be no correlation between these two quantities. These mergers therefore occur in all combinations of spin and orbit alignment, with the only common feature being that they are co-planar.

Since our galaxy sample is relatively small, we briefly check whether a broad similar trend remains if we relax the mass threshold of the analysis. As we show in the Appendix, studying the orbital configurations of similar (i.e. low f_{exsitu}) spheroids with a mass cut of $10^{10.5} M_\odot$ shows the same general tendency towards co-planar orbits, indicating that the result for our $M_* > 10^{11} M_\odot$ does not occur by chance. Note, however, that we perform this exercise only as a sanity check on our results; lower mass galaxies can naturally end up with a large in-situ stellar mass fraction via early gas accretion and not due to a peculiarity in their merger histories (Martin et al., 2018a), as a result of which the deficit of non-planar orbits in Figure A.1 is not as severe for lower masses, even though they have low f_{exsitu}. Our focus therefore remains on the most massive galaxies ($M_* > 10^{11} M_\odot$), beyond the knee of the mass function, where low f_{exsitu} is particularly anomalous.

Finally, it is also interesting to consider whether a disc could survive a co-planar orbital configuration similar to the ones that produce our population of spheroids. We find that there are some discs which have similar stellar masses as the spheroids in our study which undergo coplanar mergers but maintain their discy morphology. These systems overwhelmingly prefer *prograde* minor mergers. In addition, the mergers have higher gas fractions (×1.7 the control sample compared to ×1.1 for the spheroids) and lower mass ratios (median mass ratio of 0.12 compared to 0.2 for the spheroids). The survival of the disc is therefore due to a combination of a low mass ratio merger which is relatively gas-rich and has a prograde configuration. This disc population will be studied in detail in 3.

2.5 Summary

The most massive galaxies ($M_* > 10^{11} M_\odot$), regardless of morphology, typically exhibit rich merger histories, which results in high fractions of 'ex-situ' stellar mass i.e. mass accreted directly from external objects rather than having been formed in-situ. This is particularly true
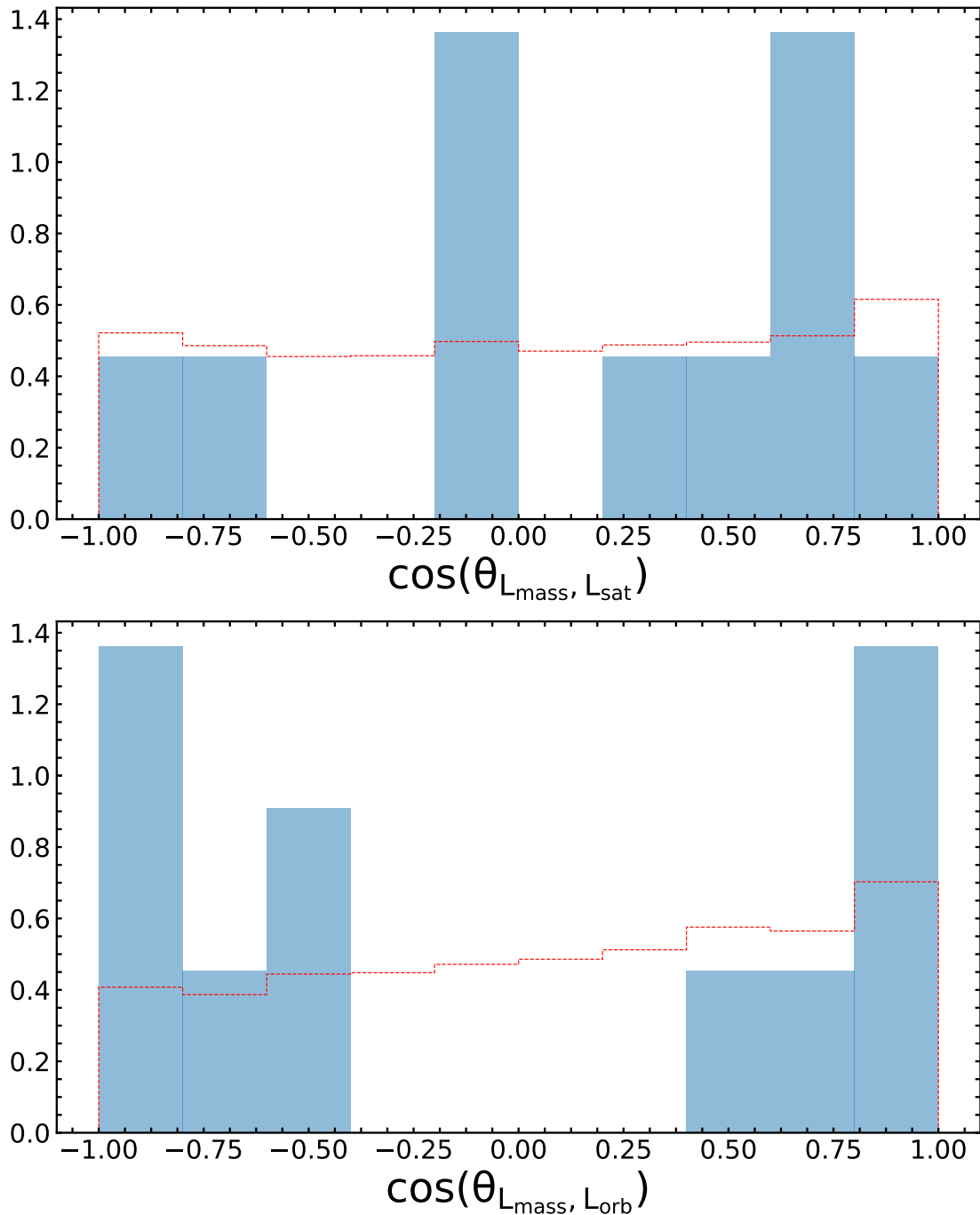
FIGURE 2.5: Top: The cosine of the angle between the spin vectors, defined using the star particles, of the massive galaxy (L_{mass}) and the satellite (L_{sat}). The corresponding distribution from a control sample is shown in red (the normalisation is arbitrary and chosen for clarity). There is no preference for the spins of the two galaxies to be aligned. Bottom: The cosine of the angle between L_{orb} (see Figure 2.4) and the spin vector of the massive galaxy (L_{mass}). The merger events cluster around a specific orbital configuration, where the satellite's orbit tends to be close to co-planar with the disk of the massive galaxy i.e. $\cos\theta$ tends to be close to either -1 or +1.
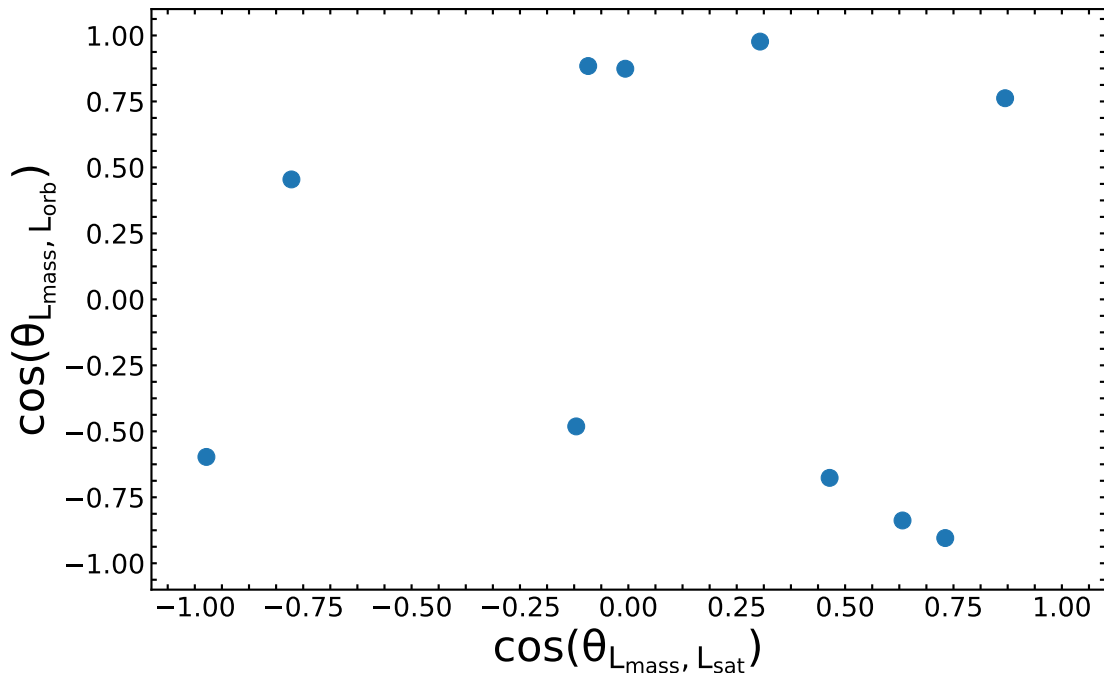
FIGURE 2.6: The cosine of the angle between the (stellar) spin vectors of the massive galaxy (L_{mass}) and the satellite (L_{sat}) plotted against the cosine of the angle between L_{orb} (see Figure 2.4) and the spin vector of the massive galaxy (L_{mass}).

for the most massive spheroids at the present day, whose stellar masses have classically been considered unattainable without significant numbers of both major and minor mergers.

In this chapter, we have studied the formation of a sample of massive ($M_* > 10^{11} M_\odot$) spheroidal systems, in the Horizon-AGN simulation, which have anomalously low (< 0.3) ex-situ mass fractions. These systems are unusual, in the sense that they are extremely massive and spheroidal, yet do not exhibit significant fractions of ex-situ stellar mass - the opposite to what is usually the case for such galaxies.

We have shown that these objects are created in a single minor merger, which triggers a catastrophic (and permanent) morphological change, with $^V/_\sigma$ declining rapidly from the disc to spheroid regime in only a few hundred Myrs. The merger event triggers strong star formation, driven by the native gas reservoir of the more massive progenitor, and an increase in the effective radius of the system. The remnant is a massive, relatively diffuse, slowly-rotating spheroidal galaxy.

We have studied the properties of the progenitor system to explore why the minor merger has such a profound effect on the remnant. Since minor mergers are thought to be able to influence the production of spheroidal systems by triggering gravitational instabilities in clumpy, gas-rich disc galaxies at high redshift, and since orbital configurations can have an impact on the properties of the remnant, we have focussed on the evolution of these properties in the progenitor systems of our spheroids.

We have shown that the properties of the individual progenitors are not anomalous. The more massive progenitors in these mergers have gas fractions and clumpiness values that are consistent with the mean values in control samples at the same redshifts. However, the relative trajectories of the merging progenitors exhibit a specific orbital configuration that likely drives the observed behaviour. The satellites approach the more massive galaxies in close to co-planar orbits, which are likely to maximize the tidal forces and therefore the transfer of orbital energy, enabling the satellite to destroy the disc in only a few hundred Myrs and drive the creation of a massive spheroidal galaxy.

The principal distinguishing feature of the spheroids described in this chapter is the high SFR of these systems for a time after the spheroid has formed. Recent ultraviolet studies have led to the the discovery of widespread star formation activity in spheroidal galaxies across cosmic time (see e.g. Yi et al., 2005; Kaviraj et al., 2007). However, this star formation is typically at a low level (e.g. Kaviraj et al., 2008), with spheroidal galaxies lying well below the star-formation main sequence (e.g. Salim et al., 2007; Kaviraj et al., 2013), even if they have had recent mergers. This is particularly true for spheroids in the low and intermediate redshift Universe.

Our spheroids on the other hand lie significantly above the star-formation main sequence (column 11 in Table 2.1) which offers a route to potentially identifying such systems in observations. Indeed, some (rare) cases of spheroids with SFRs well above the star formation main sequence are known (e.g. Fukugita et al., 2004; Schawinski et al., 2010), with number fractions of a few per cent (similar to our findings here). While such spheroids are difficult to explain via traditional channels, it is plausible that at least some of these massive spheroids with anomalously high SFRs are formed via the co-planar minor-merger channel described here.

Our study adds to the burgeoning literature that is highlighting the significant role of processes other than major mergers in driving the change in the morphological mix of massive galaxies. It demonstrates that, for close to co-planar orbital configurations, a single minor merger (with a mass ratio as low as ~1:10) is able to completely destroy a disc and create a spheroid, even at the high-mass end of the galaxy mass function. While this channel produces a minority (~5 per cent) of such galaxies, our study indicates that the formation of the *most* massive spheroids in the local Universe need not involve any major mergers – or indeed any significant merging at all – contrary to our classical assumptions.

Chapter 3

Why do extremely massive disc galaxies exist today?

3.1 Introduction

In the standard hierarchical paradigm, the morphological mix of massive galaxies is predicted to change from rotationally-supported discs to dispersion-dominated spheroids over cosmic time (e.g. Butcher and Oemler, 1984; Dressler et al., 1997; Conselice et al., 2014). Observations generally support this picture. While discs dominate the high redshift Universe, the morphologies of massive galaxies in the nearby Universe are mainly spheroidal in nature (Bernardi et al., 2003; Wuyts et al., 2011; Kaviraj, 2014b,a; Conselice et al., 2014; Buitrago et al., 2014; Shibuya et al., 2015). This disc-to-spheroid transformation is thought to be primarily driven by galaxy mergers (Toomre, 1977; Barnes, 1992a; Bournaud et al., 2007; Di Matteo et al., 2007; Oser et al., 2010; Kaviraj, 2010; Kaviraj et al., 2011; Dubois et al., 2013, 2016; Lofthouse et al., 2017; Welker et al., 2018; Martin et al., 2018a). The gravitational torques generated by mergers (especially 'major' mergers, which have nearly equal mass ratios) remove stars from ordered rotational orbits and put them on random trajectories, producing dispersion-dominated remnants (e.g. Springel and Hernquist, 2005; Hilz et al., 2013; Font et al., 2017; Martin et al., 2018a).

The role of mergers is considered to be progressively more important for more massive galaxies. At the very highest stellar masses, i.e. beyond the knee of the mass function ($M_* > 10^{10.8}$ $M_\odot$, see e.g. Li and White (2009); Kaviraj et al. (2017)), the consensus view is that mergers are essential for actually achieving the enormous stellar masses of such systems (e.g. Faber et al., 2007; McIntosh et al., 2008; Cattaneo et al., 2011). Since mergers typically create dispersion-dominated stellar components, it is not surprising that massive galaxies are dominated by spheroidal systems.

Interestingly, however, both observations (e.g. Conselice, 2006; Ogle et al., 2016, 2019) and theory (e.g. Martin et al., 2018a) indicate that, even at the highest stellar masses, a significant minority of systems (e.g. more than 10 per cent at $M_* > 10^{11.4}$ $M_\odot$) surprisingly host significant disc components. For example, in the SDSS (Abazajian et al., 2009), Ogle et al. (2016, 2019) find that a subset of the most optically luminous ($M_* = 0.3 - 3.4 \times 10^{11} M_\odot$) galaxies have clear disc components. They speculate that these 'super spirals' may have formed via gas-rich major mergers between two spiral galaxies, with the gas of the two merging galaxies combining to form large gas discs which then create the discy stellar components.

Other recent work supports the finding that such massive discs are relatively gas-rich (Li et al., 2019) and indicates that these systems can be found in a variety of environments, including clusters (Bogdán et al., 2018; Li and Chen, 2019). These studies suggest that these galaxies can even be the brightest galaxies in their respective groups and clusters, residing at the barycentres of these structures. Indeed, if such galaxies live in such high-density environments and host AGN (Ogle et al., 2016), they could provide a natural explanation for the minority of powerful radio AGN that apppear (somewhat surprisingly) to be hosted by discy systems (e.g. Tadhunter, 2016).

In the ΛCDM model, galaxy merger histories are a strong function of stellar mass, largely regardless of the morphology of the galaxy in question. The merger histories of extremely massive discs and spheroids are, therefore, very similar, both in terms of the total number of mergers they experience and the distribution of their mass ratios (e.g Martin et al., 2018a). Since mergers typically destroy discs and create spheroids, it is surprising that any discs exist at all in this extreme mass regime. It is likely, therefore, that some peculiarity in the characteristics of their merger histories causes these massive discs to either survive or for discy (i.e. rotationally-supported) components to be regenerated. This is plausible as gas-rich mergers can regenerate discs, as the gas produces new, rotationally-supported stellar components during the course of the merger event (e.g. Springel and Hernquist, 2005; Robertson et al., 2006; Governato et al., 2009; Hopkins et al., 2009; Font et al., 2017; Martin et al., 2018a; Peschken et al., 2019).

Here, we explain the origin of extremely massive disc galaxies in the nearby Universe, by exploring how details of their merger histories create these surprising systems, using the Horizon-AGN cosmological hydrodynamical simulation. It is worth noting that a cosmological simulation, such as the one used here, is essential for this exercise. While idealised and/or zoom-in simulations of galaxy mergers have often been used to study the merger process (e.g. Barnes, 1988; Hernquist and Spergel, 1992; Bois et al., 2011; Athanassoula et al., 2016; Sparre and Springel, 2016, 2017), the parameter space sampled by these experiments is typically small and not informed by a cosmological model (so that the effects of environment and gas accretion from the cosmic web cannot be fully tested).

1	2	3	4	5	6	7	8	9
Morph.	%	v/σ	$\log M_*$ [$M_\odot$]	$\log M_{BH}$ [$M_\odot$]	$\log$ acc. [$M_\odot$ yr^{-1}]	$\log M_{halo}$ [$M_\odot$]	$\log M_{gas}$ [$M_\odot$]	$\log M_{sf\text{-}gas}$ [$M_\odot$]
Rejuv.	7.7	$0.68^{0.02}$	$11.48^{0.02}$	$8.90^{0.03}$	$-2.03^{0.04}$	$12.79^{0.05}$	$10.45^{0.06}$	$10.27^{0.08}$
Const.	3.3	$0.90^{0.06}$	$11.45^{0.01}$	$8.74^{0.04}$	$-1.91^{0.08}$	$12.76^{0.09}$	$10.49^{0.04}$	$10.39^{0.04}$
Spheroids	89	$0.15^{0.01}$	$11.57^{0.01}$	$8.98^{0.02}$	$-2.08^{0.04}$	$13.19^{0.06}$	$10.29^{0.03}$	$9.86^{0.03}$

TABLE 3.1: Mean properties (errors on the means are shown as superscripts) of massive galaxies. Columns: (1) morphological class, (2) percentage of a given morphological class in the massive ($M_* > 10^{11.4}$ $M_\odot$) galaxy population, (3) v/σ, (4) $\log_{10}$ of the stellar mass, (5) $\log_{10}$ of the black-hole mass, (6) $\log_{10}$ of the mean black-hole accretion rate across the galaxy's lifetime, (7) $\log_{10}$ of the dark-matter halo mass, (8) $\log_{10}$ of the total gas mass (9) $\log_{10}$ of the star-forming gas mass (i.e. gas that is dense enough to form stars, $\rho_{gas} > 0.1$ H cm^{-3}).

The plan for this chapter is as follows. In Section 3.2, we describe how the galaxies are selected. In Section 3.3, we explain the different formation channels that lead to the formation of extremely massive discs and explore whether these massive discs can explain the discy hosts of powerful AGN (which are otherwise typically hosted by spheroidal galaxies). We summarise our findings in Section 3.4.

3.2 Selection of extremely massive disc galaxies

We define massive disc galaxies in Horizon-AGN (see Chapter 2.2 for more details) as those with $M_* > 10^{11.4}$ $M_\odot$ and $v/\sigma > 0.55$ at z = 0. These systems are, therefore, well beyond the knee of the galaxy stellar mass function ($M_* \sim 10^{10.8}$ $M_\odot$) and are in the disc regime based on v/σ, furthermore we examine mock images of these galaxies to ensure that they have a disc-like morphological appearance. The total number of galaxies with $M_* > 10^{11.4}$ $M_\odot$ is 569 and the fraction of discs in this mass range is around 11 per cent. This fraction is in good agreement with observational work. For example, Ogle et al. (2016, 2019) find that their 'super-spirals' constitute 6.5% (9.2% when accounting for inclination incompleteness) of galaxies with $M_* > 10^{11.3}$ $M_\odot$, which is consistent with our simulated values (see Table 3.1).

3.2.1 Local environment

To explore local environment we utilise information about a galaxy's host dark matter halo and its group hierarchy, i.e. whether it is a 'central' or a 'satellite'. Satellites are systems whose host dark matter haloes have merged into a larger halo where they currently reside. For some of our

1	2	3	4	5
Morph.	Redshift	Stellar mass ratio	Massive f_{gas}	Sat. f_{gas}
Rejuv. discs	$0.32^{0.07}$	$4.29^{0.36}$	$0.17^{0.02}$	$0.33^{0.02}$
Const. discs	$0.36^{0.11}$	$4.06^{0.59}$	$0.19^{0.02}$	$0.32^{0.03}$
Spheroids	$0.49^{0.02}$	$4.44^{0.11}$	$0.09^{0.01}$	$0.23^{0.01}$

TABLE 3.2: Mean properties (errors on the mean are shown as superscripts) of the most recent significant merger, defined as the last merger with a stellar mass ratio greater than 1:10. Columns: (1) morphological class (2) last merger redshift (3) stellar mass ratio of merger (4) gas fraction of the more massive galaxy, (5) gas fraction of the satellite.

analysis we also explore the vicinity of galaxies in the cosmic web produced by Horizon-AGN, via the persistence-based filament tracing algorithm `DisPerSE` (Sousbie, 2011), which uses the density field estimated via a delaunay tessellation (Schaap and van de Weygaert, 2000) of the dark matter particles. We choose a persistence of 7 sigma. `DisPerSE` identifies ridges in the density field as special lines that connect topologically robust pairs of nodes. These ridges compose the filament network of the cosmic web, and the set of all segments defining these ridges are referred to as the 'skeleton' (Pogosyan et al., 2009). We refer readers to Sousbie (2011) and Sousbie et al. (2011) for more details of the `DisPerSE` algorithm and to Dubois et al. (2014a) and Laigle et al. (2018) for a description of its implementation in Horizon-AGN.

We note that, out of the 64 massive discs in this study, 63 systems (i.e. more than 99 per cent) are central galaxies. This appears consistent with observational studies which indicate that many massive discs tend to be the brightest galaxies in their respective groups/clusters (e.g. Ledlow et al., 2001; Li and Chen, 2019; Bogdán et al., 2018). Figure 3.1 shows the positions of our three morphological classes (i.e. rejuvenated discs, constant discs and spheroids) in the cosmic web. Properties used to characterise local environment are tabulated in Table 3.1.

3.3 How do extremely massive disc galaxies form?

3.3.1 Two channels of massive disc formation

We begin by illustrating, graphically, the two channels that create galaxies that are massive discs at the present day. In Figure 3.2 we describe the evolution in morphology and the stellar mass assembly in typical galaxies that form via these channels. The left and middle columns show the change in V/σ (top) and the evolution of the stellar mass, ex-situ stellar mass (see Chapter 2.3.1) and gas mass (bottom) for a typical system that represents each of the two channels of massive-disc formation. The right-hand column shows the same for a massive spheroid. The ex-situ stellar mass is defined as the stellar mass that is directly accreted from external objects via mergers, and not formed within the galaxy's main progenitor.
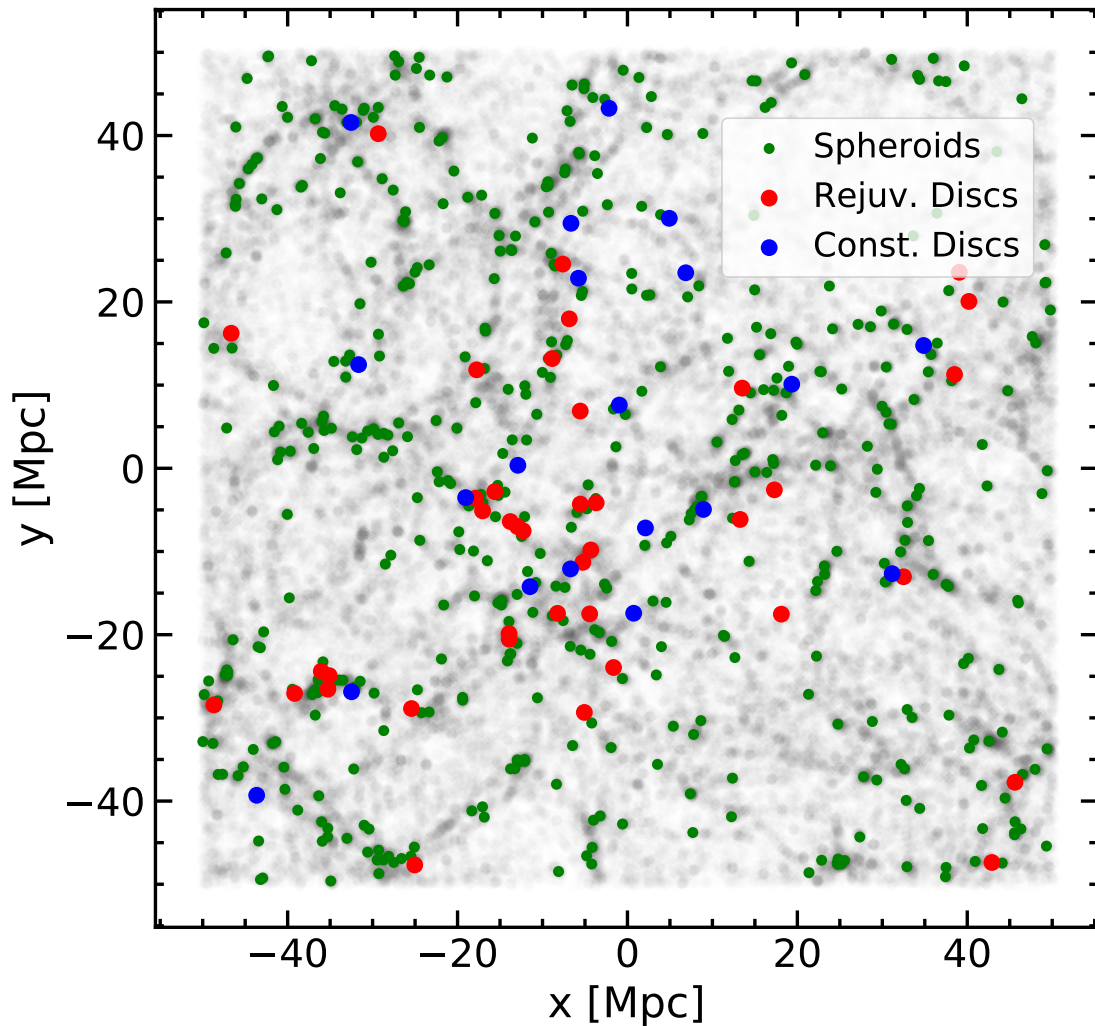
FIGURE 3.1: Positions of rejuvenated discs (red), constant discs (blue) and spheroids (green) in the cosmic web from Horizon-AGN. Grey dots indicate the general galaxy population, with darker regions indicating regions of higher density.

As this figure indicates, massive discs form in one of two ways. In the first channel (left-hand column) the progenitor is initially a spheroid, until the most recent merger event causes a significant uptick in V/σ which moves the system into the disc regime. This uptick coincides with this merger bringing in an appreciable amount of gas (since there is a coincident uptick in the gas mass) which builds a new disc component. We refer to these galaxies as 'rejuvenated discs'. As we discuss below the most recent mergers that drive this rejuvenation have significant mass ratios (> 1:10). It is worth noting that, in contrast, the most recent mergers in massive galaxies that exhibit spheroidal morphology (right-hand column) today are gas-poor. These mergers do not necessarily produce an uptick in V/σ and, when they do, these upticks are not sufficient to move the system into the disc regime. Indeed V/σ typically decreases, as is expected in mergers which are gas-poor, since the only effect of the merger is to randomise the stellar orbits and reinforce the spheroidal component of the system (e.g. Lotz et al., 2010; Taranu et al., 2013; Naab et al., 2014a; Martin et al., 2018a). In the second channel (middle column) the galaxy retains a disc
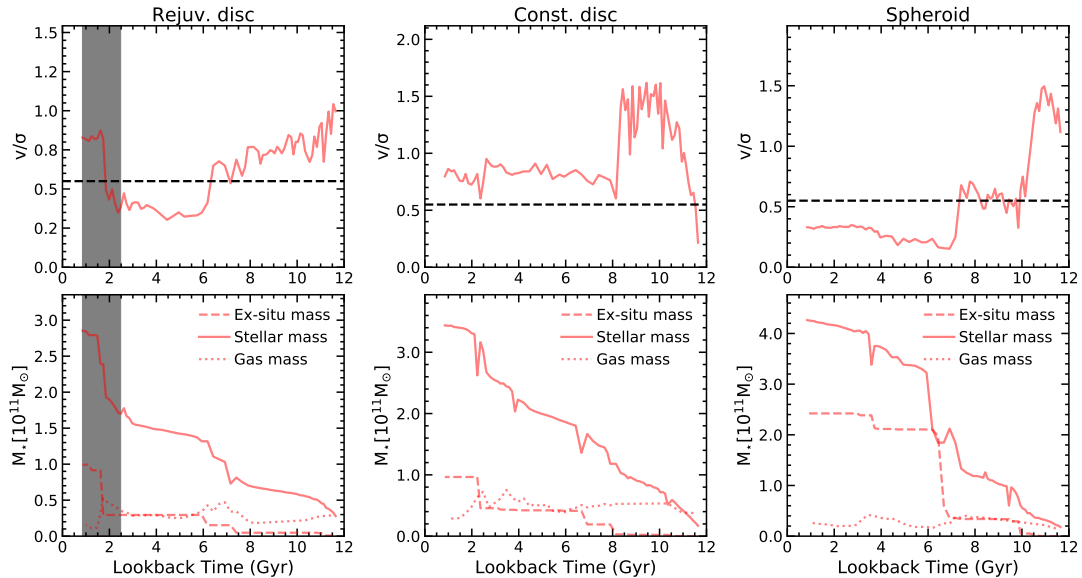
FIGURE 3.2: The evolution of the properties of the progenitor system of massive galaxies. Each column shows the evolution of an individual galaxy. The left, centre and right-hand columns show the evolution of a rejuvenated disc, a constant disc and a massive spheroid respectively (see text in Section 3.3.1 for details). The top row shows the evolution in V/σ, while the bottom row shows the change in the stellar mass (solid), ex-situ (i.e accreted) stellar mass (dashed) and gas mass (dotted) of the system. The ex-situ stellar mass shows a near-step change when mergers take place, with the magnitude of the change indicating the mass brought in by the accreted satellite. The grey region highlights the most recent merger which produces the uptick in V/σ that moves the rejuvenated disc into the disc regime. The dotted line at $V/\sigma = 0.55$ demarcates the spheroid and disc regimes.

component and remains in the disc regime throughout its lifetime. We refer to these systems as 'constant discs'.

Visual inspection of the V/σ evolution of all massive discs indicates that the rejuvenated disc channel accounts for ~ 70% of these systems (and ~ 8% of all massive galaxies), with the remaining ~ 30% having maintained a disc component over cosmic time (these systems comprise ~ 3% of all massive galaxies). Table 3.1 presents mean properties of the three morphological classes: rejuvenated discs, constant discs and spheroids. In the following sections we explore these two channels of massive disc formation in more detail.

3.3.2 The dominant channel of massive disc formation: disc rejuvenation via recent mergers

We begin by exploring the principal channel for massive disc formation - the rejuvenation of a disc by a recent merger. We note first that the rejuvenation is always driven by mergers with significant stellar mass ratios that are greater than 1:10. Given that the change in morphology from spheroid to disc appears to be driven by the properties of the most recent significant

merger, we study how the properties of these mergers differ between rejuvenated discs and their spheroidal counterparts.

As Table 3.2 indicates, the mass ratios of the most recent significant merger, defined as the last merger a galaxy has undergone with a mass ratio greater than 1:10, are similar in both the rejuvenated discs and their spheroidal counterparts. This is not unexpected, since the merger histories of galaxies with similar stellar masses tend to be comparable, regardless of morphology (Martin et al., 2018a). The rationale for the 1:10 mass ratio threshold is that mergers below this threshold affect the system very weakly and do not produce morphological change (Martin et al., 2018a). The differences between the rejuvenated discs and spheroids are, therefore, not driven by the mass ratio of the most recent significant merger.

However, differences arise when we consider both the gas content of this merger event and its redshift. The progenitor galaxies in mergers that create rejuvenated discs show higher gas fractions than those in their spheroidal counterparts. The median gas fractions are elevated by a factor of ~2 in both the more massive progenitor and the accreted satellite. Since the mass ratios of the most recent significant mergers are similar, the absolute gas mass brought into the merger therefore tends to be higher in events that create these systems. As has been shown in previous work (e.g. Lotz et al., 2010; Naab et al., 2014a; Lagos et al., 2018; Martin et al., 2018a), gas-rich mergers will 'spin up' merger remnants, as the gas creates a new rotationally-supported stellar component. As shown graphically in Figure 3.2 (top row, left-hand column), these gas-rich recent mergers produce an uptick in V/σ, that moves the system from the spheroid to the disc regime.[1]

If rejuvenated discs, which are the dominant channel of massive-disc formation, are principally created via recent gas-rich mergers, then it stands to reason that the fraction of massive galaxies that are discs should correlate positively with the availability of gas in the Universe. Figure 3.3 shows the evolution of both the gas fraction of the Universe (red) and the fraction of massive galaxies that are discs (blue) with cosmic time. At any given redshift, we define massive galaxies as those whose descendants at $z = 0$ have $M_* > 10^{11.4} M_\odot$, with massive discs defined as massive galaxies with $V/\sigma > 0.55$ at that redshift. The inset summarises this evolution by plotting the fraction of massive galaxies that are discs against the gas fraction of the Universe. This figure confirms that, as one would expect for such a rejuvenation process, a higher gas fraction in the Universe leads to a higher fraction of massive galaxies that are discs. In other words, the frequency of massive discs, and therefore the morphological mix of galaxies at the highest stellar masses, is strongly driven by the gas fraction of the Universe.

---

[1]For completeness, we have checked what fraction of massive spheroids which have a recent significant gas-rich ($f_{gas} > 0.3$) merger remain spheroids after such an event. We find that only 2% of massive spheroids fit this description. In other words, 98% of massive spheroids that undergo such a gas-rich merger become discs.
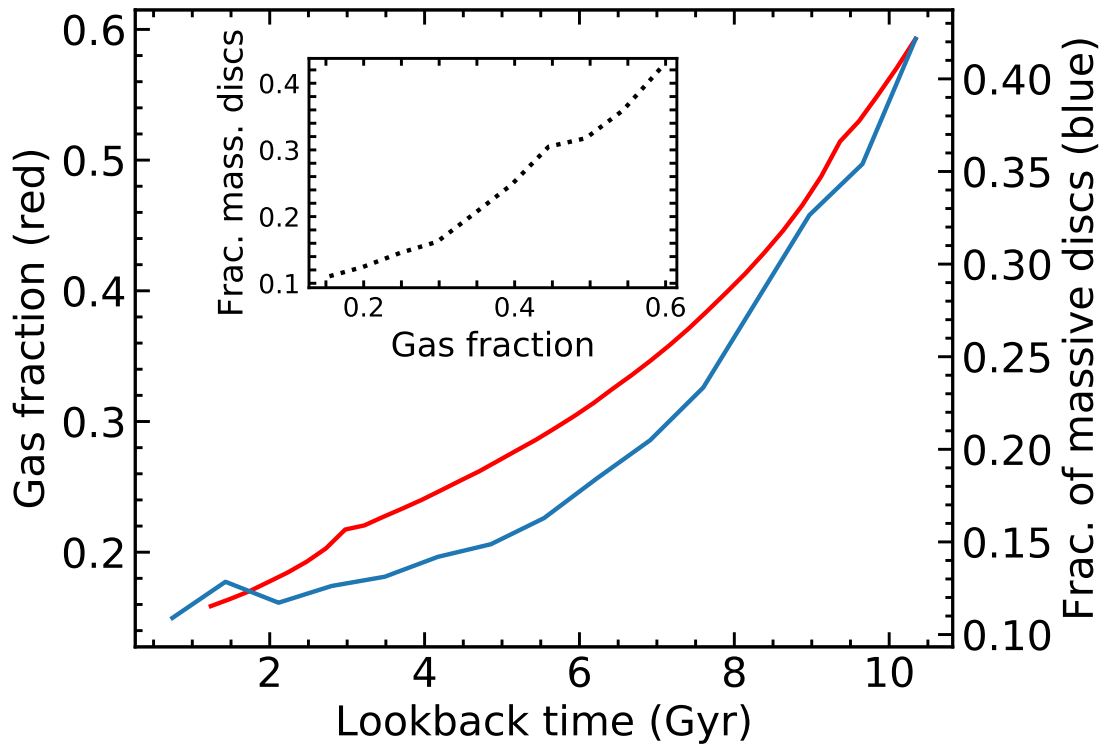
FIGURE 3.3: Evolution of the gas fraction of the Universe (red) and the fraction of massive galaxies that are discs (blue), with cosmic time. The inset summarises this evolution by plotting these quantities against each other.

Analysis of the local environment (Table 3.1) indicates that rejuvenated discs typically reside in less-massive dark-matter halo masses, i.e. they inhabit less dense environments. Galaxies in these regions will be less affected by processes like ram pressure stripping and tidal heating which can remove their constituent gas (e.g. Vollmer et al., 2001; Johansson et al., 2009; Martin et al., 2019). This enables these systems to merge with more gas-rich satellites which can then drive the disc rejuvenation process.

Finally, it is worth noting that the median redshift of the last significant merger event is lower in the rejuvenated discs ($z \sim 0.3$, which corresponds to a look-back time of ~3.5 Gyrs) compared to that in their spheroidal counterparts ($z \sim 0.49$, which corresponds to a look-back time of ~5 Gyrs). This likely assists in the survival of the discy components to the present day, because less time has elapsed since the recent merger event, reducing the possibility that further significant interactions take place which could enhance the spheroidal components of these systems.

3.3.3 The secondary channel of massive disc formation: disc preservation over cosmic time

While the majority of massive discs have formed through disc rejuvenation via recent significant gas-rich mergers, a minority of this population have remained in the disc regime over cosmic
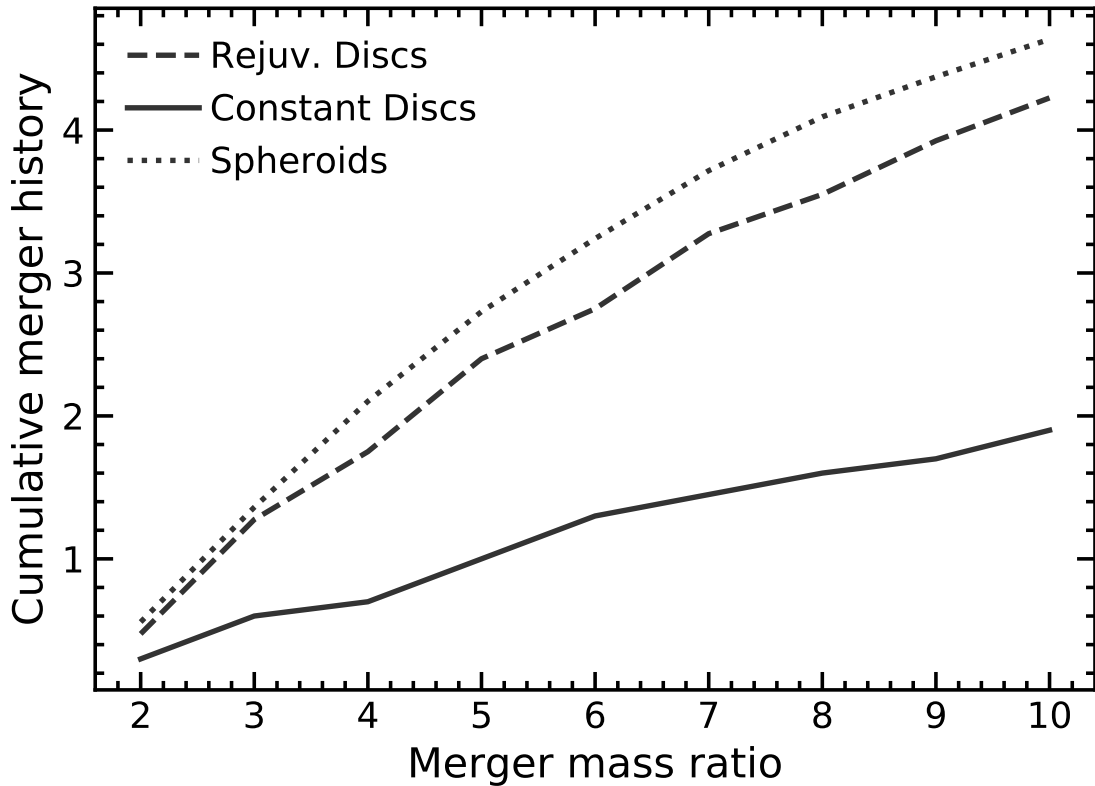
FIGURE 3.4: Cumulative merger history for our three morphological classes: rejuvenated discs (dashed line), constant discs (solid line) and spheroids (dotted line). This figure presents the average number of mergers experienced by a galaxy over its lifetime, with mass ratios less than or equal to a given value, shown on the x-axis. For example, rejuvenated discs undergo, on average, ~4.2 mergers with mass ratios greater than 1:10, while constant discs undergo ~1.9.

time. In this section, we explore how these rare systems preserve their disc components over their lifetimes.

The most recent significant mergers in these constant discs have similar properties, e.g. merger mass ratios, the redshift of the last significant merger and the gas fractions of the merging progenitors, to those in their rejuvenated counterparts (Table 3.2). The two sub-populations also occupy similar local environments in terms of their dark-matter halo masses.

However, strong differences arise when we consider the cumulative merger histories of the different morphological classes across cosmic time. Figure 3.4 presents the average number of mergers experienced by a galaxy, over its lifetime, with mass ratios less than or equal to the value shown on the x-axis. For example, rejuvenated discs undergo, on average, 4.2 mergers with mass ratios greater than 1:10, while constant discs undergo 1.9. The rate of mergers with significant mass ratios is therefore a factor of 2.2 higher in the rejuvenated discs compared to their constant counterparts. Not unexpectedly, the rejuvenated discs have similar merger histories to their spheroidal counterparts (since they were spheroidal before their most recent significant merger).

This anomalously quiet merger history enables the constant discs to maintain their discy components over their lifetimes. Furthermore, since mergers typically accelerate the consumption of gas (e.g. Martin et al., 2017), a quieter merger history also enables the system to better retain its gas, as indicated by both the higher total and star-forming gas masses in Table 3.1.

A potential explanation for this anomalously quiet merger history is the halo bias effect (e.g. Borzyszkowski et al., 2017), whereby a more massive nearby halo (typically a node in the cosmic web) effectively shields the galaxy from mergers, allowing it to continue forming stars without being disturbed by interactions. We check for the presence of a halo bias effect using the position of nodes (and other halos) in the skeleton. However, we find no evidence that this effect may be driving the properties of the constant discs. These systems are no more likely to be close to a more massive halo/node than their rejuvenated counterparts and, in most cases, their halos actually dominate the local environment. This is perhaps not unexpected because all galaxies in our sample (including the constant discs) are extremely massive. Thus, the likelihood of finding a more massive system nearby is very low. The quieter merger history of the constant discs therefore seems to be a stochastic effect, which aligns well with the extreme rarity of these systems.

3.3.4 A note about massive discy hosts of AGN

We complete our study by considering whether the massive discs studied here may provide a natural explanation for the minority of powerful AGN that appear to (surprisingly) inhabit massive disc galaxies (e.g. Tadhunter et al., 1992; de Koff et al., 2000; Canalizo and Stockton, 2001; Guyon et al., 2006; Madrid et al., 2006; Georgakakis et al., 2009; Morganti et al., 2011; Singh et al., 2015).

Recall from the analysis above that the majority of massive discs are systems that are initially spheroidal, but in which discs have been rejuvenated via a recent gas-rich merger. Table 3.1 indicates that the black-hole (BH) masses and accretion rates in the rejuvenated discs are predicted to be similar to those in their spheroidal counterparts, which is consistent with these systems originally being spheroids before the most recent significant merger. The BH masses in the constant discs are also comparable to the other morphological classes, although their BHs are slightly less massive (likely due to the quieter merger history) and their accretion rates are typically higher (due to the higher gas fractions in these systems).

These theoretical predictions appear similar to what is seen in observations. For example, Tadhunter (2016) shows that a minority of the hosts of radio AGN at high stellar masses ($M_* > 10^{11}M_\odot$), that have clearly discy morphologies, show the same patterns. They exhibit similarly high BH masses as their spheroidal counterparts ($M_{BH} > 10^8 M_\odot$), with broadly similar accretion rates.

It is worth noting, however, that while in observed AGN that are hosted by massive discs, the accretion rates are slightly lower than that in their spheroidal counterparts, the opposite appears to be true in our theoretical analysis. This is largely explained by the different mass ranges considered, because our study is focused on galaxies that are more massive than those in observational studies like Tadhunter (2016). Indeed, if we reduce our stellar mass range to M_* > 10^{11} $M_\odot$, we find that the massive discs then have lower accretion rates than their spheroidal counterparts, in line with the findings of Tadhunter (2016). Given the parallels between the massive discs in our theoretical study and their observed counterparts, the formation scenarios presented here appear to provide a natural explanation for the minority of powerful AGN that are observed to (surprisingly) inhabit disc galaxies at the highest stellar masses.

3.4   Summary

Both theory and observations indicate that the morphological mix of massive galaxies changes from being disc-dominated in the early Universe to being dominated by spheroidal systems at low redshift. In the standard ΛCDM paradigm, this morphological transformation is thought to be driven by mergers. Galaxy merger histories correlate strongly with stellar mass, largely regardless of the morphology of the galaxy in question. The frequency of mergers typically increases with stellar mass, so that galaxies at the highest stellar masses tend to have the richest merger histories. However, while most massive galaxies have spheroidal morphology, a minority of systems at the highest stellar masses are, in fact, discs. Since mergers typically destroy discs and create spheroids, and the most massive galaxies typically have the richest merger histories, it is surprising that disc galaxies exist at all at the highest stellar masses (e.g. those well beyond the knee of the mass function).

We have studied the formation mechanisms of massive (M_* > $10^{11.4}$ $M_\odot$) disc galaxies, in the Horizon-AGN simulation. Massive discs make up a significant minority ($\sim 11\%$) of systems at such high stellar masses. We have shown that there are two channels of massive disc formation. The primary channel, which accounts for ~70 per cent of these systems, is disc rejuvenation. In this channel, a massive spheroidal system experiences a recent gas-rich merger which rebuilds a disc and moves the system from the spheroid to the disc regime. The gas-rich mergers are facilitated by the fact that these systems typically inhabit less massive halos, i.e. less dense environments, than spheroidal counterparts with similar stellar masses. Galaxies in these regions are less likely to be affected by processes which deplete gas, like ram pressure and tidal stripping, making it more likely that massive galaxies can have gas-rich mergers.

In the secondary channel, a massive disc remains in the disc regime over its entire lifetime. The maintenance of the disc is the result of an anomalously quiet merger history, whereby these systems undergo a factor of ~2 fewer mergers with mass ratios greater than 1:10 than other

galaxies with similar stellar masses. Since mergers accelerate gas consumption, a quieter merger history also enables the galaxy to retain its gas reservoir more easily, further enabling it to maintain its disc component over its lifetime. The dominance of the rejuvenation channel means that the fraction of massive galaxies that are discs is progressively larger at higher redshift, since the Universe is more gas-rich. The morphological mix of galaxies at the very highest stellar masses (at any epoch) is therefore a strong function of the gas fraction of the Universe.

Finally, we have shown that the BH masses and accretion rates of massive discs are similar to those in their spheroidal counterparts. The formation mechanisms described here therefore provide a natural explanation for the minority of powerful AGN that are (surprisingly) found in disc galaxies.

Chapter 4

Extremely massive disc galaxies form through gas-rich minor mergers

4.1 Introduction

Observational studies of galaxy morphology show that, while discs dominate the high-redshift Universe, the morphologies of nearby massive galaxies are mostly spheroidal in nature (Bernardi et al., 2003; Wuyts et al., 2011; Ryan et al., 2012; Conselice et al., 2014; Buitrago et al., 2014; Shibuya et al., 2015). In our standard hierarchical structure-formation paradigm, this morphological change, from rotationally-supported discs to dispersion-dominated spheroids, is largely explained by galaxy merging (Toomre, 1977; Barnes, 1992a; Bournaud et al., 2007; Di Matteo et al., 2007; Oser et al., 2010; Kaviraj, 2010; Kaviraj et al., 2011; Dubois et al., 2013, 2016; Lofthouse et al., 2017; Welker et al., 2018; Martin et al., 2018a). The large gravitational torques produced during merger events are capable of randomising the ordered rotational orbits of stars within the merging progenitors and creating dispersion-dominated systems (e.g. Springel and Hernquist, 2005; Hilz et al., 2013; Font et al., 2017; Martin et al., 2018a).

The role of merging is thought to become increasingly more important at higher stellar masses. In particular, significant merging activity is considered essential for galaxies to achieve the highest stellar masses (e.g. Faber et al., 2007; McIntosh et al., 2008; Cattaneo et al., 2011), e.g. those well beyond the knee of the galaxy mass function ($M_* \gtrsim 10^{10.8}$ $M_\odot$, see e.g. Li and White (2009); Kaviraj et al. (2017)), because star formation via direct gas accretion is no longer sufficient to drive the requisite stellar mass growth. However, since mergers are expected to destroy discs, and the most massive galaxies have the richest merger histories, it is surprising that both observational (e.g. Conselice, 2006; Ogle et al., 2016, 2019) and theoretical (e.g. Martin et al., 2018a; Jackson et al., 2020) studies suggest that a significant minority of galaxies at the highest stellar masses ($M_* > 10^{11.4}$ $M_\odot$) are actually discs.

If discs exist in the stellar mass regime when mergers are frequent, their merger histories must involve peculiarities that either rejuvenate discy components or allow these discs to survive the mergers themselves. For example, theoretical work has shown that in gas-rich mergers, the gas brought in by the progenitors can create new discy stellar components in the remnants (e.g. Springel and Hernquist, 2005; Robertson et al., 2006; Governato et al., 2009; Hopkins et al., 2009; Font et al., 2017; Martin et al., 2018a; Peschken et al., 2019). Indeed Ogle et al. (2016, 2019) have suggested that the local massive discs in their study may have formed via major mergers (mass ratios greater than 1:4) between two gas-rich spiral galaxies.

In Jackson et al. (2020, J20 hereafter) we used Horizon-AGN, a cosmological hydrodynamical simulation (Dubois et al., 2014a; Kaviraj et al., 2017), to probe the potential channels by which massive discs may form in the standard paradigm. J20 showed that extremely massive ($M_* > 10^{11.4}$ $M_\odot$) discs do exist in the simulation and are created via two channels. In the primary channel, which accounts for ~70 per cent of these systems, a significant merger with a mass ratio greater than 1:10, between a massive spheroid and a gas-rich satellite, 'spins up' the spheroid by creating a new rotational stellar component, and leaves a massive disc as the remnant. In the secondary channel, a system maintains a disc throughout its lifetime, due to an anomalously quiet merger history which enables the galaxy to retain its gas reservoir more easily.

If massive discs are indeed formed via these channels, the simulation makes some specific predictions that are testable. For example, J20 predicts that massive discs should comprise ~11 per cent of the massive galaxy population. Since they are typically created via recent minor mergers, a large fraction of these galaxies should exhibit tidal features in deep optical images. Given the gas-rich nature of these mergers, these systems should exhibit reasonably high star-formation rates (SFRs) of a few solar masses per year. Finally, since massive ellipticals are predicted to have their last significant mergers at higher redshifts, and since these mergers are not gas-rich, both the fraction of tidally-disturbed galaxies and their SFRs should be elevated in the massive discs, compared to that in their spheroidal counterparts.

The purpose of this observational work is to confront the theoretical predictions from J20 with multi-wavelength survey data, in order to establish whether the predictions are indeed supported by the observations. This chapter is structured as follows. In Section 4.2, we describe the construction of a sample of massive galaxies and their multi-wavelength data, using the Sloan Digital Sky Survey (SDSS; York et al., 2000; Abazajian et al., 2009), the Dark Energy Camera Legacy Survey (DECaLS; Dey et al., 2019), the Galaxy Evolution Explorer (GALEX; Morrissey et al., 2007) and the Arecibo Legacy Fast ALFA (ALFALFA; Haynes et al., 2011) survey. We also describe the process of classifying galaxy morphology and identifying objects which have tidal features via visual inspection. In Section 4.3, we compare the observed properties of the massive discs in our sample with the predictions of J20. We summarise our findings in Section

4.4.

4.2   A sample of massive galaxies in the nearby Universe

We select our sample of nearby massive galaxies from the SDSS using the MPA-JHU value-added catalog [1]. We select objects which have SDSS spectroscopic redshifts in the range $0.03 < z < 0.1$ and where the lower limit of their stellar masses, taken from the MPA-JHU catalog (Brinchmann et al., 2004), is greater than $10^{11.4}$ $M_\odot$. We identify 708 galaxies which match these criteria.

The lower limit of the mass range ensures that our empirical sample of massive galaxies is comparable to those in the theoretical study of J20. The upper limit of the redshift range produces a sample with a median redshift that matches that of the simulated galaxies in J20. Standard depth SDSS imaging is typically too shallow to reveal faint tidal features from minor mergers (e.g. Kaviraj, 2010, 2014b,a). Instead, we use images from DECaLS, which provides deep optical imaging over ~14,000 square degrees in the northern hemisphere. The DECaLS images in the g, r and z bands have 5σ point-source depths of ~24.0, ~23.4 and ~22.5 magnitudes respectively, roughly 1.5 magnitudes deeper than their SDSS counterparts, with similar seeing. It is worth noting that, at our redshifts of interest, the impact of surface-brightness dimming is still relatively minor, making it possible to see faint structures like tidal features in deep optical images (e.g. Kaviraj, 2010).

To demonstrate the improvement in our ability to detect merger-induced tidal features in deeper imaging, we show, in Figure 4.1 images of the same galaxy from the SDSS, DECaLS and the Hyper Suprime-Cam Subaru Strategic Program (HSC-SSP Aihara et al., 2019), which is a further ~2 mags deeper than DECaLS. While the tidal features are invisible in the SDSS image, they are progressively more visible in the DECaLS and HSC-SSP images (and clearest in the deepest HSC-SSP image). Note that, while the HSC-SSP is the deepest wide-area optical survey currently available, its footprint ($\sim$1500 deg^2) is considerably smaller than that of DECaLS and therefore not suitable for this study. Indeed, only 4 out of the 708 massive galaxies in our sample are in the HSC-SSP footprint.

We use SFRs from the GALEX-SDSS-WISE Legacy Catalog (GSWLC; Salim et al., 2016), which are derived via spectral energy distribution (SED) fitting using total magnitudes from the GALEX and SDSS surveys. It is worth noting that SFRs derived using total magnitudes are more likely to be representative of the total SFR of the system than those derived, for example, using emission lines measured within the SDSS fibre (which will only sample the star formation activity in the central regions of the galaxy). These total SFRs are more appropriate for comparison to

---

[1]https://wwwmpa.mpa-garching.mpg.de/SDSS/DR7/
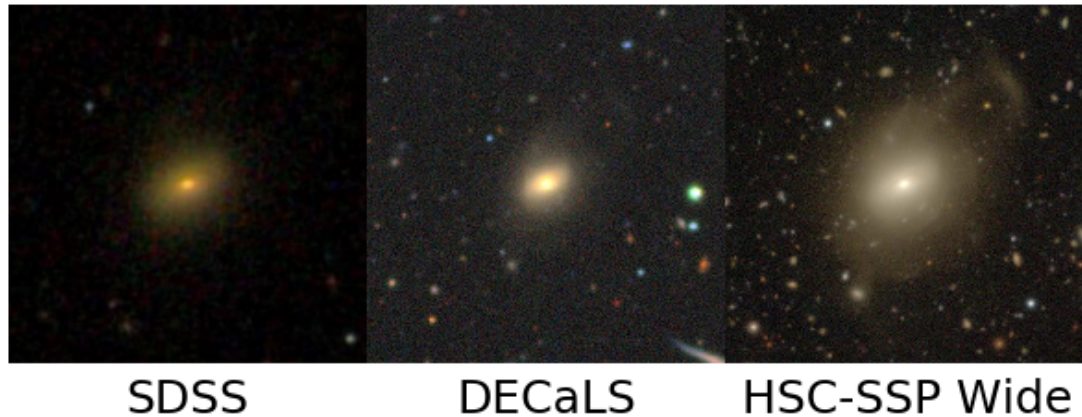
FIGURE 4.1: Images of the same galaxy from the SDSS, DECaLS and the HSC-SSP Wide surveys. DECaLS and HSC-SSP are ~1.5 and ~4 mags deeper than the SDSS respectively. While the tidal features are invisible in the SDSS, they become progressively more easily visible in the deeper images. This figure highlights the need to use a deep-wide survey like DECaLS to detect galaxies that have recently undergone a merger.

the SFRs measured in simulated galaxies, where the entire galaxy is used to measure the SFR. Finally, we use HI masses from the ALFALFA survey.

4.2.1 Morphological classification and identification of merger-induced tidal features

We visually inspect the composite grz images of each individual massive galaxy from DECaLS to morphologically classify it as either a spheroid (which includes ellipticals and lenticular systems) or a disc. For each system, we also flag the presence of tidal features. In Figure 4.2, we show a representative sample of galaxies, classified as spheroids (top panel) and discs (bottom panel) respectively. The top row of each panel shows examples of galaxies classified as 'disturbed' (i.e. those which exhibit the presence of tidal features), while the bottom row shows galaxies classified as 'relaxed' (i.e. those in which no tidal features are present).

4.3 Observed properties of massive galaxies in the local Universe

4.3.1 Morphological properties

We begin our analysis by considering the morphological properties of galaxies in our observational sample (summarised in Table 4.1). ~13 per cent of our massive galaxies are discs, of which ~64 per cent show evidence of tidal features (the corresponding value for early-types is ~31 per cent of the 87 per cent). This is a lower limit because, as indicated by Figure 4.1, it is likely that the fraction of galaxies with tidal features could be higher in deeper imaging. The
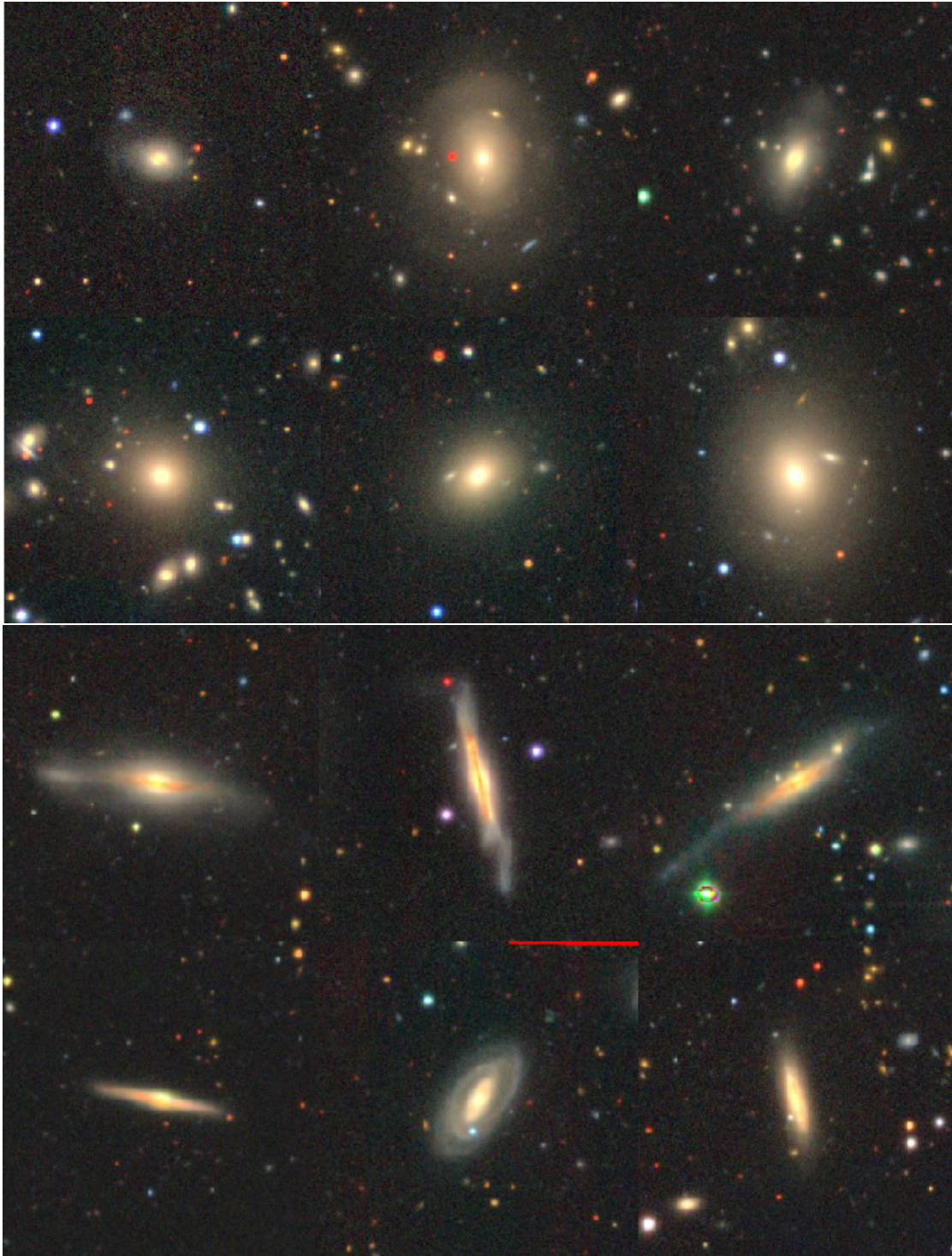
FIGURE 4.2: Examples of spheroids (top two panels) and discs (bottom two panels) from our massive galaxy sample. The images are grz composites from DECaLS. 'Disturbed' galaxies (i.e. those that show evidence of tidal features such as tidal tails, plumes and prominent shells) are shown in the top row, while 'relaxed' galaxies (i.e. those that do not show evidence of tidal features) are shown in the bottom row. This figure may look better on screen than in print.

1	2	3
Morphology	Number fraction	Fraction with tidal features
Disc	0.13	0.64
Spheroid	0.87	0.31

TABLE 4.1: The morphological properties of nearby massive galaxies. Columns: (1) morphological class (2) number fraction of galaxies in this morphological class (3) fraction of galaxies in this morphological class which exhibits tidal features in the DECaLS images. Massive discs show a high incidence of tidal features (which are significantly elevated, by at least around a factor of 4, compared to their low-mass counterparts), suggesting that the formation of these systems involves a high prevalence of mergers, consistent with the theoretical predictions in J20.

corresponding fraction of systems in the low-mass disc population, which show tidal features in SDSS Stripe 82 images (which have similar depth and seeing to DECaLS), is between ~11 and 17 per cent, depending on the specific morphology of the low-mass discs in question (e.g. Sa/Sb/Sc/Sd, see Kaviraj, 2014a). The median stellar mass of the low-mass disc population in Kaviraj (2014a) is $\sim 10^{10.3}$ M$_\odot$ (Kaviraj, 2014b). The fraction of tidal features in massive discs is therefore significantly elevated (by at least around a factor of 4) compared to their low-mass counterparts, implying that the formation of these galaxies involves a much higher incidence of recent mergers.

The high frequency of tidal features in massive discs suggests that most of these interactions are unlikely to be major mergers (mass ratios greater than 1:4). This is because, in our mass range of interest, the major merger fraction at low redshift is only a few per cent (e.g. Darg et al., 2010; Mundy et al., 2017), with the tidal features from such interactions remaining visible for 2-3 Gyrs at the depth of the DECaLS images (e.g. Mancillas et al., 2019). The majority of these events are therefore likely to be minor mergers (mass ratios between 1:4 and 1:10), which are typically 4-5 times more frequent than their major counterparts (e.g. Fakhouri and Ma, 2008; Jogee et al., 2009; López-Sanjuan et al., 2010; Lotz et al., 2011; Kaviraj, 2014a).

These observational results appear consistent with the theoretical predictions of J20, which suggest that ~11 percent of the massive galaxies in the simulation are discs, and that these systems form via recent minor mergers that take place within the last ~2-3 Gyrs. In addition, massive spheroids in the simulation typically underwent their most recent mergers at higher redshift than their discy counterparts. Since the tidal features from these mergers will have had more time to fade, this will result in fainter tidal features at $z \sim 0$, which appears consistent with the lower tidal fraction observed in the massive early-types in our observed sample.
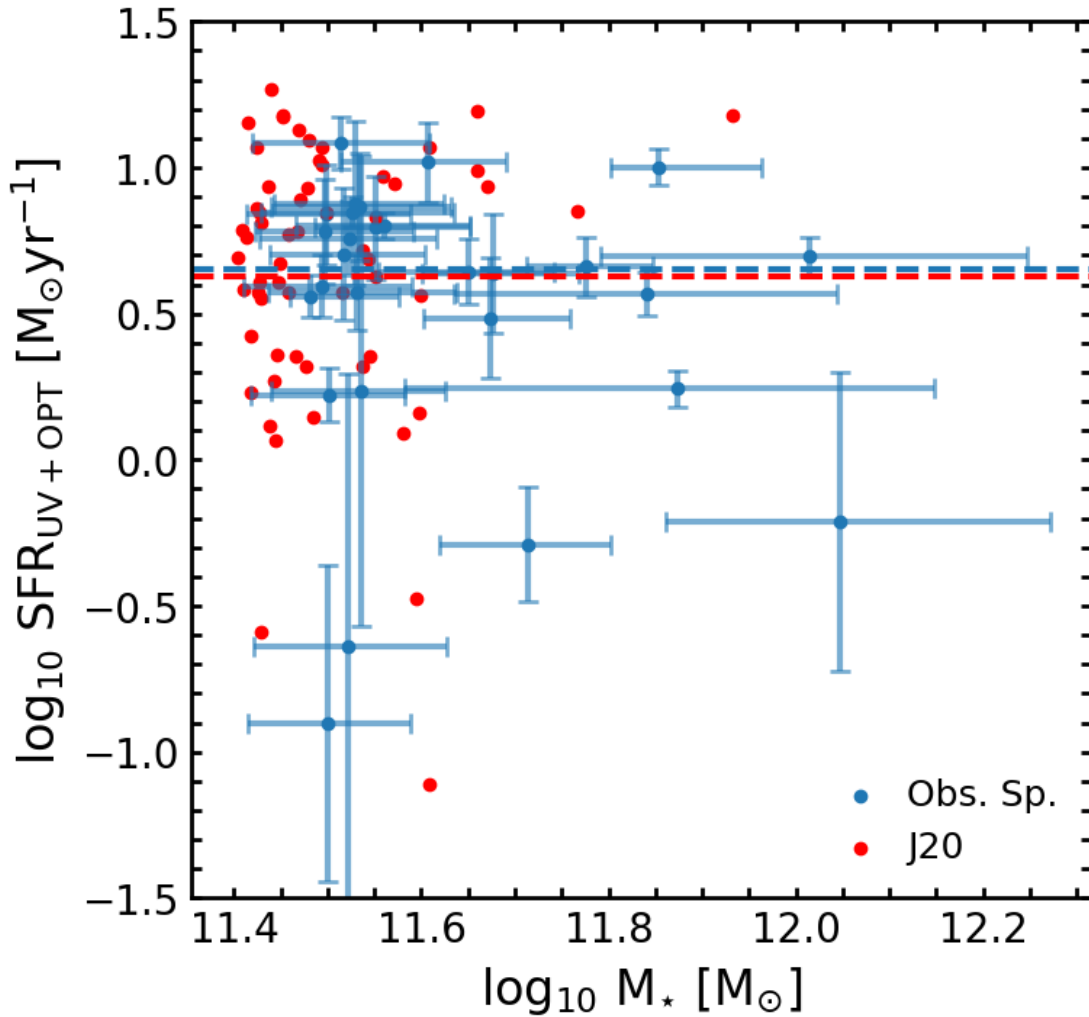
FIGURE 4.3: SFR as a function of stellar mass for massive discs in our observational sample (blue) and the simulated sample of J20 (red). Dashed lines indicate median values. The SFRs from the observations and simulations show comparable median values and distributions. While we omit spheroids for clarity, the medians and distributions for all populations are summarised in Table 4.2.

4.3.2 Star formation rates and atomic gas properties

We proceed by considering the SFRs of our observed massive galaxies. If the predicted formation mechanisms of massive discs in J20 are broadly accurate, then the expectation is that the SFRs in the observed and simulated massive discs should be comparable and that the SFRs in the discs should be significantly enhanced compared to that in the spheroids.

In Figure 4.3, we compare the total SFRs of the observed massive discs calculated using UV and optical photometry (blue) with the corresponding theoretical predictions (where the SFR is calculated as an average over ~100 Myrs) from J20 (red). Both the median values of the observed and theoretical samples (shown using the dashed lines) and the distributions of their SFRs are in good agreement with each other (the spheroids are omitted for clarity). In Table 4.2,

1	2	3	4	5
Morphology	$\log_{10}$ Sim. SFR [$M_\odot$yr^{-1}] [16th • **median** • 84th]	$\log_{10}$ Obs. SFR [$M_\odot$ yr^{-1}] [16th • **median** • 84th]	$\log_{10}$ Sim. sSFR [yr^{-1}] [16th • **median** • 84th]	$\log_{10}$ Obs. sSFR [yr^{-1}] [16th • **median** • 84th]
Discs	0.28 • **0.76** • 1.07	0.23 • **0.65** • 0.86	-11.13 • **-10.68** • -10.36	-11.53 • **-10.94** • -10.67
Spheroids	-0.73 • **0.12** • 0.68	-0.94 • **-0.37** • 0.31	-12.18 • **-11.00** • -10.39	-12.56 • **-11.96** • -11.24

TABLE 4.2: SFRs and sSFRs for massive galaxies of different morphologies (indicated in column 1). In each column we describe the 16th, 50th (i.e. the median) and 84th percentile values from the SFR and sSFR distributions. Columns are as follows: (2) SFRs of simulated massive galaxies from J20 (3) total SFRs of the observed galaxies, calculated using SED-fitting of UV + optical photometry, from the GSWLC (4) sSFRs of simulated massive galaxies from J20 (5) total sSFRs of the observed galaxies. The median values of the simulated and observed SFRs and sSFRs are in reasonably good agreement with each other for the massive disc population.

we summarise the theoretical and observed SFRs of our massive galaxies. For completeness, we also show the specific SFRs (sSFRs) of these systems. Finally, we note that, in a similar vein to what is seen in the predictions of J20, the SFRs and sSFRs of the observed massive discs are significantly elevated compared to that in their spheroidal counterparts.

While the agreement between the observed and theoretical SFRs indicates that the gas masses involved in the star formation events are broadly predicted correctly, we explore empirical constraints on what these gas masses are likely to be. While large area surveys of molecular gas are not available, we explore the HI masses of our massive galaxies using the ALFALFA survey.

None of the massive spheroids are detected in ALFALFA. However, 4 massive discs (out of 92) have ALFALFA detections. In all cases, both the spatial and velocity offsets between the SDSS and the ALFALFA sources are small, indicating reliable matches. The spatial offsets are all less than 15 arcseconds (the average positional accuracy of ALFALFA is ~24 arcseconds), while the velocity offsets (calculated from the spectroscopic redshifts and HI velocities) are within 80 km s^{-1}.

Figure 4.4 shows DECaLS images of these discs, three of which are relaxed and one is disturbed (lower-right hand panel). Figure 4.5 indicates that the HI mass (and corresponding HI fraction, defined as the HI mass divided by the sum of the HI and stellar masses) in the disturbed disc is higher than those in its relaxed counterparts. This is consistent with the idea that the gas is likely brought in by a merger and is then used up to form stars, as this merger-driven starburst progresses and the tidal features fade away. The range of HI masses and fractions in massive galaxies from J20 are shown for comparison and are consistent with that in the disturbed disc.

It is interesting to explore the possible gas fractions of the satellites that trigger the formation of these massive disc galaxies. To do this, we consider the HI content of the disturbed disc (~ $10^{10.6}$ $M_\odot$). If the hypothesis in J20 is correct, then this is likely to be more representative of the original gas mass brought in by the minor merger, since, in the relaxed systems, much of the gas is likely to have been used up by the merger-driven star formation episode before we observe the system. Using the median merger mass ratio that creates the massive discs from
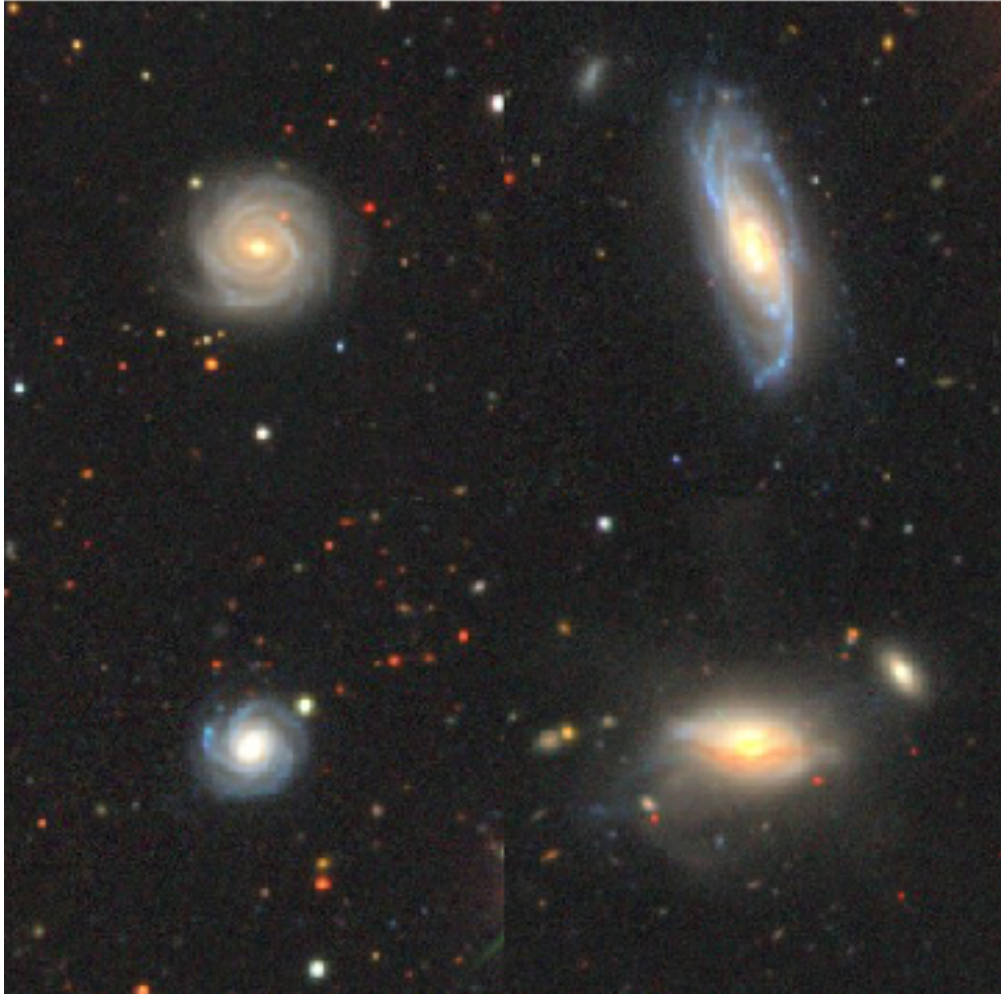
FIGURE 4.4: DECaLS images of the 4 galaxies which have HI detections from the ALFALFA survey. All 4 systems are discs, with only 1 showing evidence of tidal features (lower right-hand panel). This disturbed disc has a high signal-to-noise detection in ALFALFA, while the other three have low S/N detections, due to their lower HI content (see Figure 4.5 below).

J20 (~4.3:1) implies that the HI fraction of the satellite could be between ~39 per cent (if one assumes the lower limit of the HI mass and the upper limit of the stellar mass) and ~76 per cent (if one assumes the upper limit of the HI mass and the lower limit of the stellar mass).

While we caution that these numbers are only indicative they do suggest that the satellites are indeed likely to be gas-rich, consistent with the theoretical predictions. It is worth noting that the satellites themselves have to be relatively massive galaxies. For example, assuming a merger mass ratio of ~4.3:1 and a larger galaxy with a stellar mass of $10^{11.4}$ $M_\odot$, the satellite would have a stellar mass of ~ $10^{10.8}$ $M_\odot$). The lower end of the estimated gas fractions (~39 per cent) is a factor of ~3 higher than the median gas fractions for such systems at low redshift (e.g. Zhang et al., 2009; Catinella et al., 2010; Calette et al., 2018; Hunt et al., 2020). An important caveat in this analysis is that it is based on a very small sample of objects. Dedicated observations, or future surveys of HI which are deeper than those currently available, are needed to gain further
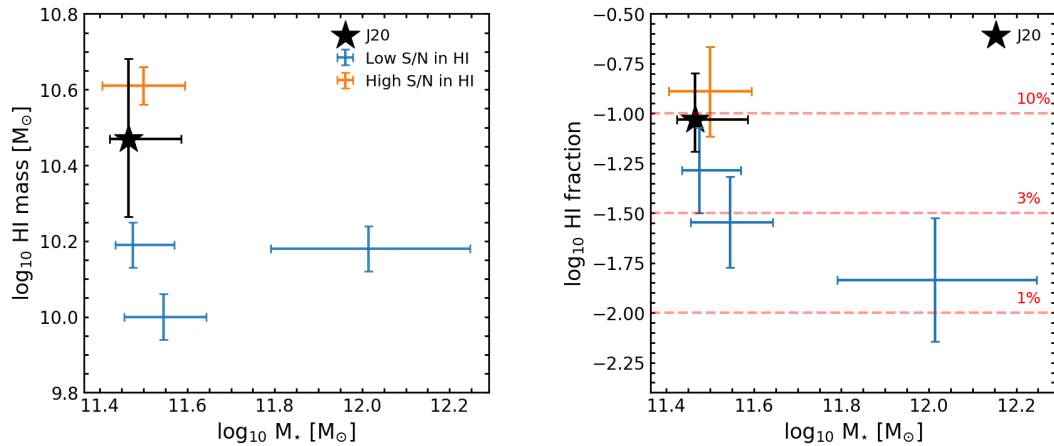
FIGURE 4.5: **Left:** HI mass vs stellar mass for galaxies that have HI detections in the ALFALFA survey. The disturbed disc (lower right-hand panel in Figure 4.4) has a high signal-to-noise (S/N) detection in ALFALFA (orange) while the other three have low S/N detections (blue). **Right:** HI fraction (defined as HI mass divided by the sum of the HI and stellar masses) vs stellar mass for the galaxies in the left-hand panel. The median values and distributions for the HI gas masses and gas fractions from the simulated galaxy sample of J20 are shown in black. The HI mass, and the corresponding HI fraction, in the disturbed disc is higher than those in its relaxed counterparts, consistent with the idea that the gas is likely brought in by a merger and is then used up to form stars as this merger-driven starburst progresses and the tidal features fade away, as suggested by J20.

statistical insights into the empirical gas properties of the massive disc population.

4.4 Summary

In our standard structure-formation paradigm, the morphological transformation of massive galaxies, from discs to spheroids, is thought to be driven largely by merging. Furthermore, the merger activity experienced by galaxies tends to be a strong function of stellar mass, with the most massive galaxies having the richest merger histories. It is, therefore, surprising that a significant minority (>10 per cent) of massive galaxies at the highest stellar masses ($M_\star > 10^{11.4}$ $M_\odot$), are in fact discs. In J20, we have used a cosmological hydrodynamical simulation to show that extremely massive discs can form via one of two channels. The dominant channel is a minor merger between a spheroid and a gas-rich satellite, while the secondary channel involves a disc galaxy which maintains its discy morphology due to an anomalously quiet merger history. In this chapter, we have studied a large statistical sample of nearby massive galaxies, using data from the SDSS, GALEX, DECaLS and ALFALFA surveys to explore whether the observations support the predicted properties and formation mechanisms of massive discs in J20. Our main conclusions are as follows:

- Massive discs account for ~13 per cent of massive galaxies in our observational sample, in good agreement with the predicted fraction of discs in J20 (~11 per cent).

- ~64 per cent of our massive discs show evidence for tidal features (compared to ~31 per cent of our massive spheroids). This is a lower limit because deeper images are likely to reveal more galaxies with tidal features (see Figure 4.1). In contrast, the tidal feature fraction in low-mass discs, in images that have similar depth and seeing, is ~11-17 per cent, depending on the specific morphology of the low-mass disc population in question. The presence of tidal features is therefore significantly elevated in massive discs, by at least a factor of 4 compared to their low-mass counterparts, indicating a significant role for merging in the formation of these systems.

- The major-merger fraction for massive galaxies at low redshift is only a few per cent, with tidal features remaining visible for 2-3 Gyrs at the depth of the DECaLS images. The majority of the interactions seen in our massive discs are therefore likely to be minor mergers (i.e. those with mass ratios greater than ~4:1), which are several times more frequent than their major counterparts. This is consistent with the predictions in J20 that minor mergers are the principal formation mechanism for massive disc galaxies.

- The SFRs of our observed massive discs are in good agreement with their predicted counterparts in J20 and also show the predicted elevation compared to that in the massive spheroids. This suggests that the minor mergers in the massive discs are gas rich, consistent with the hypothesis presented in J20.

- While none of the massive spheroids are detected in HI, four massive discs have HI detections, of which three are relaxed and one is disturbed. The HI mass (and corresponding HI fraction) in the disturbed disc is higher than those in its relaxed counterparts, consistent with the idea that the gas is brought in by a merger, and is then used up to form stars as this merger-driven starburst progresses and the tidal features fade away.

- Combining the HI content of the disturbed disc ($\sim 10^{10.6}$ M$_\odot$), which is likely to be representative of the original gas mass brought in by the merger, and the median merger mass ratio predicted in J20 for the massive discs, suggests that the gas fractions of the accreted satellites are likely to be extremely high (~40 per cent or more). Since the satellites themselves are relatively massive galaxies (e.g. assuming a merger mass ratio of ~1:4 and a larger galaxy with a stellar mass of $10^{11.4}$ M$_\odot$, M$_{sat}$ ~ $10^{10.8}$ M$_\odot$), such gas fractions are a factor of ~3 higher than the median gas fractions for such systems at low redshift. This is consistent with the predictions of J20 that massive discs are formed in gas-rich minor mergers.

In summary, the observed properties of nearby massive discs, in terms of their morphological fractions, SFRs and HI properties are in good agreement with the predictions of J20. This, in turn, suggests that massive disc galaxies in the real Universe are likely to have been formed via the mechanisms described in J20.

Chapter 5

The origin of low-surface-brightness galaxies in the dwarf regime

5.1   Introduction

Our statistical understanding of galaxy evolution is fundamentally driven by objects that are brighter than the surface brightness limits of wide-area surveys. Rapid progress has been made over the last few decades in advancing our comprehension of how galaxies form and evolve over time. The observed multi-wavelength properties of galaxies have been mapped in detail, via large surveys from both ground and space-based instruments (e.g. Beckwith et al., 2006; Bianchi et al., 2017; Blanton et al., 2017; Nayyeri et al., 2017; Aihara et al., 2019). Confrontation of these surveys with simulations in cosmological volumes (e.g. Dubois et al., 2014a; Vogelsberger et al., 2014b; Schaye et al., 2015; Kaviraj et al., 2017) has enabled us to interpret this data and understand the physics of galaxy evolution.

The current consensus from the recent literature is that galaxies form hierarchically, within a ΛCDM framework (e.g. Cole et al., 2000; Bullock et al., 2001; Hatton et al., 2003; Bower et al., 2006; Pipino et al., 2009), with models based on this paradigm broadly reproducing the observed statistical properties of galaxies in contemporary surveys (e.g. Blanton et al., 2017; Aihara et al., 2019). However, notwithstanding the successes of this standard model, our comprehension of galaxy evolution is largely restricted to relatively bright galaxies, that have effective surface brightnesses[1] greater than the surface brightness limits of past wide surveys. For example, in surveys like the SDSS (Abazajian et al., 2009), which has provided much of the discovery space in the nearby Universe, galaxy completeness decreases rapidly at $\langle \mu \rangle_{e,r} > 23$ mag arcsec^{-2} (e.g. Cross and Driver, 2002; Blanton et al., 2005; Driver et al., 2005), where $\langle \mu \rangle_{e,r}$ is the effective

---

[1]The effective surface brightness is defined here as the mean surface brightness within the effective radius.

surface brightness in the *r*-band, dropping to ~10 per cent for $\langle \mu \rangle_{e,r} \sim 24$ mag arcsec^{-2} (e.g Kniazev et al., 2004).

Thus, while our understanding of the evolution of *bright* galaxies has progressed significantly, it is worth considering the significance of 'low-surface brightness' galaxies (LSBGs), defined here as those that fall below the nominal surface brightness limits of past wide-area surveys and which are, therefore, undetectable in these datasets. Both theory (Martin et al., 2019; Kulier et al., 2019) and observational work using small, deep surveys (e.g. McGaugh et al., 1995; Bothun et al., 1997; Dalcanton et al., 1997) indicate that most galaxies are, in fact, fainter than the surface brightness limits of past wide-area surveys. These LSBGs are a heterogeneous population, ranging from massive, diffuse disks to all dwarf galaxies at cosmological distances. Current cosmological simulations indicate that these LSBGs dominate the galaxy number density, comprising more than 85 per cent of objects down to $M_\star \sim 10^7$ $M_\odot$ (Martin et al., 2019) and form a large, natural, empirically-unexplored extension of the population of bright galaxies on which our understanding of galaxy evolution is currently predicated.

The absence of these objects from past datasets has two important consequences. First, our empirical picture of galaxy formation is heavily biased. Second, since our models are statistically calibrated only to the subset of bright galaxies, our understanding of the physics of galaxy evolution remains potentially highly incomplete. It is, therefore, not surprising that many well-known tensions between theory and observation are in the low-surface brightness regime, e.g. the apparent excess of dwarfs in simulations i.e. the substructure problem (Moore et al., 1999; Bullock and Boylan-Kolchin, 2017), the core-cusp problem (de Blok, 2010) and the 'too-big-to-fail' problem (Boylan-Kolchin et al., 2011). A complete understanding of galaxy evolution therefore demands a detailed comprehension of how LSBGs evolve over cosmic time.

LSBGs have seen an explosion of interest in the recent observational literature, driven by individual or small deep pointings (e.g. Kaviraj, 2014b,a; Mihos et al., 2015; Martínez-Delgado et al., 2016; Merritt et al., 2016; Román and Trujillo, 2017b; Leisman et al., 2017; Greco et al., 2018; Kaviraj et al., 2019; Martin et al., 2020) and/or careful reprocessing of relatively shallow surveys to push fainter than their nominal detection limits (e.g. Trujillo et al., 2017; Sedgwick et al., 2019a). While these efforts have started to give us a glimpse of the LSBG regime, the galaxy samples that underpin these studies are not representative of the general population of LSBGs. In particular, the statistical properties of LSBGs in groups (e.g Smith Castelli et al., 2016; Merritt et al., 2016; Román and Trujillo, 2017a,b; Jiang et al., 2019) and the field (e.g Martínez-Delgado et al., 2016; Papastergis et al., 2017; Leisman et al., 2017) remain particularly poorly understood, largely due to the lack of surveys that are both deep and wide. However, the successful detection of LSBGs in sparser environments indicates that they are not a cluster phenomenon and are, in fact, a ubiquitous population that inhabits all regions of the observable Universe.

A burgeoning theoretical literature has explored the mechanisms that form LSBGs. For example, high halo spin (e.g. Amorisco and Loeb, 2016), bursty supernova feedback, which leads to the formation of cored dark matter haloes (e.g. Di Cintio et al., 2017; Chan et al., 2018; Martin et al., 2019), mergers (Wright et al., 2020) or formation from high angular momentum gas (Liao et al., 2019; Tremmel et al., 2019; Di Cintio et al., 2019) have all been suggested as channels for creating LSBGs and 'ultra-diffuse galaxies' (UDGs), which represent the extreme end of the LSBG population at the depth of current datasets. However, it has also been shown that environmental processes like tidal perturbations, the alignment of infalling baryons at early times and galaxy collisions are likely required to fully reproduce the variety and demographics of the LSBG/UDG populations seen in the observations (e.g. Baushev, 2018; Martin et al., 2019; Liao et al., 2019; Carleton et al., 2019; Tremmel et al., 2019; Cardona-Barrero et al., 2020). It is worth noting that LSBGs (including the more extreme UDG population) are predicted to form in all environments including the field (e.g. Di Cintio et al., 2017; Chan et al., 2018; Jiang et al., 2019; Liao et al., 2019; Wright et al., 2020), consistent with the findings of recent observational work.

A statistical comparison between observation and theory in the LSBG regime requires a hydrodynamical simulation in a cosmological volume. The hydrodynamics are essential for 2D predictions for baryons (which determines the surface brightness of the mock galaxies), while a cosmological volume is required for making statistical predictions for the properties of the LSBGs as a whole, across the full spectrum of cosmological environments (field, groups etc). In recent work, Martin et al. (2019) have performed a comprehensive study of the formation of relatively massive LSBGs, using the Horizon-AGN cosmological simulation (Kaviraj et al., 2017). They showed that, in the stellar mass range $M_\star > 10^9$ $M_\odot$, the formation of LSBGs and their eventual divergence from their high surface brightness counterparts, is triggered by a period of more intense star formation activity in the early ($z > 2$) Universe. This leads to more intense supernova feedback, which moves gas from the central regions towards the outskirts, flattening their gas profiles, but typically does not remove gas completely from the system. These shallower gas profiles then lead to shallower stellar profiles which are more susceptible to tidal processes and ram pressure stripping. Over time, these processes 'heat' the stellar and gas content of the LSBGs, increasing their effective radii further, and quench the galaxies, both of which lead to their low surface brightnesses at the present day.

While Martin et al. (2019) has offered key insights into the formation of relatively massive LSBGs, the range of stellar masses that can be probed by Horizon-AGN (and other simulations with similar box sizes such as EAGLE (Schaye et al., 2015) and Illustris (Vogelsberger et al., 2014a)) is limited by both its stellar mass resolution ($M_\star \sim 10^{8.5}$ $M_\odot$) and spatial resolution (~1 kpc). The formation of lower-mass i.e. dwarf LSBGs, which is the regime in which most observational LSBG studies are focused, requires a cosmological simulation with much better mass and spatial resolution ideally in the tens of parsecs. Recall that the scale height of the

Milky Way is ∼300 pc (e.g. Kent et al., 1991; López-Corredoira et al., 2002; McMillan, 2011), so much higher spatial resolution is needed to properly resolve dwarfs.

In this study, we use the `NewHorizon` cosmological hydro-dynamical simulation, which has stellar mass and maximum spatial resolutions of 10^4 $M_\odot$ and 40 pc respectively, to study the origin of low-mass LSBGs, drilling down deep into the dwarf regime. `NewHorizon` offers better mass and spatial resolution than any other simulation with a comparable volume, making it ideally suited for this exercise. Our aims are two fold. First, we study the surface brightness vs. stellar mass plane, for galaxies down to stellar masses of $M_\star \sim 10^{6.5}$ $M_\odot$, and compare the position of the main locus of galaxies to existing observational data. Second, we study how different processes (e.g. feedback from supernovae and active galactic nuclei (AGN), ram pressure, tidal perturbations and galaxy mergers) drive the origin of dwarf LSBGs and produce the large observed spread in galaxy surface brightness at fixed stellar mass.

This chapter is structured as follows. In Section 5.2, we briefly describe the `NewHorizon` simulation. In Section 5.3, we study the properties of galaxies in the surface brightness vs. stellar mass plane in the nearby Universe. In Section 5.4, we study how different processes contribute to the position of galaxies in the surface brightness vs. stellar mass plane at low redshift. In Section 5.5, we explore why a minority of galaxies depart strongly from the main locus of objects that hosts the majority of galaxies in this plane. We summarise our findings in Section 5.6.

5.2 Simulation

We use the `NewHorizon` cosmological, hydro-dynamical simulation (Dubois et al., 2020) [2], which is a high-resolution zoom of a region within the Horizon-AGN simulation (Dubois et al., 2014a; Kaviraj et al., 2017, H-AGN hereafter). The simulation has been run down to $z = 0.25$. NewHorizon employs the adaptive mesh refinement code RAMSES (Teyssier, 2002b). Initial conditions are taken from H-AGN, which is a cube with $L_{box} = 100$ h^{-1} comoving Mpc, using 1024^3 uniformly-distributed cubic cells with a constant mass resolution, using `MPGrafic`. For `NewHorizon`, this grid is resampled at higher resolution (using 4096^3 uniformly-distributed cubic cells), with the same cosmology (Ω_m=0.272, Ω_b=0.0455, Ω_Λ=0.728, H_0=70.4 km s^{-1} Mpc^{-1} and n_s=0.967 (Komatsu et al., 2011b)).

The high-resolution zoom has a volume of ∼(16 Mpc)^3, taken from an average density region of H-AGN. It has a dark-matter (DM) resolution of 10^6 $M_\odot$ (compared to 8×10^7 $M_\odot$ for H-AGN), stellar mass resolution of 10^4 $M_\odot$ (compared to 2×10^6 $M_\odot$ in H-AGN) and a maximum spatial resolution of 34 pc (compared to 1 kpc in H-AGN). This makes `NewHorizon` the simulation

---

[2]new.horizon-simulation.org

with the highest currently available spatial and stellar mass resolution in a cosmological volume and an ideal tool with which to study the dwarf galaxy population. Note that, given that the zoom region used to create `NewHorizon` has an average density, this simulation does not contain high-density environments like clusters.

5.2.1 Star formation and stellar feedback

Gas cools via the initial mixture of Hydrogen and Helium, which is progressively enriched by metals produced by stellar evolution (Sutherland and Dopita, 1993; Rosen and Bregman, 1995). We assume photoionized equilibrium, with an ambient UV background after the Universe is re-ionized at $z = 10$ (Haardt and Madau, 1996). Star formation occurs in gas with a hydrogen number density greater than $n_H >10$ H cm^{-3} and a temperature lower than 2×10^4 K, following a Schmidt-Kennicutt relation (Schmidt, 1959; Kennicutt, 1998). The efficiency depends on the local turbulent Mach number and virial parameter $\alpha=2E_k/|E_g|$, where E_k is the turbulent energy of the gas and E_g is the gas gravitational binding energy (Kimm et al., 2017). A probability of forming a star particle of mass $M_{\star,res}=10^4$ M$_\odot$ is drawn at each time step according to the Schmidt-Kennicutt law.

Each star particle represents a coeval collection of stars with different masses. 31 percent of the stellar mass of this star particle (corresponding to stars more massive than 6 M$_\odot$) is assumed to explode as Type II supernovae, 5 Myr after its birth. The fraction is calculated using a Chabrier initial mass function, with upper and lower mass limits of 150 M$_\odot$ and 0.1 M$_\odot$ (Chabrier, 2005).

Supernova (SN) feedback is modelled in the form of both energy and momentum, ensuring that the final radial momentum is accurately captured during the snowplough phase of the expansion (Kimm and Cen, 2014). Each supernova has an initial energy of 10^{51} erg and a progenitor mass of 10 M$_\odot$. In addition, pre-heating of the ambient gas by ultraviolet radiation from young OB stars is taken into account, by augmenting the final radial momentum from supernovae following Geen et al. (2015).

5.2.2 Supermassive black holes and black-hole feedback

Supermassive black holes (SMBHs) are considered to be sink particles, which accrete gas and impart feedback to their local surroundings, according to some fraction of the rest-mass energy of the accreted material. SMBHs form in regions with gas density larger than the threshold of star formation, with a seed mass of 10^4 M$_\odot$. New SMBHs are not allowed to form at a distance less than 50 kpc from other existing black holes. A dynamical gas drag force is applied to the SMBHs (Ostriker, 1999) and two SMBHs are allowed to merge if the distance between them is

smaller than 4 times the cell size, and if the kinetic energy of the binary is less than its binding energy.

Black holes (BHs) accrete at the Bondi-Hoyle-Lyttleton accretion rate, with its value capped at Eddington (Hoyle and Lyttleton, 1939; Bondi and Hoyle, 1944). They release energy back into the gas, both via a jet 'radio' mode and a thermal quasar mode, for accretion rates below and above 1 percent of the Eddington rate respectively (Dubois et al., 2012). SMBH spins are evolved self-consistently through gas accretion in the quasar mode and coalescence of black hole binaries (Dubois et al., 2014c). This modifies the radiative efficiencies of the accretion flow, following the models of thin Shakura & Sunyaev accretion discs, and the corresponding Eddington accretion rate, mass-energy conversion, and bolometric luminosity of the quasar mode (Shakura and Sunyaev, 1973). The quasar mode imparts a constant 15 percent of the bolometric luminosity as thermal energy back into the surrounding gas, while the radio mode has a spin-dependent variable efficiency and a spin up/down rate that follows results from simulations of magnetically choked accretion discs (McKinney et al., 2012).

5.2.3 Selection of galaxies and construction of merger trees

DM halos are identified using the AdaptaHOP algorithm (Aubert et al., 2004; Tweed et al., 2009), which efficiently removes subhalos from main structures and counts the fractional number of low-resolution DM particles within the DM virial radius. Galaxies are identified in a similar fashion using the HOP structure finder applied directly on star particles (Eisenstein and Hut, 1998). The difference with AdaptaHOP lies in the fact that HOP does not remove substructures from the main structure, since this would result in star-forming clumps being removed from galaxies. We produce merger trees for each galaxy in the final snapshot ($z = 0.25$), with an average timestep of ~ 15 Myr, which allows us to track the main branch progenitors of each galaxy with high temporal resolution.

Given that `NewHorizon` is a high resolution zoom of H-AGN, we also need to consider the DM purity of galaxies. It is possible for higher mass DM particles to enter the high resolution region of `NewHorizon` from the surrounding lower-resolution regions and, given the large mass difference, interact in unusual ways with the galaxies that they encounter. The vast majority of galaxies affected by low DM purity exist at the outer edge of the `NewHorizon` sphere. In the analysis that follows, we only consider galaxies with DM halos that are more than 99 per cent pure. We note that our results remain unchanged if we use the sample that is 100 per cent pure. We proceed with the 99 per cent pure sample because it puts our analysis on a firmer statistical footing.

5.2.4 Local environment

In some of our analysis below we explore details of the environment of galaxies in the cosmic web (e.g. their distances to nodes and filaments), using the persistence-based filament tracing algorithm `DisPerSE` (Sousbie, 2011), which uses the density field computed via a delaunay tessellation (Schaap and van de Weygaert, 2000) of the DM halo distribution. We choose a persistence of 4 sigma. `DisPerSE` identifies ridges in the density field as special lines that connect topologically robust pairs of nodes. These ridges compose the filament network of the cosmic web, and the set of all segments defining these ridges are referred to as the 'skeleton' (Pogosyan et al., 2009). The distance to the nearest filament and node is computed for each DM halo to form a filament catalog. We refer readers to Sousbie (2011) and Sousbie et al. (2011) for more details of the `DisPerSE` algorithm and to Dubois et al. (2014a) and Laigle et al. (2018) for an implementation of this algorithm on H-AGN.

5.2.5 Calculation of surface brightness

We obtain the intrinsic (i.e. unattenuated) surface brightness for each galaxy using the intensity-weighted central second-moment of the stellar particle distribution (e.g. Bernstein and Jarvis, 2002). We calculate the surface brightness in multiple orientations (*xy*, *xz* and *yz*) and use the mean value in our study. The procedure for calculating the surface brightness of individual galaxies is as follows.

We first obtain the intrinsic *r*-band magnitudes for each star particle that makes up the galaxy. To do this we obtain the full spectral energy distribution (SED) from a grid of Bruzual and Charlot (2003, BC03 hereafter) simple stellar population (SSP) models corresponding to the closest age and metallicity of each star particle. We redshift each BC03 template to the redshift of the galaxy and convolve the redshifted BC03 templates with the response curve for the SDSS *r*-band filter. We then weight by the particle mass to obtain the luminosity contribution of each star particle, and obtain the apparent *r*-band magnitude by converting the flux to a magnitude and adding the distance modulus and zero point.

We then obtain the second moment ellipse as follows. We first construct the covariance matrix of the intensity-weighted central second-moment for the star particles,

$$\text{cov}[I(x, y)] = \begin{bmatrix} Ix^2 & Ixy \\ Ixy & Iy^2 \end{bmatrix}, \tag{5.1}$$

where I is the flux of each star particle and x and y are the projected positions from the barycentre in arc seconds. We obtain major ($\alpha = \sqrt{\lambda_1/\Sigma I}$) and major ($\beta = \sqrt{\lambda_2/\Sigma I}$) axes of
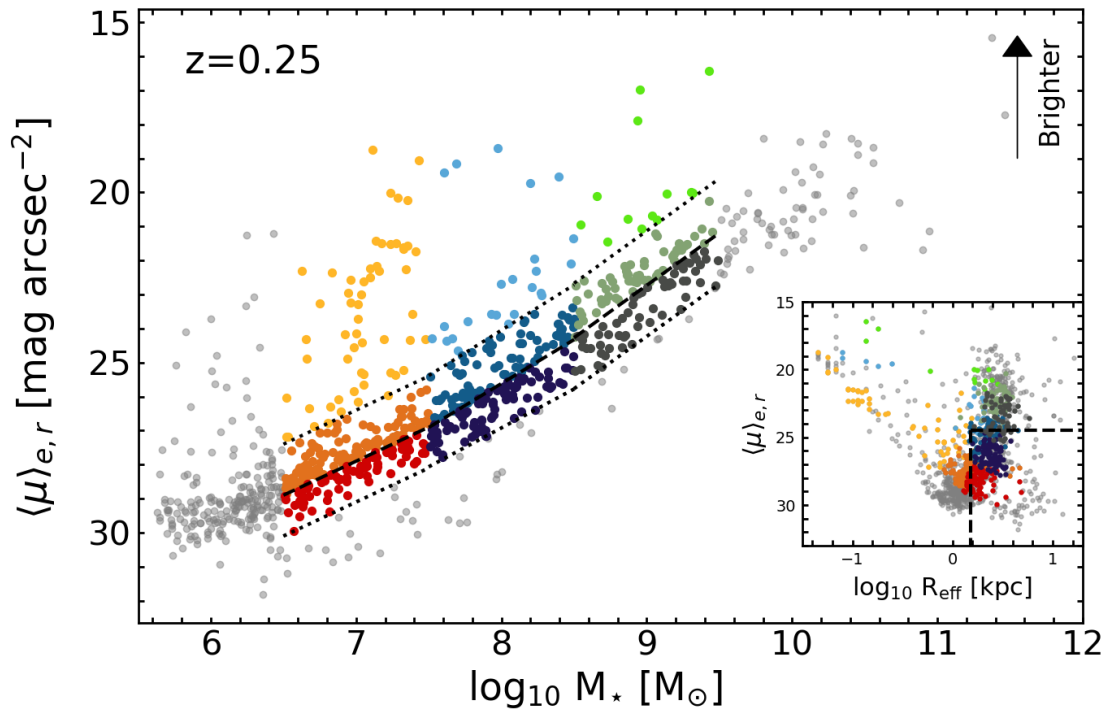
FIGURE 5.1: Intrinsic effective surface brightness vs. stellar mass for galaxies in the `NewHorizon` simulation. The bulk of the galaxy population resides on a well-defined locus with a large spread of ~3 mag, with a minority (~10-20 per cent, depending on the stellar mass range in question) departing strongly from the main locus towards higher surface brightness. The dotted lines indicate the limits of the main locus, defined by eye. The coloured points indicate different zones of the locus (described in Section 5.3) which we consider for our analysis. The inset shows the effective radius vs. intrinsic effective surface brightness for the `NewHorizon` galaxies. The dashed lines in the inset indicate the typical boundaries that demarcate 'ultra-diffuse galaxies' (UDGs) in the literature ($R_{eff} > 1.5$kpc and $\langle\mu\rangle_{e,r} > 24.5$). While UDGs are sometimes considered extreme or anomalous at the depth of current datasets, they actually dominate the predicted dwarf population, and will be routinely visible in future surveys like LSST.

the ellipse from the covariance matrix, where λ_1 and λ_2 are its eigenvalues and ΣI is the total flux, and find the scaling factor, R, which scales the ellipse so that it contains half the total flux of the object. Finally, we calculate the mean surface brightness within the effective radius, $\langle\mu\rangle_{e,r} = m - 2.5\log_{10}(2) + 2.5\log_{10}(A)$, where $A = R^2\alpha\beta\pi$ and m is the r-band apparent magnitude of the object.

5.3 The surface brightness vs. stellar mass plane in the nearby Universe

Figure 5.1 shows the intrinsic surface brightness vs. stellar mass plane for galaxies in `NewHorizon` at $z = 0.25$. The majority of galaxies populate a locus in this plane, with a large spread of ~ 3

mag arcsec^{-2}. A small minority of galaxies scatter off this locus towards high surface brightnesses. In order to understand the origin of galaxies that reside in different parts of the surface brightness vs. stellar mass plane at $z = 0.25$, we split our galaxies into three mass bins. The 'low', 'intermediate' and 'high' mass bins cover the mass ranges $10^{6.5}$ M$_\odot \geq$ M$_\star > 10^{7.5}$ M$_\odot$, $10^{7.5}$ M$_\odot \geq$ M$_\star > 10^{8.5}$ M$_\odot$ and $10^{8.5}$ M$_\odot \geq$ M$_\star > 10^{9.5}$ M$_\odot$ respectively.

We define the limits of the main locus of objects by eye as the area where galaxies are closely clustered together. This is indicated by the dotted lines in Figure 5.1. Within each mass bin, we then split the galaxy population into three zones. We use a straight line that bisects the region between the two dotted lines in each mass bin to define the 'lower' and 'upper' zones, with galaxies brighter than the upper dotted line classified as 'off-locus'. Note that surface brightness increases towards the upper end of Figure 5.1. Thus, the upper locus galaxies represent the population that is brighter in surface brightness at $z = 0.25$, while the lower locus galaxies represent their fainter counterparts. These zones and mass bins are indicated using the different colours in Figure 5.1, where colour designates the mass bin and the shade represents the position of the galaxy (lower, upper or off) on the locus. Due to the small number of galaxies, and since this regime was comprehensively explored in Martin et al. (2019), we do not study objects at the highest stellar masses (M$_\star > 10^{9.5}$ M$_\odot$). We also do not study galaxies which have M$_\star < 10^{6.5}$ M$_\odot$ because their progenitors are not massive enough to be well-resolved at early epochs.

The inset in Figure 5.1 shows the intrinsic surface brightness vs. effective radius for the `NewHorizon` galaxy population. The dashed lines indicate the typical values that are used to identify 'ultra-diffuse galaxies' (UDGs; e.g. Koda et al., 2015; van Dokkum et al., 2015c; Conselice, 2018; Laporte et al., 2019), which form the faint end of the LSBG population that is detectable at the surface brightness limits of past/current datasets. These systems are sometimes considered to be potentially extreme or anomalous, due to their low surface brightnesses and extended nature. A variety of formation mechanisms have been proposed for their formation, such as the puffing up of 'normal' dwarfs due to internal feedback processes (e.g. Amorisco and Loeb, 2016; Di Cintio et al., 2017) and the possibility that UDGs (particularly those in clusters) may be 'failed' galaxies with anomalously low star formation efficiencies (e.g. van Dokkum et al., 2015a,d; Koda et al., 2015).

However, the inset in Figure 5.1 indicates that a large number of dwarf galaxies in `NewHorizon`, particularly in the low and intermediate mass bins, have surface brightnesses and effective radii that make them consistent with the definition of UDGs in the observational literature. UDGs are, therefore, a normal component of the dwarf galaxy population at low surface brightnesses. Note that since `NewHorizon` does not contain any clusters, a clear prediction is that UDGs should exist in large numbers in groups and the field and should be routinely detectable in new and future deep surveys such as the Hyper Suprime-Cam Subaru Strategic Program (HSC-SSP Aihara et al., 2019) and the Legacy Survey of Space and time (LSST) on the Vera C. Rubin

Observatory (Robertson et al., 2019). In Figure 5.2 we present mock images of typical galaxies that occupy different regions of the locus, created using the `SKIRT9` code (Baes and Camps, 2015), which employs full radiative transfer based on the stars and gas within a galaxy.

While we study the galaxy population in terms of intrinsic surface brightness for our analysis in Sections 5.4 and 5.5, we use the attenuated surface brightness for our comparison to observations below. In Figure 5.3 we compare the predicted surface brightness vs. stellar mass plane in `NewHorizon` to that from recent work that uses the SDSS Stripe 82, which is ~2 mags deeper than standard-depth SDSS imaging (Sedgwick et al., 2019b,a). Sedgwick et al. use a novel technique that allows them to identify LSBGs that do not appear in the pipeline-constructed galaxy catalogue in the IAC Stripe 82 Legacy Project (Fliri and Trujillo, 2016) because they are too faint. They achieve this by identifying a sample of galaxies using core-collapse supernovae (CCSNe). Using custom settings in SExtractor (Bertin and Arnouts, 1996) they then extract the host galaxies of these CCSNe, many of which are not detected by the original SDSS Stripe 82 pipeline or by the IAC Stripe 82 legacy survey. The resultant sample is free of incompleteness in surface brightness in the stellar mass range $M_\star > 10^8$ $M_\odot$, with a host being identified for all 707 CCSNe candidates at $z < 0.2$. Of this sub-sample, 251 are spectroscopically confirmed CCSNe, with the remainder classified from the shape of their light-curves (see Sako et al., 2018). This sample is well-suited to a comparison with `NewHorizon`, both due to its high completeness at low surface brightness and also because we can relatively easily model the selection function and apply it to our simulated dataset.

Since the detectability of the Sedgwick et al. (2019a) galaxies depends on them hosting CCSNe, and therefore hosting star formation activity, we restrict our comparison to a subset of star-forming `NewHorizon` galaxies. The associated selection probability is correlated with the star formation rate (SFR), because the SFR determines the rate of CCSNe. We create a matching sample to the one from Sedgwick et al. (2019a) by drawing galaxies with a weight proportional to the normalised probability distribution in SFR. For the comparison in the $M_\star - \langle\mu\rangle_e$ plane, we calculate the surface brightness of each `NewHorizon` galaxy as described in Section 5.2.5. We additionally implement dust attenuation via a screen model using the SUNSET code (see Kaviraj et al., 2017). Figure 5.3 shows that the predicted surface brightness vs. stellar mass plane in `NewHorizon` corresponds well to that in the observations in the stellar mass range where the Sedgwick et al. galaxies are complete (recall that the simulation is not calibrated to produce galaxy surface brightnesses). The flattening seen in the observations is due to high levels of incompleteness at $M_\star < 10^8$. The good overlap between the `NewHorizon` galaxies and the Sedgwick et al. data suggests that, while the prescriptions used to describe baryonic processes in `NewHorizon` (e.g. SN feedback) are largely tuned to higher mass galaxies, they offer a reasonable representation of these processes also in the low-mass regime.
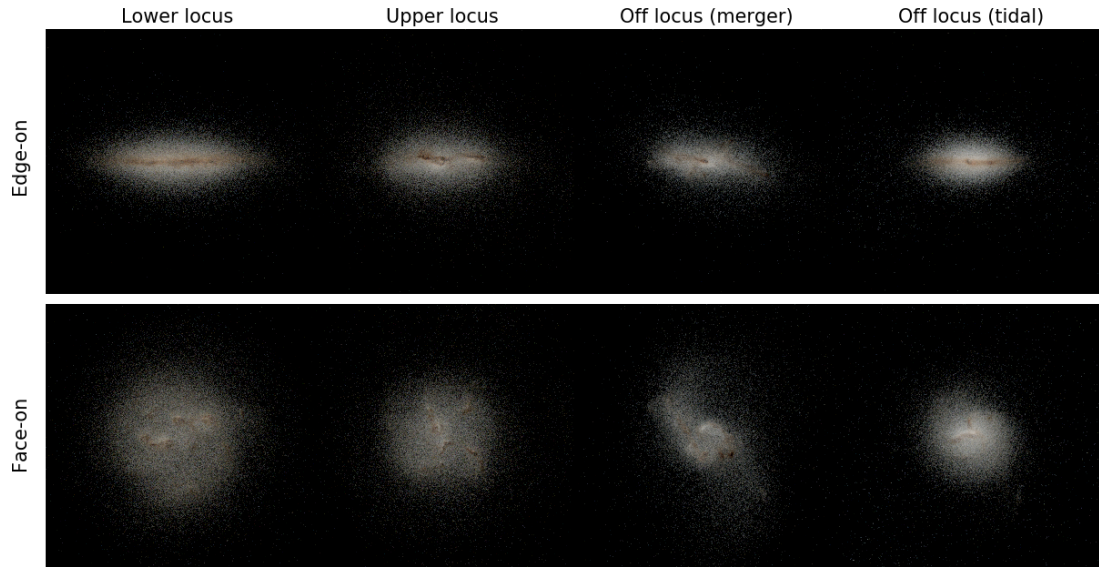
FIGURE 5.2: Mock *gri* images of dwarf galaxies in the `NewHorizon` simulation, created using the SKIRT9 code. Each column shows a typical galaxy in one of the zones on the main locus of objects – a lower and upper locus galaxy and two off-locus systems produced via tidal perturbations and mergers respectively (see Section 5.5 for an exploration of how off-locus galaxies form). The top and bottom rows show edge-on and face-on projections for each galaxy respectively. Galaxies in `NewHorizon` tend to become more compact as they move towards higher surface brightness (i.e. as we move from lower to off-locus systems).

Finally, it is worth noting that the surface-brightness limits of many past benchmark wide-area surveys lead to high levels of incompleteness in the low-mass regime. The dotted lines in Figure 5.3 indicate the galaxy completeness limits for standard-depth SDSS imaging in the local Universe (Blanton et al., 2005). Note that no evolution correction is applied to modify these completeness limits for $z = 0.25$ (the redshift of the `NewHorizon` galaxies). At an effective surface brightness of 24 mag arcsec^{-2} the galaxy completeness in SDSS is only ~10 per cent. Indeed, the `NewHorizon` locus indicates that at $M_\star < 10^8$ M$_\odot$, the overwhelming majority of galaxies in the nearby Universe are undetectable in surveys like the standard-depth SDSS, with *only* those objects that depart strongly from the locus towards very high surface brightnesses likely to be present in such datasets at all. As we show in Section 5.5, these off-locus systems host anomalous levels of star formation triggered by a recent interaction, making them highly unrepresentative of the general galaxy population in these mass regimes. Therefore, caution needs to be exercised about drawing conclusions about galaxy evolution in general using low-mass galaxies that are detected in shallow, wide-area surveys on which our understanding of the extra-galactic Universe is currently predicated. It is worth noting that future deep-wide surveys like the HSC-SSP and LSST (which have limiting surface brightnesses of ~31.5 mag arcsec^{-2} in their deepest layers), should offer 100 per cent completeness for galaxies at least down to $M_\star \sim 10^7$ M$_\odot$ in the nearby Universe, providing a revolutionary increase in discovery space over past wide surveys like the SDSS.
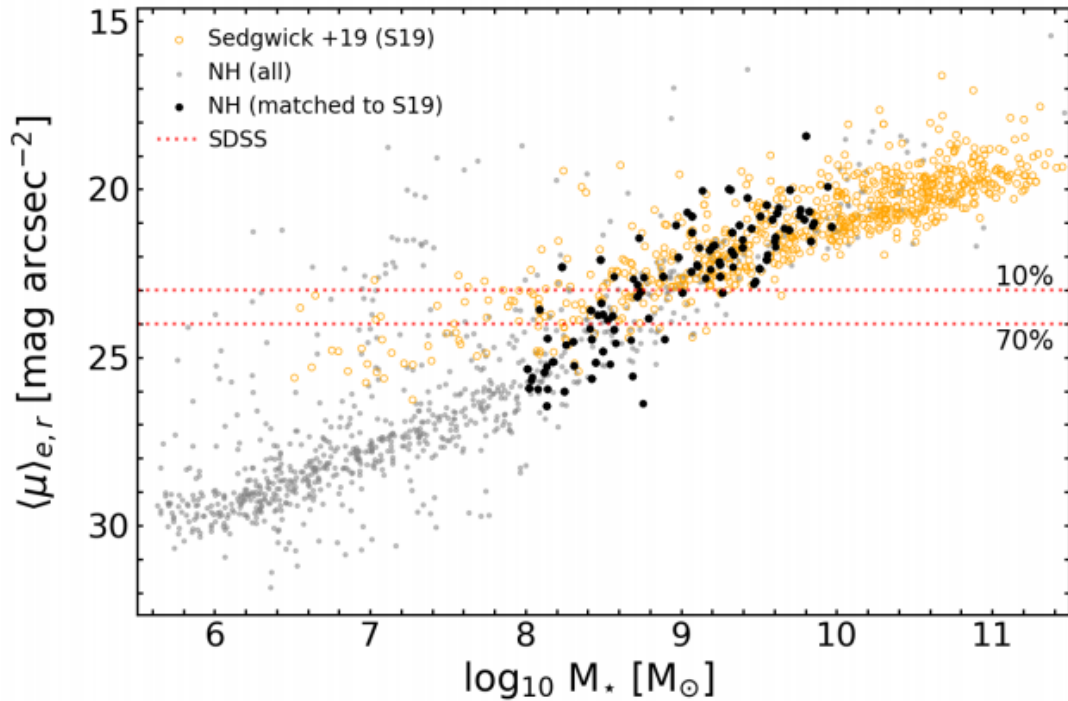
FIGURE 5.3: Surface brightness (including dust attenuation) vs. stellar mass in the `NewHorizon` simulation. Grey points indicate the entire galaxy population of `NewHorizon`, open yellow points indicate galaxies from Sedgwick et al. (2019b) and black points are `NewHorizon` galaxies that are selected to match the 2D $M_\star - z$ distribution of Sedgwick et al. (2019b). The predicted surface brightness vs. stellar mass plane in `NewHorizon` corresponds well to that in the observations, in the stellar mass range where the Sedgwick et al. galaxies are complete (recall that the simulation is not calibrated to produce galaxy surface brightnesses). The red dotted lines indicate the 70% and 10% completeness limits from the SDSS (see e.g. Table 1 in Blanton et al., 2005). The detectability of galaxies in benchmark wide area surveys like the SDSS decreases rapidly in the dwarf galaxy regime. For example, at $M_\star < 10^8$ $M_\odot$, the overwhelming majority of galaxies in the Universe lie below the surface brightness thresholds of surveys like the SDSS, with only those galaxies that depart strongly from the locus likely to be detectable in these datasets.

5.4 Galaxy evolution as a function of surface brightness: the impact of different processes

The analysis that follows studies the impact of different processes on the progenitors of galaxies in the different zones described in Figure 5.1, in order to explore how this main locus of objects forms over cosmic time. Recall that we split the locus into 'low', 'intermediate' and 'high' mass bins that cover the mass ranges $10^{6.5}$ $M_\odot \geq M_\star > 10^{7.5}$ $M_\odot$, $10^{7.5}$ $M_\odot \geq M_\star > 10^{8.5}$ $M_\odot$ and $10^{8.5}$ $M_\odot \geq M_\star > 10^{9.5}$ $M_\odot$ respectively. Each mass bin then split into upper, lower and off-locus zones. The upper and lower zones are defined by the brighter and fainter halves of the locus respectively and off-locus objects are those that scatter to higher surface brightnesses beyond the upper locus. In all the plots that follow, the colour coding of the median lines and error regions corresponds to the colours of the zones in Figure 5.1. Given the small number of

off-locus galaxies in any mass bin we do not show error regions for this population for clarity. In this section, we focus on galaxies that reside on the main locus. We study the formation of off-locus galaxies in Section 5.5.

We begin by exploring, in Figures 5.4, 5.5 and 5.6, the evolution of the median stellar mass, effective radius and surface brightness of galaxies in different zones within the locus across cosmic time. At a given stellar mass, galaxies in the lower locus show a stellar assembly bias relative to those in the upper locus, in the sense that their stellar mass assembly takes place at earlier epochs, as shown in Figure 5.4. The median effective radius of galaxies (Figure 5.5) in the lower locus increases faster than their upper locus counterparts at all epochs, including the epoch where the stellar assembly bias is most pronounced. It is worth noting that starbursts typically add new stars to the central regions of galaxies and thus act to reduce the effective radius, opposite to the trend seen in Figure 5.5. This suggests that, in the early Universe, the processes that drive the stellar assembly bias are also responsible for the differential evolution in median effective radius between the upper and lower locus galaxies.

Figure 5.6 shows the evolution of surface brightness for galaxies in different zones of the locus. The eventual divergence in surface brightness between the upper and lower locus populations (in all mass bins) is delayed compared to that in the stellar mass and effective radius, because the increase in radius is initially compensated for by the more rapid buildup of stellar mass. It is worth noting that the point at which the divergence in surface brightness takes place shows a dependence on stellar mass, with the divergence taking place later at higher stellar masses. This suggests that the depth of the potential well provides a stabilising influence against the processes that drive the surface brightness divergence between upper and lower locus galaxies.

Both these points imply that the width of the locus i.e the surface brightness separation between the upper and lower locus galaxies is likely to be driven by the assembly history of galaxies, with those forming their stellar mass earlier residing at fainter surface brightnesses at the present epoch. Therefore, in order to explain the position of galaxies in the locus, we need to understand the processes responsible for the divergence in stellar mass and effective radius of the upper and lower locus populations. These processes can be either internal or external. Internal mechanisms include feedback from either SN or AGN (or both). External processes include tidal perturbations (including mergers) and ram pressure. In the sections below, we consider how each of these processes affect galaxies, in order to identify the principal processes that determine the position of galaxies in the locus at $z = 0.25$.
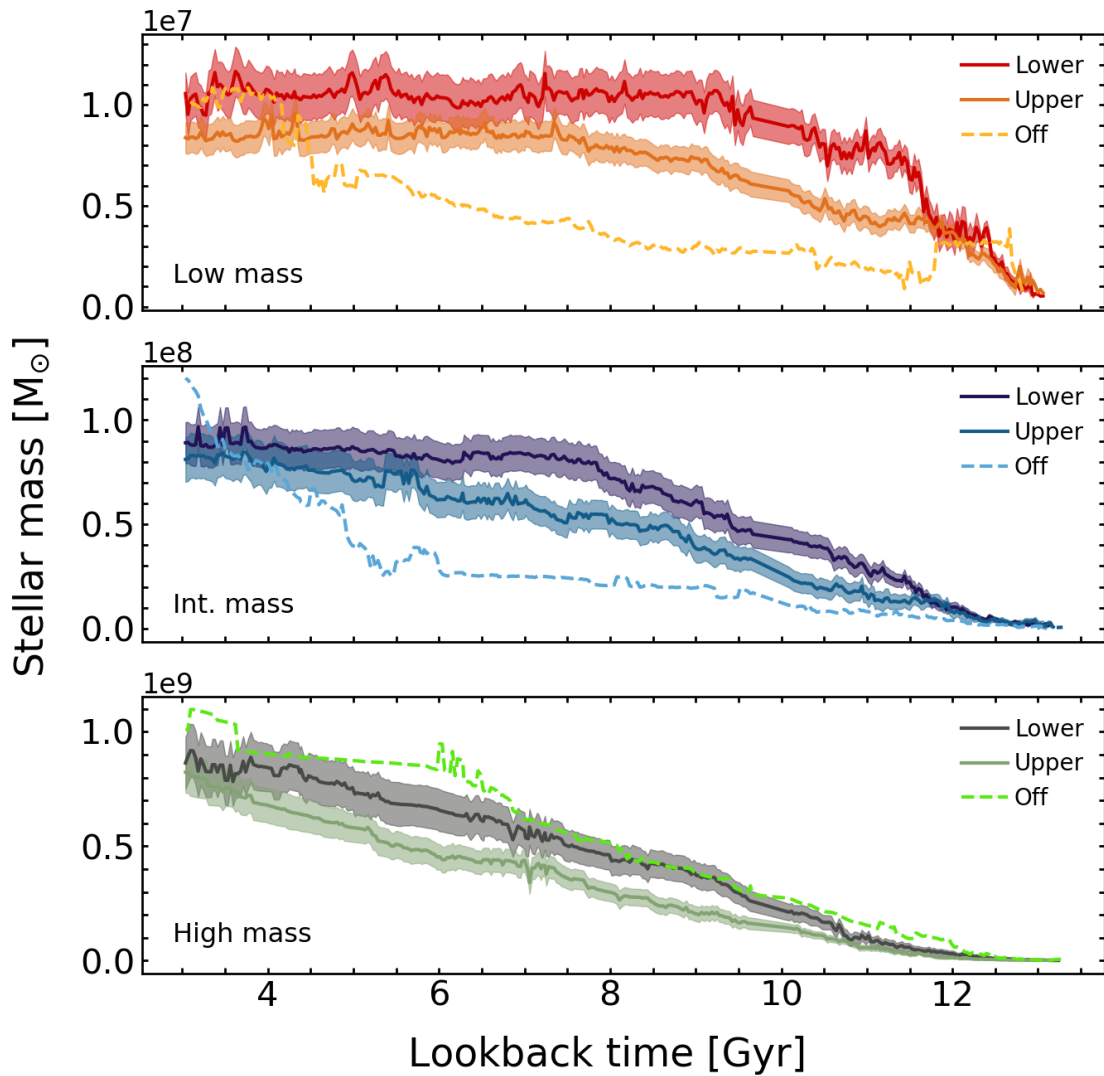
FIGURE 5.4: Evolution of the median stellar mass with look-back time. The shaded regions show the associated uncertainties. The top, middle and bottom panels represent the low ($10^{6.5}$ $M_\odot \geq M_\star > 10^{7.5}$ $M_\odot$), intermediate ($10^{7.5}$ $M_\odot \geq M_\star > 10^{8.5}$ $M_\odot$) and high ($10^{8.5}$ $M_\odot \geq M_\star > 10^{9.5}$ $M_\odot$) mass bins respectively. The colour coding indicates the upper, lower and off locus galaxy populations. Recall that lower locus galaxies represent the population that is fainter in surface brightness at $z = 0.25$, while the upper locus galaxies represent their brighter counterparts. Regardless of the mass bin in question, lower locus galaxies form their stars at earlier epochs than their upper locus counterparts. However, this stellar assembly bias takes place later at higher stellar masses.
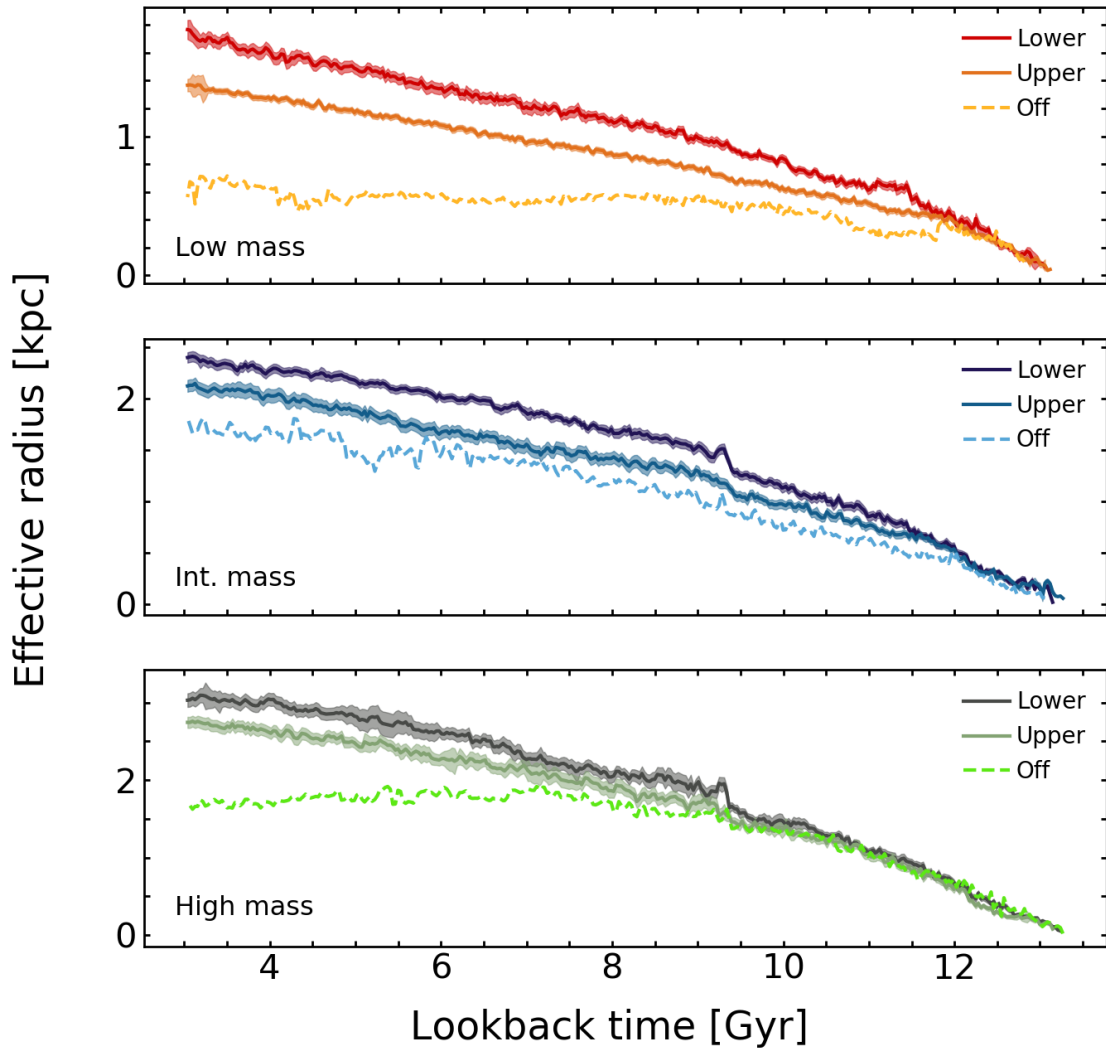
FIGURE 5.5: Evolution of the median effective radius of galaxies with look-back time. The shaded regions show the associated uncertainties. The top, middle and bottom panels represent the low ($10^{6.5}$ $M_\odot \geq M_\star > 10^{7.5}$ $M_\odot$), intermediate ($10^{7.5}$ $M_\odot \geq M_\star > 10^{8.5}$ $M_\odot$) and high ($10^{8.5}$ $M_\odot \geq M_\star > 10^{9.5}$ $M_\odot$) mass bins respectively. The colour coding indicates the upper, lower and off locus galaxy populations. Recall that lower locus galaxies represent the population that is fainter in surface brightness at $z = 0.25$, while the upper locus galaxies represent their brighter counterparts. In all mass bins, lower locus galaxies increase their effective radii faster than their upper locus counterparts.

5.4.1 Differential supernova feedback at early epochs - initiating the divergence in surface brightness

Given the coincidence of stellar assembly bias and the differential increase in the median effective radius of the upper and lower locus populations, we begin by considering the role of SN feedback in the surface brightness evolution of galaxies. Previous theoretical work has shown that, particularly at low stellar masses, where gravitational potential wells are shallow, SN feedback is capable of driving gas outflows (e.g. Dubois and Teyssier, 2008a; Di Cintio et al., 2017; Chan et al., 2018) which make the density profiles of the gas, and the stars that form from it, shallower
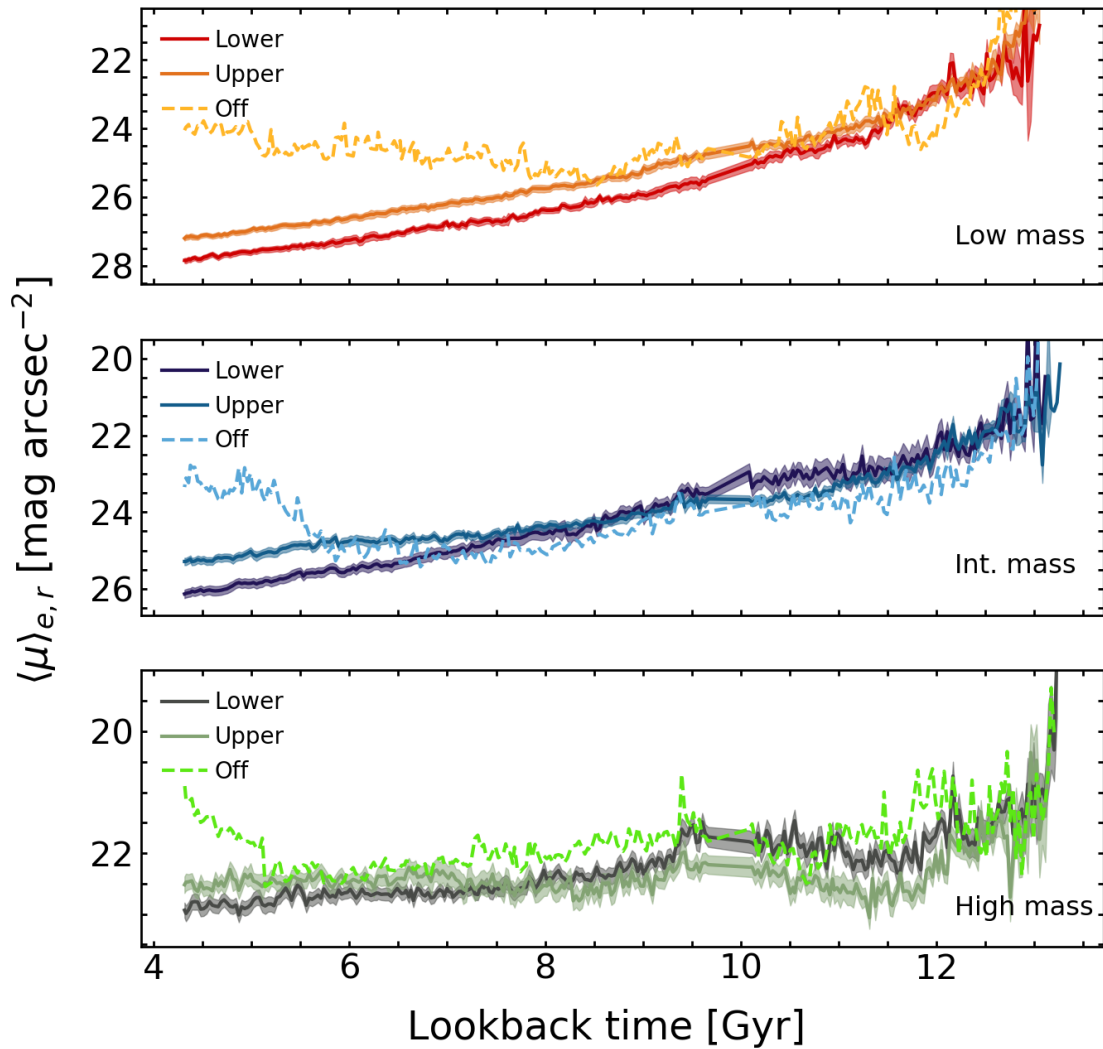
FIGURE 5.6: Evolution of the median surface brightness with look-back time. The shaded regions show the associated uncertainties. The top, middle and bottom panels represent the low ($10^{6.5}$ $M_\odot \geq M_\star > 10^{7.5}$ $M_\odot$), intermediate ($10^{7.5}$ $M_\odot \geq M_\star > 10^{8.5}$ $M_\odot$) and high ($10^{8.5}$ $M_\odot \geq M_\star > 10^{9.5}$ $M_\odot$) mass bins respectively. The colour coding indicates the upper, lower and off locus galaxy populations. Recall that lower locus galaxies represent the population that is fainter in surface brightness at $z = 0.25$, while the upper locus galaxies represent their brighter counterparts. In all mass bins, lower locus galaxies exhibit similar surface brightnesses to their upper locus counterparts at early epochs because their earlier star formation counteracts their larger effective radii. The surface brightnesses eventually diverge, with the divergence occurring later at higher stellar masses.

(e.g. Martin et al., 2019). The shallower stellar profiles naturally lead to more diffuse systems which have lower surface brightness.

In order to calculate SN feedback we define the total mechanical and thermal energy released by stellar processes between two timesteps, t_0 and t_1, by summing the energy released by each star particle in a galaxy within this interval:

$$E_{SN} = \sum_i m_{\odot,i}(E(z_1)_i - E(z_0)_i), \tag{5.2}$$

where $m_{\odot,i}$ is the mass of an individual star particle and $E(z)_i$ is the cumulative mechanical and thermal energy released by that star particle, as a result of Type II SN, between the time of its formation and a redshift z.

In Figure 5.7, we show the evolution of the SN feedback energy for galaxies in different zones of the locus. We find that galaxies which end up with fainter surface brightnesses (i.e. those in the lower locus) show higher levels of SN feedback at earlier times, regardless of the mass bin being considered. This correlates with the stellar assembly bias seen in Figure 5.4. Note also that the stellar assembly bias occurs earlier at lower stellar masses, which is mirrored in the SN feedback being more pronounced at earlier epochs in lower mass bins.

We proceed by exploring how this difference in SN feedback drives the evolution in the stellar mass, effective radius and surface brightness of galaxies shown in Figures 5.4, 5.5 and 5.6. Recall that the stellar effective radii of upper and lower locus galaxies begin diverging in the early Universe (Figure 5.5), around the epochs when there is a divergence in the SN feedback energy. This suggests that the SN feedback is likely to be impacting the gas reservoir in such a way as to drive the increase in the median effective radius.

For example, Martin et al. (2019) have shown that in the massive ($M_\star > 10^9 \, M_\odot$) galaxy regime, SN feedback acts to rapidly make the gas distribution shallower, by moving material from the central regions of the galaxy towards the outskirts (see also Governato et al., 2007). If the gas is not completely removed, new stars forming from this gas make the stellar distribution progressively shallower over time. In this mass regime at least, earlier SN feedback is central to the formation of galaxies which exhibit lower surface brightnesses at the present day.

We now consider whether a similar process operates in the dwarf galaxy regime. While galaxies in all mass bins show similar behaviour, we first demonstrate the impact of SN feedback graphically, by showing the evolution of the stacked stellar density profiles in the high mass bin. Figure 5.8 shows how the stacked stellar density profiles of all stars and that of young stars (ages < 100 Myr), which trace the star-forming gas, evolve across the epoch of divergence in SN feedback energy.
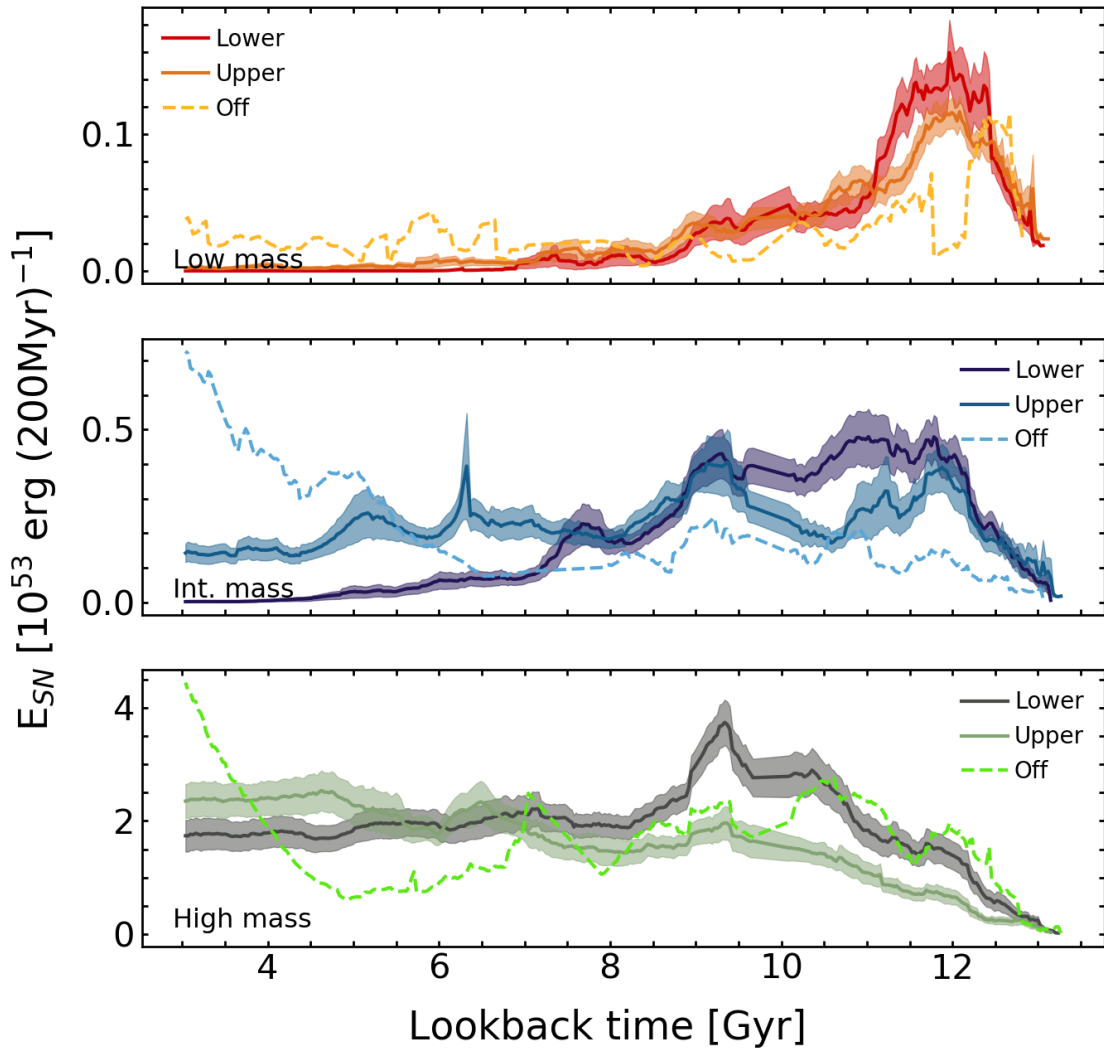
FIGURE 5.7: Evolution of the median SN feedback as a function of look-back time. The shaded regions show the associated uncertainties. The top, middle and bottom panels represent the low ($10^{6.5}$ $M_{\odot} \geq M_{\star} > 10^{7.5}$ $M_{\odot}$), intermediate ($10^{7.5}$ $M_{\odot} \geq M_{\star} > 10^{8.5}$ $M_{\odot}$) and high ($10^{8.5}$ $M_{\odot} \geq M_{\star} > 10^{9.5}$ $M_{\odot}$) mass bins respectively. The colour coding indicates the upper, lower and off locus galaxy populations. Recall that lower locus galaxies represent the population that is fainter in surface brightness at $z = 0.25$, while the upper locus galaxies represent their brighter counterparts. In all mass bins lower locus galaxies show higher levels of SN feedback (i.e. higher star formation rates) at earlier times, with the epoch of peak divergence occurring later at higher stellar masses. This drives the stellar assembly bias seen in all mass bins in Figure 5.4.
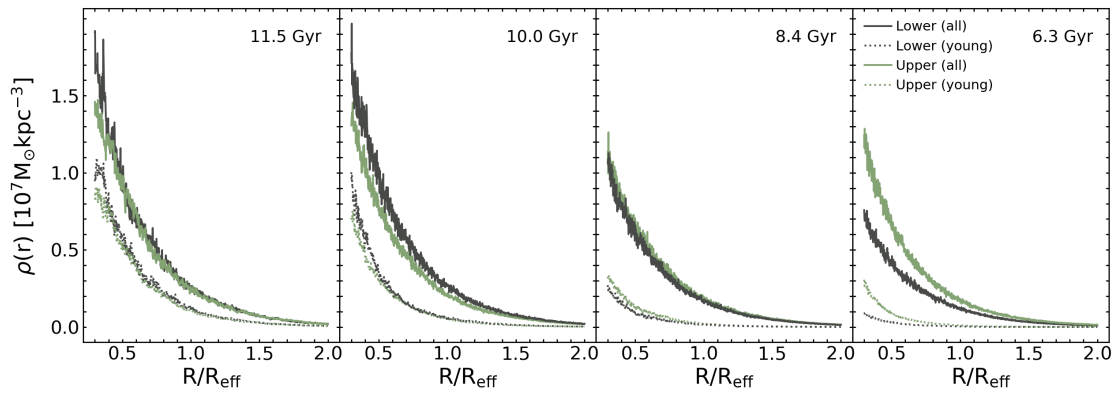
FIGURE 5.8: Evolution of the stacked stellar density profiles of galaxies in the high mass bin as a function of look-back time, as indicated in the panels. The solid lines indicate all stars, while the dotted lines indicate young (ages < 100 Myr) stars only (which trace the star-forming gas). Dark and light green curves indicate lower and upper locus galaxies respectively. As SN feedback moves material away from the centres of galaxies, the density profiles of new stars become progressively flatter which, in turn, gradually flattens the overall stellar density profiles of galaxies. The higher SN feedback experienced by lower locus galaxies (see Figure 5.7) at earlier times means that their slopes become flatter faster, as shown in the transition from the left to the right-hand panels above.

The more rapid star formation in lower locus galaxies at early epochs causes both the normalisation and the slope of the stacked young-star density profiles to decrease faster than in their upper locus counterparts, as star-forming gas is displaced from the centre towards the outskirts at a faster rate. As the systems evolve, progressive generations of young stars with flatter profiles will then drive a flattening of the overall stellar profiles. To quantify this, we fit a straight line to the inner 0.5 R_{eff} of each density profile (where the profile is roughly linear) and calculate the ratio in the slopes of the density profiles between the young stars and the total stellar population. As shown in Figure 5.9, the ratio of the slopes between young and all stars is smaller in lower locus galaxies for most of cosmic time (regardless of the mass bin being considered). This indicates that the density profiles of the young stars flatten faster in lower locus galaxies than in their upper locus counterparts. This, in turn, flattens their total stellar profiles faster, which is reflected in lower locus galaxies growing their effective radii more rapidly than their upper locus counterparts (Figure 5.5).

While initially the enhanced star formation in lower locus galaxies counteracts their larger effective radii and keeps their surface brightnesses similar to their upper locus counterparts, as star formation activity decreases in the lower locus (Figure 5.7), the two populations diverge rapidly in surface brightness (Figure 5.6). While this trend is the same in all mass bins, the divergence in the level of star formation occurs later at higher masses (Figure 5.7), and so the divergence in surface brightness also takes place at later epochs. Lower locus galaxies can be thought of as somewhat rarer events (in the peak background split sense, e.g. Schmidt et al., 2013) that start to form stars 'too early' for the depth of their potential wells to counteract the energy release of the first round of supernovae in these galaxies.
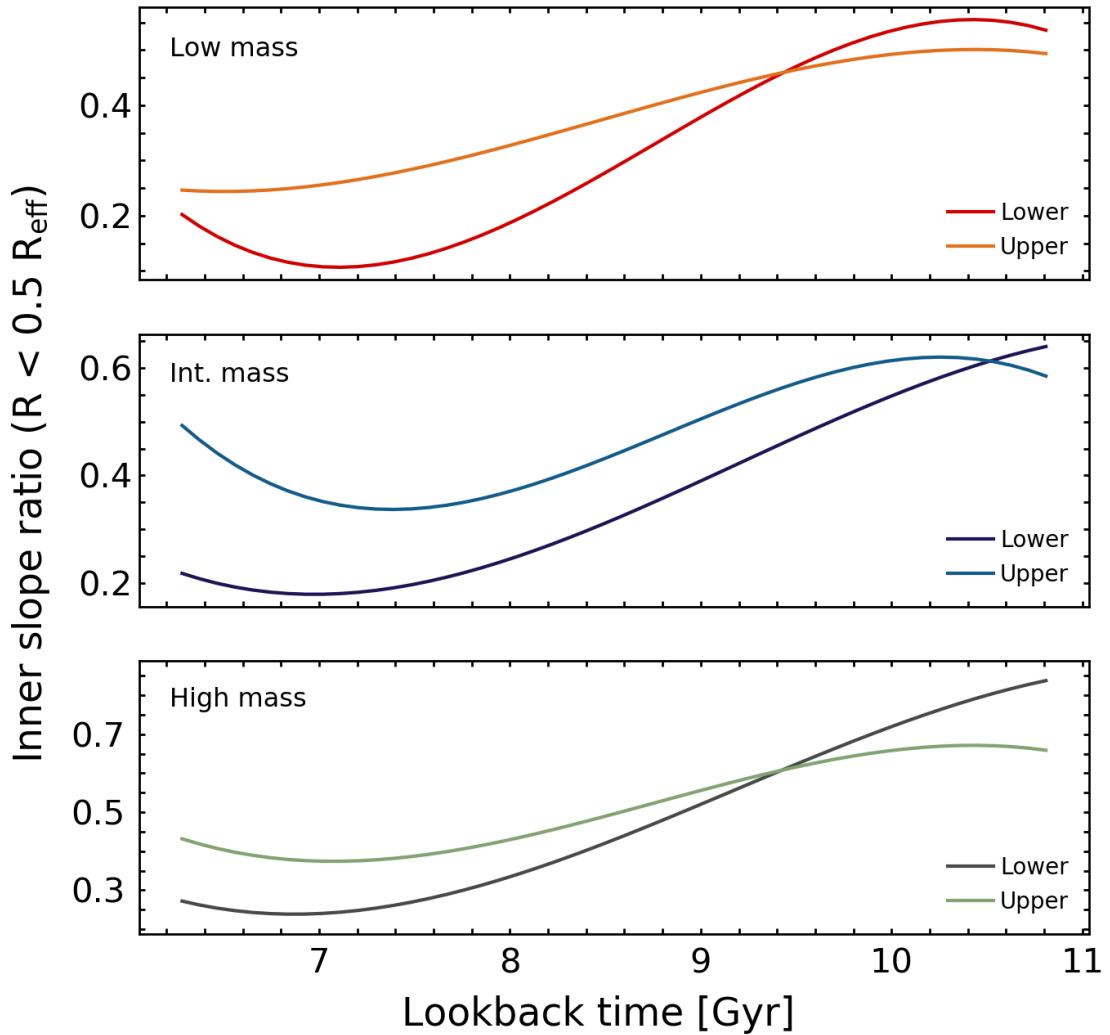
FIGURE 5.9: Evolution of the ratio between the slope of the stellar density profiles of young and all stars, for R < 0.5 R_{eff}. The slope is calculated by fitting a straight line to the inner 0.5 R_{eff} of the density profile. A value less than 1 indicates that the density profile of the young stars are flatter (i.e. shallower) than that of all stars. In lower locus galaxies, these ratios exhibit smaller values from early look-back times i.e. young stars have much flatter profiles compared to the overall stellar distribution, compared to upper locus galaxies. Since young stars will progressively flatten the entire stellar density distribution, this means that lower locus galaxies become more diffuse at a faster rate, as seen in the faster evolution of the effective radius in these galaxies (Figure 5.5).

While the role of SN feedback in initiating the surface brightness divergence is clear, we conclude this section by considering whether another internal process, AGN feedback, may contribute to this process. In Figure 5.10 (main panel) we show the location of galaxies that have central super-massive BHs (red points), compared to galaxies that do not (grey points). In the inset, we show the occupation fraction of central BHs in galaxies (defined as a galaxy having at least one BH within 1 R_{eff}) as a function of stellar mass. In the low-mass regime, which is our mass range of interest, only a small fraction of galaxies actually host BHs (the BH occupation fractions are around 10 per cent for $M_\star \sim 10^8$ $M_\odot$). It is worth noting that BHs that do exist in dwarf galaxies exhibit very little growth (e.g. Volonteri et al., 2020; Dubois et al., 2020). Finally, galaxies with
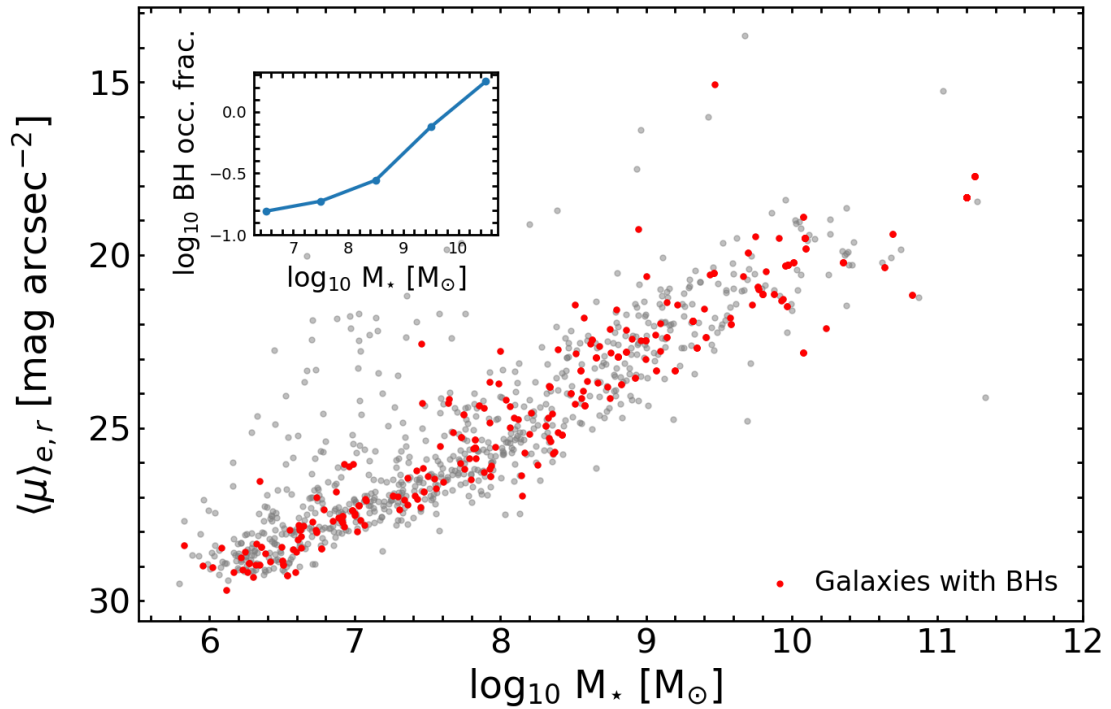
FIGURE 5.10: Main panel: Surface brightness vs stellar mass for all galaxies (grey) and galaxies hosting a supermassive black hole (red). Inset: The occupation fraction of BHs in galaxies as a function of stellar mass. A small minority of dwarf galaxies in `NewHorizon` have central BHs, and that those that do, do not occupy a preferential position in the locus.

BHs do not occupy a preferential position in the locus. Taken together, this indicates that only a small minority of dwarf galaxies in `NewHorizon` have central BHs, and that those that do, do not occupy a preferential location in the locus and show very little growth (and therefore little potential for AGN feedback). Thus AGN feedback does not play a role in determining the position of galaxies in the locus.

5.4.1.1   A cosmological trigger for the stellar assembly bias: higher local dark matter density driving higher gas accretion rates

In the previous section, we showed that galaxies that lower locus galaxies (i.e. those that end up with lower surface brightnesses at late epochs) are those that experience an earlier phase of more intense star formation. While this earlier stellar assembly is ultimately responsible for driving the initial divergence in surface brightness, we now explore the factors that are responsible for causing this bias in the first place. A faster stellar assembly implies a greater availability of gas. Thus, we explore the local environmental densities around lower and upper locus galaxies, at the epochs where the SN feedback energy diverges, since denser local environments will likely induce larger inflows of gas which can trigger stronger star formation.

Lower:upper locus ratio	Low mass	Int. mass	High mass
DM density	1.22±0.16	1.58±0.22	1.57±0.28
Gas inflow rate	1.55±0.05	1.48±0.06	1.63±0.08

TABLE 5.1: Ratio of the median dark matter density within 15 R_{vir} (first row) and the median gas inflow rate (second row) between lower and upper locus galaxies in different mass bins with associated standard errors.

In Table 5.1, we show the local DM density, on scales of 15 R_{vir} around each galaxy's halo, just before the epoch at which the SN feedback divergence takes places (lookback times of ~11.9 Gyrs, ~11.5 Gyrs and ~11 Gyrs for the low, intermediate and high mass bins respectively). In all mass bins, lower locus galaxies reside in regions of higher average dark-matter density. The local DM densities in the lower locus galaxies are elevated by 22, 58 and 57 per cent in the low, intermediate and high mass bins respectively. The gas inflow rates into this 15 R_{vir} region are, in turn, elevated by 55, 48 and 63 per cent respectively. Note that these trends remain unchanged if we calculate local DM density on different spatial scales around the galaxies (e.g. 10 R_{vir}, 20 R_{vir} etc.).

Lower locus galaxies are, therefore, born in regions of higher DM density, which enables them to access gas at a faster rate at earlier epochs. This faster gas accretion rate then drives the faster stellar assembly in the lower locus systems, leading to increased SN feedback and a faster increase in their effective radii. It is worth noting that, the idea that the density of the local environment in which dwarf galaxies form may imprint itself on their star formation histories, has been previously postulated for galaxies in the local group (e.g. Gallart et al., 2015). Our work shows that this is a general property of dwarf galaxies and not a specific feature of dwarfs in the local group.

Finally, it is worth exploring whether the higher DM densities experienced by lower locus galaxies are due to them residing in special locations in the cosmic web, or whether lower locus galaxies are simply sampling higher values of the local dark matter density distribution. We use the skeleton, described in Section 5.2.4, to check whether the locations of lower locus galaxies vary systematically from their upper locus counterparts. However, we find that both populations show similar distances to both the nearest nodes and filaments, indicating that, on average, the positions of upper and lower locus galaxies in the cosmic web are very similar. Note that, since our sample only includes galaxies that survived accretion on to more massive galaxies down to $z = 0.25$, it may be potentially biased towards objects that are born relatively further from the densest regions of the skeleton, since such systems will have a lower probability of merging with a larger galaxy (e.g. Borzyszkowski et al., 2017; Musso et al., 2018).

Our analysis has shown that the differences between the upper and locus galaxies are driven by the fact that their progenitors sample different parts of the local dark matter density distribution in the Universe at early epochs. *The stellar assembly bias which drives the divergence in galaxy surface brightness at fixed stellar mass, and therefore the width of the main locus at z = 0.25 (Figure 5.1), essentially has a purely cosmological trigger.*

5.4.2 Tidal perturbations and ram pressure: external processes that influence dwarf galaxy evolution at late epochs

At late epochs, the level of star formation in lower locus galaxies subsides and SN feedback activity in these systems falls below the levels seen in their upper locus counterparts (Figure 5.7). Nevertheless, the effective radii of lower locus systems keeps growing faster than in their upper locus counterparts (Figure 5.5). The continued divergence in surface brightness between the two populations at late epochs (Figure 5.6) is thus driven both by lower locus galaxies forming stars at a slower rate and growing their effective radii more rapidly than their upper locus counterparts. Most importantly, since the star formation activity in the lower locus galaxies is now less intense, the evolution in their radii must be driven by external processes and not by internal mechanisms like SN feedback.

The two key external processes that can influence galaxy evolution are tidal perturbations (including mergers) and ram pressure. Strong tidal perturbations from events like close fly-bys and mergers can trigger star formation. Sustained tidal perturbations over a long period of time can heat stars and gas, puffing up galaxies and reducing their star formation rate (Martin et al., 2019). Sustained ram pressure typically acts to strip the internal gas reservoir of the galaxy as it transits through a dense medium, reducing its star formation rate (e.g. Hester, 2006).

Following Choi et al. (2018) and Martin et al. (2019) we define a dimensionless 'perturbation index' (PI) that quantifies the cumulative, ambient tidal field around a galaxy:

$$PI = \sum_i \left(\frac{M_i}{M_{gal}} \right) \left(\frac{R_{\mathrm{eff}}}{D_i} \right)^3, \tag{5.3}$$

where M_{gal} is the stellar mass of the galaxy in question and R_{eff} is its effective radius, M_i is the stellar mass of the ith perturbing galaxy and D_i is the distance from the ith perturbing galaxy. We consider all perturbing galaxies within 3 Mpc of the object in question.

Figure 5.11 shows the evolution of the median PI with look-back time. We find that in all mass bins, galaxies that reside in different zones of the locus experience very similar tidal perturbations at high redshift. Therefore, perturbations caused by the ambient tidal field do not contribute to the early divergence in surface brightness. However, in the low and intermediate mass bins,
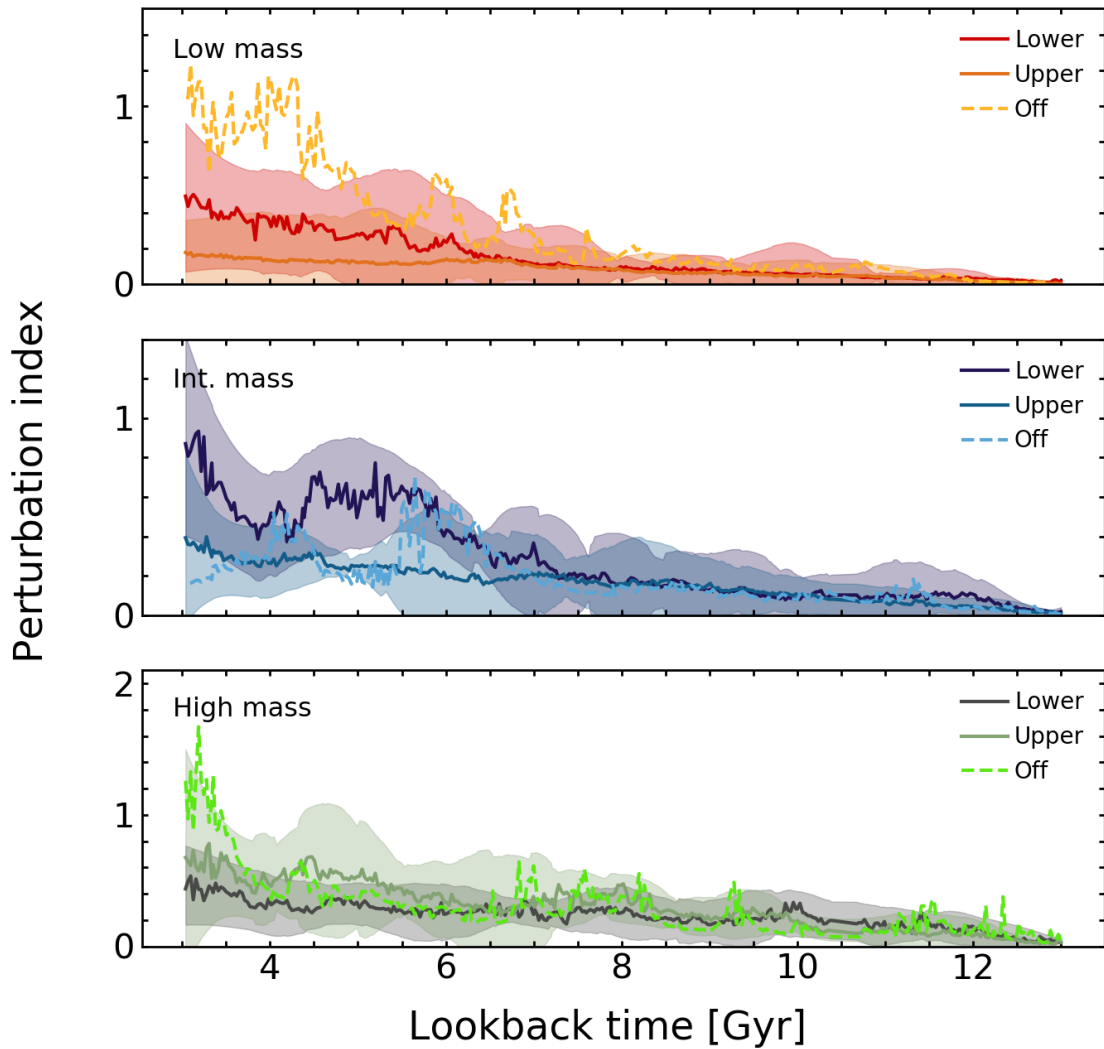
FIGURE 5.11: Evolution of the median perturbation index (PI) with look-back time. The shaded regions show the associated uncertainties. The top, middle and bottom panels represent the low ($10^{6.5}$ M$_\odot$ ≥ M$_\star$ > $10^{7.5}$ M$_\odot$), intermediate ($10^{7.5}$ M$_\odot$ ≥ M$_\star$ > $10^{8.5}$ M$_\odot$) and high ($10^{8.5}$ M$_\odot$ ≥ M$_\star$ > $10^{9.5}$ M$_\odot$) mass bins respectively. The colour coding indicates the upper, lower and off locus galaxy populations. Recall that lower locus galaxies represent the population that is fainter in surface brightness at $z = 0.25$, while the upper locus galaxies represent their brighter counterparts. Upper and lower locus galaxies exhibit similar PI evolution at early epochs, with the PI experienced by lower locus galaxies increasing at late epochs. Off-locus objects show large, recent increases in PI, which indicates that their change in surface brightness is influenced by a recent interaction.
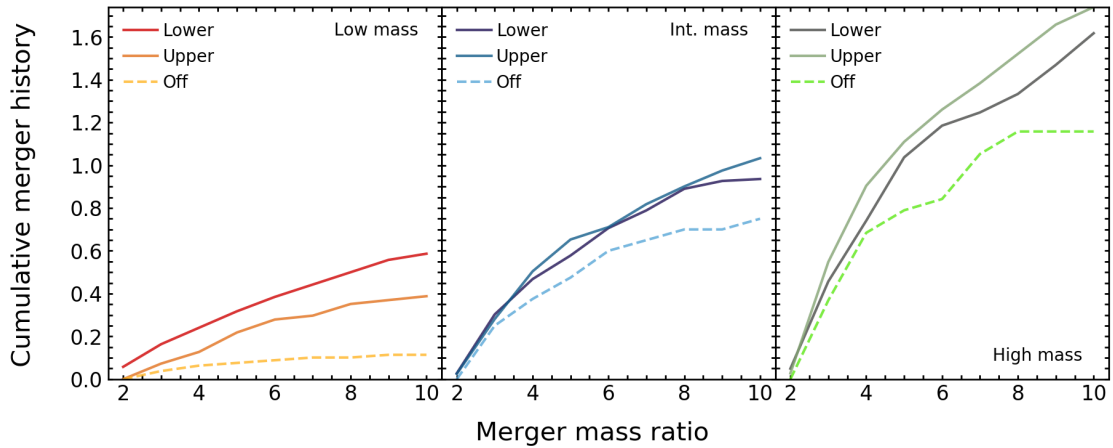
FIGURE 5.12: Cumulative merger history for galaxies in the different zones indicated in Figure 5.1. The left, centre and right panels represent the low, intermediate and high mass bins respectively. The colour coding indicates the upper, lower and off locus galaxy populations. This figure presents the average number of mergers experienced by a galaxy over its lifetime, with mass ratios less than or equal to the value shown on the x-axis.

lower locus galaxies show higher values of PI at late epochs (likely driven by the fact that these galaxies are born, and remain in, regions of higher density) which contribute to the divergence in their effective radii and surface brightnesses at late epochs. Interestingly, the trend is reversed in the high mass bin, indicating that the surface brightness divergence in this regime is driven primarily by the higher levels of star formation in the upper locus population.

Note that, while the PI includes mergers (i.e. events where the two galaxies eventually coalesce), it is worth looking separately at the merger history of galaxies, since plotting the median PI will dampen the effect of individual events, like mergers, which could cause a strong, transient change in this parameter. While mergers will increase the stellar mass of the system and can drive an increase in its radius, the smooth change in both stellar mass (Figure 5.4) and effective radius (Figure 5.5) suggests that mergers, which are stochastic and rare events (e.g. Darg et al., 2010; Uzeirbegovic et al., 2020), are unlikely to be driving this evolution. We confirm this in Figure 5.12 by exploring the cumulative merger histories of galaxies, for significant merging events which have mass ratios less than 10:1 (which is the mass ratio range where mergers typically produce measurable size and morphological change, e.g. Martin et al. (2018a)). This figure shows the average number of mergers experienced by a galaxy since the beginning of the simulation, with mass ratios less than or equal to the value shown on the x-axis. For example, a lower locus galaxy in the low mass bin (left panel) undergoes, on average, ~0.6 mergers with mass ratios greater than 1:10 at $z > 0.25$, while a lower locus galaxy in the intermediate mass bin undergoes, on average, ~0.95 mergers in the same time period.

We find that the cumulative merger histories of galaxies in the lower locus do not show a strong preference towards higher merger fractions over cosmic time in any mass bin. In addition, the number of mergers experienced by galaxies (in all zones of the locus) are indeed too small to
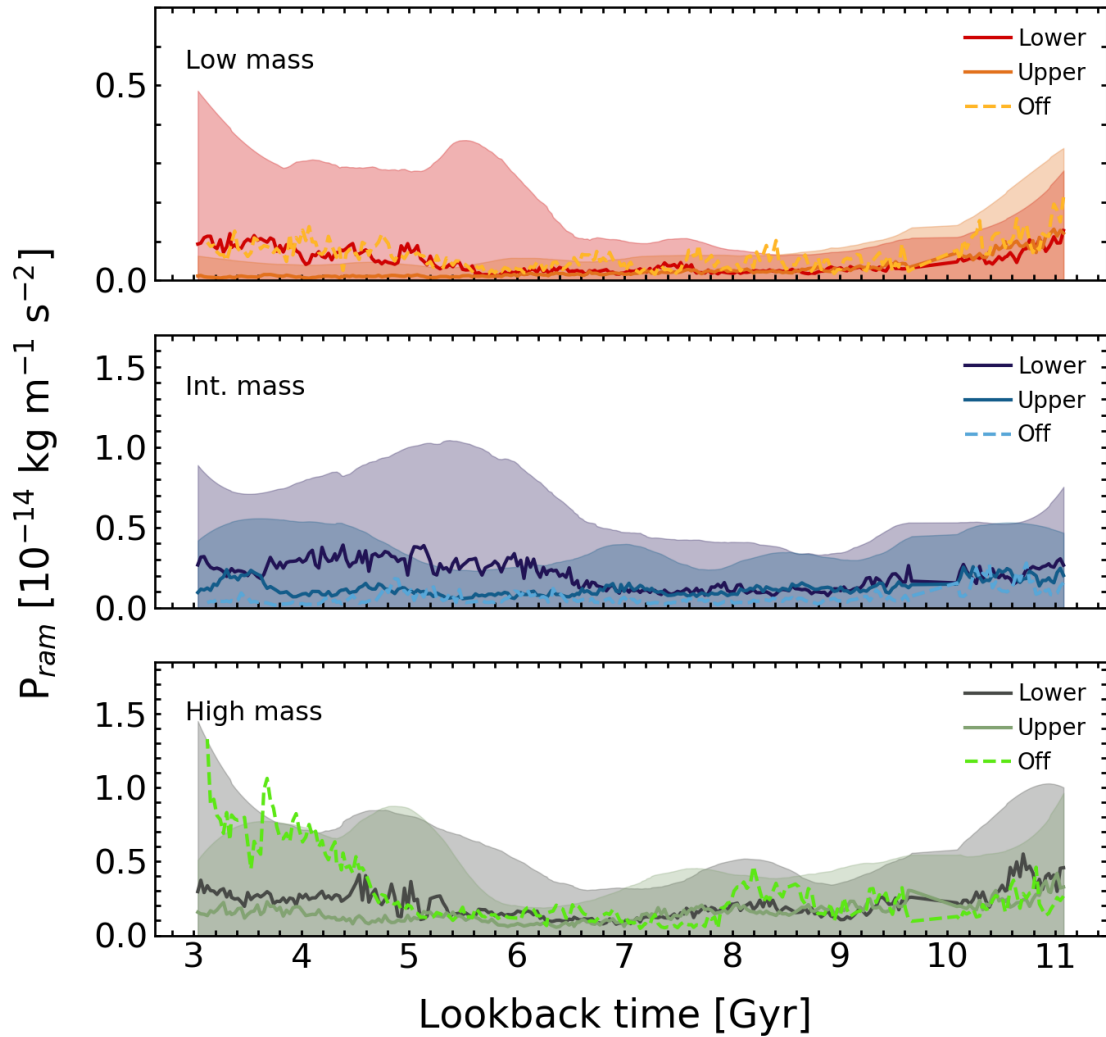
FIGURE 5.13: Evolution of the median ram pressure with look-back time. The shaded regions show the associated uncertainties. The top, middle and bottom panels represent the low ($10^{6.5}$ $M_\odot \geq M_\star > 10^{7.5}$ $M_\odot$), intermediate ($10^{7.5}$ $M_\odot \geq M_\star > 10^{8.5}$ $M_\odot$) and high ($10^{8.5}$ $M_\odot \geq M_\star > 10^{9.5}$ $M_\odot$) mass bins respectively. The colour coding indicates the upper, lower and off locus galaxy populations. Recall that lower locus galaxies represent the population that is fainter in surface brightness at $z = 0.25$, while the upper locus galaxies represent their brighter counterparts. In all mass bins, galaxies in different zones of the locus experience similar values of ram pressure over cosmic time.

explain the smooth change observed in stellar mass and effective radius. This indicates that individual mergers do not influence the eventual position of a galaxy on the locus.

Next, we consider ram pressure, which is capable of removing gas from galaxies and reducing their star formation rates, particularly in high-density environments (e.g. Gunn and Gott, 1972). While `NewHorizon` does not include the richest environments like galaxy clusters, ram pressure can still play a significant role in the evolution of low-mass galaxies, which are typically much more susceptible to gas stripping due to their shallow gravitational potential wells (e.g. Vollmer et al., 2001; Martin et al., 2019). We measure the ram pressure exerted on a galaxy by the local medium as follows:

$$P_{ram} = \rho_{\text{IGM}} v_{\text{gal}}^2, \tag{5.4}$$

where v_{gal} is the velocity of the galaxy relative to the bulk velocity of the surrounding medium and ρ_{IGM} is the mean gas density of the surrounding medium within 10 times the maximum extent of the stellar distribution of the galaxy.

Figure 5.13 shows the evolution of the median ram pressure with look-back time. In a similar vein to the PI, the ram pressure experienced by upper and lower locus galaxies is similar at large look-back times and therefore does not contribute to the surface brightness divergence at early epochs. However, the median ram pressure experienced by lower locus galaxies at late epochs is elevated compared to that in their upper-locus counterparts (although the difference is less pronounced than what is found for the PI). This is again likely to be driven by the fact that lower-locus galaxies are born, and remain in, regions of higher density. The higher ram pressure at late epochs likely assists in the faster depletion of gas in lower locus galaxies, reducing their star formation activity (which is reflected in the decrease in the SN feedback energy seen in Figure 5.7). This, in turn, helps drive the divergence in surface brightness between the two populations at late epochs.

5.5 Off-locus galaxies: transient, tidally-induced starbursts

We complete our study by exploring the formation mechanisms of galaxies that depart strongly from the locus towards higher surface brightnesses. As shown in Figure 5.1, a minority of galaxies reside 'off-locus', with the fraction of off-locus objects being 22, 12 and 10 per cent in the low, intermediate and high mass bins respectively (see Table 5.2). In particular, as noted in Section 5.3, galaxies that scatter off the main locus make up the majority of low-mass galaxies that are visible in past wide-area surveys like the SDSS. It is, therefore, important to understand how these systems form and their connection to the majority of the galaxy population which resides on the locus itself.

Figure 5.6 suggests that the off-locus population diverges in surface brightness at late look-back times, with the divergence being most pronounced in the low-mass population. The epoch of divergence coincides with an increase in both the PI (Figure 5.11) and the SN feedback energy i.e. a starburst (Figure 5.7). We first check whether the gas inflow rates in the off-locus galaxies show an increase around the time they begin to diverge from the population that resides in the locus, possibly due to abruptly entering a high-density environment. However, we find that the average gas inflow rates prior to the starburst are not anomalous and an analysis of the skeleton indicates that the off-locus galaxies do not abruptly enter high-density regions of the cosmic web.
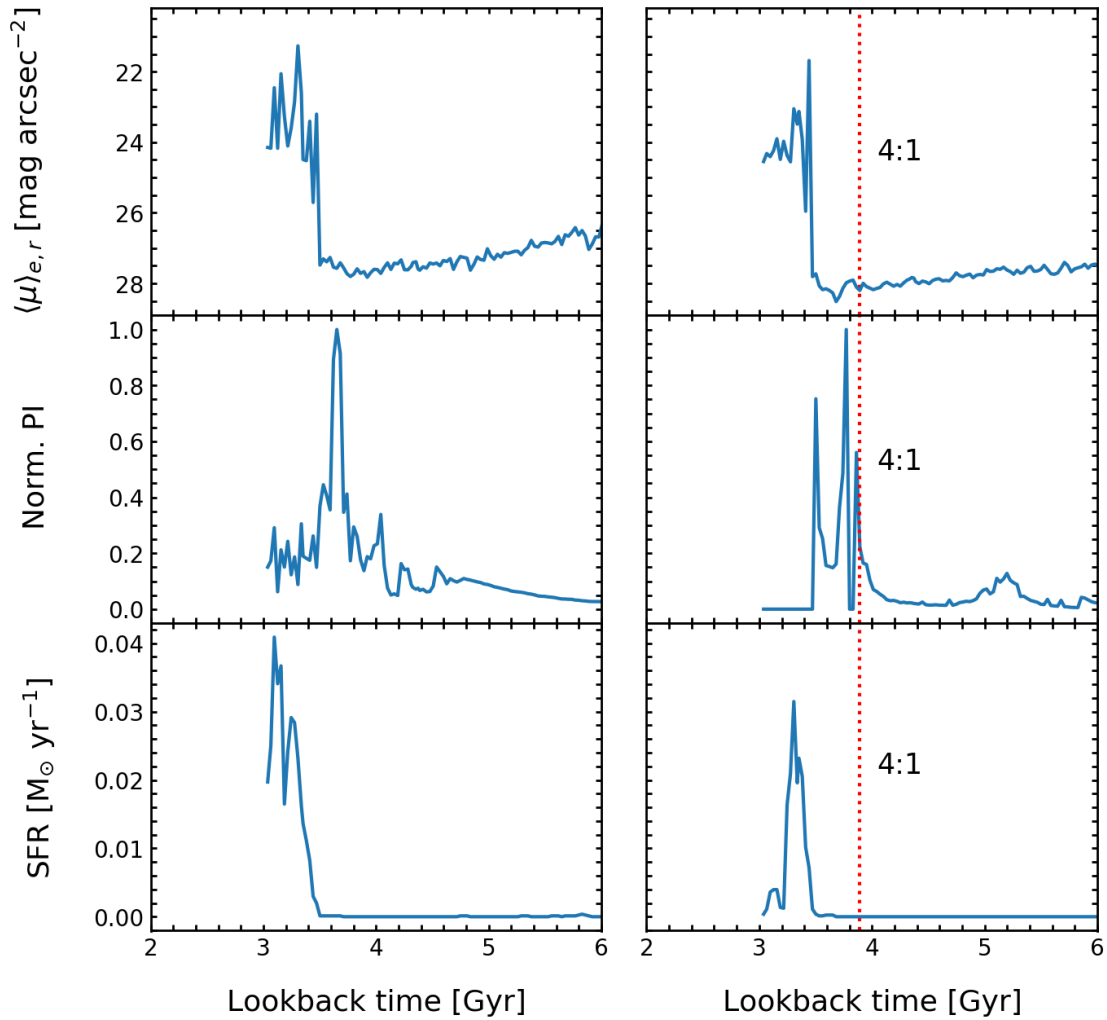
FIGURE 5.14: Top row: Evolution of surface brightness with look-back time for two off-locus galaxies in the high mass bin. Middle row: The corresponding evolution of the perturbation index with look-back time. Bottom row: Evolution of the galaxies star formation rate with look-back time. Vertical dotted red lines indicate the times at which merger events take place. While the galaxy in the right-hand column exhibits a rapid increase in surface brightness that is coincident with a merger with mass ratio 4:1, the increase in surface brightness of the galaxy in the left-hand column does not correspond to a merger event and is therefore driven by a fly-by. Both of these events induce an increase in the SFR of the galaxy.

This indicates that the off-locus galaxies depart from the main locus due to recent, tidally-induced starbursts which are essentially stochastic in nature. The epoch at which the population diverges in surface brightness (see Figure 5.6) indicates that the star formation episodes in these systems are around 1-4 Gyrs old (dependent on the mass bin). Note that this recent starburst episode is not special. While galaxies are likely to have had multiple starburst episodes in their lifetimes, the new stars produced in those episodes have since aged and faded away. The off-locus population is essentially tracing the most recent starburst episode whose signature remains visible in the *r*-band filter.

	Low mass	Int. mass	High mass
Off-locus fraction	22%	12%	10%
Fly-by induced	92%	48%	38%
Major-merger induced	4%	26%	12%
Minor-merger induced	4%	26%	50%

TABLE 5.2: The fraction of off-locus galaxies (first row) and the mechanisms that produce off-locus systems (other rows) in different mass bins. For example, in the intermediate mass bin, 12 per cent of galaxies are found off-locus. Of these 48 per cent are fly-by induced while 26 per cent are induced by major mergers (mass ratios < 4:1) and the rest are triggered by minor mergers (mass ratios > 4:1).

Since the increase in PI could either be driven by fly-bys i.e. purely tidal events where there is a rapid change in PI without a merger or by major (mass ratios < 4:1) or minor (mass ratios > 4:1) mergers, it is instructive to consider which mechanism triggers the starburst that produces off-locus galaxies in different zones of the locus. For each off-locus galaxy, we consider their merger histories in conjunction with the evolution of their PI values and compare this to their surface brightness evolution. Figure 5.14 shows examples of two cases. The right-hand column shows a system that is driven off-locus (due to the rapid brightening of the surface brightness, see top panel) by an increase in PI that coincides with a recent merger with a mass ratio of 4:1. The look-back time of the merger is indicated by the red dotted line. The left-hand column shows a case where the surface brightness is driven by a fly-by because the change in the perturbation index does not correspond with a recent merger.

We visually inspect these plots for every off-locus galaxy, in order to ascertain the principal driver of the starburst that moves them off the locus. Table 5.2 summarises the drivers of the starbursts in the off-locus objects. The impact of fly-bys is greatest in the low-mass regime, where 92 per cent of the off-locus systems are fly-by induced. Fly-bys remain important in all mass regimes, producing 48 and 38 per cent of off-locus systems in the intermediate and high mass bins respectively. However, mergers become more important at higher stellar masses, accounting for 62 per cent of off-locus objects in the high mass bin. The progressively higher minor-merger-induced off-locus fraction at higher stellar masses is due to the shape of the galaxy mass function. Since there are fewer galaxies at high stellar masses (e.g. Bell et al., 2003), equal mass mergers between massive galaxies become rarer in this mass regime.

Our analysis indicates that the recent starbursts that produce off-locus systems are largely induced by tidal perturbations that trigger the existing gas reservoirs in these galaxies, rather than being due to enhanced gas accretion from the cosmic web. As galaxies increase in stellar mass and their gravitational potential wells become deeper, a larger perturbation, via a merger rather than simply a fly-by, is required to trigger this starburst.

It is important to note that off-locus galaxies are clearly atypical of the general galaxy population because they have anomalously high levels of star formation. As has been noted before in

Section 5.3, in the $M_\star < 10^9$ M$_\odot$ regime, off-locus galaxies overwhelmingly dominate the observed galaxy population in past wide-area surveys like the (standard-depth) SDSS (see dotted red lines in Figure 5.3). Therefore, conclusions about the general galaxy population cannot be drawn using the subset of off-locus objects because they are likely to be highly unrepresentative of the overall galaxy populations in these mass regimes.

5.6 Summary

Our statistical comprehension of galaxy evolution is driven by objects that are brighter than the surface brightness limits of wide-area surveys. Given the depth of past wide surveys, our understanding of how the observable Universe evolves has been predicated largely on bright galaxies. For example, while past benchmark surveys like the SDSS become highly incomplete at effective surface brightnesses of around 24 mag arcsec^{-2}, low-surface brightness galaxies (LSBGs) that are fainter than these thresholds overwhelmingly dominate the galaxy number density (e.g. Martin et al., 2019). Understanding the evolution of the LSBG population is therefore key to a complete comprehension of galaxy evolution. Here, we have used the high resolution `NewHorizon` cosmological simulation to probe the origin and evolution of the LSBG population in the low-mass regime, where most recent observational studies are focussed. In particular, we have explored why, at a given stellar mass, LSBGs span the large observed range in surface brightness.

The `NewHorizon` galaxy population occupies a well-defined locus in the surface brightness vs. stellar mass plane, with a large spread of ∼ 3 mag arcsec^{-2}. A minority of galaxies depart strongly from this locus towards higher surface brightnesses. The fraction of these off-locus systems is ∼20 per cent in the low mass bin ($10^{6.5}$ M$_\odot$ < M$_\star$ < $10^{7.5}$ M$_\odot$) and drops to ∼10 per cent at higher stellar masses ($10^{8.5}$ M$_\odot$ < M$_\star$ < $10^{9.5}$ M$_\odot$). The predicted position of `NewHorizon` galaxies in the surface brightness vs. stellar mass plane is in good agreement with observations from the relatively deep SDSS Stripe 82 survey. This agreement suggests that, while prescriptions used in `NewHorizon` to describe baryonic physics (e.g. SN feedback) are largely tuned to higher mass galaxies, they also offer a good representation of these processes in the low-mass regime.

A large number of LSBGs in `NewHorizon`, particularly galaxies that exist in the upper locus in the low and intermediate mass bins, have surface brightnesses and effective radii that make them consistent with the definition of 'ultra-diffuse galaxies' (UDGs) in the current observational literature. These dwarfs form naturally in the standard model, through a combination of SN feedback, tidal perturbations and ram pressure as described in Section 5.4 and are, therefore, a normal component of the dwarf galaxy population (albeit one that is not readily detectable using past and current datasets). Since `NewHorizon` does not contain very high-density environments (i.e. clusters), a clear prdiction is that UDGs form ubiquitously in low-density environments like

groups and the field and will be routinely visible in new and future deep-wide surveys like the HSC-SSP and LSST.

To understand the processes that determine the eventual surface brightness of dwarf galaxies at late epochs, we have split the locus into three zones - the lower (fainter) and upper (brighter) halves and the population of off-locus galaxies that scatter towards very high surface brightnesses beyond the upper locus. We have then studied, in detail, the formation histories of galaxies in these different zones, in order to identify the processes that create the large observed spread in surface brightnesses in the dwarf galaxy population.

Regardless of the mass regime being considered, galaxies in the lower locus, i.e. those that end up with fainter surface brightnesses at late epochs, are born in denser regions of the Universe, which results in faster gas accretion and more intense star formation at high redshift. The more intense star formation in these systems leads to stronger supernova feedback. This flattens gas profiles at a faster rate which, in turn, creates shallower stellar profiles more rapidly. As star formation subsides in the lower locus, their late epoch evolution is dominated by external processes like tidal perturbations and ram pressure. Since lower locus galaxies are born in higher density environments, they remain in relatively denser environments over their lifetimes. The higher tidal perturbations they experience as a result continue to increase their effective radii at a faster rate than their upper locus counterparts. In a similar vein, the higher ram pressure they experience acts to accelerate gas depletion and reduce their star formation rates more quickly than on the upper locus. The lower locus systems thus diverge strongly from their upper locus counterparts at late epochs, both due to the fact that they are now more diffuse and because they have less star formation.

Finally, we have studied the processes that drive the formation of off-locus galaxies that deviate strongly from the main locus as they experience a recent, rapid increase in surface brightness. This increase is not driven by an uptick in the gas inflow rate but coincides with an increase in the perturbation index and a coincident rise in the star formation activity. This indicates that an interaction triggers a starburst which moves the galaxy away from the main locus. In low-mass systems ($M_\star < 10^{7.5}$ $M_\odot$) this starburst is triggered primarily by purely tidal events (i.e. fly-bys), while at high stellar masses ($M_\star > 10^{8.5}$ $M_\odot$) it is primarily induced by mergers. It is worth noting that this off-locus population makes up the bulk of the observable low-mass systems ($M_\star < 10^{8.5}$ $M_\odot$) in past benchmark wide-area surveys like the SDSS. However, since these systems are clearly anomalous in terms of their star formation activity, conclusions about the general galaxy population cannot be drawn using these galaxies.

Together with the study presented in Martin et al. (2019), the analysis in this chapter offers a theoretical counterpart to new and future deep-wide surveys like the HSC-SSP and LSST. As noted earlier, these surveys will offer galaxy completeness down to at least $M_\star \sim 10^7$ $M_\star$ in the nearby Universe, providing a revolutionary increase in discovery space. In future studies, we

will compare our theoretical studies to data from such surveys to explore LSBG formation and constrain the physics of galaxy evolution, in detail, in the low-surface-brightness regime.

Chapter 6

Dark-matter-deficient dwarf galaxies form via tidal stripping of dark matter in interactions with massive companions

6.1 Introduction

In the standard ΛCDM paradigm, dwarf galaxies ($M_\star < 10^{9.5}$ $M_\odot$) are expected to be dark matter (DM) rich, because their shallow potential wells make it easier for processes like stellar and supernova feedback to drive gas out from their central regions at early epochs. This reduces their star formation rates and produces systems that have a lower stellar content at a given DM halo mass (Dubois and Teyssier, 2008a; Di Cintio et al., 2017; Chan et al., 2018). Dwarf galaxies are expected to form a natural extension to the stellar-to-halo mass relation in massive galaxies (Moster et al., 2010; Read et al., 2017), with the $M_{halo}/M_\star$ values expected to progressively increase towards lower stellar masses. However, some recent observational studies appear to challenge this picture. A growing number of studies suggest that some dwarf galaxies may deviate strongly from the expected stellar-to-halo mass relation (e.g. van Dokkum et al., 2018a, 2019; Guo et al., 2019; Hammer et al., 2020), with unexpectedly low DM fractions. For example, Guo et al. (2019) have found 19 nearby dwarf galaxies that are DM deficient. The majority of these galaxies (14/19) appear to be relatively isolated, without many nearby bright galaxies, implying that they might have been born DM deficient. van Dokkum et al. (2018a, 2019) have studied two dwarf galaxies in group environments which could exhibit $M_{halo}/M_\star$ values (within 7.6 kpc) close to unity, suggesting that they may have DM fractions that are around 400 times lower than that expected for galaxies of their stellar mass. There is still some controversy surrounding the

validity of these findings (e.g. Oman et al., 2016; Martin et al., 2018b; Blakeslee and Cantiello, 2018; Emsellem et al., 2019; Fensch et al., 2019b; Trujillo et al., 2019), mostly focusing on the reliability of obtaining accurate distance measurements for these systems. For example, in the case of the van Dokkum et al. (2018a) galaxy, a measured distance of 13 Mpc, as suggested by Trujillo et al. (2019), rather than the quoted ~ 20 Mpc in van Dokkum et al. (2018a), would make $M_{halo}/M_\star > 20$, making it a relatively normal dwarf galaxy (but see van Dokkum et al. (2018b) for an alternate view). The existence of galaxies that are deficient in DM could pose a serious challenge to the ΛCDM model, as it is difficult for galaxies that are rich in baryons to form in halos that are deficient in DM. It is, therefore, important to investigate whether there are natural channels for the formation of such galaxies in the standard model.

Some formation methods for DM deficient galaxies have been suggested in the recent literature. A well-known channel for forming such systems are tidal dwarfs (Wetzstein et al., 2007; Bournaud et al., 2008a,b; Kaviraj et al., 2012b; Kroupa, 2012; Ploeckinger et al., 2015; Haslbauer et al., 2019). These dwarf galaxies are formed in the tidal tails that emerge as a result of gas-rich major mergers of massive galaxies, either through Jeans instabilities within the gas which lead to gravitational collapse and the formation of self-bound objects (Elmegreen et al., 1993), or a large fraction of the stellar material in the progenitor disk being ejected and providing a local potential well into which gas condenses and fuels star formation (e.g. Barnes and Hernquist, 1992; Duc et al., 2004; Hancock et al., 2009). However, the contribution of tidal dwarfs to the galaxy population, particularly at the stellar masses of the DM deficient galaxies found by recent observational studies ($\sim 10^9$ M$_\odot$), is extremely small (e.g. Kaviraj et al., 2012b).

It has been postulated that DM deficient galaxies could form via high velocity, gas-rich mergers of dwarf galaxies themselves (Silk, 2019; Shin et al., 2020). In this scenario, DM deficient galaxies form as these mergers separate DM from the warm disc gas, which is then compressed by tidal interactions and shocks to form stars. Another potential formation mechanism may involve anomalously weak stellar feedback, due to low star formation rate surface densities. As a result of this, significant amounts of gas are not ejected from the disc, resulting in a galaxy which has a high baryon fraction and therefore a relatively low DM fraction (e.g Mancera Piña et al., 2020).

A further formation channel is DM stripping of satellite galaxies, particularly in extreme environments such as clusters (Ogiya, 2018; Jing et al., 2019; Niemiec et al., 2019). Indeed, both N-body simulations in a range of environments, from Milky-Way mass halos (Hayashi et al., 2003; Kravtsov et al., 2004; Diemand et al., 2007; Rhee et al., 2017; Buck et al., 2019) to clusters (Ghigna et al., 1998; Gao et al., 2004; Tormen et al., 2004; Nagai and Kravtsov, 2005; van den Bosch et al., 2005; Giocoli et al., 2008; Xie and Gao, 2015), and analytical models (e.g. Mamon, 2000; Gan et al., 2010; Han et al., 2016; Hiroshima et al., 2018) have shown that DM stripping is capable of removing parts of a galaxy's halo in group and cluster environments. It has been

suggested that this process could drive a large scatter in the stellar-to-halo mass relation for satellite galaxies in groups and clusters, moving them from their initial positions towards lower halo masses (Vale and Ostriker, 2004; Smith et al., 2016; Bahé et al., 2017; Rhee et al., 2017; Niemiec et al., 2017, 2019), and therefore lower $M_{halo}/M_\star$ values.

A comprehensive analysis of whether DM deficient systems (dwarfs in particular) can form naturally as a by-product of the process of galaxy evolution demands a hydrodynamical simulation in a cosmological volume which has both high mass and spatial resolution. The hydrodynamics is required for spatially-resolved predictions for the DM and baryons. The cosmological volume enables us to probe galaxy populations in a statistical manner, taking into account environmental effects (which idealised studies, for instance, cannot do), and is particularly important for making meaningful comparisons to large observational surveys (e.g. forthcoming datasets like LSST, Robertson et al., 2019).

In recent years, large hydrodynamical cosmological simulations, e.g. Horizon-AGN (Dubois et al., 2014a), Illustris (Vogelsberger et al., 2014b), EAGLE (Schaye et al., 2015) and Simba (Davé et al., 2019), have been successful in reproducing many properties of (massive) galaxies over cosmic time (e.g. Kaviraj et al., 2017). For example, Saulder et al. (2020) have investigated the properties of massive ($M_\star > 10^{9.5} M_\odot$) DM deficient galaxies which are isolated in these large cosmological simulations, akin to those found in Guo et al. (2019). They find that these galaxies are probably regular objects that undergo un-physical processes at the boundary of the simulation box and are therefore artefacts. Jing et al. (2019) on the other hand have studied the formation of massive ($10^9 M_\odot < M_\star < 10^{10} M_\odot$) DM deficient galaxies in the EAGLE and Illustris simulations, in denser environments. They find that a non-negligible fraction (2.6 per cent in EAGLE, and 1.5 per cent in Illustris) of satellite galaxies, in large groups and clusters ($M_{200} > 10^{13} M_\odot$), are DM deficient in their central regions. These galaxies, which are not initially DM deficient, become so through the stripping of DM by tidal interactions with their host galaxy, an effect that has also been noted in Horizon-AGN (Volonteri et al., 2016)).

However, given that these environments are relatively rare, and since the majority of dwarfs have lower stellar masses than the galaxies in these studies, it remains unclear from these studies (1) whether DM deficient galaxies can form in low-density environments which host the majority of objects, and (2) whether they can form in the dwarf regime where galaxies are expected to be significantly more DM dominated at early epochs, and where most observational studies that have found DM deficient galaxies are focussed. It is worth noting that it is challenging to probe dwarf galaxy evolution using the large-scale cosmological simulations mentioned above due to their relatively low mass and spatial resolutions. For example, the DM mass resolution is $\sim 10^8$ $M_\odot$ in Horizon-AGN, EAGLE and Illustris and the spatial resolution of these simulations is around a kpc. Recall that the stellar scale height of the Milky Way, for example, is ~ 300 pc

(e.g. Kent et al., 1991; López-Corredoira et al., 2002; McMillan, 2011), which implies that much better spatial resolution is needed to properly resolve dwarfs.

An accurate exploration of the evolution of dwarf galaxies requires a cosmological simulation with significantly better mass and spatial resolution, in order to properly resolve the processes on the small spatial scales involved. In this study, we use the `NewHorizon` hydrodynamical cosmological simulation, to understand the formation of DM deficient galaxies in the stellar mass range $M_\star > 10^8$ $M_\odot$. `NewHorizon` is a zoom-in of an average region within Horizon-AGN simulation, which has a volume of 142 comoving Mpc^3). `NewHorizon` offers a maximum spatial resolution of 34 pc and mass resolutions of 10^4 $M_\odot$ and 10^6 $M_\odot$ in the stars and DM respectively, making it an ideal tool to study the evolution of dwarf galaxies (e.g. Martin et al., 2020). At the lower limit of our stellar mass range, a typical low-redshift dwarf galaxy contains ~10,000 stellar and ~10,000 DM particles respectively. Our aims are to (1) study whether DM deficient dwarf galaxies form naturally in `NewHorizon`, (2) estimate the frequency with which they are created and (3) quantify the processes that produce these galaxies.

This chapter is structured as follows. In Section 6.2, we briefly describe the selection of DM deficient galaxies in `NewHorizon` (see Chapter 5 for more details). In Section 6.3, we study the processes that create these objects. We summarise our findings in Section 6.4.

6.2   Selection of galaxies that are deficient in DM

Figure 6.1 shows the stellar mass ($M_\star$) vs the ratio of the DM halo (M_{halo}) and stellar mass, for galaxies in `NewHorizon` at $z = 0.25$. We study galaxies which have stellar masses above 10^8 $M_\odot$, which remain well-resolved in the simulation to early epochs. We note that, while there are some galaxies in our sample above the mass threshold that we use to define dwarfs ($M_\star < 10^{9.5}$ $M_\odot$), the overwhelming majority of galaxies in our study are dwarfs. We split this galaxy population into objects that are centrals (open black circles) and satellites (coloured circles). Centrals are defined as galaxies whose DM halo has not been accreted by a larger halo, therefore they are the main galaxy in their respective DM halo. Satellite galaxies are defined as systems whose DM halos have been accreted by a larger halo. The satellites are further divided into 'DM deficient' galaxies (blue circles), defined as objects that exhibit $M_{halo}/M_\star < 10$, satellites that coincide with the relatively tight locus defined by the centrals (orange circles) and 'DM poor' galaxies (green circles) which fall in between these populations. The satellites that occupy the same region in the $M_\star$-$M_{halo}/M_\star$ plane as the centrals (orange circles) are essentially unstripped in their DM. For the analysis below, where we study the reasons for the DM stripping in the DM deficient and DM poor populations, we use these unstripped satellites as a control sample, since these galaxies show 'normal' levels of DM (i.e. a similar DM content to that of centrals).
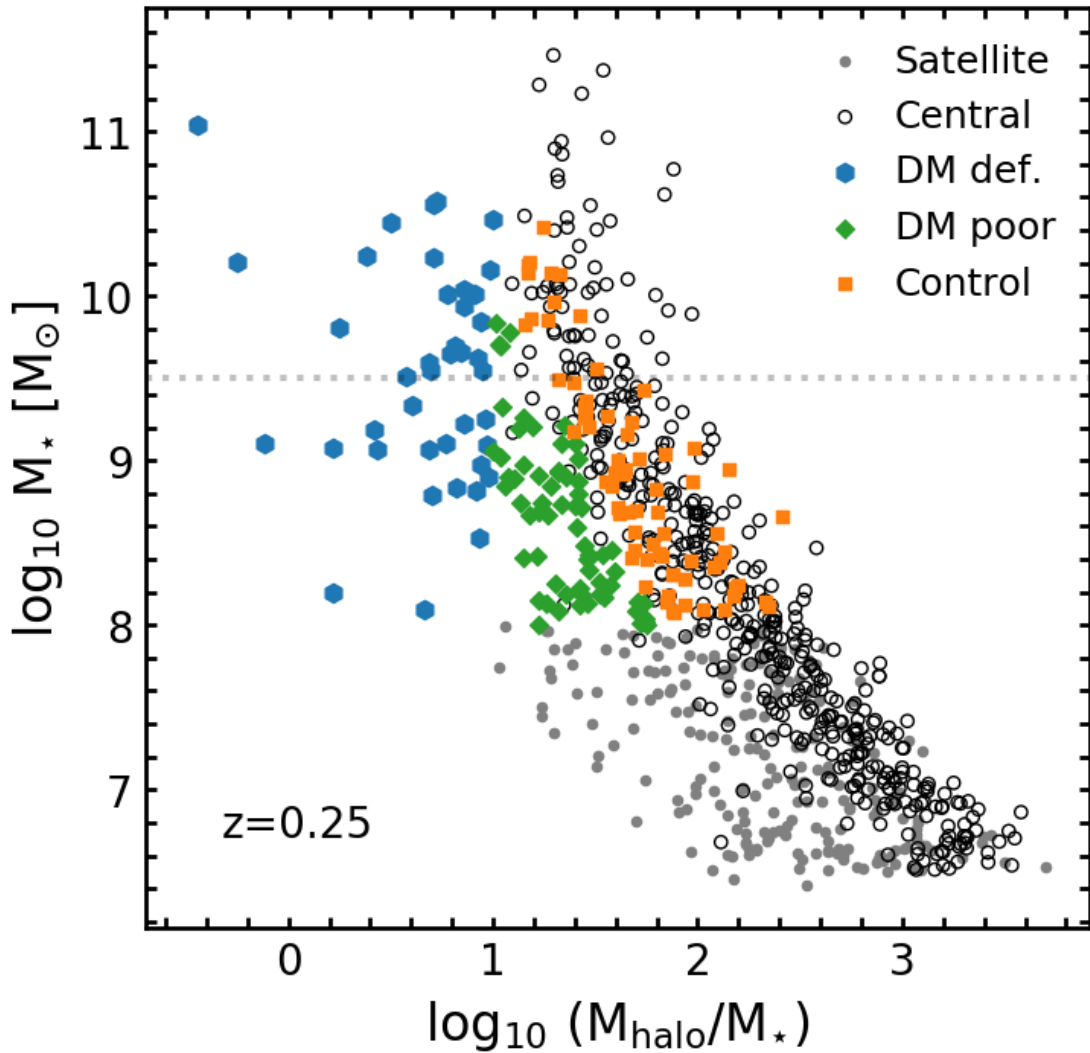
FIGURE 6.1: The stellar mass ($M_\star$) vs the ratio of the DM halo (M_{halo}) and stellar mass for galaxies in `NewHorizon` at $z = 0.25$. In this study, we focus on galaxies with $M_\star > 10^8$ $M_\odot$, which are well-resolved in the simulation to early epochs (galaxies that are less massive that this threshold are shown simply for completeness). We split this population into objects that are centrals (open black circles) and satellites (coloured symbols). The satellites are further divided into 'DM deficient' galaxies, defined as objects that exhibit $M_{halo}/M_\star < 10$ (blue symbols), satellites that coincide with the relatively tight locus defined by the centrals (orange symbols) and 'DM poor' galaxies (green symbols) which fall in between these two populations. The satellites that coincide with the centrals (orange symbols) are essentially unstripped in their DM. We use these unstripped satellites as a control sample, since these galaxies show normal levels of DM. The grey dotted line denotes the mass threshold adopted for defining dwarf galaxies. While there are some galaxies in our sample above this threshold, the overwhelming majority of galaxies in our study are dwarfs.

`NewHorizon` is a high resolution zoom of Horizon-AGN but the remaining volume of the original simulation is still simulated at much lower resolution. It is therefore possible for higher-mass (low resolution) DM particles to enter the high resolution region of `NewHorizon` from the surrounding lower-resolution regions. Given the large mass difference, these DM particles may interact with galaxies they are passing through in unusual ways. The vast majority of galaxies affected by this exist at the outer edge of the `NewHorizon` sphere. The DM deficient galaxies studied in this chapter all have DM halos that do not contain any low-resolution DM particles, ensuring that this does not influence this study.

Note that in this study we define M_{halo} to be the total mass of the DM halo associated with the galaxy. This is in contrast to previous studies (e.g. Jing et al., 2019) that have mostly looked at the central regions of the DM halo (e.g. two times the half-mass radius in the stars). The fractions of DM deficient, DM poor, control and central galaxies in `NewHorizon` are 12, 19, 18 and 51 per cent respectively. Recall that the centrals and the controls (i.e. the unstripped satellites) show normal levels of DM, so that the fraction of galaxies that show some sort of a deficiency in their DM content is around 30 per cent.

In Figure 6.2 we show the evolution of the median properties of each population. The top, middle and bottom panels show the evolution in the stellar mass, DM halo mass and the $M_{halo}/M_{\star}$ ratios respectively. While the stellar mass evolution is similar across all populations, the DM halo mass evolves differently, with the DM deficient and DM poor galaxies exhibiting declines in DM content at late epochs. The scatter in the $M_{\star}$ vs $M_{halo}/M_{\star}$ relation seen in Figure 6.1 is therefore driven by the removal of DM in these galaxies, which produces systems that are poorer in DM for their stellar mass.

While the gradual change from the locus of centrals and controls seen in Figure 6.1 indicates that the DM deficient and DM poor populations are not simply artefacts and are likely created by a persistent process that operates on these galaxies, we perform several checks to ensure that this is indeed the case. The galaxies in these populations are found in all parts of the simulation sphere (as discussed further in Section 6.3 and Figure 6.3) and not just at the edges of this volume where boundary effects can produce spurious effects. They also exhibit 100 per cent purity in DM, so that their evolution is not driven by interactions with massive low-resolution DM particles passing through them. Finally, as shown in the analysis below (Figure 6.5) the reduction of DM is very gradual, rather than abrupt, which indicates that this phenomenon is not a result of misallocation of particles between DM halos.
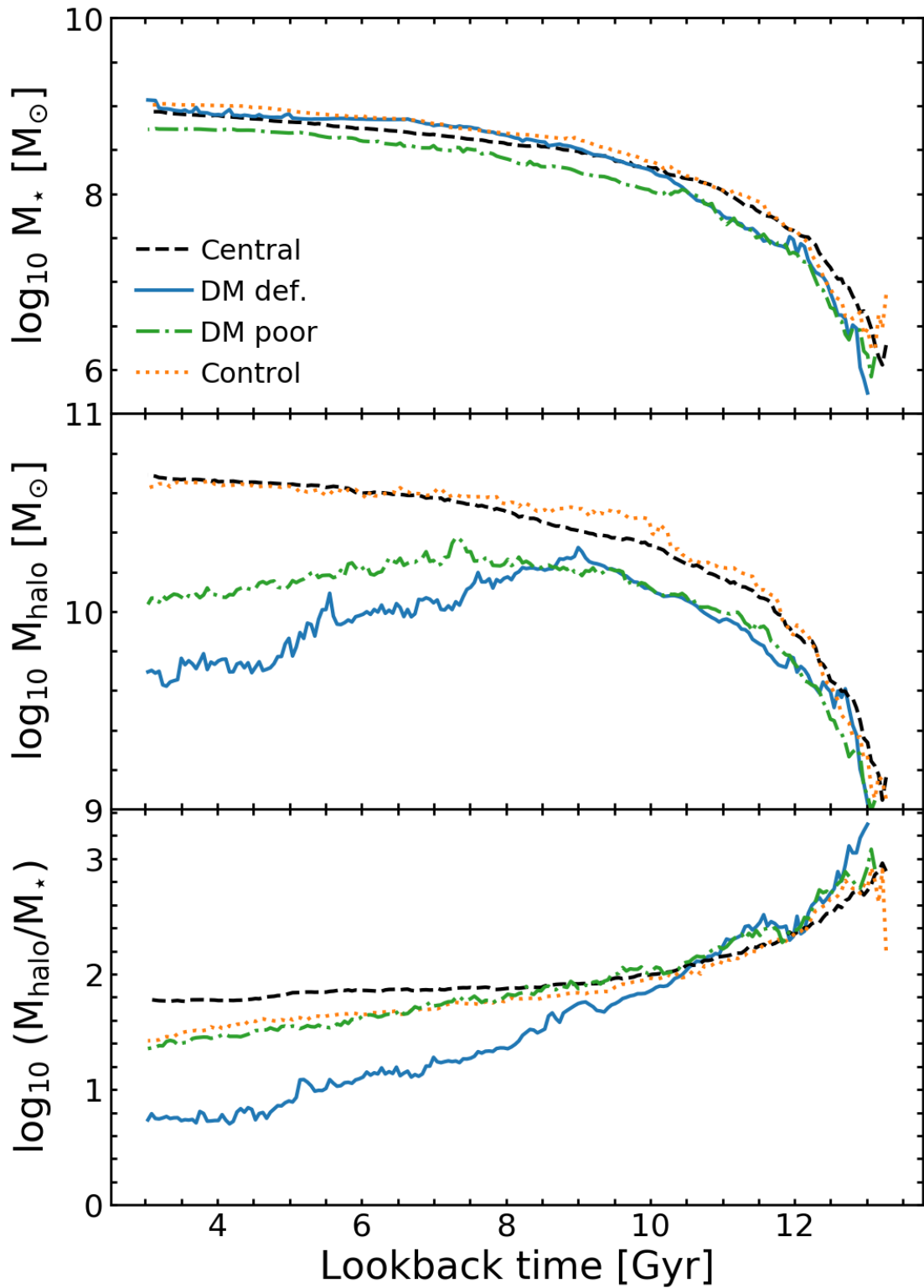
FIGURE 6.2: The evolution of the median properties of the central, DM deficient, DM poor and control populations for $M_\star > 10^8 \, M_\odot$. The top, middle and bottom panels show the evolution in the stellar mass, DM halo mass and the $M_{halo}/M_\star$ ratio respectively. While the stellar mass evolution is similar across all populations, the DM halo mass evolves differently, with the DM poor and DM deficient galaxies exhibiting sharp declines in their halo mass at late epochs (i.e. look-back times less than 8 Gyrs). This, in turn, drives the scatter in the M_{halo} vs $M_\star$ relation seen in Figure 6.1.
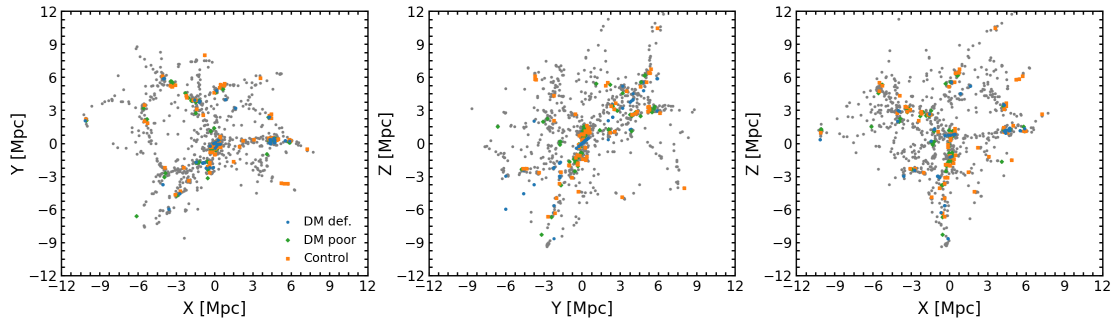
FIGURE 6.3: The locations of our different galaxy populations (DM deficient, DM poor and control) in `NewHorizon` at $z = 0.25$, in three mutually orthogonal projections (*xy*, *yz* and *xz*) of the simulation volume. The centrals are shown using small grey circles. The DM deficient and DM poor populations form in all parts of the Universe, with the DM deficient galaxies generally showing a preference for the nodes of the cosmic web.
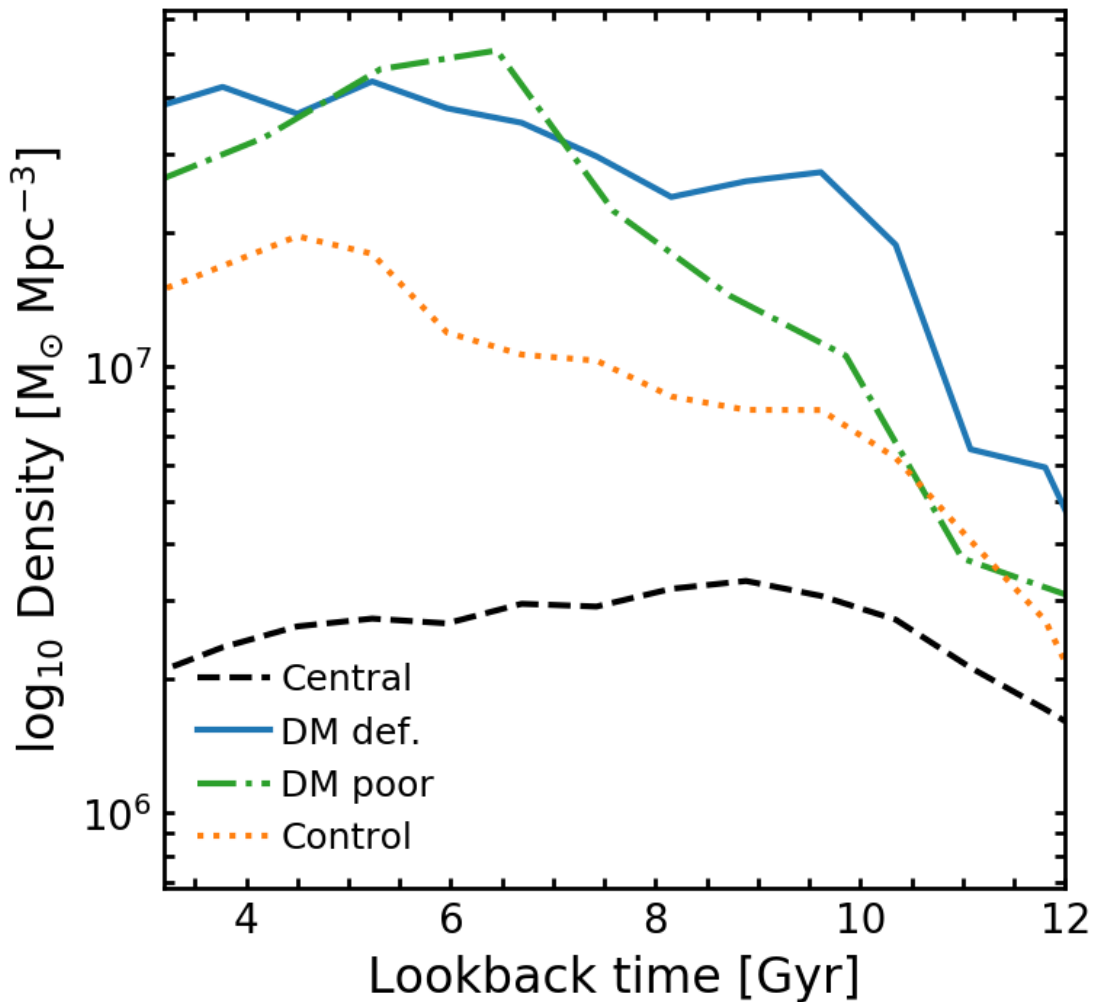
FIGURE 6.4: The local 3D density for the different populations vs look-back time for galaxies with $M_\star > 10^8$ M$_\odot$. The local 3D density is calculated using an adaptive kernel density estimation method (see text in Section 6.3 for details). Recall that `NewHorizon` does not contain rich clusters and therefore the highest density regions in the simulation correspond to large groups, with halo masses of $\sim 10^{13}$ M$_\odot$. Both the DM deficient and DM poor populations show elevated local densities, compared to the controls, indicating that local density may play a role in their formation.
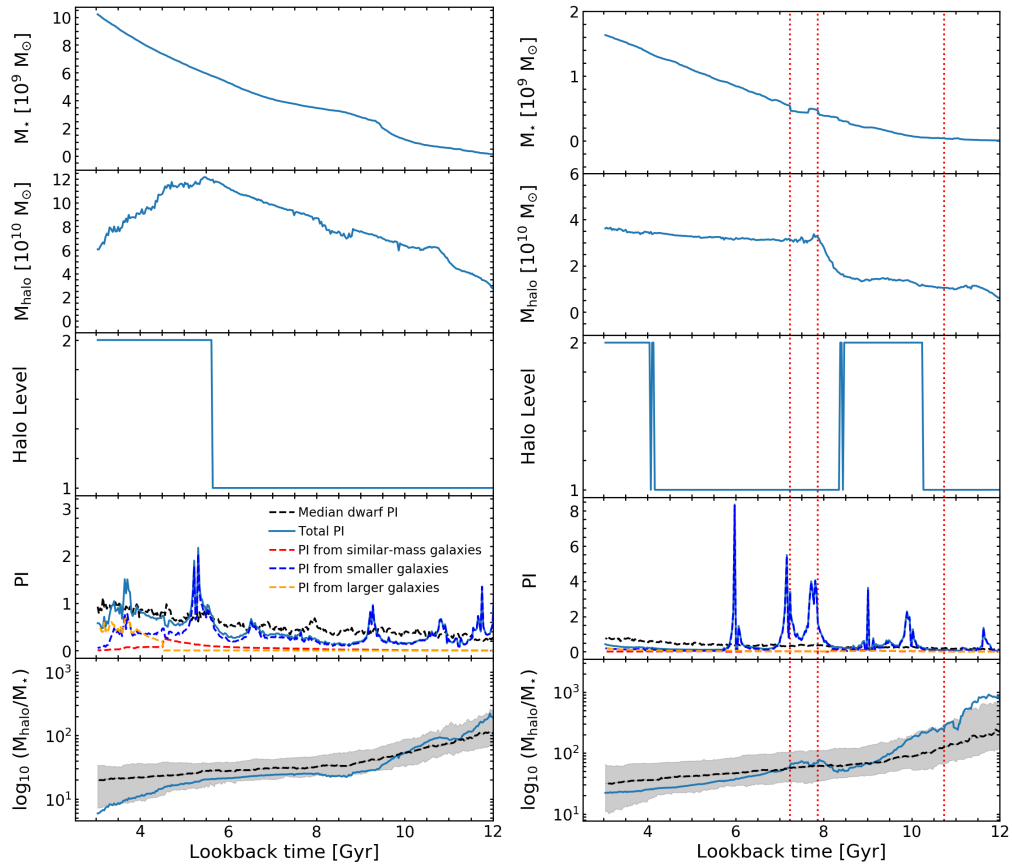
FIGURE 6.5: The rows show (from top to bottom) the evolution of the stellar mass, DM halo mass, the halo level (central [level 1] or satellite [level > 1]), perturbation index (PI) and the $M_{halo}/M_\star$ ratio of the galaxy in question. The PI is split into contributions from 'similar-mass' galaxies (those that have $0.3\,M_{gal} < M_\star < 3\,M_{gal}$, where M_{gal} is the stellar mass of the galaxy in question), 'smaller galaxies' (those that have $M_\star < 0.3\,M_{gal}$) and 'larger galaxies' (those that have $M_\star > 3\,M_{gal}$). The 'median dwarf PI' indicates the median PI experienced by galaxies with stellar masses within 0.5 dex of the galaxy in question. In the bottom panel, the dashed black line indicates the median halo-to-stellar mass ratio of galaxies with stellar masses within 0.5 dex of the galaxy in question and the shaded region is its 1σ dispersion. The left-hand column shows a DM deficient galaxy, while the right-hand column shows a control galaxy. The dotted red lines indicate times when galaxy mergers, with mass ratios greater than 10:1, take place.

6.3 Formation of DM deficient galaxies through stripping of DM in tidal interactions

We begin our analysis by exploring the local environment of our different satellite populations (DM deficient, DM poor, and control). Figure 6.3 shows the positions of these populations in the cosmic web. The DM deficient and DM poor populations form in all parts of the Universe, with the DM deficient galaxies generally showing a preference for the nodes of the cosmic web. To explore local galaxy density more quantitatively, we follow Martin et al. (2018) and define a 3-D local number density of objects around each galaxy. The local density is calculated using an
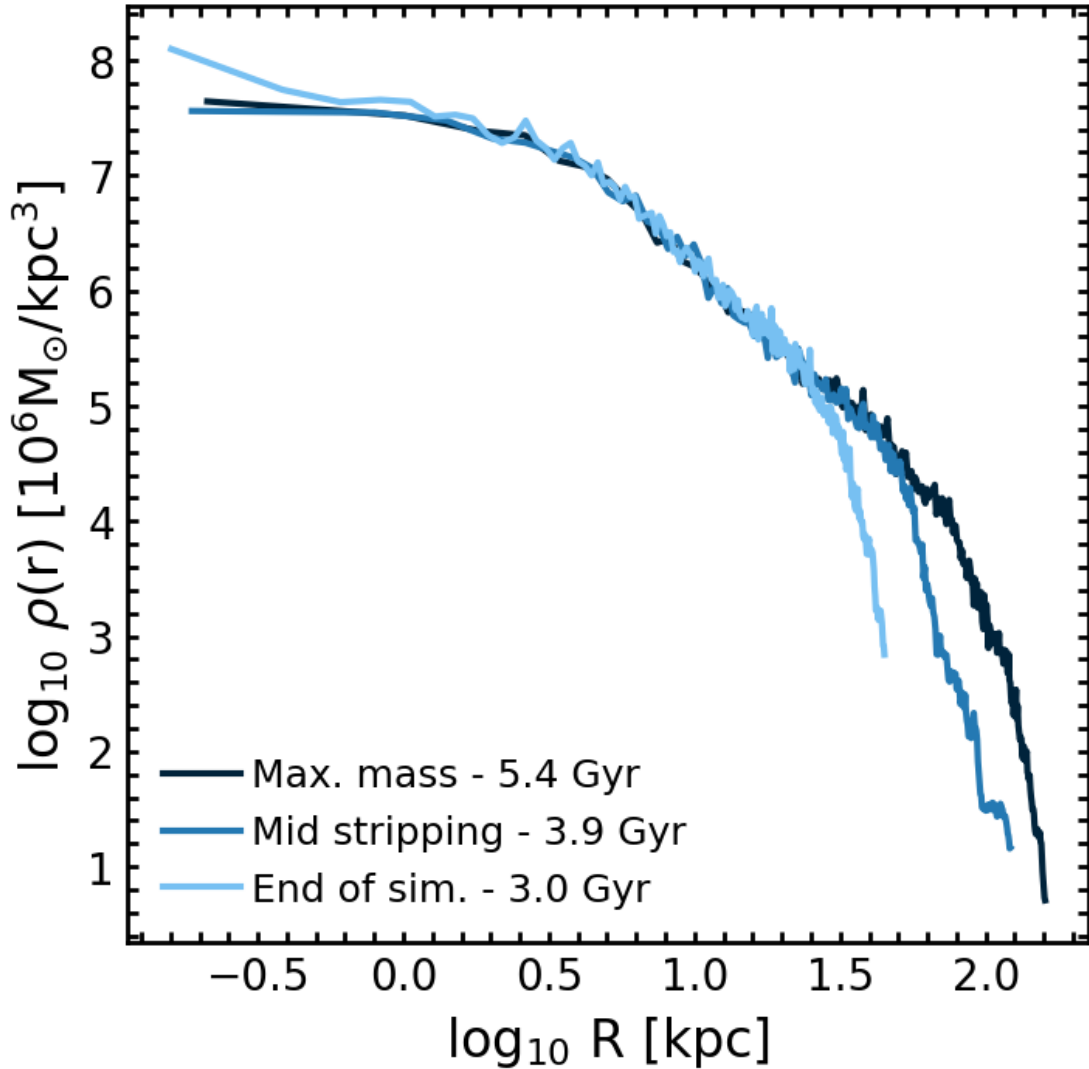
FIGURE 6.6: Evolution of the DM density profile, for various lookback times, in the DM deficient galaxy described in the left-hand column of Figure 6.5. The evolution is shown from the point at which the galaxy becomes a satellite, which is also the point at which the DM stripping starts ('max mass'), through to the end of the simulation. The DM stripping takes place in the outskirts of the dwarf where the gravitational potential well is shallowest and DM particles are more loosely bound.

adaptive kernel density estimation method[1], where the width of the kernel used for multivariate density estimation is responsive to the local density of the region, such that the error between the density estimate and the true density is minimised (Breiman et al., 1977; Ferdosi et al., 2011; Martin et al., 2018). The density estimate takes into account all galaxies with stellar masses above 10^8 M$_\odot$. In Figure 6.4 we show the evolution of the local density occupied by our different populations. Recall that `NewHorizon` does not contain rich clusters and therefore the highest density regions in the simulation correspond to large groups with halo masses of $\sim 10^{13}$ M$_\odot$.

---

[1]Code available at github.com/garrethmartin/MBEtree
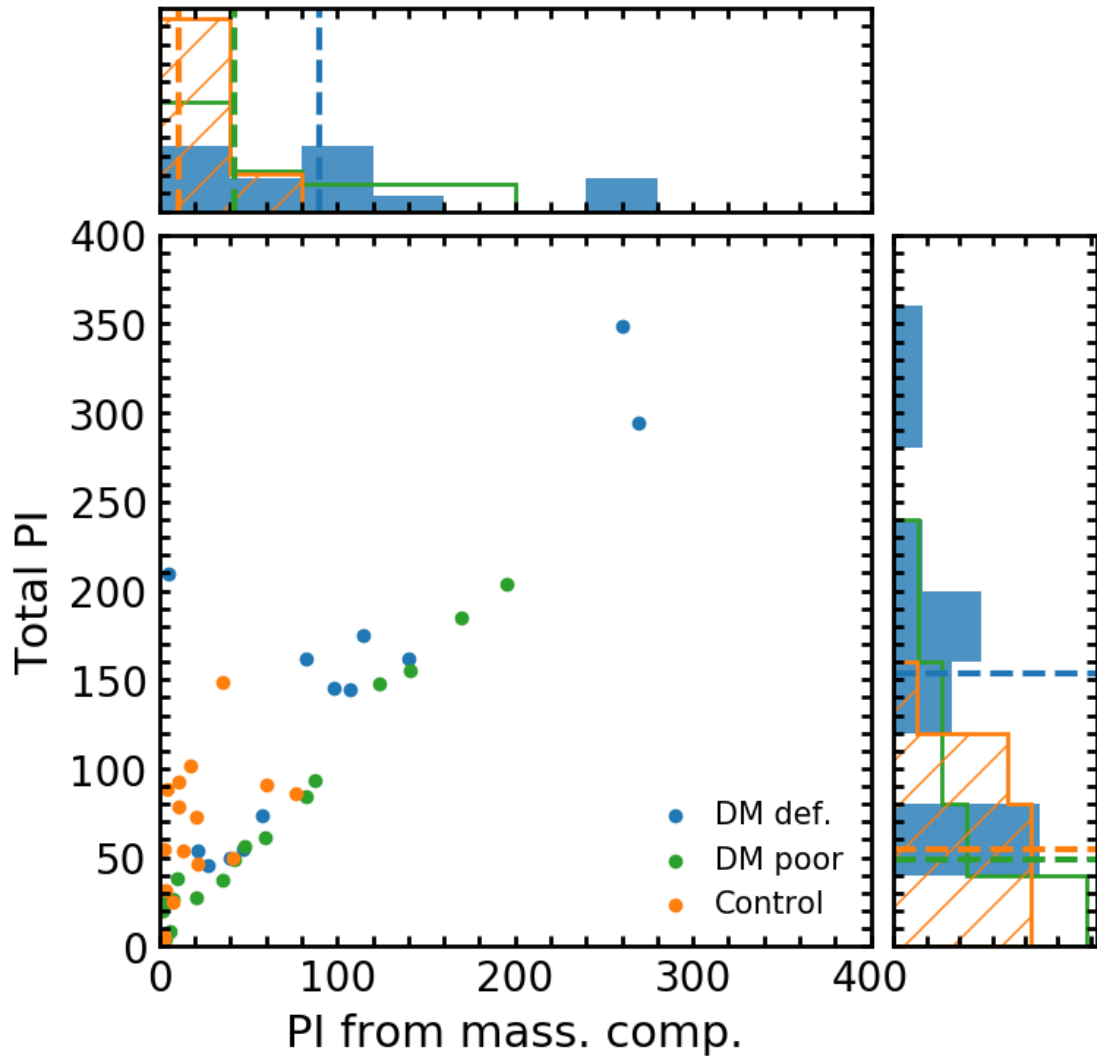
FIGURE 6.7: The total perturbation index (PI) from all companions vs that just from the massive companion, integrated over the period from when the dwarf becomes a satellite until the end of the simulation. The different satellite populations are shown using different colours. The histograms are normalised and the dashed lines indicate median values. DM deficient galaxies show both larger values for the total PI and the PI from massive companions, compared to their control counterparts (with the DM poor galaxies falling in between these two populations). Note also that the PI from the massive companion dominates the total PI in the DM deficient and DM poor populations.

Figures 6.3 and 6.4 indicate that the DM deficient and DM poor populations form in all regions of the Universe. The DM deficient galaxies generally show a preference for the nodes of the cosmic web. Both the DM deficient and DM poor populations show elevated local densities, compared to the controls, indicating that local density may play a role in their formation. Not unexpectedly, the dwarf centrals reside in lower density environments, where the probability of interacting with, and becoming the satellite of, a more massive galaxy is lower.

The evolution of galaxies is influenced by a combination of internal processes, like supernova (e.g. Kimm and Cen, 2014) and AGN (e.g. Croton et al., 2006) feedback, and external processes
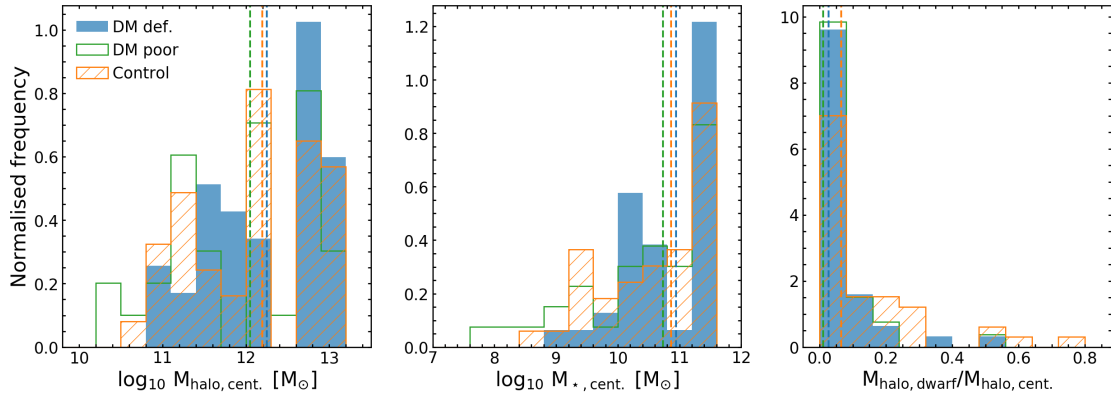
FIGURE 6.8: The DM halo (left) and stellar (centre) mass of the massive centrals that host our dwarf satellites and the halo mass ratio (right) between the dwarf satellite and its massive central. The dashed lines indicate the median values of the histograms. The distribution of massive central masses and halo mass ratios are similar for all dwarf populations and are therefore not the principal reason for the differences in perturbation index (PI) in these populations.
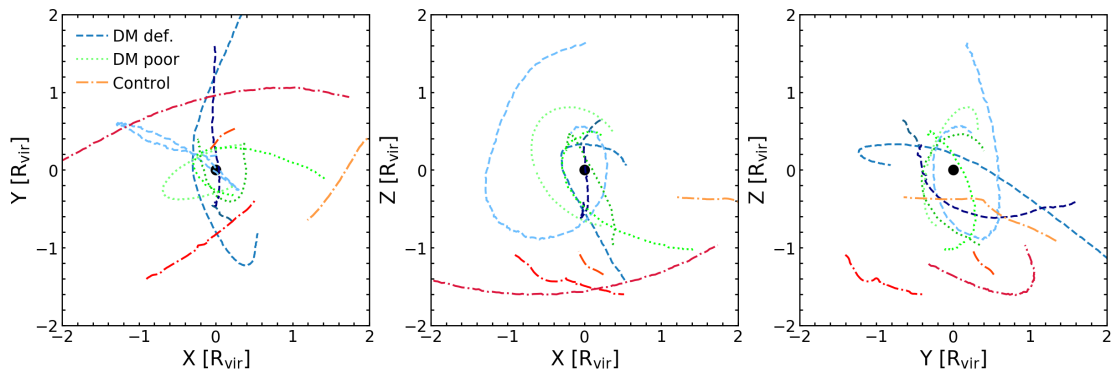
FIGURE 6.9: The orbits of four galaxies in each of the DM deficient (shades of blue), DM poor (shades of green) and control (shades of orange) populations around their centrals. Individual galaxy orbits are shown using different shades of the colour in question (see legend). We show orbits from the point at which the dwarf in question becomes a satellite through to the end of the simulation. The orbital distances are normalised by the virial radius of the central, which is always shown at the origin.

such as tidal perturbations (e.g. Martin et al., 2019), mergers (e.g. Kaviraj, 2014b,a; Kaviraj et al., 2019) and ram pressure (e.g. Hester, 2006). Baryonic feedback and ram pressure are not capable of removing significant amounts of DM in galaxies, except in the very central regions through rapid expansion of gas (Navarro et al., 1996; Governato et al., 2012; Teyssier et al., 2013). Furthermore, the steady stripping of DM, which drives the creation of the DM poor and DM deficient populations, requires a dynamical process, suggesting that tidal perturbations (possibly including mergers) are likely to be important in giving rise to these systems. In particular, interactions between a massive galaxy and a lower mass companion typically results in the stripping of material from the smaller companion. This is because, while the same tidal force acts on both objects, the smaller companion is not as strongly bound and stripping typically takes place from the outskirts of the system where the depth of the gravitational potential well is shallowest (Smith et al., 2016).
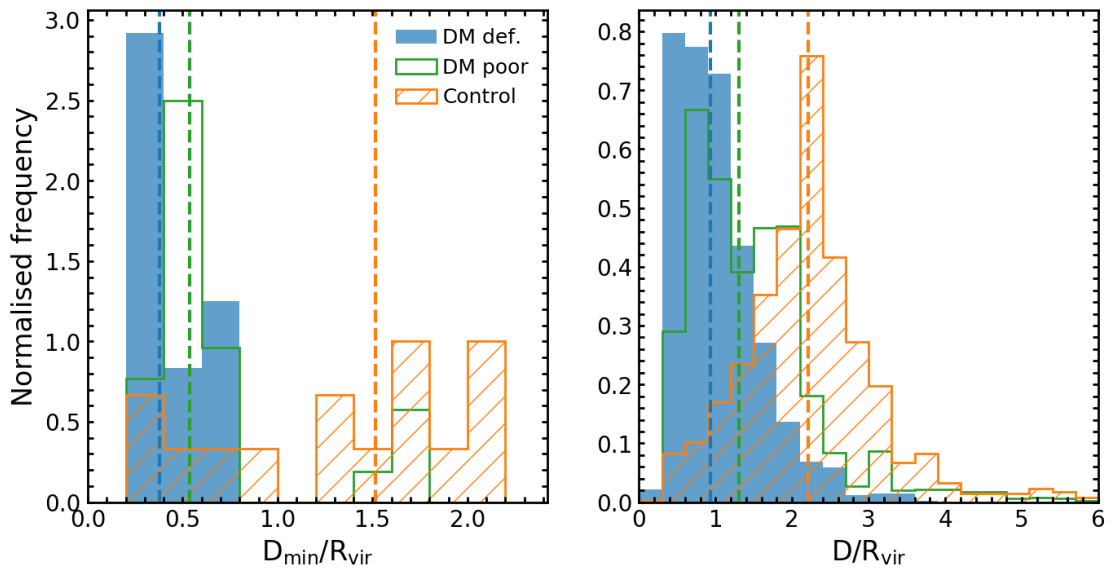
FIGURE 6.10: **Left:** Minimum distance between dwarfs and their massive centrals for our different satellite populations. The dashed lines indicate the median value of each distribution. **Right:** Orbital distances (normalised by the virial radius of the central) between the dwarf and their massive central at all timesteps in the period between the dwarf becoming a satellite and the end of the simulation. The DM deficient and DM poor populations exhibit closer orbits than their control counterparts which drives the higher perturbation index (PI) values seen in these populations.
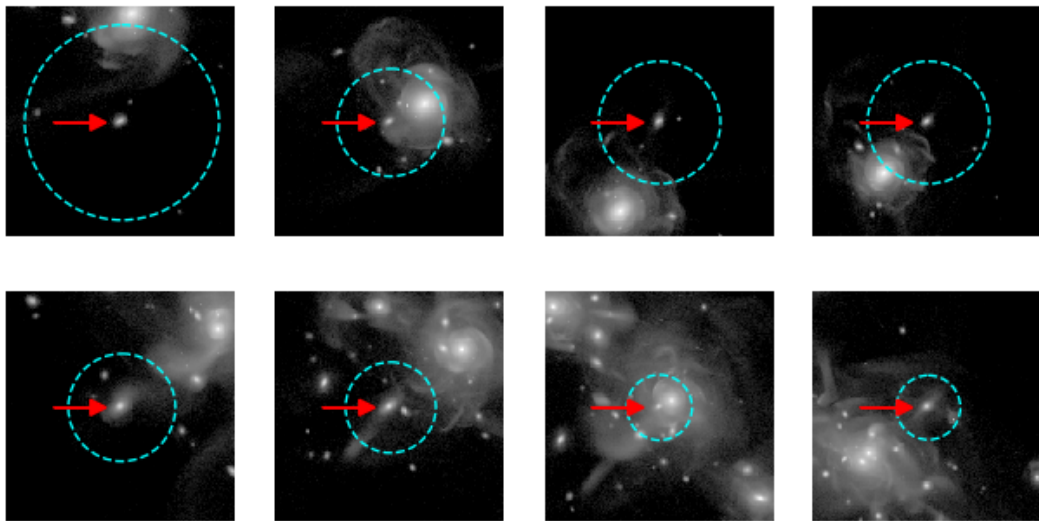
FIGURE 6.11: *r*-band mock images of two example systems that bracket the types of interactions that lead to DM stripping. Each image is 200 proper kpc across. In all images, the DM deficient galaxy in question is at the centre of the image and indicated by the red arrow. The blue circle shows the virial radius of the DM deficient galaxy. The sequence (where time moves forward from left to right) shows ~3 Gyrs of evolution. The top row shows a two body interaction, while the bottom row shows a more complex interaction where the dwarf interacts with a larger companion which dominates a group. In both cases, the dwarf undergoes significant DM stripping and ends up as a DM deficient galaxy.

To quantify the effect of tidal perturbations, we follow Martin et al. (2019) to define a dimensionless 'perturbation index' (PI) that quantifies the strength of the ambient tidal field around a galaxy:

$$PI = \sum_i \left(\frac{M_i}{M_{halo}} \right) \left(\frac{R_{vir}}{D_i} \right)^3, \tag{6.1}$$

where M_{halo} is the halo mass of the galaxy in question, R_{vir} is the virial radius of its DM halo, M_i is the DM halo mass of the ith perturbing galaxy and D_i is the distance to the ith perturbing galaxy. We consider all perturbing galaxies within 3 Mpc of the object in question.

We use the PI to explore the trends in the tidal perturbations in our different populations and study how these perturbations may be driving the DM stripping in the DM poor and DM deficient populations. In Figure 6.5, we visually illustrate the evolution of two typical objects (selected randomly) in the DM deficient and control populations. The left-hand column shows the DM deficient galaxy, while the right-hand column shows the control galaxy. Recall that the control galaxies are satellites in which DM is not stripped and that the DM deficient galaxies are systems which have the lowest values of $M_{halo}/M_\star$ (Figure 6.1). These two populations therefore bracket the dwarf population as a whole. The rows show (from top to bottom) the evolution of the stellar mass, DM halo mass, halo level (central [level 1] or satellite [level > 1]), PI and the $M_{halo}/M_\star$ ratio of the galaxy in question. The halo level determines whether a DM halo is subsumed within a larger halo, if the halo level is 1 then it is not inside a larger halo and is therefore a central. If halo level is greater than 1 then the halo is inside a larger halo and therefore is a satellite. For example a level 2 halo is inside a level 1 halo, a level 3 halo is inside a level 2 halo which is inside a level 1 halo etc.

The PI is split into contributions from 'similar-mass' galaxies (those that have $0.3 \, M_{gal} < M_\star < 3 \, M_{gal}$, where M_{gal} is the stellar mass of the galaxy in question), 'smaller galaxies' (those that have $M_\star < 0.3 \, M_{gal}$) and 'larger galaxies' (those that have $M_\star > 3 \, M_{gal}$). While the DM deficient galaxy shows a steady increase in stellar mass (row 1), it exhibits sustained DM stripping after a look-back time of around 6 Gyrs (row 2). The stripping coincides with the galaxy transitioning from being a central to a satellite (row 3) and an increase in the PI from massive galaxies, even as that from smaller galaxies decreases (row 4). The DM stripping drives the $M_{halo}/M_\star$ ratio down, until it is below the region traced by the median ratio for galaxies which have stellar masses within ±0.5 dex (row 5). The principal difference between the DM deficient galaxy and its control counterpart is that, even after the control object becomes a satellite, the PI due to massive galaxies does not increase and the control galaxy does not exhibit significant DM stripping. This shows that the simulation does not assume that DM halos should be stripped when they become a satellite and that it is indeed some physical process that causes the DM stripping.

PI	PI frac.	Cumul. PI	Mass ratio	PI	PI frac.	Cumul. PI	Mass ratio
0.48	0.78	0.78	5.75	0.09	0.25	0.25	10.98
0.05	0.08	0.86	0.01	0.04	0.12	0.37	0.67
0.01	0.02	0.88	0.88	0.04	0.12	0.49	0.02
0.01	0.01	0.89	0.01	0.02	0.04	0.53	0.01

TABLE 6.1: The four largest perturbation index (PI) contributions from individual companions for the DM deficient (left hand table) and control (right hand table) galaxy shown in Figure 6.5, at the point where the galaxy becomes a satellite. Columns in each table show (from left to right) the PI contributed by the individual companion, the fraction this represents of the total PI, the cumulative fraction of PI contributed by this companion and those in previous rows and the mass ratio of the companion and the dwarf galaxy in question. The left hand table, which corresponds to the DM deficient galaxy, shows that ~80 per cent of the total PI comes from one larger companion with the next largest PI contribution being an order of magnitude smaller. For the control galaxy the largest PI contribution, while also derived from a larger companion, is a factor of 5 smaller than that in the DM deficient galaxy and contributes only 25 per cent of the total PI, with many smaller companions contributing PI values which are within a factor of 2 of that from the larger companion.

In Figure 6.6, we show the evolution of the DM density profile (calculated using all DM particles associated with the galaxy) of the DM deficient galaxy described in the left-hand column of Figure 6.5. The evolution is shown from the point at which the galaxy becomes a satellite (which is also the point at which the DM stripping starts), through to the end of the simulation. Not unexpectedly, the DM stripping typically takes place in the outskirts of the dwarf, where the gravitational potential well is shallower and DM particles are less well bound. The trends are identical in all DM deficient and DM poor galaxies.

In Table 6.1, we present the four largest PI contributions from individual companions, for the DM deficient and control galaxy in Figure 6.5, at the point where each galaxy becomes a satellite. The left hand table, which corresponds to the DM deficient galaxy, shows that ~80 per cent of the total PI comes from one larger companion (which is the central that hosts this dwarf), with the next largest PI contribution being an order of magnitude smaller. For the control galaxy, on the other hand, the largest PI contribution, while also derived from a larger companion (again the host central), is a factor of 5 smaller than that in the DM deficient galaxy and contributes only 25 per cent of the total PI. Indeed, many smaller companions contribute PI values which are within a factor of 2 of that from the larger companion. Note that, in all cases, the larger companion which dominates the PI in the DM deficient and DM poor galaxies is the central that hosts the dwarf satellite in question. While Figure 6.5 illustrates the trends seen in typical galaxies in the DM deficient and control populations, Figure 6.7 summarises the differences in the PI from massive galaxies seen in our different satellite populations, after the galaxies become satellites. We show both the total PI from all companions vs that just from the massive companion, integrated over the period from when the dwarf becomes a satellite until the end of the simulation. DM deficient galaxies show both larger values for the total PI and the PI from massive companions, compared to their control counterparts (with the DM poor galaxies falling in between these two

populations). Note also that the PI from the massive companion dominates the total PI in the DM deficient and DM poor populations. This indicates that the DM stripping in the DM deficient and DM poor galaxies is indeed driven by stronger interactions with a massive (central) companion.

We proceed by exploring why the DM deficient dwarfs exhibit higher values of PI due to their massive companions. Figure 6.8 indicates that both the halo (left panel) and stellar (centre panel) masses of the central that host the dwarfs are similar. In addition, the mass ratios between the dwarfs and their host centrals (right panel), are comparable across all the different populations. Therefore, these quantities are unlikely to be driving the higher values of PI in the DM deficient and DM poor populations.

However, given the strong dependence of the PI on the distance between galaxies (Equation 1), it is likely that the higher PI in DM deficient and DM poor galaxies is driven by orbits that bring them closer to their corresponding centrals. In Figure 6.9, we first illustrate this graphically by plotting the orbits of four galaxies (selected to span the mass range in our study) in each of the DM deficient, DM poor and control populations around their centrals. The orbital distances are normalised by the virial radius of the central and orbits are shown from the point at which the dwarf in question becomes a satellite to the end of the simulation. It is clear that DM deficient galaxies have orbits that bring them significantly closer to their massive central than in their control counterparts.

Figure 6.10 presents this more quantitatively, by comparing both the orbital distances (normalised by the virial radius of the central) in the period after individual galaxies become satellites, and the minimum distances between the satellites and centrals during these orbits. DM deficient dwarfs spend most of their orbits at significantly smaller distances from their centrals compared to their control counterparts, with the DM poor galaxies lying in between these two populations. The same patterns are apparent in the minimum orbital distances. The larger PI values from larger galaxies in these populations are therefore driven by orbits which bring these galaxies closer to their massive central companions. The degree of DM stripping is correlated with these orbital distances, with members of the DM deficient population (which exhibits the largest amount of stripping) spending their orbits at much smaller distances than their DM poor and control counterparts.

Given that the DM deficient galaxies are in tight orbits around nearby massive companions, it is worth considering how long these dwarfs may survive. We explore this by considering the evolution of the DM deficient population (selected in an identical way) at $z = 0.7$ i.e. around 3.5 Gyrs before the epoch ($z = 0.25$) at which the analysis above is performed. The stellar mass distribution of DM deficient galaxies at both epochs is similar. We find that only 30 per cent of DM deficient galaxies that exist at $z = 0.7$ still survive at $z = 0.25$. This indicates that the creation of DM deficient galaxies is a constant process over cosmic time. In other words, satellites that are in close orbits are not only stripped of their DM, but many also do not survive after the stripping

starts as they are accreted by their larger companions. Thus, the DM deficient population at a given redshift are largely systems that have formed recently enough that they still exist in the simulation at that epoch.

We also consider whether dwarfs that may be candidates for being DM deficient systems could potentially be identified using quantities that are readily available in imaging survey data. As described above, the process that drives the creation of these objects are tidal interactions with more massive companions on very close orbits. In the appendix we show a version of the right-hand panel of Figure 6.10 without normalising the orbital distances of the dwarfs by the virial radius of the massive companion (Figure B.1), because virial radii are not measurable quantities in imaging data. Combining Figures 6.8, 6.10, 6.11 and B.1 indicates that dwarfs that are found close to massive companions with $M_\star > 10^{10}$ $M_\odot$ (Figure 6.8) at distances less ~150 kpc (Figure B.1) and show stellar tidal features (Figure 6.11) are likely to be good candidates for being DM deficient systems. As is typical of interactions between massive galaxies and dwarf companions (e.g. Kaviraj, 2010, 2014a), the tidal features (e.g. the ones visible in Figure 6.11) are faint with surface brightnesses typically fainter than 29 mag arcsec^{-2}. This suggests that finding large samples of DM deficient candidates would ideally require deep wide-area surveys, such as LSST (Robertson et al., 2019; Kaviraj, 2020), which have limiting surface-brightnesses that are fainter than such values.

6.3.1 Comparison to observational studies

We complete our study by considering our results in the context of recent observational work. DM deficient galaxies form in `NewHorizon` via tidal interactions in close orbits with a more massive (central) companion. It is worth noting that the theoretical study of Macciò et al. (2020) comes to similar conclusions, albeit using a small sample of three zoom-in simulations of individual galaxies. The formation mechanism described in our study is strongly supported by the recent empirical work of Montes et al. (2020), who have used deep optical imaging to demonstrate that the DM deficient galaxy NGC 1052-DF4 exhibits tidal tails, similar to those predicted in Figure 6.11. They show that these tidal features are driven by an interaction with its neighboring galaxy NGC 1035, and argue that the DM-deficient nature of this dwarf galaxy is caused by the DM stripping produced by this interaction.

Our proposed mechanism is also consistent with the recent studies by van Dokkum et al. (2018a) and van Dokkum et al. (2019), who find multiple DM deficient dwarf galaxies in group environments. These galaxies are likely to have been subjected to strong tidal forces that would have stripped their DM halo (see e.g. the lower panel of Figure 6.11 which shows a possible analog of this in `NewHorizon`). The formation of DM deficient dwarfs via tidal interactions also appears consistent with the excess number of globular clusters (GCs) reported in these systems

(e.g. Fensch et al., 2019b; Müller et al., 2020). Since tidal interactions between dwarfs and larger companions can trigger enhanced GC formation (e.g. Fensch et al., 2019a; Carleton et al., 2020; Somalwar et al., 2020), systems like DM deficient dwarfs, that undergo strong tidal interactions, could be expected to show an excess number of GCs. Note, however, that the resolution of `NewHorizon` is not sufficient for us to directly study the formation of GCs.

The formation channel outlined in this chapter appears less well-aligned with the findings of Guo et al. (2019), who suggest that most of their DM deficient galaxies lie at distances greater than three times the virial radius of the nearest group or cluster. However, it is worth noting that the nearest groups and clusters in Guo et al. are significantly more massive than those in our study. It is possible that the tidal forces required to strip dwarfs of their DM can be produced at larger distances around much more massive groups. Furthermore, without deep images it is difficult to identify tidal features which are the tell-tale signatures of the tidal stripping process that creates DM deficient galaxies. Nevertheless, the relatively isolated nature of these galaxies, coupled with other potential mechanisms for producing such objects, e.g. weak baryonic feedback (Mancera Piña et al., 2020) suggests that other channels maybe required to satisfactorily explain the entire DM deficient population.

6.4 Summary

In the standard ΛCDM paradigm, dwarf galaxies are expected to be DM-rich, because their shallow gravitational potential wells make it easier for processes like stellar and supernova feedback to deplete their gas reservoirs. This results in a rapid depletion of gas and reduction of star formation at early epochs, leaving these objects with relatively high DM fractions. However, recent observational work suggests that some local dwarfs exhibit DM fractions as low as unity, around 400 times lower than what is expected for systems of their stellar mass. The existence of such DM deficient galaxies appears to contradict our classical expectations of the DM properties of dwarf galaxies, potentially bringing the validity of the standard paradigm into serious question. Understanding the origins of these galaxies, using a high-resolution cosmological simulation which can make realistic statistical predictions of dwarf galaxies, is, therefore, a key exercise.

Here, we have used the `NewHorizon` cosmological hydrodynamical simulation to explain the formation of DM deficient galaxies. We are able to perform this exercise, for the first time, in a statistical fashion, as the cosmological volume of `NewHorizon` allows us to study large numbers of dwarf galaxies, while its high spatial resolution enables us to resolve these systems with the requisite detail. We have shown that interactions between massive central galaxies and dwarf satellites can drive sustained and significant stripping of DM from the dwarfs, which reduces their DM content. The level of stripping is determined by the details of the orbit, with dwarfs that

are heavily stripped typically spending significant fractions of their time in tight orbits around their corresponding massive central, after they turn into satellites.

DM stripping is responsible for the large dispersion in the stellar-to-halo mass relation in the dwarf regime (see Figure 6.1), with the DM deficient and DM poor populations, which comprise ~30 per cent of dwarfs, scattering off the tight main locus defined by the dwarf centrals and the dwarf satellites that remain unstripped. In extreme cases, this DM stripping produces dwarfs which exhibit $M_{halo}/M_\star$ ratios as low as unity, consistent with the findings of recent observational studies. Given their close orbits, a significant fraction of DM deficient dwarfs will merge with their massive companions and disappear from the galaxy population (e.g. ~70 per cent of such dwarfs will merge over timescales of ~3.5 Gyrs). But the DM deficient population is replenished by new interactions between dwarfs and massive companions. It is worth noting that our results are robust with respect to the details of the sub-grid recipes implemented in `NewHorizon`, as this formation mechanism is principally driven by gravitational forces.

The formation of DM deficient galaxies through tidal stripping of DM, as hypothesised here, is strongly supported by recent observational studies (e.g. Montes et al., 2020), which are located in similar environments to the DM deficient galaxies in `NewHorizon`. Observations of an excess of GCs in these galaxies, although not directly testable in `NewHorizon`, also appear to support this formation mechanism (although, as noted above, contributions from other pathways may be required to explain the DM deficient population as a whole).

The results of our study offer a route to identifying dwarf galaxies that may have low DM content, purely from data that is typically available in imaging surveys. Dwarfs that are found close to massive companions with $M_\star > 10^{10}$ M$_\odot$, at distances less than ~150 kpc, and show stellar tidal features, are likely to be good candidates for being DM deficient systems. The surface brightness of the tidal features produced by such interactions (typically fainter than 29 mag arcsec^{-2}) suggests that new and future deep wide surveys, like the Hyper Suprime-Cam SSP or LSST, could be used to identify large samples of such DM deficient dwarf candidates.

Our study demonstrates that stripping of DM via a tidal interaction, a process that takes place in all environments, can routinely create dwarfs that have DM fractions that deviate significantly from their initial values in the early Universe and, in extreme cases, produces systems that are DM deficient. The existence of such galaxies is therefore an integral feature of galaxy evolution in the standard ΛCDM paradigm and their existence is not in tension with the predictions of this model.

Chapter 7

Conclusions

In this thesis we have shown how the processes that operated both on and within galaxies are capable of creating many of the diverse populations of galaxies which we see in our Universe today. We have shown how merging and tidal interactions can produce galaxies that seem to be counter-intuitive, based on our theories of galaxy evolution. We also demonstrate that most low mass galaxies are below the surface brightness limits of current wide-area surveys and investigate the physical processes that form and evolve dwarf galaxies. These are key predictions that can be tested with the next generation of deep-wide survey instruments such as the Rubin Observatory, EUCLID and JWST.

7.1   The role of mergers in creating galaxy populations

Understanding how rotationally-supported discs transform into dispersion-dominated spheroids is central to our comprehension of galaxy evolution. The most massive galaxies ($M_* > 10^{11} M_\odot$) are believed to have rich merger histories in order to grow to these large masses. This results in high fractions of 'ex-situ' stellar mass i.e. mass accreted directly from external objects rather than having been formed in-situ. It has been shown that major mergers are capable of inducing morphological change and can efficiently create spheroids with high 'ex-situ' mass fractions.

In Chapter 2 we show that a population of spheroids exist which go against these preconceptions. These spheroids are massive but have low 'ex-situ' mass fractions, indicating that their formation has not involved a major merger. Indeed other recent work has highlighted the significant role of other processes, like minor mergers, in driving morphological change. We used Horizon-AGN to show that 5% of spheroids above 10^{11} $M_\odot$ are formed in a single minor merger. In these minor mergers, the satellite orbit is virtually co-planar with the disc of the massive galaxy, which triggers a rapid transformation from a disc to a spheroid within just a few dynamical timescales.

Similarly, Chapter 3 used the Horizon-AGN simulation to explain the existence of extremely massive disc galaxies, with $M_\star > 10^{11.4}$ $M_\odot$. While these objects have been found in recent observational work (Ogle et al., 2016), explaining their formation within ΛCDM has been difficult. This is because merging is believed to destroy discs, and massive galaxies are thought to have the richest merger histories, since their high stellar masses cannot typically be attained without mergers (e.g. Martin et al., 2018a). We showed that extremely massive discs form naturally in the standard model making up around 11% of extremely massive galaxies in Horizon-AGN.

These galaxies form via 2 distinct channels. In the principal channel (which accounts for 70% of these objects), a merger between a massive spheroid and a gas-rich satellite rebuilds the galaxy's disc component. This process moves the galaxy from the spheroid to disc regime where it remains. While in the secondary channel, a system maintains a disc throughout its lifetime. These galaxies have an anomalously quiet merger history, for galaxies of comparable stellar mass, allowing them to retain their gas reservoir more easily and therefore maintain a disc. Finally, we examined the BH properties of these galaxies, finding them to be consistent with their spheroidal counterparts. These galaxies could therefore be potential hosts of AGN, with observations suggesting that some powerful AGN are found in disc galaxies.

In Chapter 4 we show the results of an observational follow up of Chapter 3 to test this theoretical hypothesis for massive-disc formation. To do this we created a complete sample of local, massive galaxies drawn from the DECaLS survey (which is around 1.5 mags deeper than the SDSS). Our results indicate that the observations support the theoretical hypothesis. 13% of the observed massive galaxies are spirals (compared to 11% in Horizon-AGN), of which 64% show tidal features indicative of minor mergers. The incidence of tidal features is significantly higher than that seen in a control sample of low mass spirals ($\sim 11 - 17\%$) and is higher than our spheroid sample ($\sim 31\%$).

Furthermore, the massive spirals show elevated levels of star formation (measured using UV data from GALEX) compared to the control spheroids. The SFRs and sSFRs of the observed massive discs are in good agreement with the results from Horizon-AGN. We also look at the HI gas properties of these galaxies, where available in ALFALFA, we find 4 detections in the massive disc population and none in the control spheroid population. One of these detections is associated to a clearly disturbed disc, indicative of a recent merger, which shows similar HI mass/fraction to the predictions from the simulated galaxies. These results suggest that massive spirals do indeed form via the channels predicted by Chapter 3.

7.2   The formation and evolution of dwarf galaxies

In Chapter 5 we used the `NewHorizon` hydrodynamical, cosmological simulation to perform a comprehensive, high-resolution, theoretical study of the key processes that drive the formation of dwarf galaxies and determine their surface brightnesses (SB) at the present day. Such a study is timely because, while dwarf galaxies dominate the galaxy number density, dwarfs at cosmological distances remain unexplored since they are too faint to be visible in past wide-area surveys (e.g. the SDSS). This means that our current understanding of galaxy evolution is potentially highly incomplete. We showed that galaxies occupy a well-defined locus from low-mass and low-SB to high-mass and high-SB, with a spread of ~3 mag arcsec^{-2}. Therefore, LSB galaxies are a natural extension of the dwarf galaxy population, rather than a new population of galaxies. Some of these dwarfs, in the low and intermediate mass range, have SB and effective radii that would make them ultra diffuse galaxies in the observational literature. These galaxies do not form in any special way and are also part of the normal dwarf galaxy population. The `NewHorizon` locus is consistent with observations from SDSS Stripe 82, suggesting that the feedback recipes employed by the simulation, offer a good representation of these physical processes.

We find that galaxies with fainter SB at the present day are born in regions of higher dark matter density at early epochs. This leads to faster gas accretion, higher levels of star formation and more intense supernova feedback at earlier times. This flattens their gas profiles quicker, which, in turn, creates shallower stellar profiles (i.e. more diffuse systems) more rapidly. As star formation declines towards late epochs, the continued tidal perturbations and ram pressure experienced by these systems (due to their local environments) accelerate the divergence in surface brightness, by increasing their effective radii and reducing star formation respectively. We also show that a small minority of dwarfs have anomalously high levels of star formation (driven by mergers and fly bys), making them detectable in past surveys (like the SDSS), but that they are not representative of the general dwarf population. The results of this chapter offer a suite of testable predictions for the properties of dwarf galaxies that will be visible in new, and future, deep-wide surveys (e.g. the Hyper Suprime-Cam SSP and LSST).

7.3   A potential challenge to ΛCDM

A recent potential challenge to the ΛCDM paradigm, has been the discovery of dwarf galaxies that are deficient in dark matter (DM) (e.g. van Dokkum et al., 2018a), with DM fractions around 400 times lower than expected. Dwarf galaxies are expected to be dark-matter-rich, as baryonic feedback is thought to quickly drive gas out of their shallow potential wells and quench star formation at early epochs. Therefore existence of DM deficient dwarfs appears to bring the

validity of the standard model into question, and understanding their formation is therefore an essential exercise.

Chapter 6 used the `NewHorizon` simulation, to perform the first statistical study of how DM deficient dwarfs may form in the ΛCDM paradigm. We find that these galaxies form readily in the simulation, and around 30% of dwarf galaxies in `NewHorizon` show DM fractions that deviate from what is expected. The formation of these DM deficient galaxies is caused by tidal interactions between a massive galaxy and a dwarf satellite. These interactions are capable of inducing sustained stripping of DM from the dwarf, naturally producing galaxies that resemble the DM deficient galaxies seen in the observations. This process is responsible for the large scatter seen in the stellar-to-halo mass relation in the dwarf regime, with the degree of stripping being correlated with the distance between the galaxy pair during the orbit. We find that these galaxies are typically within 150kpc of a more massive companion (with $M_\star > 10^{10} M_\odot$), this provides a guide for future observations attempting to detect more of these objects. This study shows that the existence of DM deficient galaxies is not in tension with the ΛCDM model but rather a natural consequence of it.

Chapter 8

Future work

The simulations used throughout this thesis have been largely successful at reproducing many of the bulk properties of the observed galaxy population. They are also in agreement with other simulations, despite the use of different methodologies (Vogelsberger et al., 2014b; Schaye et al., 2015). However, there are some key disagreements between the models and observations, particularly in the LSB/dwarf galaxy regime. A current limitation of observations is the relatively shallow depth of wide-area surveys, which could result in an incomplete observational galaxy sample. This is particularly problematic when studying LSB galaxies and it is currently unclear whether observations agree with the theoretical predictions in this regime. For example, current observations predict that dwarf/LSB galaxies in the field have blue colours and are therefore star forming (Greco et al., 2018) but in NewHorizon most of these galaxies are predicted to be quenched.

In order to understand the LSB regime state-of-the-art simulations, such as Horizon-AGN (Kaviraj et al., 2017), NewHorizon (Dubois et al., 2020) and Illustris-TNG (Nelson et al., 2019), need to be used alongside deep observational data. Upcoming deep-wide surveys such as HSC-SSP, Rubin Observatory and Euclid will allow for the statistical study of dwarf and LSB galaxies, which can be compared to the results of high-resolution simulations. For example, the HSC-SSP will offer 1400/30 deg^2 down to surface-brightness depths of ~28.5/30 mag arcsec^{-2} in its wide/deep layers. This will allow for the construction of large catalogues of LSB and dwarf galaxies and their properties (e.g. stellar masses, SED-fitted star formation rates and visually-classified morphologies). Combining these new datasets we will be able to address the following key questions in the field: *Can we resolve the small scale challenges to ΛCDM with new observational data and high-resolution simulations? What role does merging play in the dwarf galaxy regime? How do minor mergers drive massive galaxy evolution? Do current galaxy formation models (which are calibrated to reproduce massive galaxies) correctly model the dwarf galaxy population?.*
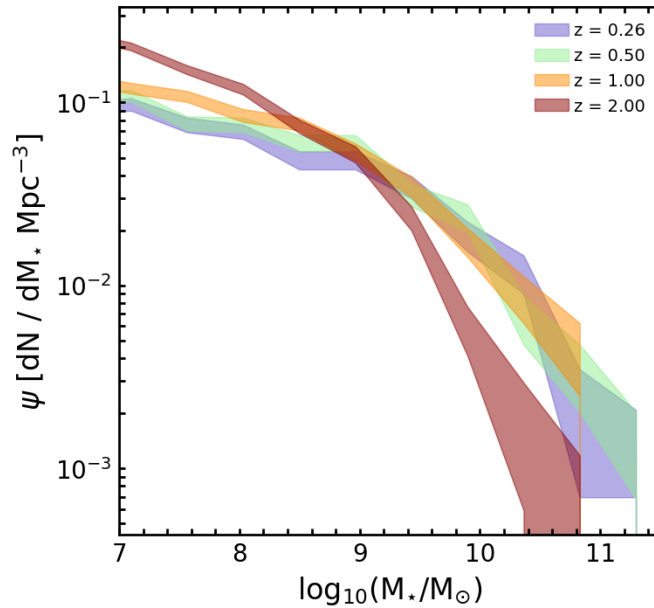
FIGURE 8.1: Galaxy stellar mass function at various redshifts in NewHorizon. The NewHorizon simulation clearly predicts that dwarf galaxies should dominate the number density at all redshifts. It is worth noting that NewHorizon does not contain any cluster environments, so this predicts that dwarf galaxies outnumber massive galaxies in the field and groups. This prediction can be tested with deep-wide surveys such as HSC and LSST.

8.1 Tackling the tensions between theory and data in the low mass regime

Many historical tensions exist in ΛCDM between theory and data in the dwarf regime, driven, at least partly, by the prior unavailability of deep-wide surveys and high resolution cosmological simulations.

The over-production of dwarf galaxies in simulations is a long-standing problem in the ΛCDM paradigm (Bullock and Boylan-Kolchin, 2017). While past explanations have included the existence of warm dark matter and/or an incomplete understanding of the physics of baryonic feedback in the dwarf regime, recent studies suggest that this tension is at least partly due to missing dwarf galaxies in shallow surveys (Martin et al. 2019, Chapter 5). While recent work suggests that ΛCDM-based models could match Local Group number densities (Sawala et al., 2016), a comprehensive exploration of the dwarf galaxy population at cosmological distances is necessary to fully explore this issue. Leveraging the unprecedented depth and area of the upcoming observational instruments (HSC-SSP, LSST, Euclid etc.), it is possible to construct empirical dwarf mass functions down to $M_\star \sim 10^{7.5}$ $M_\odot$ in the local ($z < 0.3$) Universe. These observed mass functions can then be compared to theoretical predictions from the NewHorizon and Illustris-TNG50 simulations. This will explore whether missing dwarfs in past large observational surveys (which are relatively shallow) can account for the apparent dwarf excess in simulations (see Figure 8.1). If theory and observations match, this would indicate

that the substructure problem does not generally exist in the nearby Universe. However, if a discrepancy remains, then this would indicate a need for improved feedback physics in dwarfs and studying this will be able to inform the development of such future models.

The 'core-cusp problem' is another apparent discrepancy between theory and data. While DM-only ΛCDM simulations show that DM halos have density profiles that rise steeply in the central regions (cusps) (Navarro et al., 2010) this appears inconsistent with observations of low mass galaxies which find approximately constant central DM densities (cores) (Kuzio de Naray et al., 2008). Although recent simulations have shown that baryonic feedback processes can possibly remove cusps (Read et al., 2017), these studies are based on small samples of galaxies and do not probe different environments. As NewHorizon has a spatial resolution of ~34 pc, it is capable of resolving the inner DM density profiles of dwarf galaxies down to stellar masses of ~$10^{6.5}$ M$_\odot$. This means that we now have the simulations to probe the core-cusp problem in a statistical manner across a large of environments (e.g. the field through to large groups) for the first time.

In addition to these two main problems, it is also possible to address other challenges to the ΛCDM paradigm in the dwarf regime. The too-big-to-fail problem (Boylan-Kolchin et al., 2011) can be investigated using NewHorizon in a statistical manner, since it contains many galaxies with $M_\star > 10^{10}$ with multiple satellites. A potential solution could be DM stripping. For example, in Chapter 6 we show that substantial DM stripping is possible in dwarf satellite galaxies around centrals of Milky-Way mass. In a further problem, some studies have shown that satellites of the Milky Way and M31 have a planar (disk-like) spatial configuration (Metz et al., 2007; Pawlowski et al., 2013), suggesting that these satellites may not be DM substructures, potentially in contradiction with the predictions of ΛCDM. Using NewHorizon, the spatial distribution of satellite galaxies can be analysed in detail, to understand whether such planar configurations could occur naturally in ΛCDM and, if so, what processes cause it to occur.

8.2 LSB galaxies - comparing theory and observations

Our current statistical understanding of galaxy evolution is driven by objects and structures that are brighter than the SB limits of past wide area surveys, like the SDSS ($\mu_r > 24$-25 mag arcsec^{-2}). The standard paradigm postulates hierarchical structure formation, with ΛCDM-based models broadly reproducing the properties of *bright* objects in past large surveys. However, recent studies (e.g. Chapter 5) have shown that the majority of galaxies are, in fact, fainter than the SB limits of past wide-area surveys. This LSB population, which comprises all dwarfs at cosmological distances and massive diffuse disks, dominates the galaxy number density (~85% of galaxies down to 10^7 M$_\odot$; Martin et al. (2019)) but is largely missing from past datasets. In particular the search for ultra-diffuse galaxies (UDGs), has been largely limited to deep cluster surveys (van Dokkum et al., 2015b; Koda et al., 2015). These galaxies are of particular interest as they
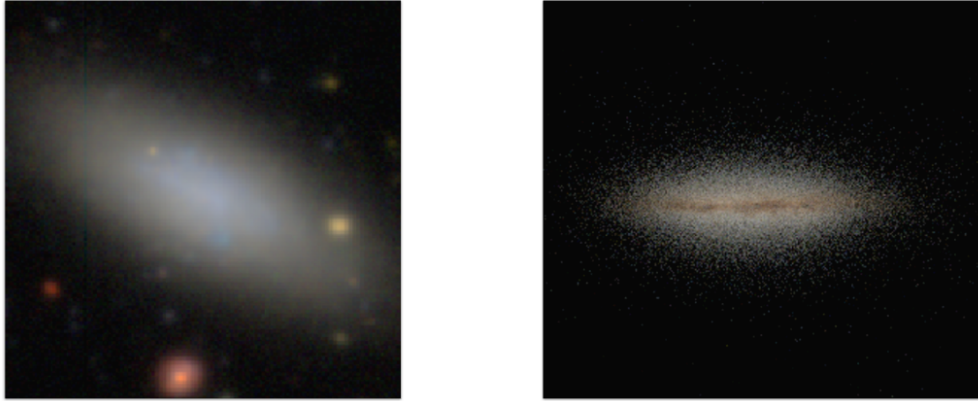
FIGURE 8.2: Left: A HSC image of a $10^8 M_\odot$ galaxy. Right: Mock image of a $10^8 M_\odot$ galaxy in NewHorizon. NewHorizon is able to produce realistic looking galaxies even down to these low stellar masses. This is evidence that the physical processes dwarf galaxies undergo in NewHorizon are realistic and therefore we can use it to make testable predictions about galaxies in this mass regime.

could be good tests of black hole and stellar feedback. This incompleteness has two important consequences. First, our empirical picture of galaxy formation is heavily biased. Second, since our models are statistically calibrated only to the subset of bright galaxies, our understanding of the physics of galaxy evolution remains potentially highly incomplete. A complete understanding of galaxy evolution therefore demands a detailed comprehension of how LSB galaxies evolve over cosmic time.

The currently available HSC-SSP, and eventually LSST, will allow for the statistical exploration of the distributions, and redshift evolution, of key properties of LSB galaxies e.g. morphology (see Figure 8.2), effective radii, colours and star-formation rates, extending fundamental diagnostics like the star-formation main sequence into the LSB regime. Using other instruments (such as JWST), we will be able to probe the high redshift progenitors of these galaxies to explore when, and why, these galaxies deviate from their high SB counterparts. Potentially increasing own knowledge of how supernovae and AGN feedback influence the formation of these galaxies at high redshift.

These observational studies can be compared to results from the Horizon-AGN/NewHorizon simulations (and LSB-galaxy predictions from other cosmological simulations, if available). This will yield novel tests of the implementation of key processes, such as SN feedback, in current simulations. For example, a key test of SN feedback recipes would be to compare the quenched (red) dwarf galaxy fractions, as a function of redshift, in observations and simulations. We can then analyse how and when quenching is taking place, to understand if these recipes (which are based on bright galaxies) are applicable in the dwarf regime. Discrepancies between theory and data found in these tests can inform the development of the next generation of sub-grid recipes in theoretical models. In addition, using the increased mass and spatial resolution of NewHorizon and Illustris-TNG50, we can for the first time analyse the evolution of morphology
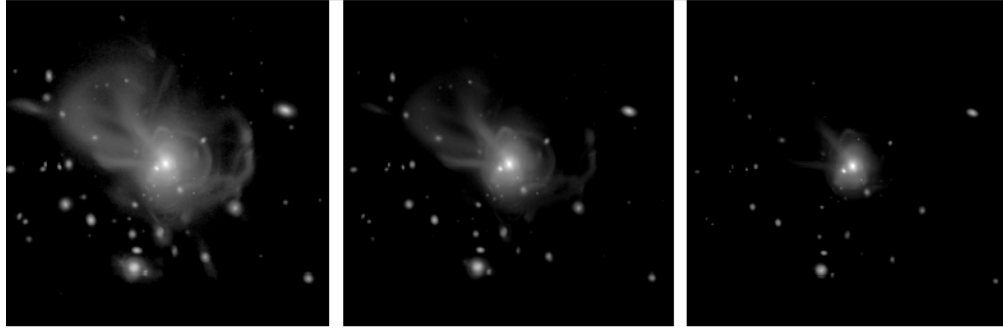
FIGURE 8.3: *r*-band mock image at various surface-brightness limits of the remnant of a minor merger (mass ratio ~1:10) at *z* ~ 0.5 from NewHorizon. The left image is representative of HSC-SSP Deep/LSST. The detection of tidal features, and therefore identification of minor merger remnants, requires the depth of surveys like HSC-SSP and LSST.

in dwarf galaxies and the processes that give rise to the morphological mix of the present day Universe across the galaxy mass range.

8.3   A definitive study of how mergers shape galaxy evolution

Although merging underpins our theoretical paradigm, significant topics, such as mergers between dwarf galaxies and the role of minor mergers between massive galaxies and low-mass companions remain poorly understood. As dwarf galaxies dominate the number density of the galaxy population, and form the building blocks of all massive galaxies seen today, understanding merging in this regime is key to gaining a complete knowledge of galaxy evolution.

The role of mergers in dwarf galaxy evolution is currently unknown, due to size and SB of these galaxies and the tidal features produced. In (Martin et al., 2020), the role of how mergers and fly-bys influenced galaxy evolution in the dwarf regime using NewHorizon is analysed. It shows that fly-bys are the main drivers of morphological disturbances in dwarf galaxies and that neither merging nor fly-bys had a strong impact on increasing SFRs, with these galaxies typically only undergoing a single major and minor merger in their lifetime. In order to test these predictions a SB complete catalogue of galaxies (including dwarfs) over a large area is required, making use of the next generation of instruments, such as Rubin Observatory, Euclid and JWST. Such a catalogue will allow, for the first time, the construction of merger fractions in the dwarf regime up to cosmological distances. We can then use this merger fraction to quantify the role of merging in the dwarf regime, such as the observational merger fraction/rate, the enhancement of star formation in these mergers and the influence of these mergers on morphology.

Minor mergers between massive galaxies and low-mass companions dominate the merger activity of massive galaxies but, due to the low surface brightness of tidal features they produce, are

difficult to study in a statistical way in past surveys. Mock images from NewHorizon indicate that, at the depth of the HSC-SSP, minor-merger-induced tidal features will be visible out to intermediate and high redshift (Figure 8.3). With HSC-SSP, thousands of mergers and postmergers (single objects with tidal features) can be detected up to $z \sim 1.5$, down to mass ratios of 1:10, for galaxies with $M_\star > 10^{10}$ $M_\odot$, a number that will only increase further once Rubin Observatory data becomes available in the next few years. For the first time, we will be able to observationally determine *statistical* properties of minor mergers, such as the minor merger rate/fraction and the contribution of minor mergers to the star formation budget over around 75% of cosmic time. These results can then be compared to predictions from Horizon-AGN (Martin et al., 2017) to understand how these mergers affect massive galaxies across cosmic time.

Appendix A

Massive spheroid Appendix

A.1 Orbital configurations with a relaxed mass cut

Section 2.4.2 indicates that the principal difference in the formation mechanism of our massive, low f_{exsitu} spheroids compared to typical (i.e. high f_{exsitu}) spheroids of similar mass is that they form via minor mergers where the satellite orbit is close to being co-planar with the disc of the massive galaxy. As noted in Section 2.4.2, since our sample size is relatively small, we check whether this result could have originated by chance, by exploring whether this tendency towards co-planar orbits persists with more relaxed selection criteria.

For this exercise, we reduce the mass threshold of our sample to $M_* > 10^{10.5} M_\odot$ but leave constraints on the other variables (i.e. $V/\sigma < 0.3$ and $f_{exsitu} < 0.3$) the same. We perform an identical orbital configuration analysis on this sample as that described in Section 2.4.2. As Figure A.1 indicates this analysis shows the same tendency towards close-to-co-planar orbits creating low f_{exsitu} spheroids, indicating that the result for the more massive spheroids does not occur by chance.

Note, however, that, as described in Section 2.4.2, we use this only as a sanity check of our results. Lower-mass galaxies naturally produce larger in-situ mass fractions because they produce more mass via gas accretion, as opposed to mergers (Martin et al., 2018a). As a result, the deficit of non co-planar orbits in Figure A.1 is not as severe in this lower-mass regime as it is for their more massive counterparts which are the subject of this paper. Our focus, therefore, remains on the most massive galaxies ($M_* > 10^{11} M_\odot$) in which low f_{exsitu} is particularly anomalous.
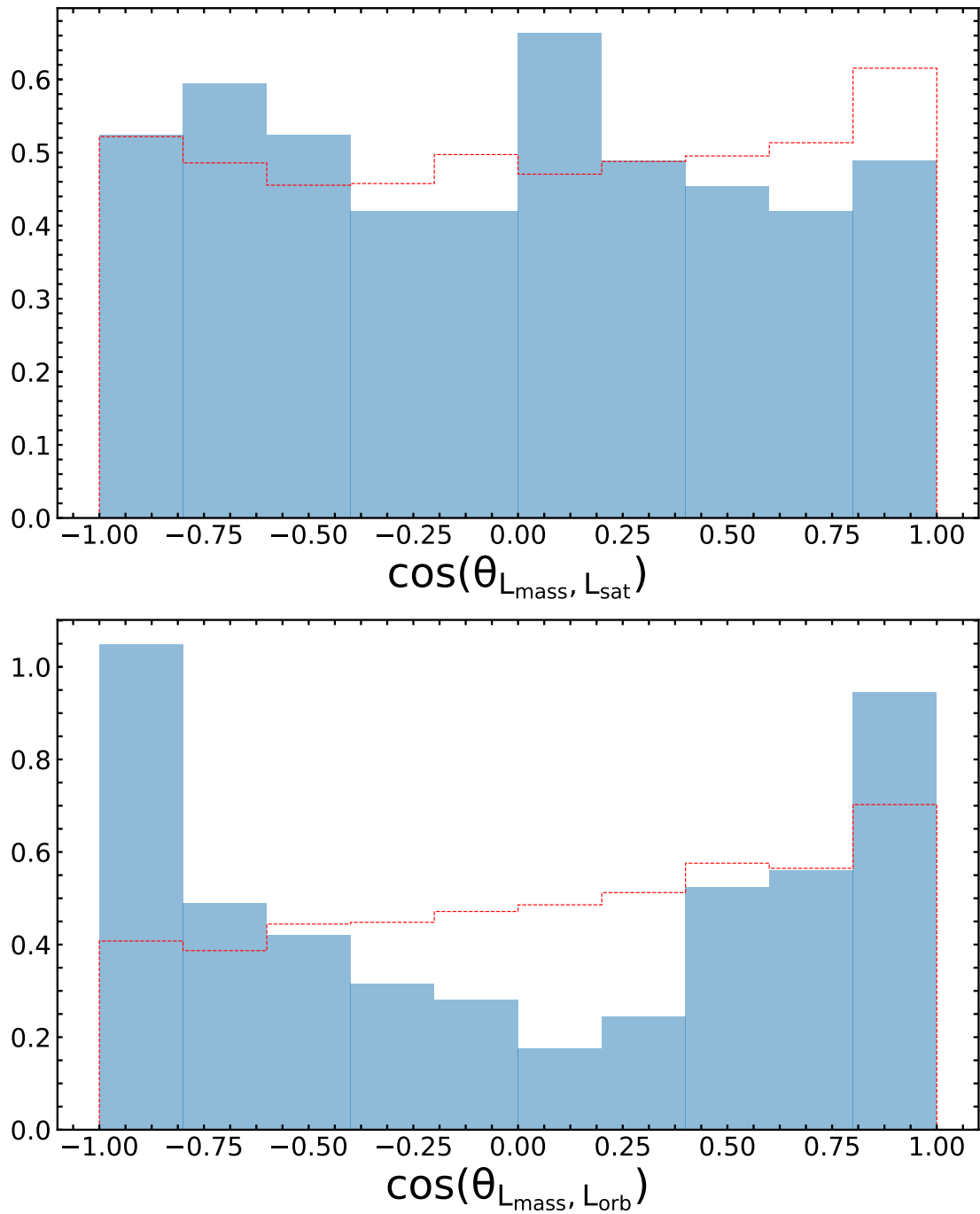
FIGURE A.1: Same as Figure 2.5 but for a sample where the mass threshold is $M_* > 10^{10.5}$ $M_\odot$, with other parameters unchanged (i.e. $V/\sigma < 0.3$ and $f_{exsitu} < 0.3$). As is the case for the $M_* > 10^{11}$ $M_\odot$, low $f_{ex-situ}$ spheroids continue to show a tendency towards mergers that have close to co-planar orbits.

Appendix B

Dark-matter-deficient galaxies Appendix

B.1 Orbital distances of dwarfs around their massive centrals

Figure B.1 shows the orbital distances of dwarfs around their massive centrals in our different satellite populations. This figure is a version of the right-hand panel of Figure 6.10, without the distance being normalised by the virial radius of the halo of the massive central. These distances are directly comparable to measured distances between massive galaxies and nearby dwarfs in deep-wide surveys in order to identify DM deficient galaxy candidates.
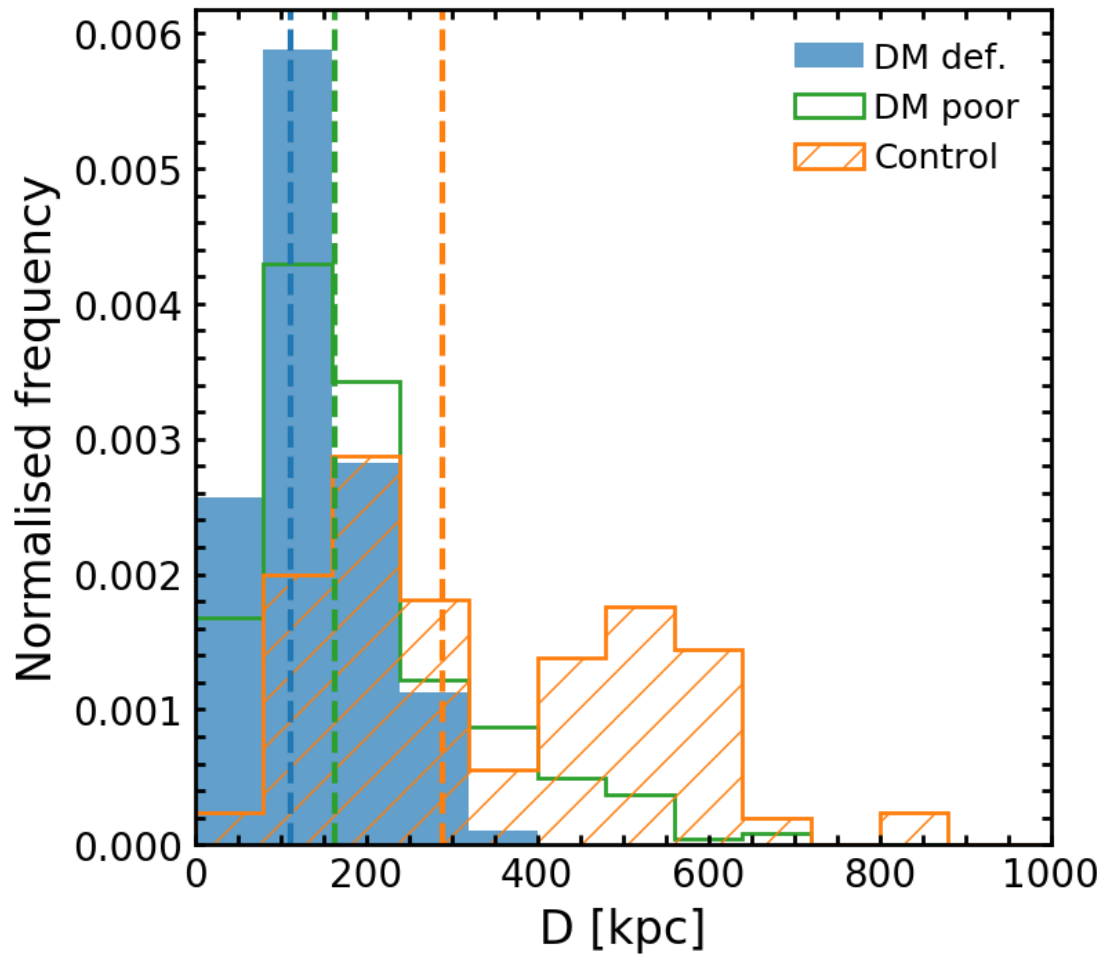
FIGURE B.1: Orbital distances of our different satellite populations, in the period after individual dwarfs become satellites through to the end of the simulation. The dashed lines indicate the median value of each distribution.

Bibliography

Abazajian, K.N., Adelman-McCarthy, J.K., Agüeros, M.A., et al., 2009. The Seventh Data Release of the Sloan Digital Sky Survey. *ApJS*, 182(2):543.

Aihara, H., AlSayyad, Y., Ando, M., et al., 2019. Second data release of the Hyper Suprime-Cam Subaru Strategic Program. *PASJ*, page 106.

Amorisco, N.C. and Loeb, A., 2016. Ultradiffuse galaxies: the high-spin tail of the abundant dwarf galaxy population. *MNRAS*, 459:L51.

Antonuccio-Delogu, V. and Silk, J., 2008. Active galactic nuclei jet-induced feedback in galaxies - I. Suppression of star formation. *MNRAS*, 389(4):1750.

Athanassoula, E., Rodionov, S.A., Peschken, N., et al., 2016. Forming Disk Galaxies in Wet Major Mergers. I. Three Fiducial Examples. *ApJ*, 821(2):90.

Aubert, D., Pichon, C., and Colombi, S., 2004. The origin and implications of dark matter anisotropic cosmic infall on ˜L∗ haloes. *MNRAS*, 352:376.

Baes, M. and Camps, P., 2015. Skirt: The design of a suite of input models for monte carlo radiative transfer simulations. *Astronomy and Computing*, 12:33 .

Bahé, Y.M., Barnes, D.J., Dalla Vecchia, C., et al., 2017. The Hydrangea simulations: galaxy formation in and around massive clusters. *MNRAS*, 470(4):4186.

Baldry, I.K., Driver, S.P., Loveday, J., et al., 2012. Galaxy And Mass Assembly (GAMA): the galaxy stellar mass function at z < 0.06. *MNRAS*, 421(1):621.

Balogh, M.L., Morris, S.L., Yee, H.K.C., et al., 1999. Differential Galaxy Evolution in Cluster and Field Galaxies at z˜0.3. *ApJ*, 527(1):54.

Barnes, J.E., 1988. Encounters of disk/halo galaxies. *ApJ*, 331:699.

Barnes, J.E., 1992a. Transformations of galaxies. I - Mergers of equal-mass stellar disks. *ApJ*, 393:484.

Barnes, J.E., 1992b. Transformations of galaxies. I - Mergers of equal-mass stellar disks. *ApJ*, 393:484.

Barnes, J.E. and Hernquist, L., 1992. Formation of dwarf galaxies in tidal tails. *Nature*, 360(6406):715.

Baushev, A.N., 2018. Galaxy collisions as a mechanism of ultra diffuse galaxy (UDG) formation. *New Astron.*, 60:69.

Beckmann, R.S., Devriendt, J., Slyz, A., et al., 2017. Cosmic evolution of stellar quenching by AGN feedback: clues from the Horizon-AGN simulation. *MNRAS*, 472(1):949.

Beckwith, S.V.W., Stiavelli, M., Koekemoer, A.M., et al., 2006. The hubble ultra deep field. *The Astronomical Journal*, 132(5):1729–1755.

Bell, E.F., McIntosh, D.H., Katz, N., et al., 2003. The Optical and Near-Infrared Properties of Galaxies. I. Luminosity and Stellar Mass Functions. *ApJS*, 149(2):289.

Bell, E.F., Wolf, C., Meisenheimer, K., et al., 2004. Nearly 5000 Distant Early-Type Galaxies in COMBO-17: A Red Sequence and Its Evolution since z~1. *ApJ*, 608:752.

Benson, A.J. and Bower, R., 2011. Accretion shocks and cold filaments in galaxy formation. *MNRAS*, 410(4):2653.

Benson, A.J., Bower, R.G., Frenk, C.S., et al., 2003. What Shapes the Luminosity Function of Galaxies? *ApJ*, 599:38.

Bernardi, M., Meert, A., Sheth, R.K., et al., 2013. The massive end of the luminosity and stellar mass functions: dependence on the fit to the light profile. *MNRAS*, 436(1):697.

Bernardi, M., Shankar, F., Hyde, J.B., et al., 2010. Galaxy luminosities, stellar masses, sizes, velocity dispersions as a function of morphological type. *MNRAS*, 404:2087.

Bernardi, M., Sheth, R.K., Annis, J., et al., 2003. Early-Type Galaxies in the Sloan Digital Sky Survey. I. The Sample. *AJ*, 125:1817.

Bernstein, G.M. and Jarvis, M., 2002. Shapes and Shears, Stars and Smears: Optimal Measurements for Weak Lensing. *AJ*, 123(2):583.

Bertin, E. and Arnouts, S., 1996. Sextractor: Software for source extraction. *Astronomy and Astrophysics Supplement Series*, 117(2):393.

Bianchi, L., Shiao, B., and Thilker, D., 2017. Revised Catalog of GALEX Ultraviolet Sources. I. The All-Sky Survey: GUVcat_AIS. *ApJS*, 230(2):24.

Bielby, R., Hudelot, P., McCracken, H.J., et al., 2012. The WIRCam Deep Survey. I. Counts, colours, and mass-functions derived from near-infrared imaging in the CFHTLS deep fields. *A&A*, 545:A23.

Birnboim, Y. and Dekel, A., 2003. Virial shocks in galactic haloes? *MNRAS*, 345(1):349.

Blake, C., Pracy, M.B., Couch, W.J., et al., 2004. The 2dF Galaxy Redshift Survey: the local E+A galaxy population. *MNRAS*, 355:713.

Blakeslee, J.P. and Cantiello, M., 2018. Independent Analysis of the Distance to NGC 1052-DF2. *Research Notes of the American Astronomical Society*, 2(3):146.

Blanton, M.R., Bershady, M.A., Abolfathi, B., et al., 2017. Sloan Digital Sky Survey IV: Mapping the Milky Way, Nearby Galaxies, and the Distant Universe. *AJ*, 154(1):28.

Blanton, M.R., Lupton, R.H., Schlegel, D.J., et al., 2005. The Properties and Luminosity Function of Extremely Low Luminosity Galaxies. *ApJ*, 631:208.

Blumenthal, G.R., Faber, S.M., Primack, J.R., et al., 1984. Formation of galaxies and large-scale structure with cold dark matter. *Nature*, 311:517.

Bogdán, Á., Lovisari, L., Kovács, O.E., et al., 2018. Detection of a Star-forming Galaxy in the Center of a Low-mass Galaxy Cluster. *ApJ*, 869(2):105.

Bois, M., Emsellem, E., Bournaud, F., et al., 2011. The ATLAS^{3D} project - VI. Simulations of binary galaxy mergers and the link with fast rotators, slow rotators and kinematically distinct cores. *MNRAS*, 416:1654.

Bondi, H. and Hoyle, F., 1944. On the mechanism of accretion by stars. *MNRAS*, 104:273.

Booth, C.M. and Schaye, J., 2009. Cosmological simulations of the growth of supermassive black holes and feedback from active galactic nuclei: method and tests. *MNRAS*, 398(1):53.

Borzyszkowski, M., Porciani, C., Romano-Díaz, E., et al., 2017. ZOMG - I. How the cosmic web inhibits halo growth and generates assembly bias. *MNRAS*, 469(1):594.

Bothun, G., Impey, C., and McGaugh, S., 1997. Low-Surface-Brightness Galaxies: Hidden Galaxies Revealed. *PASP*, 109:745.

Bournaud, F., Bois, M., Emsellem, E., et al., 2008a. Galaxy mergers at high resolution: From elliptical galaxies to tidal dwarfs and globular clusters. *Astronomische Nachrichten*, 329:1025.

Bournaud, F., Duc, P.A., and Emsellem, E., 2008b. High-resolution simulations of galaxy mergers: resolving globular cluster formation. *MNRAS*, 389(1):L8.

Bournaud, F., Jog, C.J., and Combes, F., 2007. Multiple minor mergers: formation of elliptical galaxies and constraints for the growth of spiral disks. *A&A*, 476:1179.

Bower, R.G., Benson, A.J., Malbon, R., et al., 2006. Breaking the hierarchy of galaxy formation. *MNRAS*, 370:645.

Boylan-Kolchin, M., Bullock, J.S., and Kaplinghat, M., 2011. Too big to fail? The puzzling darkness of massive Milky Way subhaloes. *MNRAS*, 415(1):L40.

Breiman, L., Meisel, W., and Purcell, E., 1977. Variable kernel estimates of multivariate densities. *Technometrics*, 19(2):135.

Brinchmann, J., Charlot, S., White, S.D.M., et al., 2004. The physical properties of star-forming galaxies in the low-redshift Universe. *MNRAS*, 351(4):1151.

Bruzual, G. and Charlot, S., 2003. Stellar population synthesis at the resolution of 2003. *MNRAS*, 344:1000.

Buck, T., Macciò, A.V., Dutton, A.A., et al., 2019. NIHAO XV: the environmental impact of the host galaxy on galactic satellite and field dwarf galaxies. *MNRAS*, 483(1):1314.

Buitrago, F., Conselice, C.J., Epinat, B., et al., 2014. SINFONI/VLT 3D spectroscopy of massive galaxies: evidence of rotational support at z ~ 1.4. *MNRAS*, 439:1494.

Buitrago, F., Trujillo, I., Conselice, C.J., et al., 2013. Early-type galaxies have been the predominant morphological class for massive galaxies since only z ~ 1. *MNRAS*, 428(2):1460.

Bullock, J.S. and Boylan-Kolchin, M., 2017. Small-Scale Challenges to the ΛCDM Paradigm. *ARA&A*, 55(1):343.

Bullock, J.S., Kravtsov, A.V., and Weinberg, D.H., 2001. Hierarchical Galaxy Formation and Substructure in the Galaxy's Stellar Halo. *ApJ*, 548(1):33.

Bundy, K., Ellis, R.S., and Conselice, C.J., 2005. The Mass Assembly Histories of Galaxies of Various Morphologies in the GOODS Fields. *ApJ*, 625:621.

Bundy, K., Ellis, R.S., Conselice, C.J., et al., 2006. The Mass Assembly History of Field Galaxies: Detection of an Evolving Mass Limit for Star-Forming Galaxies. *ApJ*, 651:120.

Butcher, H.R. and Oemler, Jr., A., 1984. Nature of blue galaxies in the cluster C11447 + 2619. *Nature*, 310:31.

Calette, A.R., Avila-Reese, V., Rodríguez-Puebla, A., et al., 2018. The HI- and H_2-to-Stellar Mass Correlations of Late- and Early-Type Galaxies and their Consistency with the Observational Mass Functions. *Rev. Mex. Astron. Astrofis.*, 54:443.

Canalizo, G. and Stockton, A., 2001. Quasi-stellar objects, ultraluminous infrared galaxies, and mergers. *The Astrophysical Journal*, 555(2):719.

Cardona-Barrero, S., Di Cintio, A., Brook, C.B.A., et al., 2020. NIHAO XXIV: rotation- or pressure-supported systems? Simulated Ultra Diffuse Galaxies show a broad distribution in their stellar kinematics. *MNRAS*, 497(4):4282.

Carleton, T., Errani, R., Cooper, M., et al., 2019. The formation of ultra-diffuse galaxies in cored dark matter haloes through tidal stripping and heating. *MNRAS*, 485(1):382.

Carleton, T., Guo, Y., Munshi, F., et al., 2020. An Excess of Globular Clusters in UDGs Formed Through Tidal Heating. *arXiv e-prints*, arXiv:2008.11205.

Carpineti, A., Kaviraj, S., Darg, D., et al., 2012. Spheroidal post-mergers in the local Universe. *MNRAS*, 420:2139.

Catinella, B., Schiminovich, D., Kauffmann, G., et al., 2010. The GALEX Arecibo SDSS Survey - I. Gas fraction scaling relations of massive galaxies and first data release. *MNRAS*, 403(2):683.

Cattaneo, A., Faber, S.M., Binney, J., et al., 2009. The role of black holes in galaxy formation and evolution. *Nature*, 460(7252):213.

Cattaneo, A., Mamon, G.A., Warnick, K., et al., 2011. How do galaxies acquire their mass? *A&A*, 533:A5.

Cava, A., Schaerer, D., Richard, J., et al., 2018. The nature of giant clumps in distant galaxies probed by the anatomy of the cosmic snake. *Nature Astronomy*, 2:76.

Chabrier, G., 2003. The Galactic Disk Mass Function: Reconciliation of the Hubble Space Telescope and Nearby Determinations. *ApJ*, 586:L133.

Chabrier, G., 2005. *The Initial Mass Function: From Salpeter 1955 to 2005*, volume 327 of *Astrophysics and Space Science Library*, page 41.

Chan, T.K., Kereš, D., Wetzel, A., et al., 2018. The origin of ultra diffuse galaxies: stellar feedback and quenching. *MNRAS*, page 1094.

Chilingarian, I.V., Di Matteo, P., Combes, F., et al., 2010. The GalMer database: galaxy mergers in the virtual observatory. *A&A*, 518:A61.

Choi, H., Yi, S.K., Dubois, Y., et al., 2018. Early-type Galaxy Spin Evolution in the Horizon-AGN Simulation. *ApJ*, 856.

Cole, S., Lacey, C.G., Baugh, C.M., et al., 2000. Hierarchical galaxy formation. *MNRAS*, 319:168.

Conselice, C.J., 2003. The Relationship between Stellar Light Distributions of Galaxies and Their Formation Histories. *ApJS*, 147:1.

Conselice, C.J., 2006. Early and Rapid Merging as a Formation Mechanism of Massive Galaxies: Empirical Constraints. *ApJ*, 638:686.

Conselice, C.J., 2007. Galaxy Mergers and Interactions at High Redshift. In F. Combes and J. Palouš, editors, *Galaxy Evolution across the Hubble Time*, volume 235, pages 381–384.

Conselice, C.J., 2014. The Evolution of Galaxy Structure Over Cosmic Time. *ARA&A*, 52:291.

Conselice, C.J., 2018. Ultra-diffuse Galaxies Are a Subset of Cluster Dwarf Elliptical/Spheroidal Galaxies. *Research Notes of the American Astronomical Society*, 2(1):43.

Conselice, C.J., Bluck, A.F.L., Mortlock, A., et al., 2014. Galaxy formation as a cosmological tool - I. The galaxy merger history as a measure of cosmological parameters. *MNRAS*, 444:1125.

Conselice, C.J., Mortlock, A., Bluck, A.F.L., et al., 2013. Gas accretion as a dominant formation mode in massive galaxies from the GOODS NICMOS Survey. *MNRAS*, 430(2):1051.

Conselice, C.J., Yang, C., and Bluck, A.F.L., 2009a. The structures of distant galaxies - III. The merger history of over 20000 massive galaxies at z < 1.2. *MNRAS*, 394:1956.

Conselice, C.J., Yang, C., and Bluck, A.F.L., 2009b. The structures of distant galaxies - III. The merger history of over 20000 massive galaxies at z < 1.2. *MNRAS*, 394:1956.

Cox, T.J., Jonsson, P., Somerville, R.S., et al., 2008. The effect of galaxy mass ratio on merger-driven starbursts. *MNRAS*, 384:386.

Cross, N. and Driver, S.P., 2002. The bivariate brightness function of galaxies and a demonstration of the impact of surface brightness selection effects on luminosity function estimations. *MNRAS*, 329(3):579.

Croton, D.J., Springel, V., White, S.D.M., et al., 2006. The many lives of active galactic nuclei: cooling flows, black holes and the luminosities and colours of galaxies. *MNRAS*, 365:11.

Croton, D.J., Stevens, A.R.H., Tonini, C., et al., 2016. Semi-Analytic Galaxy Evolution (SAGE): Model Calibration and Basic Results. *ApJS*, 222(2):22.

Dalcanton, J.J., Spergel, D.N., Gunn, J.E., et al., 1997. The Number Density of Low-Surface Brightness Galaxies with 23 < mu_0 < 25 V Mag/arcsec$\hat{2}$. *AJ*, 114:635.

Darg, D.W., Kaviraj, S., Lintott, C.J., et al., 2010. Galaxy Zoo: the fraction of merging galaxies in the SDSS and their morphologies. *MNRAS*, 401(2):1043.

Davé, R., Anglés-Alcázar, D., Narayanan, D., et al., 2019. SIMBA: Cosmological simulations with black hole growth and feedback. *MNRAS*, 486(2):2827.

Davidzon, I., Ilbert, O., Laigle, C., et al., 2017. The COSMOS2015 galaxy stellar mass function . Thirteen billion years of stellar mass assembly in ten snapshots. *A&A*, 605:A70.

de Blok, W.J.G., 2010. The Core-Cusp Problem. *Advances in Astronomy*, 2010:789293.

de Koff, S., Best, P., Baum, S.A., et al., 2000. The Dust-Radio Connection in 3CR Radio Galaxies. *ApJS*, 129(1):33.

Deeley, S., Drinkwater, M.J., Cunnama, D., et al., 2017. Galaxy and Mass Assembly (GAMA): formation and growth of elliptical galaxies in the group environment. *MNRAS*, 467:3934.

Dekel, A. and Birnboim, Y., 2006. Galaxy bimodality due to cold flows and shock heating. *MNRAS*, 368(1):2.

Dekel, A. and Burkert, A., 2014. Wet disc contraction to galactic blue nuggets and quenching to red nuggets. *MNRAS*, 438:1870.

Dekel, A., Sari, R., and Ceverino, D., 2009. Formation of Massive Galaxies at High Redshift: Cold Streams, Clumpy Disks, and Compact Spheroids. *ApJ*, 703:785.

Dey, A., Schlegel, D.J., Lang, D., et al., 2019. Overview of the DESI Legacy Imaging Surveys. *AJ*, 157(5):168.

Di Cintio, A., Brook, C.B., Dutton, A.A., et al., 2017. NIHAO - XI. Formation of ultra-diffuse galaxies by outflows. *MNRAS*, 466:L1.

Di Cintio, A., Brook, C.B., Macciò, A.V., et al., 2019. NIHAO XXI: the emergence of low surface brightness galaxies. *MNRAS*, 486(2):2535.

Di Matteo, P., Combes, F., Melchior, A.L., et al., 2007. Star formation efficiency in galaxy interactions and mergers: a statistical study. *A&A*, 468:61.

Di Matteo, T., Springel, V., and Hernquist, L., 2005. Energy input from quasars regulates the growth and activity of black holes and their host galaxies. *Nature*, 433(7026):604.

Diemand, J., Kuhlen, M., and Madau, P., 2007. Formation and Evolution of Galaxy Dark Matter Halos and Their Substructure. *ApJ*, 667(2):859.

Dong, S., Lin, D.N.C., and Murray, S.D., 2003. Star Formation and Feedback in Dwarf Galaxies. *ApJ*, 596(2):930.

Draine, B.T. and Li, A., 2007. Infrared Emission from Interstellar Dust. IV. The Silicate-Graphite-PAH Model in the Post-Spitzer Era. *ApJ*, 657:810.

Dressler, A., 1980. Galaxy morphology in rich clusters: implications for the formation and evolution of galaxies. *ApJ*, 236:351.

Dressler, A., Oemler, Jr., A., Couch, W.J., et al., 1997. Evolution since z = 0.5 of the Morphology-Density Relation for Clusters of Galaxies. *ApJ*, 490:577.

Driver, S.P., Liske, J., Cross, N.J.G., et al., 2005. The Millennium Galaxy Catalogue: the space density and surface-brightness distribution(s) of galaxies. *MNRAS*, 360:81.

D'Souza, R., Vegetti, S., and Kauffmann, G., 2015. The massive end of the stellar mass function. *MNRAS*, 454(4):4027.

Dubois, Y., Beckmann, R., Bournaud, F., et al., 2020. Introducing the NewHorizon simulation: galaxy properties with resolved internal dynamics across cosmic time. *arXiv e-prints*, arXiv:2009.10578.

Dubois, Y., Devriendt, J., Slyz, A., et al., 2012. Self-regulated growth of supermassive black holes by a dual jet-heating active galactic nucleus feedback mechanism: methods, tests and implications for cosmological simulations. *MNRAS*, 420:2662.

Dubois, Y., Gavazzi, R., Peirani, S., et al., 2013. AGN-driven quenching of star formation: morphological and dynamical implications for early-type galaxies. *MNRAS*, 433:3297.

Dubois, Y., Peirani, S., Pichon, C., et al., 2016. The HORIZON-AGN simulation: morphological diversity of galaxies promoted by AGN feedback. *MNRAS*, 463:3948.

Dubois, Y., Pichon, C., Welker, C., et al., 2014a. Dancing in the dark: galactic properties trace spin swings along the cosmic web. *MNRAS*, 444:1453.

Dubois, Y. and Teyssier, R., 2008a. Cosmological MHD simulation of a cooling flow cluster. *A&A*, 482(2):L13.

Dubois, Y. and Teyssier, R., 2008b. On the onset of galactic winds in quiescent star forming galaxies. *A&A*, 477:79.

Dubois, Y., Volonteri, M., and Silk, J., 2014b. Black hole evolution - III. Statistical properties of mass growth and spin evolution using large-scale hydrodynamical cosmological simulations. *MNRAS*, 440(2):1590.

Dubois, Y., Volonteri, M., and Silk, J., 2014c. Black hole evolution - III. Statistical properties of mass growth and spin evolution using large-scale hydrodynamical cosmological simulations. *MNRAS*, 440(2):1590.

Duc, P.A., Bournaud, F., and Masset, F., 2004. A top-down scenario for the formation of massive Tidal Dwarf Galaxies. *A&A*, 427:803.

Duc, P.A., Cuillandre, J.C., Serra, P., et al., 2011. The ATLAS^{3D} project - IX. The merger origin of a fast- and a slow-rotating early-type galaxy revealed with deep optical imaging: first results. *MNRAS*, 417:863.

Dunkley, J., Komatsu, E., Nolta, M.R., et al., 2009. Five-Year Wilkinson Microwave Anisotropy Probe Observations: Likelihoods and Parameters from the WMAP Data. *ApJS*, 180(2):306.

Eisenstein, D.J. and Hut, P., 1998. HOP: A New Group-Finding Algorithm for N-Body Simulations. *ApJ*, 498(1):137.

Elbaz, D., Daddi, E., Le Borgne, D., et al., 2007. The reversal of the star formation-density relation in the distant universe. *A&A*, 468(1):33.

Elbaz, D., Dickinson, M., Hwang, H.S., et al., 2011. GOODS-Herschel: an infrared main sequence for star-forming galaxies. *A&A*, 533:A119.

Ellison, S.L., Mendel, J.T., Scudder, J.M., et al., 2013. Galaxy pairs in the Sloan Digital Sky Survey - VII. The merger-luminous infrared galaxy connection. *MNRAS*, 430(4):3128.

Ellison, S.L., Patton, D.R., Simard, L., et al., 2008. Galaxy Pairs in the Sloan Digital Sky Survey. I. Star Formation, Active Galactic Nucleus Fraction, and the Mass-Metallicity Relation. *AJ*, 135:1877.

Elmegreen, B.G., Elmegreen, D.M., Sánchez Almeida, J., et al., 2013. Massive Clumps in Local Galaxies: Comparisons with High-redshift Clumps. *ApJ*, 774:86.

Elmegreen, B.G., Kaufman, M., and Thomasson, M., 1993. An Interaction Model for the Formation of Dwarf Galaxies and 10 8 M$_{sun}$ Clouds in Spiral Disks. *ApJ*, 412:90.

Emsellem, E., van der Burg, R.F.J., Fensch, J., et al., 2019. The ultra-diffuse galaxy NGC 1052-DF2 with MUSE. I. Kinematics of the stellar body. *A&A*, 625:A76.

Faber, S.M., Willmer, C.N.A., Wolf, C., et al., 2007. Galaxy Luminosity Functions to z˜1 from DEEP2 and COMBO-17: Implications for Red Galaxy Formation. *ApJ*, 665:265.

Fabian, A.C., 2012. Observational Evidence of Active Galactic Nuclei Feedback. *ARA&A*, 50:455.

Fakhouri, O. and Ma, C.P., 2008. The nearly universal merger rate of dark matter haloes in ΛCDM cosmology. *MNRAS*, 386(2):577.

Fall, S.M. and Efstathiou, G., 1980. Formation and rotation of disc galaxies with haloes. *MNRAS*, 193:189.

Fensch, J., Duc, P.A., Boquien, M., et al., 2019a. Massive star cluster formation and evolution in tidal dwarf galaxies. *A&A*, 628:A60.

Fensch, J., van der Burg, R.F.J., Jeřábková, T., et al., 2019b. The ultra-diffuse galaxy NGC 1052-DF2 with MUSE. II. The population of DF2: stars, clusters, and planetary nebulae. *A&A*, 625:A77.

Ferdosi, B.J., Buddelmeijer, H., Trager, S.C., et al., 2011. Comparison of density estimation methods for astronomical datasets. *A&A*, 531:A114.

Ferreras, I., Lisker, T., Pasquali, A., et al., 2009. On the formation of massive galaxies: a simultaneous study of number density, size and intrinsic colour evolution in GOODS. *MNRAS*, 396:1573.

Fiacconi, D., Feldmann, R., and Mayer, L., 2015. The Argo simulation - II. The early build-up of the Hubble sequence. *MNRAS*, 446:1957.

Fliri, J. and Trujillo, I., 2016. The iac stripe 82 legacy project: a wide-area survey for faint surface brightness astronomy. *Monthly Notices of the Royal Astronomical Society*, 456(2):1359.

Font, A.S., McCarthy, I.G., Le Brun, A.M.C., et al., 2017. The diversity of assembly histories leading to disc galaxy formation in a LambdaCDM model. *ArXiv e-prints*.

Fontana, A., Dunlop, J.S., Paris, D., et al., 2014. The Hawk-I UDS and GOODS Survey (HUGS): Survey design and deep K-band number counts. *A&A*, 570:A11.

Fukugita, M., Nakamura, O., Turner, E.L., et al., 2004. Actively star-forming elliptical galaxies at low redshifts in the sloan digital sky survey. *The Astrophysical Journal Letters*, 601(2):L127.

Gallart, C., Monelli, M., Mayer, L., et al., 2015. The ACS LCID Project: On the Origin of Dwarf Galaxy Types—A Manifestation of the Halo Assembly Bias? *ApJ*, 811(2):L18.

Gan, J., Kang, X., van den Bosch, F.C., et al., 2010. An improved model for the dynamical evolution of dark matter subhaloes. *MNRAS*, 408(4):2201.

Gao, L., White, S.D.M., Jenkins, A., et al., 2004. The subhalo populations of ΛCDM dark haloes. *MNRAS*, 355(3):819.

Gardner, J.P., Mather, J.C., Clampin, M., et al., 2006. The James Webb Space Telescope. *Space Sci. Rev.*, 123:485.

Geen, S., Rosdahl, J., Blaizot, J., et al., 2015. A detailed study of feedback from a massive star. *MNRAS*, 448(4):3248.

Georgakakis, A., Coil, A.L., Laird, E.S., et al., 2009. Host galaxy morphologies of X-ray selected AGN: assessing the significance of different black hole fuelling mechanisms to the accretion density of the Universe at z∼ 1. *Monthly Notices of the Royal Astronomical Society*, 397(2):623.

Ghigna, S., Moore, B., Governato, F., et al., 1998. Dark matter haloes within clusters. *MNRAS*, 300(1):146.

Giocoli, C., Tormen, G., and van den Bosch, F.C., 2008. The population of dark matter subhaloes: mass functions and average mass-loss rates. *MNRAS*, 386(4):2135.

Girardi, L., Bressan, A., Bertelli, G., et al., 2000. Evolutionary tracks and isochrones for low- and intermediate-mass stars: From 0.15 to 7 M$_{sun}$, and from Z=0.0004 to 0.03. *A&AS*, 141:371.

González, V., Labbé, I., Bouwens, R.J., et al., 2011. Evolution of Galaxy Stellar Mass Functions, Mass Densities, and Mass-to-light Ratios from z ∼7 to z ∼4. *ApJ*, 735(2):L34.

Governato, F., Brook, C.B., Brooks, A.M., et al., 2009. Forming a large disc galaxy from a z < 1 major merger. *MNRAS*, 398(1):312.

Governato, F., Willman, B., Mayer, L., et al., 2007. Forming disc galaxies in ΛCDM simulations. *MNRAS*, 374(4):1479.

Governato, F., Zolotov, A., Pontzen, A., et al., 2012. Cuspy no more: how outflows affect the central dark matter and baryon distribution in Λ cold dark matter galaxies. *MNRAS*, 422(2):1231.

Grazian, A., Fontana, A., Santini, P., et al., 2015. The galaxy stellar mass function at 3.5 ≤z ≤ 7.5 in the CANDELS/UDS, GOODS-South, and HUDF fields. *A&A*, 575:A96.

Greco, J.P., Greene, J.E., Strauss, M.A., et al., 2018. Illuminating Low Surface Brightness Galaxies with the Hyper Suprime-Cam Survey. *ApJ*, 857(2):104.

Gunn, J.E. and Gott, J. Richard, I., 1972. On the Infall of Matter Into Clusters of Galaxies and Some Effects on Their Evolution. *ApJ*, 176:1.

Guo, Q., Hu, H., Zheng, Z., et al., 2019. Further evidence for a population of dark-matter-deficient dwarf galaxies. *Nature Astronomy*, 4:246.

Guyon, O., Sanders, D.B., and Stockton, A., 2006. Near-Infrared Adaptive Optics Imaging of QSO Host Galaxies. *ApJS*, 166(1):89.

Haardt, F. and Madau, P., 1996. Radiative Transfer in a Clumpy Universe. II. The Ultraviolet Extragalactic Background. *ApJ*, 461:20.

Hambleton, K.M., Gibson, B.K., Brook, C.B., et al., 2011. Advanced morphological galaxy classification: a comparison of observed and simulated galaxies. *MNRAS*, 418:801.

Hammer, F., Yang, Y., Arenou, F., et al., 2020. Orbital Evidences for Dark-matter-free Milky Way Dwarf Spheroidal Galaxies. *ApJ*, 892(1):3.

Han, J., Cole, S., Frenk, C.S., et al., 2016. A unified model for the spatial and mass distribution of subhaloes. *MNRAS*, 457(2):1208.

Hancock, M., Smith, B.J., Struck, C., et al., 2009. Candidate Tidal Dwarf Galaxies in Arp 305: Lessons on Dwarf Detachment and Globular Cluster Formation. *AJ*, 137(6):4643.

Häring, N. and Rix, H.W., 2004. On the Black Hole Mass-Bulge Mass Relation. *ApJ*, 604(2):L89.

Haslbauer, M., Dabringhausen, J., Kroupa, P., et al., 2019. Galaxies lacking dark matter in the Illustris simulation. *A&A*, 626:A47.

Hatton, S., Devriendt, J.E.G., Ninin, S., et al., 2003. GALICS- I. A hybrid N-body/semi-analytic model of hierarchical galaxy formation. *MNRAS*, 343(1):75.

Hayashi, E., Navarro, J.F., Taylor, J.E., et al., 2003. The Structural Evolution of Substructure. *ApJ*, 584(2):541.

Haynes, M.P., Giovanelli, R., Martin, A.M., et al., 2011. The Arecibo Legacy Fast ALFA Survey: The α.40 H I Source Catalog, Its Characteristics and Their Impact on the Derivation of the H I Mass Function. *AJ*, 142(5):170.

Hayward, C.C. and Hopkins, P.F., 2017. How stellar feedback simultaneously regulates star formation and drives outflows. *MNRAS*, 465(2):1682.

Hernquist, L. and Spergel, D.N., 1992. Formation of shells in major mergers. *ApJ*, 399:L117.

Hernquist, L. and Springel, V., 2003. An analytical model for the history of cosmic star formation. *MNRAS*, 341(4):1253.

Hester, J.A., 2006. Ram Pressure Stripping in Clusters and Groups. *ApJ*, 647(2):910.

Hilz, M., Naab, T., and Ostriker, J.P., 2013. How do minor mergers promote inside-out growth of ellipticals, transforming the size, density profile and dark matter fraction? *MNRAS*, 429:2924.

Hiroshima, N., Ando, S., and Ishiyama, T., 2018. Modeling evolution of dark matter substructure and annihilation boost. *Phys. Rev. D*, 97(12):123002.

Hopkins, P.F., Cox, T.J., Younger, J.D., et al., 2009. How do Disks Survive Mergers? *ApJ*, 691(2):1168.

Hoyle, F. and Lyttleton, R.A., 1939. The evolution of the stars. *Mathematical Proceedings of the Cambridge Philosophical Society*, 35(4):592–609.

Hubble, E.P., 1926. Extragalactic nebulae. *ApJ*, 64:321.

Huertas-Company, M., Pérez-González, P.G., Mei, S., et al., 2015. The Morphologies of Massive Galaxies from z ∼ 3 - Witnessing the Two Channels of Bulge Growth. *ApJ*, 809:95.

Hunt, L.K., Tortora, C., Ginolfi, M., et al., 2020. Scaling relations and baryonic cycling in local star-forming galaxies. II. Gas content and star-formation efficiency. *A&A*, 643:A180.

Ilbert, O., McCracken, H.J., Le Fèvre, O., et al., 2013. Mass assembly in quiescent and star-forming galaxies since z ≃ 4 from UltraVISTA. *A&A*, 556:A55.

Jackson, R.A., Martin, G., Kaviraj, S., et al., 2020. Why do extremely massive disc galaxies exist today? *MNRAS*, 494(4):5568.

Jiang, F., Dekel, A., Freundlich, J., et al., 2019. Formation of ultra-diffuse galaxies in the field and in galaxy groups. *MNRAS*, 487(4):5272.

Jing, Y., Wang, C., Li, R., et al., 2019. Dark-matter-deficient galaxies in hydrodynamical simulations. *MNRAS*, 488(3):3298.

Jogee, S., Miller, S.H., Penner, K., et al., 2009. History of Galaxy Interactions and Their Impact on Star Formation Over the Last 7 Gyr from GEMS. *ApJ*, 697(2):1971.

Johansson, P.H., Naab, T., and Ostriker, J.P., 2009. Gravitational Heating Helps Make Massive Galaxies Red and Dead. *ApJ*, 697(1):L38.

Joung, M.R., Putman, M.E., Bryan, G.L., et al., 2012. Gas Accretion is Dominated by Warm Ionized Gas in Milky Way Mass Galaxies at z ∽0. *ApJ*, 759(2):137.

Karim, A., Schinnerer, E., Martínez-Sansigre, A., et al., 2011. The Star Formation History of Mass-selected Galaxies in the COSMOS Field. *ApJ*, 730:61.

Kaviraj, S., 2010. Peculiar early-type galaxies in the Sloan Digital Sky Survey Stripe82. *MNRAS*, 406:382.

Kaviraj, S., 2014a. The importance of minor-merger-driven star formation and black hole growth in disc galaxies. *MNRAS*, 440:2944.

Kaviraj, S., 2014b. The significant contribution of minor mergers to the cosmic star formation budget. *MNRAS*, 437:L41.

Kaviraj, S., 2020. The low-surface-brightness Universe: a new frontier in the study of galaxy evolution. *arXiv e-prints*, arXiv:2001.01728.

Kaviraj, S., Cohen, S., Ellis, R.S., et al., 2013. Newborn spheroids at high redshift: when and how did the dominant, old stars in today's massive galaxies form? *MNRAS*, 428:925.

Kaviraj, S., Darg, D., Lintott, C., et al., 2012a. Tidal dwarf galaxies in the nearby Universe. *MNRAS*, 419:70.

Kaviraj, S., Darg, D., Lintott, C., et al., 2012b. Tidal dwarf galaxies in the nearby Universe. *MNRAS*, 419:70.

Kaviraj, S., Devriendt, J., Dubois, Y., et al., 2015. Galaxy merger histories and the role of merging in driving star formation at z > 1. *MNRAS*, 452:2845.

Kaviraj, S., Khochfar, S., Schawinski, K., et al., 2008. The UV colours of high-redshift early-type galaxies: evidence for recent star formation and stellar mass assembly over the last 8 billion years. *MNRAS*, 388:67.

Kaviraj, S., Laigle, C., Kimm, T., et al., 2017. The Horizon-AGN simulation: evolution of galaxy properties over cosmic time. *MNRAS*, 467:4739.

Kaviraj, S., Martin, G., and Silk, J., 2019. AGN in dwarf galaxies: frequency, triggering processes and the plausibility of AGN feedback. *MNRAS*, 489(1):L12.

Kaviraj, S., Schawinski, K., Devriendt, J.E.G., et al., 2007. UV-Optical Colors As Probes of Early-Type Galaxy Evolution. *ApJS*, 173:619.

Kaviraj, S., Tan, K.M., Ellis, R.S., et al., 2011. A coincidence of disturbed morphology and blue UV colour: minor-merger-driven star formation in early-type galaxies at z ∼ 0.6. *MNRAS*, 411:2148.

Kennicutt, Jr., R.C., 1998. The Global Schmidt Law in Star-forming Galaxies. *ApJ*, 498:541.

Kent, S.M., Dame, T.M., and Fazio, G., 1991. Galactic Structure from the Spacelab Infrared Telescope. II. Luminosity Models of the Milky Way. *ApJ*, 378:131.

Kereš, D., Katz, N., Weinberg, D.H., et al., 2005. How do galaxies get their gas? *MNRAS*, 363(1):2.

Khandai, N., Di Matteo, T., Croft, R., et al., 2015. The MassiveBlack-II simulation: the evolution of haloes and galaxies to z ∼ 0. *MNRAS*, 450:1349.

Kimm, T. and Cen, R., 2014. Escape Fraction of Ionizing Photons during Reionization: Effects due to Supernova Feedback and Runaway OB Stars. *ApJ*, 788(2):121.

Kimm, T., Katz, H., Haehnelt, M., et al., 2017. Feedback-regulated star formation and escape of LyC photons from mini-haloes during reionization. *MNRAS*, 466(4):4826.

Knapen, J.H., Whyte, L.F., de Blok, W.J.G., et al., 2004. The nuclear ring in the unbarred galaxy NGC 278: Result of a minor merger? *A&A*, 423:481.

Kniazev, A.Y., Grebel, E.K., Pustilnik, S.A., et al., 2004. Low Surface Brightness Galaxies in the Sloan Digital Sky Survey. I. Search Method and Test Sample. *AJ*, 127:704.

Koda, J., Yagi, M., Yamanoi, H., et al., 2015. Approximately a Thousand Ultra-diffuse Galaxies in the Coma Cluster. *ApJ*, 807(1):L2.

Komatsu, E., Dunkley, J., Nolta, M.R., et al., 2009. Five-Year Wilkinson Microwave Anisotropy Probe Observations: Cosmological Interpretation. *ApJS*, 180(2):330.

Komatsu, E., Smith, K.M., Dunkley, J., et al., 2011a. Seven-year Wilkinson Microwave Anisotropy Probe (WMAP) Observations: Cosmological Interpretation. *ApJS*, 192:18.

Komatsu, E., Smith, K.M., Dunkley, J., et al., 2011b. Seven-year Wilkinson Microwave Anisotropy Probe (WMAP) Observations: Cosmological Interpretation. *ApJS*, 192:18.

Kravtsov, A.V., Gnedin, O.Y., and Klypin, A.A., 2004. The Tumultuous Lives of Galactic Dwarfs and the Missing Satellites Problem. *ApJ*, 609(2):482.

Kroupa, P., 2012. The Dark Matter Crisis: Falsification of the Current Standard Model of Cosmology. *Publ. Astron. Soc. Australia*, 29(4):395.

Kulier, A., Galaz, G., Padilla, N.D., et al., 2019. Massive Low Surface Brightness Galaxies in the EAGLE Simulation. *arXiv e-prints*, arXiv:1910.05345.

Kuzio de Naray, R., McGaugh, S.S., and de Blok, W.J.G., 2008. Mass Models for Low Surface Brightness Galaxies with High-Resolution Optical Velocity Fields. *ApJ*, 676(2):920.

Lagos, C.d.P., Stevens, A.R.H., Bower, R.G., et al., 2018. Quantifying the impact of mergers on the angular momentum of simulated galaxies. *MNRAS*, 473(4):4956.

Laigle, C., Pichon, C., Arnouts, S., et al., 2018. COSMOS2015 photometric redshifts probe the impact of filaments on galaxy properties. *MNRAS*, 474(4):5437.

Laporte, C.F.P., Agnello, A., and Navarro, J.F., 2019. Reconciling mass estimates of ultradiffuse galaxies. *MNRAS*, 484(1):245.

Laureijs, R., Amiaux, J., Arduini, S., et al., 2011. Euclid Definition Study Report. *ArXiv e-prints*.

Ledlow, M.J., Owen, F.N., Yun, M.S., et al., 2001. A Large-Scale Jet and FR I Radio Source in a Spiral Galaxy: The Host Properties and External Environment. *ApJ*, 552(1):120.

Lee, N., Sanders, D.B., Casey, C.M., et al., 2015. A Turnover in the Galaxy Main Sequence of Star Formation at $M_* \sim 10^{10}\,M_\odot$ for Redshifts $z < 1.3$. *ApJ*, 801:80.

Leisman, L., Haynes, M.P., Janowiecki, S., et al., 2017. (Almost) Dark Galaxies in the ALFALFA Survey: Isolated H I-bearing Ultra-diffuse Galaxies. *ApJ*, 842:133.

Leitherer, C., Ortiz Otálvaro, P.A., Bresolin, F., et al., 2010. A Library of Theoretical Ultraviolet Spectra of Massive, Hot Stars for Evolutionary Synthesis. *ApJS*, 189:309.

Leitherer, C., Schaerer, D., Goldader, J.D., et al., 1999. Starburst99: Synthesis Models for Galaxies with Active Star Formation. *ApJS*, 123:3.

Li, C. and White, S.D.M., 2009. The distribution of stellar mass in the low-redshift Universe. *MNRAS*, 398(4):2177.

Li, J.T., Zhou, P., Jiang, X., et al., 2019. Molecular Gas of the Most Massive Spiral Galaxies. I. A Case Study of NGC 5908. *ApJ*, 877(1):3.

Li, Y.T. and Chen, L.W., 2019. First ranked galaxies of non-elliptical morphology. *MNRAS*, 482(3):4084.

Liao, S., Gao, L., Frenk, C.S., et al., 2019. Ultra-diffuse galaxies in the Auriga simulations. *MNRAS*, 490(4):5182.

Lofthouse, E.K., Kaviraj, S., Conselice, C.J., et al., 2017. Major mergers are not significant drivers of star formation or morphological transformation around the epoch of peak cosmic star formation. *MNRAS*, 465:2895.

López-Corredoira, M., Cabrera-Lavers, A., Garzón, F., et al., 2002. Old stellar Galactic disc in near-plane regions according to 2MASS: Scales, cut-off, flare and warp. *A&A*, 394:883.

López-Sanjuan, C., Balcells, M., Pérez-González, P.G., et al., 2010. The Minor Role of Gas-Rich Major Mergers in the Rise of Intermediate-Mass Early Types at z <= 1. *ApJ*, 710(2):1170.

Lotz, J.M., Jonsson, P., Cox, T.J., et al., 2010. The effect of gas fraction on the morphology and time-scales of disc galaxy mergers. *Monthly Notices of the Royal Astronomical Society*, 404(2):590.

Lotz, J.M., Jonsson, P., Cox, T.J., et al., 2011. The Major and Minor Galaxy Merger Rates at z < 1.5. *ApJ*, 742(2):103.

Macciò, A.V., Huterer Prats, D., Dixon, K.L., et al., 2020. Creating a galaxy lacking dark matter in a dark matter dominated universe. *arXiv e-prints*, arXiv:2010.02245.

Madau, P. and Dickinson, M., 2014. Cosmic Star-Formation History. *ARA&A*, 52:415.

Madrid, J.P., Chiaberge, M., Floyd, D., et al., 2006. Hubble Space Telescope Near-Infrared Snapshot Survey of 3CR Radio Source Counterparts at Low Redshift. *ApJS*, 164(2):307.

Mamon, G.A., 2000. Theory of Galaxy Dynamics in Clusters and Groups. In F. Combes, G.A. Mamon, and V. Charmandaris, editors, *Dynamics of Galaxies: from the Early Universe to the Present*, volume 197 of *Astronomical Society of the Pacific Conference Series*, page 377.

Mancera Piña, P.E., Fraternali, F., Oman, K.A., et al., 2020. Robust H I kinematics of gas-rich ultra-diffuse galaxies: hints of a weak-feedback formation scenario. *MNRAS*, 495(4):3636.

Mancillas, B., Duc, P.A., Combes, F., et al., 2019. Probing the merger history of red early-type galaxies with their faint stellar substructures. *A&A*, 632:A122.

Martin, G., Jackson, R.A., Kaviraj, S., et al., 2020. The role of mergers and fly-bys in driving the evolution of dwarf galaxies over cosmic time. *arXiv e-prints*, arXiv:2007.07913.

Martin, G., Kaviraj, S., Devriendt, J.E.G., et al., 2017. The limited role of galaxy mergers in driving stellar mass growth over cosmic time. *MNRAS*, 472:L50.

Martin, G., Kaviraj, S., Devriendt, J.E.G., et al., 2018. Identifying the progenitors of present-day early-type galaxies in observational surveys: correcting ?progenitor bias? using the horizon-agn simulation. *MNRAS*, 474(3):3140.

Martin, G., Kaviraj, S., Devriendt, J.E.G., et al., 2018a. The role of mergers in driving morphological transformation over cosmic time. *MNRAS*, 480:2266.

Martin, G., Kaviraj, S., Laigle, C., et al., 2019. The formation and evolution of low-surface-brightness galaxies. *MNRAS*, 485(1):796.

Martin, N.F., Collins, M.L.M., Longeard, N., et al., 2018b. Current Velocity Data on Dwarf Galaxy NGC 1052-DF2 do not Constrain it to Lack Dark Matter. *ApJ*, 859(1):L5.

Martínez-Delgado, D., Läsker, R., Sharina, M., et al., 2016. Discovery of an Ultra-diffuse Galaxy in the Pisces–Perseus Supercluster. *AJ*, 151(4):96.

Martínez-Delgado, D., Läsker, R., Sharina, M., et al., 2016. Discovery of an Ultra-diffuse Galaxy in the Pisces–Perseus Supercluster. *AJ*, 151:96.

Matteucci, F. and Greggio, L., 1986. Relative roles of type I and II supernovae in the chemical enrichment of the interstellar gas. *A&A*, 154:279.

Matteucci, F. and Recchi, S., 2001. On the Typical Timescale for the Chemical Enrichment from Type Ia Supernovae in Galaxies. *ApJ*, 558:351.

McGaugh, S.S., Schombert, J.M., and Bothun, G.D., 1995. The Morphology of Low Surface Brightness Disk Galaxies. *AJ*, 109:2019.

McIntosh, D.H., Guo, Y., Hertzberg, J., et al., 2008. Ongoing assembly of massive galaxies by major merging in large groups and clusters from the SDSS. *MNRAS*, 388:1537.

McKinney, J.C., Tchekhovskoy, A., and Blandford, R.D., 2012. General relativistic magnetohydrodynamic simulations of magnetically choked accretion flows around black holes. *Monthly Notices of the Royal Astronomical Society*, 423(4):3083.

McMillan, P.J., 2011. Mass models of the Milky Way. *MNRAS*, 414(3):2446.

Merritt, A., van Dokkum, P., Danieli, S., et al., 2016. The Dragonfly Nearby Galaxies Survey. II. Ultra-Diffuse Galaxies near the Elliptical Galaxy NGC 5485. *ApJ*, 833:168.

Metz, M., Kroupa, P., and Jerjen, H., 2007. The spatial distribution of the Milky Way and Andromeda satellite galaxies. *MNRAS*, 374(3):1125.

Mihos, C., 2000. Interactions and mergers at higher redshift. *arXiv e-prints*, astro-ph/0010249.

Mihos, J.C., Durrell, P.R., Ferrarese, L., et al., 2015. Galaxies at the Extremes: Ultra-diffuse Galaxies in the Virgo Cluster. *ApJ*, 809(2):L21.

Mihos, J.C. and Hernquist, L., 1996. Gasdynamics and Starbursts in Major Mergers. *ApJ*, 464:641.

Montes, M., Infante-Sainz, R., Madrigal-Aguado, A., et al., 2020. The Galaxy "Missing Dark Matter" NGC 1052-DF4 is Undergoing Tidal Disruption. *ApJ*, 904(2):114.

Moody, C.E., Romanowsky, A.J., Cox, T.J., et al., 2014. Simulating multiple merger pathways to the central kinematics of early-type galaxies. *MNRAS*, 444:1475.

Moore, B., Ghigna, S., Governato, F., et al., 1999. Dark Matter Substructure within Galactic Halos. *ApJ*, 524(1):L19.

Morganti, R., Holt, J., Tadhunter, C., et al., 2011. PKS 1814-637: a powerful radio-loud AGN in a disk galaxy. *A&A*, 535:A97.

Morrissey, P., Conrow, T., Barlow, T.A., et al., 2007. The Calibration and Data Products of GALEX. *ApJS*, 173(2):682.

Moster, B.P., Somerville, R.S., Maulbetsch, C., et al., 2010. Constraints on the Relationship between Stellar Mass and Halo Mass at Low and High Redshift. *ApJ*, 710(2):903.

Müller, O., Marleau, F.R., Duc, P.A., et al., 2020. Spectroscopic study of MATLAS-2019 with MUSE: An ultra-diffuse galaxy with an excess of old globular clusters. *A&A*, 640:A106.

Mundy, C.J., Conselice, C.J., Duncan, K.J., et al., 2017. A consistent measure of the merger histories of massive galaxies using close-pair statistics - I. Major mergers at z < 3.5. *MNRAS*, 470(3):3507.

Musso, M., Cadiou, C., Pichon, C., et al., 2018. How does the cosmic web impact assembly bias? *MNRAS*, 476(4):4877.

Naab, T. and Burkert, A., 2003. Statistical Properties of Collisionless Equal- and Unequal-Mass Merger Remnants of Disk Galaxies. *ApJ*, 597:893.

Naab, T., Oser, L., Emsellem, E., et al., 2014a. The ATLAS^{3D} project - XXV. Two-dimensional kinematic analysis of simulated galaxies and the cosmological origin of fast and slow rotators. *MNRAS*, 444:3357.

Naab, T., Oser, L., Emsellem, E., et al., 2014b. The ATLAS^{3D} project - XXV. Two-dimensional kinematic analysis of simulated galaxies and the cosmological origin of fast and slow rotators. *MNRAS*, 444:3357.

Nagai, D. and Kravtsov, A.V., 2005. The Radial Distribution of Galaxies in Λ Cold Dark Matter Clusters. *ApJ*, 618(2):557.

Navarro, J.F., Eke, V.R., and Frenk, C.S., 1996. The cores of dwarf galaxy haloes. *MNRAS*, 283(3):L72.

Navarro, J.F., Ludlow, A., Springel, V., et al., 2010. The diversity and similarity of simulated cold dark matter haloes. *MNRAS*, 402(1):21.

Nayyeri, H., Hemmati, S., Mobasher, B., et al., 2017. CANDELS Multi-wavelength Catalogs: Source Identification and Photometry in the CANDELS COSMOS Survey Field. *ApJS*, 228(1):7.

Negroponte, J. and White, S.D.M., 1983. Simulations of mergers between disc-halo galaxies. *MNRAS*, 205:1009.

Nelson, D., Springel, V., Pillepich, A., et al., 2019. The IllustrisTNG simulations: public data release. *Computational Astrophysics and Cosmology*, 6(1):2.

Newman, A.B., Ellis, R.S., Bundy, K., et al., 2012. Can Minor Merging Account for the Size Growth of Quiescent Galaxies? New Results from the CANDELS Survey. *ApJ*, 746:162.

Niemiec, A., Jullo, E., Giocoli, C., et al., 2019. Dark matter stripping in galaxy clusters: a look at the stellar-to-halo mass relation in the Illustris simulation. *MNRAS*, 487(1):653.

Niemiec, A., Jullo, E., Limousin, M., et al., 2017. Stellar-to-halo mass relation of cluster galaxies. *MNRAS*, 471(1):1153.

Ogiya, G., 2018. Tidal stripping as a possible origin of the ultra diffuse galaxy lacking dark matter. *MNRAS*, 480(1):L106.

Ogle, P.M., Lanz, L., Appleton, P.N., et al., 2019. A Catalog of the Most Optically Luminous Galaxies at z < 0.3: Super Spirals, Super Lenticulars, Super Post-mergers, and Giant Ellipticals. *ApJS*, 243(1):14.

Ogle, P.M., Lanz, L., Nader, C., et al., 2016. SUPERLUMINOUS SPIRAL GALAXIES. *The Astrophysical Journal*, 817(2):109.

Oman, K.A., Navarro, J.F., Sales, L.V., et al., 2016. Missing dark matter in dwarf galaxies? *MNRAS*, 460(4):3610.

Oser, L., Ostriker, J.P., Naab, T., et al., 2010. The Two Phases of Galaxy Formation. *ApJ*, 725:2312.

Ostriker, E.C., 1999. Dynamical Friction in a Gaseous Medium. *ApJ*, 513(1):252.

Pace, C. and Salim, S., 2014. Satellites of Radio AGN in SDSS: Insights into AGN Triggering and Feedback. *ApJ*, 785:66.

Papastergis, E., Adams, E.A.K., and Romanowsky, A.J., 2017. The HI content of isolated ultra-diffuse galaxies: A sign of multiple formation mechanisms? *A&A*, 601:L10.

Pawlowski, M.S., Kroupa, P., and Jerjen, H., 2013. Dwarf galaxy planes: the discovery of symmetric structures in the Local Group. *MNRAS*, 435(3):1928.

Peebles, P.J.E., 1982. Large-scale background temperature and mass fluctuations due to scale-invariant primeval perturbations. *ApJ*, 263:L1.

Peirani, S., Crockett, R.M., Geen, S., et al., 2010. Composite star formation histories of early-type galaxies from minor mergers: prospects for WFC3. *MNRAS*, 405:2327.

Peschken, N., Łokas, E.L., and Athanassoula, E., 2019. Disc galaxies formed from major mergers in Illustris. *arXiv e-prints*, arXiv:1909.01033.

Pichon, C., Pogosyan, D., Kimm, T., et al., 2011. Rigging dark haloes: why is hierarchical galaxy formation consistent with the inside-out build-up of thin discs? *MNRAS*, 418(4):2493.

Pichon, C., Thiébaut, E., Prunet, S., et al., 2010. ASKI: full-sky lensing map-making algorithms. *MNRAS*, 401(2):705.

Pipino, A., Kaviraj, S., Bildfell, C., et al., 2009. Evidence for recent star formation in BCGs: a correspondence between blue cores and UV excess. *MNRAS*, 395(1):462.

Ploeckinger, S., Recchi, S., Hensler, G., et al., 2015. Chemodynamical evolution of tidal dwarf galaxies - II. The long-term evolution and influence of a tidal field. *MNRAS*, 447(3):2512.

Pogosyan, D., Pichon, C., Gay, C., et al., 2009. The local theory of the cosmic skeleton. *MNRAS*, 396:635.

Postman, M. and Geller, M.J., 1984. The morphology-density relation - The group connection. *ApJ*, 281:95.

Pozzetti, L., Bolzonella, M., Lamareille, F., et al., 2007. The VIMOS VLT Deep Survey. The assembly history of the stellar mass in galaxies: from the young to the old universe. *A&A*, 474(2):443.

Putman, M.E., 2017. *An Introduction to Gas Accretion onto Galaxies*, volume 430, page 1.

Qu, Y., Di Matteo, P., Lehnert, M.D., et al., 2011. Minor mergers and their impact on the kinematics of old and young stellar populations in disk galaxies. *A&A*, 535:A5.

Read, J.I., Iorio, G., Agertz, O., et al., 2017. The stellar mass-halo mass relation of isolated field dwarfs: a critical test of ΛCDM at the edge of galaxy formation. *MNRAS*, 467(2):2019.

Rees, M.J. and Ostriker, J.P., 1977. Cooling, dynamics and fragmentation of massive gas clouds - Clues to the masses and radii of galaxies and clusters. *MNRAS*, 179:541.

Rhee, J., Smith, R., Choi, H., et al., 2017. Phase-space Analysis in the Group and Cluster Environment: Time Since Infall and Tidal Mass Loss. *ApJ*, 843(2):128.

Robertson, B., Bullock, J.S., Cox, T.J., et al., 2006. A Merger-driven Scenario for Cosmological Disk Galaxy Formation. *ApJ*, 645:986.

Robertson, B.E., Banerji, M., Brough, S., et al., 2019. Galaxy formation and evolution science in the era of the Large Synoptic Survey Telescope. *Nature Reviews Physics*, 1(7):450.

Robertson, B.E., Banerji, M., Cooper, M.C., et al., 2017. Large Synoptic Survey Telescope Galaxies Science Roadmap. *ArXiv e-prints*.

Rodrigues, M., Hammer, F., Flores, H., et al., 2017. Morpho-kinematics of z ~ 1 galaxies probe the hierarchical scenario. *MNRAS*, 465:1157.

Rodriguez-Gomez, V., Sales, L.V., Genel, S., et al., 2017. The role of mergers and halo spin in shaping galaxy morphology. *MNRAS*, 467:3083.

Román, J. and Trujillo, I., 2017a. Spatial distribution of ultra-diffuse galaxies within large-scale structures. *MNRAS*, 468:703.

Román, J. and Trujillo, I., 2017b. Ultra-diffuse galaxies outside clusters: clues to their formation and evolution. *MNRAS*, 468:4039.

Rosen, A. and Bregman, J.N., 1995. Global Models of the Interstellar Medium in Disk Galaxies. *ApJ*, 440:634.

Ryan, R. E., J., McCarthy, P.J., Cohen, S.H., et al., 2012. The Size Evolution of Passive Galaxies: Observations from the Wide-Field Camera 3 Early Release Science Program. *ApJ*, 749(1):53.

Saha, K. and Cortesi, A., 2018. Forming Lenticular Galaxies via Violent Disk Instability. *ApJ*, 862:L12.

Sako, M., Bassett, B., Becker, A.C., et al., 2018. The Data Release of the Sloan Digital Sky Survey-II Supernova Survey. *PASP*, 130(988):064002.

Salim, S., Lee, J.C., Janowiecki, S., et al., 2016. GALEX-SDSS-WISE Legacy Catalog (GSWLC): Star Formation Rates, Stellar Masses, and Dust Attenuations of 700,000 Low-redshift Galaxies. *ApJS*, 227(1):2.

Salim, S., Rich, R.M., Charlot, S., et al., 2007. UV Star Formation Rates in the Local Universe. *ApJS*, 173:267.

Sandage, A., Tammann, G.A., and Yahil, A., 1979. The velocity field of bright nearby galaxies. I. The variation of mean absolute magnitude with redshift for galaxies in a magnitude-limited sample. *ApJ*, 232:352.

Sanders, D.B. and Mirabel, I.F., 1996. Luminous Infrared Galaxies. *ARA&A*, 34:749.

Saulder, C., Snaith, O., Park, C., et al., 2020. Isolated dark-matter-deprived galaxies in hydrodynamical simulations: real objects or artefacts? *MNRAS*, 491(1):1278.

Sawala, T., Frenk, C.S., Fattahi, A., et al., 2016. The APOSTLE simulations: solutions to the Local Group's cosmic puzzles. *MNRAS*, 457(2):1931.

Schaap, W.E. and van de Weygaert, R., 2000. Continuous fields and discrete samples: reconstruction through Delaunay tessellations. *A&A*, 363:L29.

Schawinski, K., Dowlin, N., Thomas, D., et al., 2010. The role of mergers in early-type galaxy evolution and black hole growth. *The Astrophysical Journal Letters*, 714(1):L108.

Schaye, J., Crain, R.A., Bower, R.G., et al., 2015. The EAGLE project: simulating the evolution and assembly of galaxies and their environments. *MNRAS*, 446:521.

Schaye, J., Dalla Vecchia, C., Booth, C.M., et al., 2010. The physics driving the cosmic star formation history. *MNRAS*, 402(3):1536.

Schmidt, F., Jeong, D., and Desjacques, V., 2013. Peak-background split, renormalization, and galaxy clustering. *Phys. Rev. D*, 88(2):023515.

Schmidt, M., 1959. The rate of star formation. *The Astrophysical Journal*, 129:243.

Schreiber, C., Pannella, M., Elbaz, D., et al., 2015. The Herschel view of the dominant mode of galaxy growth from z = 4 to the present day. *A&A*, 575:A74.

Searle, L. and Zinn, R., 1978. Composition of halo clusters and the formation of the galactic halo. *ApJ*, 225:357.

Sedgwick, T.M., Baldry, I.K., James, P.A., et al., 2019a. The galaxy stellar mass function and low surface brightness galaxies from core-collapse supernovae. *MNRAS*, 484(4):5278.

Sedgwick, T.M., Baldry, I.K., James, P.A., et al., 2019b. The galaxy stellar mass function from CCSNe with improved photo-z techniques. *arXiv e-prints*, arXiv:1909.04535.

Shakura, N.I. and Sunyaev, R.A., 1973. Reprint of 1973A&A....24..337S. Black holes in binary systems. Observational appearance. *A&A*, 500:33.

Shibuya, T., Ouchi, M., and Harikane, Y., 2015. Morphologies of ~190,000 Galaxies at z = 0-10 Revealed with HST Legacy Data. I. Size Evolution. *ApJS*, 219:15.

Shin, E.j., Jung, M., Kwon, G., et al., 2020. Dark Matter Deficient Galaxies Produced via High-velocity Galaxy Collisions in High-resolution Numerical Simulations. *ApJ*, 899(1):25.

Silk, J., 2011. Feedback in Galaxy Formation. In C. Carignan, F. Combes, and K.C. Freeman, editors, *Tracing the Ancestry of Galaxies*, volume 277, pages 273–281.

Silk, J., 2019. Ultra-diffuse galaxies without dark matter. *MNRAS*, 488(1):L24.

Silk, J. and Mamon, G.A., 2012. The current status of galaxy formation. *Research in Astronomy and Astrophysics*, 12(8):917.

Singh, V., Ishwara-Chandra, C.H., Sievers, J., et al., 2015. Discovery of rare double-lobe radio galaxies hosted in spiral galaxies. *MNRAS*, 454(2):1556.

Smith, R., Choi, H., Lee, J., et al., 2016. The Preferential Tidal Stripping of Dark Matter versus Stars in Galaxies. *ApJ*, 833(1):109.

Smith Castelli, A.V., Faifer, F.R., and Escudero, C.G., 2016. Stellar systems in the direction of the Hickson Compact Group 44. I. Low surface brightness galaxies. *A&A*, 596:A23.

Solanes, J.M. and Perea, J.D., 2015. The dependency of merger time-scales on the orbital parameters and internal spins of galaxies. Implications on the observability of AGN pairs. In A.J. Cenarro, F. Figueras, C. Hernández-Monteagudo, J. Trujillo Bueno, and L. Valdivielso, editors, *Highlights of Spanish Astrophysics VIII*, pages 337–342.

Solanes, J.M., Perea, J.D., and Valentí-Rojas, G., 2018. Timescales of major mergers from simulations of isolated binary galaxy collisions. *A&A*, 614:A66.

Somalwar, J.J., Greene, J.E., Greco, J.P., et al., 2020. Hyper Suprime-Cam Low Surface Brightness Galaxies II: A Hubble Space Telescope Study of the Globular Cluster Systems of Ultra-Diffuse Galaxies in Groups. *arXiv e-prints*, arXiv:2008.02806.

Somerville, R.S. and Davé, R., 2015. Physical Models of Galaxy Formation in a Cosmological Framework. *ARA&A*, 53:51.

Somerville, R.S. and Primack, J.R., 1999. Semi-analytic modelling of galaxy formation: the local Universe. *MNRAS*, 310:1087.

Song, M., Finkelstein, S.L., Ashby, M.L.N., et al., 2016. The Evolution of the Galaxy Stellar Mass Function at z = 4-8: A Steepening Low-mass-end Slope with Increasing Redshift. *ApJ*, 825(1):5.

Sousbie, T., 2011. The persistent cosmic web and its filamentary structure – I. Theory and implementation. *Monthly Notices of the Royal Astronomical Society*, 414(1):350.

Sousbie, T., Pichon, C., and Kawahara, H., 2011. The persistent cosmic web and its filamentary structure – II. Illustrations. *Monthly Notices of the Royal Astronomical Society*, 414(1):384.

Sparre, M. and Springel, V., 2016. Zooming in on major mergers: dense, starbursting gas in cosmological simulations. *MNRAS*, 462(3):2418.

Sparre, M. and Springel, V., 2017. The unorthodox evolution of major merger remnants into star-forming spiral galaxies. *MNRAS*, 470:3946.

Speagle, J.S., Steinhardt, C.L., Capak, P.L., et al., 2014. A Highly Consistent Framework for the Evolution of the Star-Forming "Main Sequence" from z ~0-6. *ApJS*, 214(2):15.

Springel, V. and Hernquist, L., 2005. Formation of a Spiral Galaxy in a Major Merger. *ApJ*, 622:L9.

Steinmetz, M. and Navarro, J.F., 2002. The hierarchical origin of galaxy morphologies. *New Astron.*, 7(4):155.

Sutherland, R.S. and Dopita, M.A., 1993. Cooling functions for low-density astrophysical plasmas. *ApJS*, 88:253.

Swinbank, A.M., Smail, I., Sobral, D., et al., 2012. The Properties of the Star-forming Interstellar Medium at z = 0.8-2.2 from HiZELS: Star Formation and Clump Scaling Laws in Gas-rich, Turbulent Disks. *ApJ*, 760:130.

Tacconi, L.J., Genzel, R., Smail, I., et al., 2008. Submillimeter Galaxies at z ~ 2: Evidence for Major Mergers and Constraints on Lifetimes, IMF, and CO-H_2 Conversion Factor. *ApJ*, 680:246-262.

Tadhunter, C., 2016. Radio AGN in the local universe: unification, triggering and evolution. *A&ARv*, 24(1):10.

Tadhunter, C.N., Scarrott, S.M., Draper, P., et al., 1992. The optical polarizations of high- and intermediate-redshift radio galaxies. *MNRAS*, 256(4):53P.

Taranu, D., Dubinski, J., and Yee, H.K.C., 2015. Mergers in Galaxy Groups. II. The Fundamental Plane of Elliptical Galaxies. *ApJ*, 803:78.

Taranu, D.S., Dubinski, J., and Yee, H.K.C., 2013. Mergers in Galaxy Groups. I. Structure and Properties of Elliptical Remnants. *ApJ*, 778:61.

Tasca, L.A.M., Le Fèvre, O., Hathi, N.P., et al., 2015. The evolving star formation rate: $M_\star$ relation and sSFR since z ≃ 5 from the VUDS spectroscopic survey. *A&A*, 581:A54.

Taylor, P. and Kobayashi, C., 2016. Time evolution of galaxy scaling relations in cosmological simulations. *MNRAS*, 463:2465.

Teyssier, R., 2002a. Cosmological hydrodynamics with adaptive mesh refinement. A new high resolution code called RAMSES. *A&A*, 385:337.

Teyssier, R., 2002b. Cosmological hydrodynamics with adaptive mesh refinement. A new high resolution code called RAMSES. *A&A*, 385:337.

Teyssier, R., Pontzen, A., Dubois, Y., et al., 2013. Cusp-core transformations in dwarf galaxies: observational predictions. *MNRAS*, 429(4):3068.

Tomczak, A.R., Quadri, R.F., Tran, K.V.H., et al., 2016. The SFR-M* Relation and Empirical Star-Formation Histories from ZFOURGE* at 0.5 < z < 4. *ApJ*, 817(2):118.

Tonini, C., Mutch, S.J., Croton, D.J., et al., 2016. The growth of discs and bulges during hierarchical galaxy formation - I. Fast evolution versus secular processes. *MNRAS*, 459(4):4109.

Toomre, A., 1977. Mergers and Some Consequences. In B.M. Tinsley and R.B.G. Larson D. Campbell, editors, *Evolution of Galaxies and Stellar Populations*, page 401.

Tormen, G., Moscardini, L., and Yoshida, N., 2004. Properties of cluster satellites in hydrodynamical simulations. *MNRAS*, 350(4):1397.

Tremmel, M., Wright, A.C., Brooks, A.M., et al., 2019. The Formation of Ultra-Diffuse Galaxies from Passive Evolution in the RomulusC Galaxy Cluster Simulation. *arXiv e-prints*, arXiv:1908.05684.

Trujillo, I., Beasley, M.A., Borlaff, A., et al., 2019. A distance of 13 Mpc resolves the claimed anomalies of the galaxy lacking dark matter. *MNRAS*, 486(1):1192.

Trujillo, I., Förster Schreiber, N.M., Rudnick, G., et al., 2006. The Size Evolution of Galaxies since z~3: Combining SDSS, GEMS, and FIRES. *ApJ*, 650:18.

Trujillo, I., Roman, J., Filho, M., et al., 2017. The Nearest Ultra Diffuse Galaxy: UGC 2162. *ApJ*, 836(2):191.

Tweed, D., Devriendt, J., Blaizot, J., et al., 2009. Building merger trees from cosmological N-body simulations. Towards improving galaxy formation models using subhaloes. *A&A*, 506:647.

Tyson, J.A., 2002. Large Synoptic Survey Telescope: Overview. In J.A. Tyson and S. Wolff, editors, *Survey and Other Telescope Technologies and Discoveries*, volume 4836 of *Proc. SPIE*, pages 10–20.

Uzeirbegovic, E., Geach, J.E., and Kaviraj, S., 2020. Eigengalaxies: describing galaxy morphology using principal components in image space. *arXiv e-prints*, arXiv:2004.06734.

Vale, A. and Ostriker, J.P., 2004. Linking halo mass to galaxy luminosity. *MNRAS*, 353(1):189.

van den Bosch, F.C., Tormen, G., and Giocoli, C., 2005. The mass function and average mass-loss rate of dark matter subhaloes. *MNRAS*, 359(3):1029.

van Dokkum, P., Danieli, S., Abraham, R., et al., 2019. A Second Galaxy Missing Dark Matter in the NGC 1052 Group. *ApJ*, 874(1):L5.

van Dokkum, P., Danieli, S., Cohen, Y., et al., 2018a. A galaxy lacking dark matter. *Nature*, 555(7698):629.

van Dokkum, P., Danieli, S., Cohen, Y., et al., 2018b. The Distance of the Dark Matter Deficient Galaxy NGC 1052-DF2. *ApJ*, 864(1):L18.

van Dokkum, P.G., 2005. The Recent and Continuing Assembly of Field Elliptical Galaxies by Red Mergers. *AJ*, 130:2647.

van Dokkum, P.G., Abraham, R., Merritt, A., et al., 2015a. Forty-seven Milky Way-sized, Extremely Diffuse Galaxies in the Coma Cluster. *ApJ*, 798(2):L45.

van Dokkum, P.G., Nelson, E.J., Franx, M., et al., 2015b. Forming Compact Massive Galaxies. *ApJ*, 813:23.

van Dokkum, P.G., Romanowsky, A.J., Abraham, R., et al., 2015c. Spectroscopic Confirmation of the Existence of Large, Diffuse Galaxies in the Coma Cluster. *ApJ*, 804(1):L26.

van Dokkum, P.G., Romanowsky, A.J., Abraham, R., et al., 2015d. Spectroscopic Confirmation of the Existence of Large, Diffuse Galaxies in the Coma Cluster. *ApJ*, 804(1):L26.

Vassiliadis, E. and Wood, P.R., 1993. Evolution of low- and intermediate-mass stars to the end of the asymptotic giant branch with mass loss. *ApJ*, 413:641.

Veilleux, S., Meléndez, M., Sturm, E., et al., 2013. Fast Molecular Outflows in Luminous Galaxy Mergers: Evidence for Quasar Feedback from Herschel. *ApJ*, 776(1):27.

Vogelsberger, M., Genel, S., Springel, V., et al., 2014a. Introducing the Illustris Project: simulating the coevolution of dark and visible matter in the Universe. *MNRAS*, 444:1518.

Vogelsberger, M., Genel, S., Springel, V., et al., 2014b. Properties of galaxies reproduced by a hydrodynamic simulation. *Nature*, 509:177.

Vollmer, B., Cayatte, V., Balkowski, C., et al., 2001. Ram Pressure Stripping and Galaxy Orbits: The Case of the Virgo Cluster. *ApJ*, 561:708.

Volonteri, M., Dubois, Y., Pichon, C., et al., 2016. The cosmic evolution of massive black holes in the Horizon-AGN simulation. *MNRAS*, 460:2979.

Volonteri, M., Pfister, H., Beckmann, R.S., et al., 2020. Black hole mergers from dwarf to massive galaxies with the NewHorizon and Horizon-AGN simulations. *MNRAS*, 498(2):2219.

Wagner, A.Y. and Bicknell, G.V., 2011. Relativistic Jet Feedback in Evolving Galaxies. *ApJ*, 728(1):29.

Welker, C., Dubois, Y., Devriendt, J., et al., 2017. The rise and fall of stellar across the peak of cosmic star formation history: effects of mergers versus diffuse stellar mass acquisition. *MNRAS*, 465:1241.

Welker, C., Dubois, Y., Pichon, C., et al., 2018. Caught in the rhythm. I. How satellites settle into a plane around their central galaxy. *A&A*, 613:A4.

Wetzstein, M., Naab, T., and Burkert, A., 2007. Do dwarf galaxies form in tidal tails? *MNRAS*, 375(3):805.

Whitaker, K.E., van Dokkum, P.G., Brammer, G., et al., 2012. The Star Formation Mass Sequence Out to z = 2.5. *ApJ*, 754:L29.

White, S.D.M. and Rees, M.J., 1978. Core condensation in heavy halos - A two-stage theory for galaxy formation and clustering. *MNRAS*, 183:341.

Wild, V., Almaini, O., Dunlop, J., et al., 2016. The evolution of post-starburst galaxies from z=2 to 0.5. *MNRAS*, 463:832.

Willett, K.W., Schawinski, K., Simmons, B.D., et al., 2015. Galaxy Zoo: the dependence of the star formation-stellar mass relation on spiral disc morphology. *MNRAS*, 449(1):820.

Williams, C.C., Giavalisco, M., Cassata, P., et al., 2014. The Progenitors of the Compact Early-type Galaxies at High Redshift. *ApJ*, 780:1.

Wong, O.I., Schawinski, K., Kaviraj, S., et al., 2012. Galaxy Zoo: building the low-mass end of the red sequence with local post-starburst galaxies. *MNRAS*, 420:1684.

Wright, A.C., Tremmel, M., Brooks, A.M., et al., 2020. The Formation of Isolated Ultra-Diffuse Galaxies in Romulus25. *arXiv e-prints*, arXiv:2005.07634.

Wuyts, S., Förster Schreiber, N.M., van der Wel, A., et al., 2011. Galaxy Structure and Mode of Star Formation in the SFR-Mass Plane from z ~ 2.5 to z ~ 0.1. *ApJ*, 742:96.

Xie, L. and Gao, L., 2015. Assembly history of subhalo populations in galactic and cluster sized dark haloes. *MNRAS*, 454(2):1697.

Yi, S.K., Yoon, S.J., Kaviraj, S., et al., 2005. Galaxy Evolution Explorer Ultraviolet Color-Magnitude Relations and Evidence of Recent Star Formation in Early-Type Galaxies. *ApJ*, 619:L111.

York, D.G., Adelman, J., Anderson, John E., J., et al., 2000. The Sloan Digital Sky Survey: Technical Summary. *AJ*, 120(3):1579.

Zhang, W., Li, C., Kauffmann, G., et al., 2009. Estimating the HI gas fractions of galaxies in the local Universe. *MNRAS*, 397(3):1243.

Zolotov, A., Dekel, A., Mandelker, N., et al., 2015. Compaction and quenching of high-z galaxies in cosmological simulations: blue and red nuggets. *MNRAS*, 450:2327.